AN ABSTRACT OF THE DISSERTATION OF

Alison M. Koleszar for the degree of Doctor of Philosophy in Geology presented on July 21, 2011.

Title: Controls on Eruption Style and Magma Compositions at Mount Hood, Oregon

Abstract approved:

Adam J. R. Kent

This study is an effort to characterize the magma sources, plumbing system, and eruptive behavior of Mount Hood, a low-explosivity recharge-dominated volcano in the Oregon Cascades. The three manuscripts in this dissertation make use of melt inclusion data, phenocryst compositions, and whole rock petrology and geochemistry to build a schematic model of plumbing, mixing, and eruption at Mount Hood.

Volatile contents in melt inclusions were measured by Fourier Transform Infrared Spectroscopy (FTIR) and Secondary Ion Mass Spectometry (SIMS). These measurements indicate that the pre-eruptive volatile contents at Mount Hood are comparable to concentrations in more explosive volcanoes, and do not sufficiently explain the low explosivity of Mount Hood. Measured H_2O contents were also used to test the validity of multiple different hygrometers.

Various geothermobarometers were applied to the melt inclusions and phenocrysts from Mount Hood, and demonstrate that pre-eruptive temperatures increase

by 100-150˚C immediately after mafic recharge, which occurs days to weeks prior to eruption and is accompanied by a 5-10 fold decrease in magma viscosity. Numerical simulations of magma ascent indicate that magma fragmentation is significantly delayed with this magnitude of pre-eruptive heating, which reduces the likelihood of explosive eruption.

Analyses of amphibole demonstrate two markedly different populations, which correspond to different magma compositions, temperatures, and pressures. Pressure and temperature calculations were compared to other geothermobarometers to crosscheck the validity of these results and generally agreed well.

Trace element concentrations in lavas, enclaves, and inclusions from Mount Hood confirm previous models for simple binary mixing at Mount Hood. A linear regression technique for extrapolating the major element contents of the mixing endmembers works acceptably well to characterize the trace element budgets of these endmembers.

Additionally, we observe that the "recharge filter" that is responsible for the compositionally monotonous lavas at Mount Hood is also the likely cause of long-term low explosivity, and is indicative of a two-part magma plumbing system that may be a general model for a number of other recharge-dominated arc volcanoes. The results presented in this dissertation, in concert with previous results by other authors, converge on a generally consistent model for the production, hybridization, and eruption of intermediate lavas at Mount Hood and elsewhere.

©Copyright by Alison M. Koleszar
July 21, 2011
All Rights Reserved

Controls on Eruption Style and Magma Compositions at Mount Hood, Oregon

by
Alison M. Koleszar

A DISSERTATION

submitted to

Oregon State University

in partial fulfillment of
the requirements for the
degree of

Doctor of Philosophy

Presented July 21, 2011
Commencement June 2012

Doctor of Philosophy dissertation of Alison M. Koleszar presented July 21, 2011.

APPROVED:

Major Professor, representing Geology

Chair of the Department of Geosciences

Dean of the Graduate School

I understand that my thesis will become part of the permanent collection of Oregon State University libraries. My signature below authorizes release of my thesis to any reader upon request.

Alison M. Koleszar, Author

ACKNOWLEDGEMENTS

I would like to thank a number of wonderful people for their active participation in the academic pursuits that produced the contents of these pages:

- My PhD advisor, Adam Kent, for his assistance, support, and guidance through the completion of this dissertation—without his mentorship I would have never progressed beyond olivine
- The faculty of the OSU VIPER group, including Anita Grunder, Dave Graham, and Shan de Silva for their mentorship, guidance, and willingness to serve on my committee; and Frank Tepley for his expertise in analytical techniques and his philosophical discourses on magma mixing
- All of the kind and encouraging folks at the USGS Cascades Volcano Observatory, especially Willie Scott, who gave me my first real introduction to Mount Hood
- My inspiring undergraduate advisor, Karen Harpp, who got me keen on geology and taught me how to sample massive volcanics IYP
- My fellow VIPER grad students at OSU, especially Erin Lieuallen, Ashley Bromley, and Matt Loewen, who provided moral support, stimulating discussion, and countless hours of engaging conversation about volcanoes, amphibole, and beer
- My dear friend, former housemate, and fellow TFL student, Cori Myers, whose emotional, philosophical, and geological support made graduate school a lot of fun
- My fantastic parents, Rick and Edith Koleszar, who always encouraged my scientific pursuits and let me turn the kitchen into my own experimental lab (even after I broke the oven). My dad, who taught me to always know the location of the fire

extinguisher, and my mom, who let me lead her up volcanoes without a fire extinguisher in sight

- And finally, I would like to thank my wonderful other half, Joe Levy, who joins me in all of my adventures and explorations, both academic and otherwise, and saves me from getting too lost in any of them.

Much of the work for this dissertation was funded by NSF EAR grant EAR-038421 to AJRK, with additional funding from a USGS Kleinman Grant to AMK.

CONTRIBUTION OF AUTHORS

Dr. Adam J. R. Kent provided oversight for all three of the manuscripts presented here, training and assistance with Laser Ablation Inductively Coupled Plasma Mass Spectroscopy analyses, and assistance with fieldwork. Dr. Paul J. Wallace provided training and assistance with Fourier Transform Infrared Spectroscopy and interpretation of results. Dr. William E. Scott provided access to samples and valuable background information on the geology of Mount Hood.

TABLE OF CONTENTS

TABLE OF CONTENTS (Continued)

TABLE OF CONTENTS (Continued)

TABLE OF CONTENTS (Continued)

LIST OF FIGURES

LIST OF FIGURES (Continued)

LIST OF TABLES

CONTROLS ON ERUPTION STYLE AND MAGMA COMPOSITIONS AT MOUNT HOOD, OREGON

CHAPTER ONE

GENERAL INTRODUCTION

Mount Hood is a 3426 m intermediate stratocone in the Cascade arc, and is located approximately 75 km east of Portland, Oregon. The current edifice is relatively young (~0.5 my) and has erupted as recently as ~220 years ago (Scott et al., 1997a). Volcanism in convergent margins like the Cascadia subduction zone often focuses in regions of localized extension (Smith and Leeman, 2005), and Hood is no exception. Mount Hood is located at the northern tip of the northward-propagating High Cascades Graben and is bounded to the east by the Hood River normal fault (Guffanti and Weaver, 1988). Much of the earthquake activity at Mount Hood, including the 2002 earthquake swarm, is often attributed to extensional stress from the Basin and Range province (Jones and Malone, 2005), which some authors suggest partly underlies the High Cascades (e.g., Guffanti and Weaver, 1988).

Eruptive products at Mount Hood have remained remarkably consistent both in composition and eruptive style through time. Andesitic (54-63 wt% SiO_2) domes, lava flows, and related debris make up the bulk of the current edifice. Eruptions of minor amounts of low-SiO_2 dacite (63-66 wt% SiO_2) from Mount Hood are evident in the record of the past 15,000 years, but are rarely preserved in the older record. The most mafic material erupted at Hood did not come from the vent itself, but erupted from peripheral vents including Cloud Cap, a 55 ka flow approximately 5 km northeast of Hood's summit, and Parkdale, a 7.7 ka basaltic andesite flow located 11 km north of the

summit (Darr, 2006). The remaining lavas erupted from Mount Hood are compositionally resticted, and 95% of the lavas have between 58-66 wt% SiO_2 (Kent et al., 2010). In contrast, many other Cascade volcanoes, including nearby Mount Jefferson and Mount St. Helens (located 80 km and 100 km from Mount Hood, respectively) have erupted more compositionally diverse lavas. Mount Jefferson has produced material from 50-71 wt% SiO_2, and Mount St. Helens has erupted lavas from 48-70 wt% SiO_2 (Blundy and Cashman, 2008; Clynne et al., 2008; Conrey et al., 2001; Hildreth, 2007). None of the lavas erupted from Mount Hood can be characterized are primitive, but like many of the intermediate lavas of the Cascades, they are likely derived from one of the common primitive basaltic parents known from the region (see Chapter Four).

Kent et al. (2010) suggest that the restricted compositional range at Mount Hood is the result of a "recharge filter," where eruption only occurs following mixing between mafic and silicic magmas, limiting eruptible products to mixed andesitic-dacitic compositions. Magma mixing exerts great influence on the initiation of eruptions (Eichelberger, 1980; Murphy et al., 1998), the composition of erupted lavas (Anderson, 1976; Kent et al., 2010; Reubi and Blundy, 2009), and the style of eruption (Koleszar et al., in review; Ruprecht and Bachmann, 2010; Sparks and Sigurdsson, 1977). In the following chapters we explore how these processes are influenced by dominantly bimodal magma mixing at Mount Hood.

The eruptive history of Mount Hood is somewhat different from most of the other High Cascades volcanoes. During the growth of the current edifice over the last ~500,000 years, eruptions at Mount Hood have been dominated lava domes and flows, with block-and-ash flows produced by dome collapse (Scott et al., 1997a). Evidence for significant

explosive activity at Mount Hood is absent from the available tephra record (Scott et al., 1997b). Although there is general agreement about the driving forces behind explosive volcanic eruptions (e.g., Scandone et al., 2007; Wilson, 1980), it is often difficult to assess the exact causes and potential for explosive activity associated with individual volcanoes and for individual eruptions because of the large number of factors that affect eruptive style including magma composition and flux, plumbing system characteristics, conduit geometry, and time of repose (e.g., Woods, 1995). Despite the lack of significant explosive activity at Mount Hood, neighboring volcanoes to the north (e.g., Mount St. Helens) and south (e.g., Mount Jefferson, The Three Sisters, Mazama) have experienced significant explosive eruptions of magmas with compositions that broadly overlap those erupted from Mount Hood (e.g., Conrey et al., 2001; Hildreth, 2007; McBirney, 1978). The long-term dearth of explosive activity at Mount Hood thus provides a unique opportunity to address the factors that lead to non-explosive eruptions in an andesite-dominated arc volcano.

A number of studies have identified the importance of magma mixing in generating the intermediate compositions that are erupted at Mount Hood, (Cribb and Barton, 1997; Darr, 2006; Kent et al., 2010; Woods, 2004), and recent work has suggested that Mount Hood may be an appropriate general model for the production of andesites at mixing-dominated intermediate arc volcanoes (see Chapter Three and Kent et al., 2010).

The three main chapters of this dissertation address the ways that Mount Hood can be considered somewhat of a general model for an intermediate arc volcano. Chapter Two addresses the tendency for intermediate arc volcanoes to erupt effusively rather than explosively, perhaps as a consequence of magma reheating that accompanies mafic

recharge. At Mount Hood, where virtually every eruption is preceded by mafic recharge and therefore by magma reheating, eruptive behavior consists exclusively of effusive domes, flows, and block-and-ash flows. Chapter Three addresses phenocrystic evidence for multiple magma bodies below intermediate arc volcanoes. At Mount Hood, where compositionally restricted intermediate lavas are consistently bimodal mixtures of two parent magmas, we see clear evidence of two discrete magma bodies that differ in terms of composition, pressure, and temperature. Chapter Four integrates whole rock, phenocryst, and melt inclusion data to estimate the compositions of endmember magmas involved in mixing. At Mount Hood, where multiple Cascade parent magma compositions could be involved in mixing, we observe trace element variations consistent with simple bimodal mixing between calc-alkaline basalt and partial melts of crustal amphibolite.

The clear relationship between two sources, two parent magmas, and two populations of phenocrysts make Mount Hood an ideal natural laboratory for assessing how processes like magma mixing exert control on eruptive behavior.

REFERENCES

Anderson, A.T., 1976, Magma mixing: Petrological process and volcanological tool: Journal of Volcanology and Geothermal Research, v. 1, p. 3-33.

Blundy, J., and Cashman, K., 2008, Petrologic reconstruction of magmatic system variables and processes, *in* Putirka, K.D., and Tepley, F.J.I., eds., Minerals, Inclusions, and Volcanic Processes, Volume 69: Reviews in Mineralogy and Geochemistry: Chantilly, Mineralogical Society of America, p. 179-239.

Clynne, M.A., Calvert, A.T., Wolfe, E.W., Evarts, R.C., Fleck, R.J., and Lanphere, M.A., 2008, The Pleistocene Eruptive History of Mount St. Helens, Washington, from 300,000 to 12,800 Years Before Present, *in* Sherrod, D.R., Scott, W.E., and Stauffer, P.H., eds., A Volcano Rekindled: The Renewed Eruption of Mount St.

Helens, 2004-2006, Volume Professional Paper 1750: Reston, U.S. Geological Survey.

Conrey, R.M., Hooper, P.R., Larson, P.B., Chesley, J., and Ruiz, J., 2001, Trace element and isotopic evidence for two types of crustal melting beneath a High Cascades volcanic center, Mt. Jefferson, Oregon: Contributions to Mineralogy and Petrology, v. 141, p. 710-732.

Cribb, J.W., and Barton, M., 1997, Significance of crustal and source region processes on the evolution of compositionally similar calc-alkaline lavas, Mt. Hood, Oregon: Journal of Volcanology and Geothermal Research, v. 76, p. 229-249.

Darr, C.M., 2006, Magma chamber processes over the past 475,000 years at Mount Hood, Oregon: Insights from crystal zoning and crystal size distribution studies: Corvallis, Oregon State University.

Eichelberger, J.C., 1980, Vesiculation of mafic magma during replenishment of silicic magma reservoirs: Nature, v. 288, p. 446-450.

Guffanti, M., and Weaver, C.S., 1988, Distribution of late Cenozoic volcanic vents in the Cascade Range; volcanic arc segmentation and regional tectonic considerations: Journal of Geophysical Research, v. B93, p. 6513-6529.

Hildreth, W., 2007, Quaternary Magmatism in the Cascades— Geologic Perspectives: Reston, VA, U.S. Geological Survey.

Jones, J., and Malone, S.D., 2005, Mount Hood earthquake activity: Volcanic or tectonic origins?: Bulletin of the Seismological Society of America, v. 95, p. 818-832.

Kent, A.J.R., Darr, C.M., Koleszar, A.M., Salisbury, M.J., and Cooper, K.M., 2010, Preferential eruption of andesitic magmas through recharge filtering: Nature Geoscience, v. 3, p. 631-636.

Koleszar, A.M., Kent, A.J.R., Wallace, P.J., and Scott, W.E., in review, Controls on long-term low explosivity at andesitic arc volcanoes: Insights from Mount Hood, Oregon: Journal of Volcanology and Geothermal Research.

McBirney, A.R., 1978, Volcanic evolution of the Cascades Range: Annual Review in Earth and Planetary Sciences, v. 6, p. 437-456.

Murphy, M.D., Sparks, R.S.J., Barclay, J., Carroll, M.R., Lejeune, A.-M., Brewer, T.S., Macdonald, R., Black, S., and Young, S., 1998, The role of magma mixing in triggering the current eruption at the Soufriere Hills volcano, Montserrat, West Indies: Geophysical Research Letters, v. 25, p. 3433-3436.

Reubi, O., and Blundy, J., 2009, A dearth of intermediate melts at subduction zone volcanoes and the petrogenesis of arc andesites: Nature, v. 461, p. 1269-1273.

Ruprecht, P., and Bachmann, O., 2010, Pre-eruptive reheating during magma mixing at Quizapu volcano and the implications for the explosiveness of silicic arc volcanoes: Geology, v. 38, p. 919-922.

Scandone, R., Cashman, K.V., and Malone, S.D., 2007, Magma supply, magma ascent and the style of volcanic eruptions: Earth and Planetary Science Letters, v. 253, p. 513-529.

Scott, W.E., Gardner, C.A., Tilling, R.I., and Lanphere, M.A., 1997a, Geologic History of Mount Hood Volcano, Oregon: A Field-Trip Guidebook: U.S. Geological Survey Open-File Report, v. 97, p. 38p.

Scott, W.E., Pierson, T.C., Schilling, S.P., Costa, J.E., Gardner, C.A., Vallance, J.W., and Major, J.J., 1997b, Volcano hazards in the Mount Hood Region, Oregon, *in* Interior, U.S.D.o.t., ed., Volume Open-File Report 97-89, U.S. Geological Survey, p. 14.

Smith, D.R., and Leeman, W.P., 2005, Chromian spinel-olivine phase chemistry and the origin of primitive basalts of the southern Washington Cascades: Journal of Volcanology and Geothermal Research, v. 140, p. 49-66.

Sparks, R.S.J., and Sigurdsson, H., 1977, Magma mixing: a mechanism for triggering acid explosive eruptions: Nature, v. 267, p. 315-318.

Wilson, L., 1980, Relationships between pressure, volatile content, and ejecta velocity in three types of volcanic explosive: Journal of Volcanology and Geothermal Research, v. 8, p. 297-313.

Woods, A.W., 1995, The dynamics of explosive volcanic eruptions: Reviews of Geophysics, v. 33, p. 495-530.

Woods, M.M., 2004, Compositional and mineralogical relationships between mafic inclusions and host lavas as key to andesite petrogenesis at Mount Hood Volcano, Oregon: Portland, Portland State University.

CHAPTER TWO

CONTROLS ON LONG-TERM LOW EXPLOSIVITY AT ANDESITIC ARC VOLCANOES: INSIGHTS FROM MOUNT HOOD, OREGON

Alison M. Koleszar
Adam J. R. Kent
Paul J. Wallace
William E. Scott

This manuscript submitted to:
Journal of Volcanology and Geothermal Research
3251 Riverport Lane
Maryland Heights, MO 63043
USA

ABSTRACT

The factors that control the explosivity of silicic volcanoes are critical for hazard assessment, but are often poorly constrained for specific volcanic systems. Mount Hood, Oregon, is a somewhat atypical arc volcano in that it is characterized by a lack of large explosive eruptions over the entire lifetime of the current edifice (~500,000 years). Erupted Mount Hood lavas are also compositionally homogeneous, with ~95% having SiO_2 contents between 58-66 wt%. The last three eruptive periods in particular have produced compositionally homogeneous andesite-dacite lava domes and flows.

In this paper we report major element and volatile (H_2O, CO_2, Cl, S, F) contents of melt inclusions and selected phenocrysts from these three most recent eruptive phases, and use these and other data to consider possible origins for the low explosivity of Mount Hood. Measured volatile concentrations of melt inclusions in plagioclase, pyroxene, and amphibole from pumice indicate that the volatile contents of Mount Hood magmas are comparable to those in more explosive silicic arc volcanoes, including Mount St. Helens, Mount Mazama, and others, suggesting that the lack of explosive activity is unlikely to result solely from low intrinsic volatile concentrations or from substantial degassing prior to magma ascent and eruption. We instead argue that an important control over explosivity is the increased temperature and decreased magma viscosity that results from mafic recharge and magma mixing prior to eruption, similar to a model recently proposed by Ruprecht and Bachmann (2010). Erupted Mount Hood magmas show extensive evidence for mixing between magmas of broadly basaltic and rhyolitic compositions, and mineral zoning studies show that mixing occurred immediately prior to eruption. Amphibole chemistry and thermobarometry also reveal the presence of multiple

amphibole populations and indicate that the mixed andesites and dacites are at least 100°C hotter than the rhyolitic resident magma prior to mixing. Viscosity models suggest that recharge by hot, mafic magma prior to eruption can lower magmatic viscosity by at least a factor of four. Lower viscosity during ascent delays fragmentation and allows volatile escape through degassing, thus lowering the potential for explosive eruptions. These results suggest that low explosivity should be more common in volcanoes where eruption is primarily controlled by mafic recharge events.

INTRODUCTION

Explosive eruptions are relatively common phenomena in volcanoes associated with subduction zone environments, and explosive events can have dramatic and deleterious effect on human populations and infrastructure (Baxter, 2000; Blong, 1984). High explosivity in arc volcanoes typically occurs in high silica magmas that are often crystal-rich, and as a result have elevated viscosity, although explosive eruptions of andesite and even basalt are also known (e.g., Ross et al., 2005). Silicic arc magmas also typically have high volatile concentrations (particularly H_2O). Collectively these factors can combine to lead to catastrophic fragmentation during the rapid decompression that accompanies magma ascent (Dingwell, 1996).

Although there is general agreement about the driving forces behind explosive volcanic eruptions (e.g., Scandone et al., 2007; Wilson, 1980), it is often difficult to assess the exact causes and potential for explosive activity associated with individual volcanoes and for individual eruptions because of the large number of factors that affect eruptive style (e.g., Woods, 1995). Magma composition and flux, plumbing system

characteristics, and conduit geometry, time of repose, and other factors, complicate our ability to identify the reasons why any particular eruption proceeded in a particular way. Despite this, such information is critical to assessing the hazards posed by individual volcanic systems and to understand why some volcanoes transition between effusive and explosive behavior (e.g., Huppert and Woods, 2002; Scandone et al., 2007).

One potential way forward is to study intermediate and silicic arc volcanoes that consistently exhibit low-explosive or non-explosive eruptions, in order to illustrate the parameters that control this long-term behavior. In particular, a number of andesitic arc volcanoes appear to be dominated (perhaps not exclusively) by lava flow or dome eruptions, with little or no explosive activity, over extended time intervals. This behavior appears to be more common in volcanoes where andesitic magmas are produced through mixing between mafic and silicic magmas shortly before eruption, such as at Unzen (Sato et al., 1999), Soufrière Hills (Murphy et al., 1998), Mount Dutton (Miller et al., 1999), and others. Although magma mixing is a well-known trigger for explosive volcanic activity (e.g., Pallister et al., 1996; Sparks and Sigurdsson, 1977), it has also been recently suggested that in some situations the increase in magmatic temperature (and concomitant decrease in magmatic viscosity) that results from mafic recharge can play a dominant role in reducing eruption explosivity (Ruprecht and Bachmann, 2010).

Mount Hood, Oregon, is an endmember example of this type of low-explosivity andesitic arc volcano. During the growth of the current edifice over the last ~500,000 years, eruptions are dominated by lava extrusion to form domes and flows, and evidence for an explosive eruption from Mount Hood is entirely lacking from the available tephra record (Scott et al., 1997b). Despite this, neighboring volcanoes to the north (e.g., Mount

St. Helens) and south (e.g., Mount Jefferson, The Three Sisters, Crater Lake) have experienced significant explosive eruptions of magmas with compositions that broadly overlap those erupted from Mount Hood (e.g., Conrey et al., 2001; Hildreth, 2007; McBirney, 1978). The long-term dearth of explosive activity at Mount Hood thus provides a unique opportunity to address the factors that lead to non-explosive eruptions in an andesite-dominated arc volcano.

Multiple factors are likely to exert influence over whether a given magma will erupt explosively or effusively, including volatile content, ascent rate, conduit and vent geometry (e.g., Scandone et al., 2007; Wilson, 1980; Wilson et al., 1980). To a first order, exsolution of magmatic volatiles drive explosive fragmentation and thus magmas that have inherently low volatile contents are less likely to experience an explosive eruption (Roggensack et al., 1997). Previous studies have examined multiple eruptions from a single volcano and found that explosive versus effusive eruption style correlates with pre-eruptive volatile contents, with more effusive eruptions resulting from magma that has degassed extensively prior to eruption and consequently has lower volatile contents (e.g., Roggensack et al., 1997). Explosive eruptions require magma fragmentation to occur during magma ascent, and this is dependent on a number of additional factors. One important mechanism for fragmentation is the formation of interconnected vesicles once the gas volume fraction in the ascending magma exceeds a critical amount, typically regarded as 75% (Sparks, 1978). More broadly, fragmentation is a consequence of increasing strain rate during magma ascent, and the gas volume at fragmentation can vary from ~62-95% depending on the magma viscosity (Papale, 1999).

A high-viscosity magma will fragment at a lower gas volume fraction, and thus be more prone to explosive eruptions, than a low-viscosity magma.

Degassing style also plays a key role. With closed-system degassing (where exsolved volatiles remain entrained in the magma rather than escaping through the conduit or conduit walls), volatile escape prior to eruption is minimal, leading to an increase in vesicularity (Villemant and Boudon, 1998) and consequently a greater potential for explosive eruption. In contrast, open-system behavior (where volatiles are lost from the system through permeable conduit walls or upwards along conduit margins), permits the loss of volatiles prior to eruption, resulting in a relatively gas-poor magma that may then erupt effusively (Eichelberger et al., 1986; Melnik and Sparks, 1999; Scandone et al., 2007). Open-system degassing can result from a number of factors: volatile loss through porous (permeable) flow of gas (Eichelberger et al., 1986; Jaupart and Allegre, 1991), non-explosive fragmentation along conduit walls (Gonnermann and Manga, 2003), and/or volatile loss to hydrothermal fluids (Villemant and Boudon, 1998). In many eruption sequences explosivity decreases during the course of a single volcanic eruption, and this has been attributed to decreasing overpressure and/or decreasing ascent rate and a subsequent transition from closed- to open-system degassing (Jaupart and Allegre, 1991; Scandone et al., 2007). The transition from open-system to closed-system degassing behavior has also been invoked as an explanation for eruptions that have become more explosive with time (Melnik and Sparks, 1999; Villemant and Boudon, 1998).

Understanding the dynamics of magma ascent also allows characterization of the key factors that control the tendency for a particular volcano to exhibit non- (or low-)

explosive behavior. In addition to the important role played by volatiles and degassing style, magma viscosity will strongly influence the likelihood of fragmentation by affecting magma strength, ascent rate, and ability to degas (Dingwell, 1996; Gonnermann and Manga, 2003; Jaupart and Allegre, 1991; Papale, 1999). Lower melt viscosity allows rapid bubble formation and coalescence, contributing to open-system degassing through permeable flow (Ruprecht and Bachmann, 2010 and references therein). Additionally, higher viscosity magmas will suffer strain-induced fragmentation at a lower gas volume fraction than magma with lower viscosity (Papale, 1999). As viscosity is a function of magma composition, temperature, and crystallinity, important feedbacks between these factors will also influence eruptive style. One means by which magma viscosity can decrease is through an increase in temperature, as recently proposed for Volcán Quizapu by Ruprecht and Bachmann (2010). In the 1846-1847 eruption of Quizapu, recharge by a hotter mafic magma led to an overall increase in magmatic temperature after recharge. Ruprecht and Bachmann (2010) argue that the corresponding decrease in viscosity resulted in a less explosive eruption than that which occurred at Quizapu in 1932, when pre-eruptive magma temperatures were lower. Ruprecht and Bachmann (2010) suggest that this viscosity decrease reduced the depth at which fragmentation occurred, enabling more time for degassing to occur, or possibly preventing fragmentation entirely.

In this paper we present data for volatile abundances in melt inclusions hosted in a variety of phenocryst phases from Mount Hood and investigate the causes of long-term low-explosivity eruptive behavior at this volcano and at other similar arc volcanoes, such as Soufriére Hills Volcano (Montserrat) and Augustine Volcano (Alaska). These data, when combined with phenocryst compositions and other published studies, suggest that

the temperature-dependent viscosity of ascending magma is a key parameter during magma ascent and that magma mixing immediately prior to eruption plays a decisive role in the resulting eruptive style.

REGIONAL SETTING

Mount Hood rises to 3426 meters and is the northernmost Cascade volcano in the state of Oregon, located approximately 75 km east of Portland, Oregon. Eruptive products at Mount Hood have remained remarkably consistent both in composition and eruptive style through time. Andesitic (54-63 wt% SiO_2) domes, lava flows, and related debris make up the bulk of the current edifice, most of which has been constructed over the last ~500,000 years (Scott et al., 1997a). Eruptions of minor amounts of low-SiO_2 dacite (63-66 wt% SiO_2) from Mount Hood are evident in the record of the past 15,000 years, but are rarely preserved in the older record. Overall, approximately 95% of the lavas erupted at Mount Hood have between 58-66 wt% SiO_2. Tephra and other records also contain no evidence for major explosive eruptions over this eruptive history (Scott et al., 1997b). In contrast, many other Cascade volcanoes, including nearby Mount Jefferson and Mount St. Helens (located 80 km and 100 km from Mount Hood, respectively) have erupted more compositionally diverse lavas. Mount Jefferson has prodduced material from 50-71 wt% SiO_2, and Mount St. Helens has erupted lavas from 48-70 wt% SiO_2 (Blundy and Cashman, 2008; Clynne et al., 2008; Conrey et al., 2001; Hildreth, 2007). Mount Jefferson and Mount St. Helens, as well as many other major Cascade volcanoes, have also experienced large explosive eruptions in the past 50,000-100,000 years (Hildreth, 2007). Kent et al. (2010) suggest that the restricted compositional range at

Mount Hood is the result of a "recharge filter," where eruption only occurs following mixing between mafic and silicic magmas, limiting eruptible products to mixed andesitic-dacitic compositions. Further details regarding the magmatic components and processes involved in creating compositionally homogeneous andesite-dacite at Mount Hood are discussed elsewhere in more detail (Cribb and Barton, 1997; Darr, 2006; Kent et al., 2010; Woods, 2004).

In this study we have focused on material from the three most recent eruptive periods at Mount Hood (Old Maid ~200 years ago, Timberline ~1500 years ago, and Polallie 13,000-20,000 years ago). These and some earlier periods were all characterized by growth of lava dome(s) followed by subsequent dome collapse, producing block and ash flows (Scott et al., 1997a). Pumiceous deposits are rare and of small volume. Crater Rock, located in the south-facing summit crater, is the remains of an Old Maid- and Timberline-age lava dome, and deposits from these two eruptive periods are concentrated on the south side of the edifice. In contrast, deposits from the Polallie-age eruptive sequence are present on nearly all sides of the volcano, because lava domes of this age form much of summit. Two well-exposed domes are located above Eliot Glacier and at Steel Cliff near the summit (Scott et al., 1997a).

SAMPLES AND METHODS

Pumice samples from the Old Maid eruptive period and prismatically jointed blocks (PJBs) from the Old Maid and Timberline eruptive periods were collected in the summer of 2008. Additional pumice samples from the Timberline and Polallie eruptive periods were provided from the USGS Cascades Volcano Observatory collection.

Volatile contents were measured in melt inclusions using a combination of techniques. Concentrations of H_2O and CO_2 in one suite of inclusions were measured in doubly exposed melt inclusions using a Thermo Nicolet 670 Fourier Transform Infrared (FTIR) Spectrometer interfaced with a Continuum IR microscope at the University of Oregon. Total H_2O was determined using the band at 3570 cm^{-1}; this was compared to the sum obtained by adding the molecular H_2O concentration (1630 cm^{-1}) to the OH concentration (4500 cm^{-1}) for analyses in which all three peaks were resolvable. Reproducibility assessed from replicate measurements was within ~5% relative for H_2O. CO_2 concentrations were determined using the band at 2350 cm^{-1} and typical detection limits were ~25-50 μg/g, however CO_2 was not detected in any of the melt inclusions analyzed by FTIR.

Many melt inclusions were too small to be doubly-exposed and polished for FTIR analysis (inclusion diameter <60-80 μm), so a second suite of melt inclusions was analyzed for H_2O, CO_2, S, Cl, and F using the Cameca IMS 1280 ion microprobe at the Northeast National Ion Microprobe Facility at Woods Hole Oceanographic Institution. General analysis techniques followed those in Hauri et al. (2002), using a Cs^+ beam rastered over 20 μm. Analyzed species were ^{12}C, $^{16}O^1H$, ^{19}F, ^{30}Si, ^{32}S, and ^{35}Cl. Calibration curves were fit to five rhyolitic glasses (Mangan and Sisson, 2000) for H_2O and CO_2 and seven in-house basaltic glasses for S, Cl, and F. The root mean squared error (RMSE) of the calibration lines was 0.2 wt% for H_2O and 30-90 μg/g for CO_2, S, Cl, and F. The RMSE for CO_2 represents an error of approximately 20% at the concentrations of the calibration standards. A lack of suitable standards with >540 μg/g CO_2 required us to extrapolate the calibration line to the highest concentrations observed

in samples from Mount Hood (~2400 μg/g), therefore CO_2 concentrations beyond ~1000 μg/g are presented as information values only. Melt inclusions were visually inspected in reflected light and backscattered electron (BSE) images to eliminate any analyses near a crack, where CO_2 contamination is most likely to occur. In addition, analyses where ^{12}C count rates changed significantly through the analysis were disregarded.

Major and minor elements (SiO_2, TiO_2, Al_2O_3, CaO, MgO, MnO, FeO^T, Na_2O, K_2O) and select volatiles (S, Cl, F) in melt inclusions and phenocrysts (plagioclase, orthopyroxene, clinopyroxene, amphibole, and oxides) were determined by Electron Microprobe Analysis (EMPA) using a Cameca SX-100 at Oregon State University. Well-characterized standard reference materials and procedures were used for the different phases analyzed. Analytical uncertainty (as assessed by replicate analyses) was typically within 2% for SiO_2, Al_2O_3, CaO, K_2O, and Cl and within 5% for TiO_2, MgO, FeO^T, and Na_2O. Concentrations of MnO, S, and F were below detection limits (0.8 wt%, 100 μg/g, and 700 μg/g, respectively) in most minerals and glasses.

RESULTS

Melt inclusion compositions

Melt inclusions analyzed for this study contain 69-77 wt% SiO_2 and are dacitic to rhyolitic in composition (Fig. 2.1, Table 2.2), typical for melt inclusions from intermediate composition volcanic systems (e.g., Reubi and Blundy, 2009). Clinopyroxene-hosted inclusions have SiO_2 contents restricted to the lower end of total range (69-71 wt%). As commonly observed in melt inclusions from other arc volcanoes,

there are no systematic differences in the major element compositions of plagioclase-, orthopyroxene-, and amphibole-hosted inclusions that would indicate significant compositional modification by post-entrapment crystallization (PEC) in these different host minerals (Reubi and Blundy, 2009). Additionally, melt inclusions examined in this study were collected from pumice produced in block-and-ash flows or from small fallout deposits and were therefore rapidly quenched to glass during eruption, minimizing any effects of PEC during eruption (Kress and Ghiorso, 2004; Luhr, 2001). On this basis we have made no extra corrections for PEC.

Melt inclusion compositions differ only slightly among the three most recent eruptive periods. Melt inclusions from the Polallie eruptive period have slightly lower SiO_2 and K_2O and higher CaO, Al_2O_3, and Na_2O contents than inclusions of Timberline- and Old Maid-age, but major element ranges exhibit extensive overlap (Figs. 2.1, 2.2).

Volatile analyses by SIMS and FTIR indicate that Mount Hood melt inclusions contain 0.8-5.4 wt% H_2O and 0-2400 μg/g CO_2 (Fig. 2.3). Volatile contents are consistent across all three eruptive periods considered in this study (Fig. 2.3). The highest measured H_2O concentrations in inclusions from Mount Hood are equivalent to P_{H2O} of ~1.8 kbar (Newman and Lowenstern, 2002). CO_2 measurements up to ~ 2400 μg/g suggest that saturation pressures could be as high as 5 kbar (Newman and Lowenstern, 2002; Papale et al., 2006).

Measurements of H_2O by FTIR range from 0.8-3.6 wt%, whereas SIMS measurements range from 0.9-5.4 wt%. The higher values measured by SIMS likely reflect the larger number of inclusions measured by SIMS: only 12 inclusions were analyzed by FTIR (compared to 28 analyzed by SIMS), and only larger (>60 μm)

plagioclase-hosted inclusions were analyzed by FTIR. Analyses by SIMS do not require the inclusion to be doubly-polished and can therefore be performed on a wider range of inclusion sizes (down to ~30 μm). The SIMS-analyzed inclusions were hosted in plagioclase, amphibole, and pyroxenes. Thus we conclude that the difference between the two techniques does not represent a bias in measurements, and we note that previous studies have demonstrated good agreement between SIMS and FTIR measurements of H_2O in glasses (e.g., Hauri et al., 2002).

The majority of melt inclusions analyzed in this study contain 0.2-0.3 wt% Cl (Fig. 2.4), consistent with many other intermediate to silicic volcanic systems (Webster et al., 1999), although some inclusions contain up to 0.36 wt% Cl. Concentrations of S are <100 μg/g (the detection limit for analyses by EMPA) in approximately 75% of the melt inclusions analyzed for this study. The remaining 25% contain up to nearly 300 μg/g, and in general S concentrations are slightly higher in melt inclusions from the Polallie eruptive period. Concentrations of F were below EMPA detection limits (~700 μg/g) in nearly all melt inclusions, and SIMS analyses indicate typical F contents of ~500 μg/g. As a result of their low concentrations, S and F are omitted from further discussion in this paper.

Plagioclase-melt hygrometry

We have also evaluated the H_2O contents of melt inclusions from this study using plagioclase-melt hygrometers (Table 2.3). Cribb and Barton (1997) used the plagioclase-melt hygrometer of Housh and Luhr (1991) to estimate 3.9-6.1 wt% H_2O in Mount Hood magmas based on albite and anorthite exchange. We have applied the hygrometer

calibrations of Housh and Luhr (1991), Putirka (2005) and Lange et al. (2009) to our melt inclusion data. A summary of results is shown in Fig. 2.5. Plagioclase compositions used in the hygrometer calculations were measured in duplicate or triplicate near the margin of each melt inclusion. Where necessary, an equilibrium temperature of 900˚C was used in hygrometer calculations.

Hygrometers can provide an estimate of H_2O concentrations in silicate melts, with the limitations that they rely on accurate knowledge of equilibrium plagioclase compositions, pre-eruptive temperatures, and an appropriate calibration. All of the tested hygrometers yielded H_2O concentrations that overlap broadly with H_2O contents measured by SIMS and FTIR (Fig. 2.5). The hygrometer of Housh and Luhr (1991) returns two separate H_2O concentrations (one for albite exchange and one for anorthite exchange) that may differ by >2.5 wt%. The plagioclase-melt hygrometer (Model H) of Putirka (2005) gives a more limited range of H_2O contents but also underestimates H_2O concentrations for over half of the plagioclase-hosted inclusions that were measured for volatiles in this study. The plagioclase-melt hygrometer described in Lange et al. (2009) overestimates H_2O contents by up to 3.5 wt%, but only underestimates H_2O for two inclusions included in this study. One possible explanation for this is that the consistently high values returned by the hygrometer are indicative of post-entrapment loss of H_2O, either by vapor bubble formation (many of the inclusions contain vapor bubbles), inclusion rupture, or diffusive loss. In this interpretation, plagioclase-melt compositions were previously in equilibrium with higher H_2O contents (which are recorded by the hygrometer), whereas the measured H_2O concentrations may have been subject to pre- and/or syn-eruptive volatile loss. From this we conclude that the Lange et al. (2009)

hygrometer provides the most realistic estimate of pre-eruptive volatile contents, because it is more likely that the inclusions have lost H_2O (through rupture, diffusive loss, or rapid decompression prior to trapping) than gained H_2O (as required for a substantial number of inclusions by the Putirka (2005) hygrometer).

In addition, two melt inclusions had higher measured H_2O concentrations than predicted by the Lange et al. (2009) hygrometer and both of these inclusions appear to be compromised: one of the inclusions is devitrified and the other inclusion is cracked. Both inclusions also have extremely high CO_2 concentrations consistent with carbon contamination during analysis near a crack. Hygrometer calculations therefore also appear to be a potentially useful way of identifying compromised inclusions. These two inclusions are omitted from all figures and further discussion. If these two inclusions are omitted, the highest P_{H2O} recorded by a plagioclase-hosted melt inclusion is 1.4 kbar using the highest measured H_2O concentration and 1.7 kbar using the highest calculated H_2O concentration from the Lange et al. (2009) hygrometer. Interestingly, none of the calculated H_2O values are less than 3 wt%, suggesting entrapment pressures (P_{H2O}) of at least 0.7 kbar.

A reliable hygrometer also provides an excellent way to estimate H_2O concentrations when direct measurements are unavailable. Applying the Lange et al. (2009) hygrometer to the 62 plagioclase-hosted melt inclusions with unmeasured H_2O expands our dataset considerably, and allows more complete comparisons between H_2O contents and other volatile species (e.g., Fig. 2.4).

As noted in Results, melt inclusion compositions were not corrected for post-entrapment crystallization (PEC) because we see no evidence for substantial PEC in

major element concentrations. Although PEC can be difficult to account for in plagioclase-hosted melt inclusions (e.g., Kent, 2008), model corrections for 10% PEC by incremental addition of the host plagioclase lowers the concentration of H_2O returned by the Lange et al. (2009) and Putirka (2005) hygrometers by 0.5-0.6 wt%, which is minor relative to the abundances and variations that we see within the sample suite.

DISCUSSION

Behavior of the magmatic system at Mount Hood

Previous studies provide insight into the behavior of the magmatic system at Mount Hood and the relation between eruption initiation and magma evolution, and provide context for interpreting the volatile contents of melt inclusions. Over the 500,000 year lifetime of the current edifice (and particularly during the most recent three eruptive periods) Mount Hood has erupted compositionally similar andesite-dacite lavas (Kent et al., 2010). In addition, the common presence of mafic enclaves, together with evidence from whole rock and mineral compositions and mineral textures and zoning patterns, suggest that erupted magmas are produced by mixing between separate silicic and mafic magmas shortly before eruption (Darr, 2006; Kent et al., 2010; Woods, 2004). Kent et al. (2010) proposed a model whereby Mount Hood magmas are produced by mafic recharge and mixing between a rhyolitic (70.9 ± 2.1 wt% SiO_2) magma stored within the shallow crust and a more mafic magma (50.7 ± 4.3 wt% SiO_2) derived ultimately from the underlying mantle. On the basis of this and other evidence, Kent et al. (2010) suggested that mafic recharge is the only mechanism by which the magmatic system beneath Mount Hood can consistently initiate an eruption. As recharge is

inextricably linked with mixing and formation of mixed andesitic-dacitic compositions, this "recharge filtering" mechanism results in continued eruption of compositionally restricted andesitic-dacitic magmas.

Origin of melt inclusions in Mount Hood magmas

Although bulk rock compositions at Mount Hood represent a mixed magma, melt inclusions examined in this study are exclusively dacite-rhyolite in composition (Fig. 2.1). Globally, melt inclusion compositions are bimodal but those in arc-related intermediate rocks are predominately high SiO_2 (Reubi and Blundy, 2009), as we observe at Mount Hood. The composition of these melt inclusions also overlaps with the estimated silicic endmember at Mount Hood (70.9 ± 2.1 wt% SiO_2; Fig. 2.1) (Kent et al., 2010), although the inclusion compositions also extend to lower total alkali contents. We suggest that these high-SiO_2 melt inclusions trap melt that originated with the silicic parental melt. To date we have observed no melt inclusions with lower SiO_2 corresponding to the mafic mixing endmember. Again, this is consistent with the near-absence of low-SiO_2 melt inclusions in arc rocks where the whole rock composition contains >60 wt% SiO_2 (Reubi and Blundy, 2009). A plausible explanation for the lack of low-SiO_2 melt inclusions (even in phenocrysts that clearly originated in the mafic magma, such as pargasitic amphibole and high-An plagioclase) is that melt inclusion formation requires significant undercooling (e.g., Kent, 2008; Kohut and Nielsen, 2004). Phenocrysts in the mafic magma may not experience sufficient undercooling until they come into contact with the cooler high-SiO_2 magma, at which point magma mixing has begun and trapped inclusions will be typical of those trapped in intermediate systems

(i.e., high-SiO_2). If mixing does not occur (i.e., in mafic, rather than intermediate, systems), significant undercooling will not occur until the mafic magma ascends to shallow depths. This is consistent with the relatively low (<2 kbar) vapor saturation pressures typically observed in mafic melt inclusions (e.g., Ruscitto et al., 2010). In addition, the cooler silicic magma involved in mixing probably exists as a crystal-rich mush prior to recharge and therefore contributes substantially more crystals to the mixed andesite-dacite, further reducing the probability of finding any mafic melt inclusions that may have formed.

Our interpretations of the volatile budget at Mount Hood therefore rely on the volatile contents derived from the silicic endmember, and it is not possible to determine the volatile content of the mafic endmember, or its contribution to the overall volatile budget at Mount Hood, from the available data. However, comparison with other studies of mafic Cascade magmas (e.g., Ruscitto et al., 2010) would suggest that mafic magmas could have volatile contents as high as 3-4 wt%. The presence of pargasitic amphibole derived from mafic magmas (see 5.4.1) also suggests that H_2O contents in this magma are likely to be ~4-6 wt% (Pichavant et al., 2002; Sato et al., 1999). The lack of a mafic signal in melt inclusions is a likely explanation for the lack of measurable S (>100 µg/g) in melt inclusions from this study—as with Soufrière Hills Volcano (Humphreys et al., 2009b), the S budget of Mount Hood is probably controlled by the mafic magma that recharges the system shortly before eruption.

Volatile contents of Mount Hood magmas

H_2O and CO_2

Melt inclusions from the Mount Hood magmas considered in this study contain 0.8-5.4 wt% H_2O. In general the inclusions with the highest H_2O have among the lowest SiO_2, suggesting concurrent degassing and crystallization during magma ascent (Fig. 2.6). A subset of inclusions have anomalously low H_2O contents at a given SiO_2; Blundy and Cashman (2008) describe melt inclusions with these characteristics as "ruptured inclusions" that have lost some of their H_2O during syn-eruptive rupture, at a rate faster than the SiO_2 content of the melt inclusion could readjust. All of the melt inclusions that fall on the "ruptured inclusion" trend (with one exception) contain <500 μg/g CO_2, also consistent with volatile loss through late-stage rupture of the melt inclusion at shallow pressures, where CO_2 is low (Newman and Lowenstern, 2002; Papale et al., 2006). Volatile loss by diffusion would have a similar effect on measured concentrations of H_2O in these inclusions (see Results). Plagioclase-hosted melt inclusions that fall the furthest off the broad H_2O-SiO_2 trend have H_2O measured concentrations at least 1 wt% lower than predicted by the hygrometer of (Lange et al., 2009), consistent with H_2O loss after entrapment. Concentrations of H_2O and CO_2 within our range of analytical calibration (see Results) suggest that saturation pressures for melt inclusions in this study are up to 3.3 kbar, and higher CO_2 values indicate that saturation pressures could be as high as ~5 kbar (Newman and Lowenstern, 2002; Papale et al., 2006). Much of the variation in H_2O and CO_2 contents appear to broadly fall along closed- or open-system degassing paths, starting from parental melt with 4-6 wt% H_2O, although some inclusions also have high CO_2 (relative to their H_2O content) inconsistent with either style of degassing (Fig.

2.3). The high X_{CO2} in these inclusions may represent mixing between variably degassed magmas or fluxing by CO_2-rich vapor, as suggested for melt inclusions from the 1980 eruption of Mount St. Helens (Blundy et al., 2010), eruptions of Mount Etna (Collins et al., 2009), and eruptions from mafic cinder cones in central Mexico (Johnson et al., 2010; Johnson et al., 2008).

Chlorine

Most melt inclusions from Mount Hood have Cl concentrations comparable to other arc volcanoes (Webster et al., 1999), but individual inclusions contain up to 0.36 wt% Cl (Fig. 2.4). These concentrations are higher than those measured in melt inclusions from other Cascade volcanoes such as Mount St. Helens (Blundy et al., 2008) and Mount Mazama (Bacon et al., 1992), but they extend to the higher values observed in other arc volcanoes such as Augustine (Roman et al., 2006) and Soufrière Hills (Humphreys et al., 2009b).

Humphreys et al. (2009b) suggested that Cl concentrations in the melt will decrease during closed-system degassing because Cl will partition into a coexisting vapor phase, which will overwhelm the Cl increase that occurs due to incompatibility during crystallization. To add further complexity, Cl solubility in the melt decreases as SiO_2 increases during crystallization and as pressure decreases during ascent (Webster, 1997).

At Mount Hood, the relatively limited range of Cl concentrations in most inclusions (between 0.2-0.3 wt%) over a range of H_2O concentrations suggests the presence of a Cl-buffering liquid ± vapor phase during coupled degassing and crystallization (Webster, 1997). At temperatures and pressures consistent with crustal

magmas, a miscibility gap in the NaCl-H_2O system produces a coexisting vapor and brine (Lowenstern, 2000). This miscibility gap is enhanced by the presence of CO_2, which concentrates in the vapor phase (Lowenstern, 2000). These coexisting volatile phases will buffer the Cl contents of the melt at a value approximating the solubility limit for Cl in that melt. In felsic liquids at 2 kbar, this is typically 0.26-0.30 wt% (Métrich and Rutherford, 1992; Webster, 1997 and references therein), consistent with the upper range of Cl concentrations in melt inclusions from Mount Hood, which, with the exception of a smaller number of high Cl inclusions, cluster along a path broadly similar to the Cl solubility line (Fig. 2.4). From this we infer that the melts trapped in inclusions were likely saturated, or nearly saturated, with a Cl-rich liquid ± vapor. Inclusions with higher Cl (i.e., ≥0.28 wt% Cl) are mostly from the Timberline eruptive period and are otherwise geochemically indistinguishable from other melt inclusions of the same eruptive period. These melt inclusions mostly occur on the lower end of the SiO_2 range, consistent with increased Cl solubility at lower SiO_2 concentrations in the melt (Webster, 1997).

Causes of low explosivity at Mount Hood

Explosive volcanic eruptions are the result of magma fragmentation during magma ascent (e.g., Dingwell, 1996; Papale, 1999). Highly explosive eruptions occur when magmas reach a critical fragmentation limit during ascent, whereas magmas erupted non-explosively or with low explosivity do not reach that limit prior to reaching the surface, either due to low concentrations of volatile elements (the driving force for expansion) or other physical properties that inhibit fragmentation (e.g., Dingwell, 1996; Papale, 1999; Scandone et al., 2007). Low volatile contents may be intrinsic to the

magma, or may have developed as a result of degassing prior to, or during, ascent (Eichelberger et al., 1986). Here we examine the combined effects of intrinsic volatile concentration, volatile loss by degassing, and changes to the physical properties of the magma as we consider the potential causes for low explosivity at Mount Hood and other recharge-driven volcanoes.

Intrinsic volatile concentration

Comparison of the measured concentrations of H_2O and other volatiles in melt inclusions from Mount Hood indicate that the pre-eruptive volatile concentrations in the silicic endmember magma were as high as those observed in other, more explosive, volcanoes from the Cascade arc and from other subduction zones (Figs. 2.3, 2.7). Although we cannot directly measure the volatile abundances in the mafic component, the presence of pargasitic amphibole in the mafic component prior to mixing (see above) suggests that H_2O contents in this magma would be ~4-6 wt% (Pichavant et al., 2002; Sato et al., 1999). The comparison shown in Fig. 2.7 illustrates that H_2O (the primary volatile for driving explosive expansion and fragmentation) contents are similar to those observed in both the plinian and dome eruptions from Mount St Helens (1980), Soufrière Hills (2007), Mount Mazama (~7.7 ka), and Augustine Volcano (1986) (Bacon et al., 1992; Blundy and Cashman, 2008; Humphreys et al., 2009b; Roman et al., 2006; Wallace, 2005). Although volatile contents from these various volcanoes are highly variable, it is clear that erupted Mount Hood magmas have similar volatile abundances, with H_2O contents ranging up to >5 wt%, to other systems where magmas have erupted

explosively. From this we infer that the cause of low explosivity at Mount Hood is unlikely to relate solely to intrinsically low volatile contents.

Volatile loss by degassing prior to eruption

The extent of pre-eruptive degassing is difficult to quantify for ancient eruptions (such as the three eruptive periods considered in this study), although the fumarole field located in the crater of Mount Hood confirms the presence of modern day degassing. Near-mantle values for $^{3}He/^{4}He$ (7.48-7.59 R_C/R_A) and high $^{40}Ar/^{36}Ar$ (341-470) suggest active degassing from relatively shallow (<5 km) magma (Symonds et al., 2003), presumably related to the Old Maid eruptive phase that ended ~220 years ago. Heat flow calculations indicate that in addition to the continued cooling of the Old Maid dome complex, there is also a deep-seated heat source beneath the volcano that most likely represents unerupted magma (Friedman and Williams, 1982).

Estimates of volatile loss by degassing are possible from plagioclase-melt hygrometry results (Fig. 2.5), which can be a useful way to estimate the H_2O concentrations last recorded by plagioclase-melt equilibrium and thus to assess the extent of degassing prior to eruption. Inclusions that record H_2O concentrations close to the estimate from the hygrometer are likely to be less degassed than inclusions for which the hygrometer value is significantly higher than the measured H_2O concentration (see Results). As degassing occurs, volatiles can be lost rapidly from the melt but the plagioclase and melt compositions will not record this change immediately, so the calculated hygrometer H_2O values can be used to predict a minimum H_2O concentration prior to degassing. The highest H_2O concentration in Mount Hood melt inclusions

calculated by hygrometer is 6 wt% (Lange et al., 2009), and the differences between the hygrometer and measured H_2O values range from 0 to 3.5 wt% (Fig. 2.5).

It is also possible to reconstruct where in the system degassing occurs by combining volatile measurements with estimates from hygrometry. A rhyolitic magma containing 6 wt% H_2O (but no CO_2) at 900°C will become vapor saturated at ~2 kbar (Newman and Lowenstern, 2002), or a depth of ~6 km. When measured values of CO_2 are included to calculate P_{Total}, we determine entrapment pressures >3 kbar (Newman and Lowenstern, 2002; Papale et al., 2006). Barring the effects of supersaturation, these observations suggest that melt inclusion entrapment must have started at a depth of at least ~9 km, giving a minimum depth at which crystallization and volatile exsolution must have begun. Conversely, the lowest H_2O in a melt inclusion that does not fall on the "ruptured inclusion" trend described above is 1.4 wt%, coupled with 372 μg/g CO_2. This gives a saturation pressure of 0.8 kbar at 900°C (Newman and Lowenstern, 2002), corresponding to depth slightly greater than 2 km. Presumably, then, all of the non-compromised melt inclusions examined in this study were trapped at a depth of at least 2 km, and any degassing (either closed system or open system) that can be inferred from these melt inclusions must occur at depths between ~2 and 9 km. Degassing certainly would have continued as the magma ascended above 2 km, but melt that records those extremely degassed compositions was not trapped by any of melt inclusions examined in this study.

For degassing to prevent fragmentation during ascent, volatiles must be lost quickly enough to prevent bubble nucleation and expansion, a necessary criteria for fragmentation whether it occurs through vesicle interconnection (Eichelberger et al.,

1986; Villemant and Boudon, 1998) or strain-induced brittle magma failure (Papale, 1999). Additionally, gas loss and ascent rate form a feedback loop and magmas that have degassed extensively will ascend more slowly, which leads to further gas loss because the magma spends more time at shallow depths (Jaupart and Allegre, 1991).

Previous studies suggest that rapid open-system behavior typically occurs in silicic magmas at depths less than ~1 km (Eichelberger et al., 1986; Villemant and Boudon, 1998), and is probably most effective where shear-induced fragmentation can occur along conduit walls (Gonnermann and Manga, 2003). Experimental studies by Okumura et al. (2006), however, demonstrate that shear-induced vesicle coalescence can occur at vesicularities as low as 20-30%, allowing open-system loss of volatiles through interconnected vesicles at much greater depths. Assuming magmas started with approximately 6 wt% H_2O at 900°C the vesicularity would reach 30% at approximately 3 km depth (Okumura et al., 2009). This may represent an approximate depth at which open-system degassing begins to exert a significant control on the volatile budget of the ascending magma.

The variable H_2O and CO_2 concentrations of melt inclusions from Mount Hood indicate that variable extents of degassing have occurred over a range of crustal depths. Again, however, this observation appears unlikely to explain low explosivity, as similar composition magmas that have erupted explosively elsewhere also commonly record evidence of extensive pre-eruptive degassing. Although some studies show that extrusive and explosively erupted materials from the same volcanic system may have systematic differences in pre-eruptive volatile abundances (e.g., Roggensack et al., 1997), pre-eruptive volatile abundances at Mount Hood overlap with those from a number of

explosive eruptions in the Cascadia subduction zone and elsewhere (Fig. 2.3). For example, melt inclusions from Mount Hood have H_2O contents that overlap with those measured in melt inclusions from both the dome and plinian phases (1980-1986, 2004-2006) from Mount St. Helens (Blundy et al., 2008), the climactic and pre-climactic eruptions of Mount Mazama at ~7.7 ka (Mandeville et al., 2009), and volcanoes of the Trans-Mexican Volcanic Belt (Wallace, 2005 and references therein). Melt inclusions from Mount Mazama also record extensive degassing, confirmed with analyses of δD (Mandeville et al., 2009). Concentrations of H_2O in melt inclusions from the climatic and preclimactic eruptions of Mount Mazama are variable and range from 3.1-6.9 wt% H_2O with concentrations of CO_2 that are below FTIR detection limits (Mandeville et al., 2009). Melt inclusions from Mount Hood have H_2O abundances that broadly overlap with those measured in the Mazama inclusions, although inclusions from Hood extend to lower H_2O concentrations (0.8-5.4 wt%) and higher CO_2 (Fig. 2.3). The maximum recorded saturation pressures at Mount Hood (>3 kbar) are greater than the maximum saturation pressures recorded at Mount Mazama, suggesting that they are less degassed. The similarities between the volatile contents of melt inclusions from Mount Hood and melt inclusions from the highly explosive Mount Mazama eruption (as well as other explosive eruptions), together with the extensive evidence for magma degassing preserved by both melt inclusion suites, suggest that the extent of degassing prior to eruption at Mount Hood is insufficient to be the sole explanation for the lack of explosive eruptions.

Changes to the physical properties of the magma

Recent work by Ruprecht and Bachmann (2010) has emphasized the control that temperature has on magma viscosity, and specifically suggests that magmas that have been heated by mafic recharge immediately prior to eruption may be less likely to erupt explosively. Ruprecht and Bachmann (2010) studied high- and low-explosivity eruptions at a single volcano (Volcán Quizapu), and argued that the potential for explosive eruptions can be reduced by mafic recharge and efficient mixing prior to eruption, which increases the magma temperature of the more silicic magma into which mafic recharge occurs. This produces a decrease in viscosity that delays fragmentation and allows more extensive degassing during ascent, and thus decreases the potential for explosive eruptions. Although Ruprecht and Bachmann (2010) used this line of reasoning to understand high- and low-explosivity eruptions from a single volcano, this model is also applicable to understanding the long-term behavior of Mount Hood, as previous studies have shown that mafic recharge and magma mixing is implicated in almost all eruptions (Kent et al., 2010). The presence of intermediate composition lavas at Mount Hood and the apparent lack of erupted material from the unmixed mafic and silicic magmas that mix to form erupted andesites and dacites led Kent et al. (2010) to argue that eruptions at Mount Hood are initiated by recharge of mafic magmas into shallow silicic crustal magma chambers. Mixing between the mafic recharging magma and a more silicic resident magma creates a mixed magma with intermediate composition, density, and viscosity. In addition to the impetus provided by volatile exchange and other processes during recharge and mixing (e.g., Eichelberger, 1980; Murphy et al., 1998), the intermediate density and viscosity of the mixed magma promotes magma mobility and

eruption. We suggest that the decrease in magma viscosity following mixing also provides a viable mechanism to explain the long-term low explosivity of Mount Hood.

To test this model we use mineral thermometry to estimate temperatures in erupted magmas at Mount Hood. Previous studies of the plagioclase compositions and textures in lavas from Mount Hood have found evidence for multiple plagioclase populations related to mixing (Darr, 2006; Kent et al., 2010; Woods, 2004), and we likewise find similar evidence for multiple amphibole populations (Fig. 2.8). Multiple populations of amphibole have been observed in material erupted from other volcanoes where mafic recharge and magma mixing appear to play important roles in magma genesis, including Mount Pinatubo (Prouteau et al., 1999), Mount Unzen (Sato et al., 1999), and Soufrière Hills (Humphreys et al., 2009b), indicating coexistence of amphiboles derived from a more mafic melt and those derived from a more silicic melt. At Mount Hood, amphiboles that formed from mafic and silicic magmas also show consistent major and trace element differences (see Chapter Three). In particular, amphiboles that crystallized from the mafic and silicic melts are readily distinguishable in terms of their SiO_2 contents (mafic-derived amphiboles contain <45 wt% SiO_2 whereas silicic-derived amphiboles contain >45 wt% SiO_2), and we have used this to subdivide our amphiboles on Fig. 2.8. Following the nomenclature of Kent et al. (2010) for two populations of plagioclase (which are also derived from mafic and silicic sources) we refer to amphiboles from mafic magma as Group 1 and those from silicic magma as Group 2.

Equilibration temperatures for amphiboles were calculated using the amphibole geothermobarometer of Ridolfi et al. (2010) and the hornblende-plagioclase

geothermometer of Holland and Blundy (1994). We have also calculated equilibrium temperatures for magnetite-ilmentite pairs in groundmass using the Fe-Ti oxide thermometer of Ghiorso and Evans (2008). Results are summarized in Fig. 2.8. Two temperature groups are clearly apparent using the amphibole thermobarometer of Ridolfi et al. (2010) and, to a lesser extent, with the hornblende-plagioclase thermometer of Holland and Blundy (1994). Using the model of Ridolfi et al. (2010), we find that Group 1 amphiboles (pargasite, 946 ± 15°C, 1σ) were formed at temperatures approximately 100°C hotter than Group 2 amphiboles (magnesiohornblende, 843 ± 14°C, 1σ). As the phase stability of pargasite limits formation temperatures to approximately <1000°C (Ridolfi et al., 2010), temperatures indicated by Group 1 amphiboles represent a minimum for the mafic recharge magma. Hornblende-plagioclase thermometry indicates temperatures of approximately 950 ± 12˚C for Group 1-Population 1 pairs and 902 ± 16˚C for Group 2-Population 2 pairs (Holland and Blundy, 1994). Pre-eruptive temperatures were also calculated using the two-oxide geothermometer of Ghiorso and Evans (2008) using touching oxide pairs that were tested for Mg-Mn equilibrium according to the criteria of Bacon and Hirschmann (1988). The total range of oxide temperatures is 888-1028°C (Table 2.4), slightly higher than that recorded by plagioclase-hornblende pairs and amphibole thermobarometry. Such a large range of temperatures suggests that the final magma temperatures were variable (not unexpected during magma mixing) and/or not all of the oxides reached thermal equilibrium with each other prior to eruption (Blundy and Cashman, 2008). Higher oxide temperatures relative to temperatures calculated from amphibole compositions is probably the result of the rapid re-equilibration of oxides to changing magmatic conditions (Putirka, 2008) and the

lack of amphibole stability at higher temperatures. In addition, because of the rapid equilibration timescales of oxide pairs (days), the slightly higher two-oxide temperatures are likely to better record the actual temperature following mafic recharge and decompression-induced crystallization during ascent. Temperatures recorded by Group 1 amphiboles probably represent minimum temperatures for the mafic magma prior to mixing (the magmatic temperature is only recorded once the magma has cooled enough for amphibole to become stable); those for Group 2 probably represent a maximum temperature for the silicic magma prior to reheating by mafic recharge (see Chapter Two).

Temperature is an important factor in controlling magma viscosity (e.g., Giordano et al., 2008), and as shown by Ruprecht and Bachmann (2010) temperature increases can have a significant effect on the ability of a magma to ascend without reaching the fragmentation limit. To determine if the observed temperature increase, and concomitant viscosity decrease, is sufficient to prevent an explosive eruption at Mount Hood, we simulated two different eruptions using the program CONFLOW, which assumes that fragmentation occurs when vesicularity reaches the critical threshold of 75% (Mastin and Ghiorso, 2002). In reality, fragmentation may occur within a range of gas fractions depending on other factors such as melt viscosity and strain rate, although a value of ~60% seems to represent a minimum gas volume fraction for fragmentation to occur (Papale, 1999).

For simplicity, parameters other than temperature (such as bulk composition, conduit dimensions, starting pressure, crystallinity, and H_2O content) were kept constant for all CONFLOW simulations reported here. In addition, for some parameters we have

no direct constraints (starting depth for magma ascent, conduit dimensions, etc.) and thus used reasonable values from the literature for similar volcanoes (Table 2.1 lists all simulation parameters). Magma temperature was 843°C for the pre-recharge simulation and 946°C for the post-recharge simulation (Table 2.1). We also performed an additional simulation for the higher temperature (975°C) suggested by oxide pairs.

A temperature increase of 100°C following mixing decreases the melt viscosity by a factor of ~5-10 (Giordano et al., 2008; Mastin and Ghiorso, 2002) (Fig. 2.9A), and results in a considerably higher fragmentation level for the ascending magma (Fig. 2.9B). Although the CONFLOW model is schematic, these results confirm that a ~100°C temperature increase is sufficient to significantly delay fragmentation, which allows more time for degassing to occur during ascent and increases the potential for effusive eruptions. Additionally, magma viscosity is inversely correlated with gas volume fraction at fragmentation, so magmas with lower viscosity will require higher gas volume fractions for fragmentation to occur. Reducing magma viscosity by a factor of ~10 results in an increase of the gas volume fraction at fragmentation by ~15% (Papale, 1999).

When we run the CONFLOW simulation with the higher temperature of 975˚C (indicated by Fe-Ti oxide thermometry), as expected we see an even greater decrease in viscosity and associated delay in fragmentation (Fig. 2.9B). Ruprecht and Bachmann (2010) report similar results for the temperature increase of ~130˚C they observed for magmas from Volcán Quizapu. It should be noted, however, that this is a largely qualitative simulation that requires the user to speculate on parameters such as magma starting depth and conduit dimensions. The CONFLOW model also does not address fragmentation that occurs without vesicle coalescence (Dingwell, 1996). Additionally,

fragmentation does not necessarily result in explosive eruptions and some workers have suggested that localized fragmentation can facilitate degassing, thus inhibiting explosive eruptions (Gonnermann and Manga, 2003). Despite these limitations, the CONFLOW simulations provide convincing qualitative evidence of significant changes in magma conditions (including eruptive style) as a result of a significant 100-150°C temperature increase following recharge and mixing, and the effect of this temperature increase would be to decrease the overall potential for explosive eruptions. The potential effects on eruptive style of decreasing magma viscosity are apparent even when considered outside the confines of the CONFLOW model.

We also note that a number of other factors could influence explosivity and we discuss these below. Magma ascent rates exert important controls over eruption dynamics (Jaupart and Allegre, 1991; Scandone et al., 2007), and higher ascent rates can contribute to brittle failure and fragmentation of the magma (Dingwell, 1996; Papale, 1999). Ascent rate is influenced by a number of factors including magma viscosity and magma density (Huppert and Woods, 2002; Jaupart and Allegre, 1991; Scandone et al., 2007), both of which are effected by mafic recharge. Small changes to magma overpressure have also been invoked as a possible explanation for transitions from explosive to effusive activity (Jaupart and Allegre, 1991), suggesting that low overpressures could result in low explosivity. Although this could be a contributing factor to the low explosivity of Mount Hood, we stress that the long-term record of low explosivity at Mount Hood (a volcano that appears to have never experienced a significant explosive eruption) makes it unlikely that such low overpressures would be consistent and sustained over the lifetime of the

edifice (~500,000 years), particularly given the critical control that small changes in overpressure are suggested to have by Jaupart and Allegre (1991).

Magma crystallinity is another factor that strongly influences viscosity (Marsh, 1981). Crystallization driven by decompression during ascent will act to increase viscosity, but could also potentially produce a temperature increase due to rapid release of latent heat. Blundy et al. (2006) report that the latent heat of crystallization in ascending hydrous silicic magmas at shallow pressures accounts for a temperature increase of 2-3˚C per 1% crystallization. The release of latent heat in magmas from Mount Hood is a potential cause of the relatively high two-oxide temperatures described above. However, despite this, calculations based on the Giordano (2008) viscosity model combined with the recommended constant of ϕ_m=0.6 from Marsh (1981) in the Roscoe-Einstein equation suggest that the effect of decompression crystallization on viscosity will be minor relative to the effect of temperature increase following recharge. Variation from 20% to 30% crystallinity will increase magma viscosity by a factor of ~2, comparable to the increase in viscosity during dehydration (magmatic water reduced from 4 wt% to 2 wt%). Both of these viscosity increases are smaller than the 5 to 10 fold *decrease* that we estimate for temperature increase alone. Moreover, the increased temperatures produced by any latent heat release will act to offset the viscosity effect of crystallization. As noted above, our estimate of the viscosity decrease based on oxide pair temperatures may already incorporate this effect as the rapid equilibration times of oxides allow them to record temperatures during magma ascent (Putirka, 2008). Finally, we also note that the growth of new microlites during ascent of Mount Hood magmas appears to be relatively minor and the high FeO, Sr, and MgO contents of plagioclase (the dominant

modal phase) with sizes < 0.5 mm suggests that they derive from the mafic magma involved in recharge, rather than growing during ascent from a mixed magma composition (Kent et al., 2010). This is consistent with studies of other andesitic volcanoes indicating that populations of microphenocrysts or microlites largely derive from mafic magmas (Clynne, 1999; Humphreys et al., 2009a; Martel et al., 2006; Salisbury et al., 2008).

Implications for eruptive behavior at andesitic volcanoes

From the above discussion we conclude that reduction in magma viscosity following recharge and mixing between mafic and silicic magma components is likely to have played a decisive role in preventing explosive eruptions at Mount Hood over the lifetime of the current edifice. This hypothesis also fits well with the observed processes of magma genesis at this volcano and provides a guide for a general model for the development of mixed andesitic-dacitic volcanic systems with low explosivity. As discussed above, Kent et al. (2010) argued that eruptions at Mount Hood are repeatedly initiated by mafic recharge, and that separate eruption of the mafic and silicic magmas that mix to produce erupted magmas is prohibited by viscosity, density, or other barriers to magma movement within the crust under the volcano.

In addition, if, as we have argued in above and has been suggested elsewhere (i.e., Ruprecht and Bachmann, 2010), that temperature increases and concomitant viscosity decrease following mafic recharge and mixing delays fragmentation during magma ascent and promotes non-explosive eruptions, then there is a clear link at Mount Hood between magma genesis, the homogeneity of erupted magma compositions, eruption

initiation, and eruptive style. Simply put, the dependence on mafic recharge to initiate eruptions at Mount Hood not only favors the eruption of mixed andesites-dacites, but also appears to favor non-explosive effusive eruptions. This does not necessarily mean that all eruptive events or volcanic systems dominated by magma mixing will be devoid of explosive eruptions. Magma mixing is well known as a trigger for explosive volcanic activity (e.g., Pallister et al., 1996; Sparks and Sigurdsson, 1977). There is also evidence to suggest that individual eruptive sequences involving mixed magmas can include transitions from extrusive to explosive such as Mount Pinatubo (Hammer et al., 1999), and that andesitic-dacitic volcanoes that appear mixing-driven can also have plinian or subplinian eruptions in addition to dome formation (e.g., Browne and Gardner, 2006; Martel et al., 1998; Sato et al., 1999). Nevertheless we view Mount Hood as a near-endmember in the spectrum of arc andesitic-dacitic volcanic systems where recharge and mixing have a particularly dominant effect on eruption initiation and style. From this we would predict that similar mixing-driven intermediate volcanoes that appear to require mafic recharge and mixing to initiate eruptions would also have relatively restricted compositional ranges and would typically erupt through dome formation, lava flows, and related processes, rather than consistently through larger explosive eruptions. Note that large pyroclastic flows related to dome collapse are not considered to represent explosive activity in this context, even though these flows can be highly destructive. Our model also predicts less variation in the eruptive style of volcanoes where mixing ratios and timescales remain somewhat constant through time (such as Mount Hood), and a greater variety of eruptive styles at volcanoes where the relative proportions of mixed components and the timescales of mixing are more variable, such as Mount Pinatubo

(Hammer et al., 1999) and Volcán Quizapu (Ruprecht and Bachmann, 2010). Variations in the eruptive style of these volcanoes are also likely related to local conditions such as magma flux, crustal strength and stress fields, edifice size, etc. (e.g., Eichelberger et al., 1986; Jaupart and Allegre, 1991; Pinel and Jaupart, 2005; Scandone et al., 2007).

There are a number of well-characterized volcanoes that appear to broadly match the characteristics of Mount Hood and thus may have their low explosivity explained by a model similar to that we propose.

Mount Unzen has produced material with a relatively narrow compositional range (57-67 wt% SiO_2) in periods of dominantly effusive activity for the past 0.5 m.y. (Browne and Gardner, 2006). These dome-forming eruptions have included porphyritic mafic enclaves that record temperatures 150˚C hotter than the host magmas (Browne and Gardner, 2006), indicating extensive recharge-driven reheating shortly before eruption.

Soufriére Hills Volcano in Montserrat has produced at least five lava domes that have experienced growth and repeated collapse (Webster, 1997). An influx of mafic magma shortly before eruption is consistent with geochemical and seismic observations during the most recent (and on-going) eruptive period that began in 1995 (Murphy et al., 1998; Watts et al., 2002). Eruptions over the past 18,000 years have produced andesites with a narrow compositional range (58-63.5 wt% SiO_2) but all erupted materials have included mafic enclaves (Murphy et al., 1998), which record a temperature increase associated with mafic recharge (Humphreys et al., 2009a; Humphreys et al., 2009b).

The >10,000 year eruptive history of Mount Pelée transitioned from plinian (explosive) to dome-forming eruptions approximately 650 years B.P. (Martel et al., 2000)

and experimental studies initially suggested identical pre-eruptive conditions for both eruptive styles, invoking variations in degassing patterns for changing eruptive styles (Martel et al., 1998). Recent work, however, has identified extensive evidence for magma mixing, including multiple populations of plagioclase and amphibole, the presence of mafic enclaves, and compositional differences that indicate a temperature difference of approximately 150˚C between the mixing magmas (Martel and Poussineau, 2007).

Multiple volcanoes in Alaska also exhibit periods of low explosivity that may be linked to reheating by recharge. Mount Dutton effusively erupts lavas that contain mafic enclaves, and Miller et al. (1999) suggested a link between enclave-bearing eruptions and low explosivity. Augustine Volcano has erupted mafic enclaves (51.3-57.3 wt% SiO_2) hosted in andesitic lavas (59.1-62.6 wt% SiO_2) and eruptions over the past 2200 years have varied in both the extent of magma mixing and in eruption style (Steiner, 2009). Eruptive activity of the past 50 years at Redoubt Volcano has ranged from effusive dome emplacement to brief explosive eruptions that produced modest tephra fallout (Coombs et al., 2010; Miller and Chouet, 1994). Lavas from Redoubt also show abundant evidence for magma mixing, including two compositionally distinct populations of amphibole (Wolf and Eichelberger, 1997) and two populations of plagioclase identified by crystal size distributions (Morrissey, 1997).

Reheating by mafic injection is likely an important factor in deciding the eruptive style of recharge-driven volcanoes. The effects on eruptive style from variations in recharge reheating are likely clouded by concurrent variations in degassing, crystallization, and ascent rate, and also in differences between magma plumbing systems. Studies that integrate investigations of all of these processes are necessary to

determine the exact role in reducing explosivity that is played by magma reheating prior to eruption.

CONCLUSIONS

In examining the causes of low explosivity at Mount Hood, we conclude the following:

1. Pre-eruptive volatile contents are as high in Mount Hood magmas as in other, more explosive, arc-related volcanoes, and suggest that low explosivity is not solely related to intrinsically low volatile abundances;

2. Pre-eruptive degassing is also unlikely to be the sole cause of the low explosivity, although significant amounts of pre-eruptive and syn-eruptive degassing did demonstrably occur at Mount Hood. However large variations in the extent of degassing are also evident in explosively erupted magmas, including those associated with plinian eruptions, suggesting pre-eruptive degassing is not necessarily a deterministic factor for eruptive style;

3. A critical factor in controlling explosivity at Mount Hood and at other volcanoes that erupt mixed andesitic-dacitic magmas is the reduction in viscosity following mafic recharge (Ruprecht and Bachmann, 2010), that delays or prevents fragmentation during magma ascent. This favors dome forming and other non-explosive eruptive styles. Geothermometry results, coupled with a simple viscosity model and simulations using CONFLOW (Mastin and Ghiorso, 2002), support this suggestion, showing that mafic recharge may be associated with a 5-10 fold decrease in viscosity in the silicic resident magma;

4. Our model for Mount Hood may represent a general model for non-explosive recharge-driven andesitic-dacitic volcanoes that links the processes that lead to eruption initiation, formation of mixed magma compositions, and non-explosive eruptive styles. A number of other andesitic-dacitic volcanoes show similarly limited compositional ranges, abundant evidence for mafic recharge and magma mixing, and a predilection for eruption via dome extrusive or other non-explosive means.

ACKNOWLEDGEMENTS

We thank Andy Ungerer, Frank Tepley, Dale Burns, Dan Ruscitto, Nobu Shimizu, and Andrey Gurenko for analytical assistance. This manuscript benefited greatly from stimulating discussions with Cynthia Gardner and members of the VIPER group at OSU. This work was supported by National Science Foundation grant EAR-038421 to AJRK and a USGS Kleinman Grant to AMK.

REFERENCES

Bacon, C.R., and Hirschmann, M.M., 1988, Mg/Mn partitioning as a test for equilibrium between coexisting Fe-Ti oxides: American Mineralogist, v. 73, p. 57-61.

Bacon, C.R., Newman, S., and Stolper, E.M., 1992, Water, CO2, Cl, and F in melt inclusions in phenocrysts from three Holocene explosive eruptions, Crater Lake, Oregon: American Mineralogist, v. 77, p. 1021-1030.

Baxter, P.J., 2000, Impacts of Eruptions on Human Health, *in* Sigurdsson, H., ed., Encyclopedia of Volcanoes: San Diego, Academic Press.

Blong, R.J., 1984, Volcanic Hazards: Sydney, Academic Press.

Blundy, J., and Cashman, K., 2008, Petrologic reconstruction of magmatic system variables and processes, *in* Putirka, K.D., and Tepley, F.J.I., eds., Minerals, Inclusions, and Volcanic Processes, Volume 69: Reviews in Mineralogy and Geochemistry: Chantilly, Mineralogical Society of America, p. 179-239.

Blundy, J., Cashman, K., and Humphreys, M., 2006, Magma heating by decompression-driven crystallization beneath andesite volcanoes: Nature, v. 443, p. 76-80.

Blundy, J., Cashman, K.V., and Berlo, K., 2008, Evolving magma storage conditions beneath Mount St. Helens inferred from chemical variations in melt inclusions from the 1980-1986 and current (2004-2006) eruptions, *in* Sherrod, D.R., Scott, W.E., and Stauffer, P.H., eds., A Volcano Rekindled: The Renewed Eruption from Mount St. Helens, 2004-2006, Volume 1750, U.S.G.S. Professional Paper.

Blundy, J., Cashman, K.V., Rust, A., and Witham, F., 2010, A case for CO2-rich arc magmas: Earth and Planetary Science Letters, v. 290, p. 289-301.

Browne, B.L., and Gardner, J.E., 2006, The influence of magma ascent path on the texture, mineralogy, and formation of hornblende reaction rims: Earth and Planetary Science Letters, v. 246, p. 161-176.

Clynne, M.A., 1999, A complex magma mixing origin for rocks erupted in 1915, Lassen Peak, California: Journal of Petrology, v. 40, p. 105-132.

Clynne, M.A., Calvert, A.T., Wolfe, E.W., Evarts, R.C., Fleck, R.J., and Lanphere, M.A., 2008, The Pleistocene Eruptive History of Mount St. Helens, Washington, from 300,000 to 12,800 Years Before Present, *in* Sherrod, D.R., Scott, W.E., and Stauffer, P.H., eds., A Volcano Rekindled: The Renewed Eruption of Mount St. Helens, 2004-2006, Volume Professional Paper 1750: Reston, U.S. Geological Survey.

Collins, S.J., Pyle, D.M., and Maclennan, J., 2009, Melt inclusions track pre-eruption storage and dehydration of magmas at Etna: Geology, v. 37, p. 571-574.

Conrey, R.M., Hooper, P.R., Larson, P.B., Chesley, J., and Ruiz, J., 2001, Trace element and isotopic evidence for two types of crustal melting beneath a High Cascades volcanic center, Mt. Jefferson, Oregon: Contributions to Mineralogy and Petrology, v. 141, p. 710-732.

Coombs, M.L., Bull, K.F., Vallance, J.W., Schneider, D.J., Thoms, E.E., Wessels, R.L., and McGimsey, R.G., 2010, Timing, distribution, and volume of proximal products of the 2006 eruption of Augustine Volcano, *in* Power, J.A., Coombs, M.L., and Freymueller, J.T., eds., The 2006 Eruption of Augustine Volcano, Alaska: U.S. Geological Survey Professional Paper 1769.

Cribb, J.W., and Barton, M., 1997, Significance of crustal and source region processes on the evolution of compositionally similar calc-alkaline lavas, Mt. Hood, Oregon: Journal of Volcanology and Geothermal Research, v. 76, p. 229-249.

Darr, C.M., 2006, Magma chamber processes over the past 475,000 years at Mount Hood, Oregon: Insights from crystal zoning and crystal size distribution studies: Corvallis, Oregon State University.

Dingwell, D.B., 1996, Volcanic Dilemma: Flow or Blow?: Science, v. 273.

Eichelberger, J.C., 1980, Vesiculation of mafic magma during replenishment of silicic magma reservoirs: Nature, v. 288, p. 446-450.

Eichelberger, J.C., Carrigan, C.R., Westrich, H.R., and Price, R.H., 1986, Non-explosive silicic volcanism: Nature, v. 323, p. 598-602.

Friedman, J.D., and Williams, D.L., 1982, Structural and heat flow implications of infrared anomalies at Mt. Hood, Oregon, 1972-1977: Journal of Geophysical Research, v. 87, p. 2793-2803.

Ghiorso, M.S., and Evans, B.W., 2008, Thermodynamics of rhombohedral oxide solid solutions and a revision of the Fe-Ti two-oxide geothermometer and oxygen-barometer: American Journal of Science, v. 308, p. 957-1039.
Giordano, D., Russell, J.K., and Dingwell, D.B., 2008, Viscosity of magmatic liquids: A model: Earth and Planetary Science Letters, v. 271, p. 123-134.
Gonnermann, H.M., and Manga, M., 2003, Explosive volcanism may not be an inevitable consequence of magma fragmentation: Nature, v. 426, p. 432-435.
Hammer, J.E., Cashman, K.V., Hoblitt, R.P., and Newman, S., 1999, Degassing and microlite crystallization during the pre-climatic events of the 1991 eruption of Mt. Pinatubo, Phillipines: Bulletin of Volcanology, v. 60, p. 355-380.
Hauri, E.H., Wang, J., Dixon, J.E., King, P.L., Mandeville, C., and Newman, S., 2002, SIMS analysis of volatiles in silicate glasses 1. Calibration, matrix effects and comparisons with FTIR: Chemical Geology, v. 183, p. 99-114.
Hildreth, W., 2007, Quaternary Magmatism in the Cascades— Geologic Perspectives: Reston, VA, U.S. Geological Survey.
Holland, T., and Blundy, J., 1994, Non-ideal interactions in calcic amphiboles and their bearing on amphibole-plagioclase thermometry: Contributions to Mineralogy and Petrology, v. 116, p. 433-447.
Housh, T.B., and Luhr, J.F., 1991, Plagioclase-melt equilibria in hydrous systems: American Mineralogist, v. 76, p. 477-492.
Humphreys, M.C.S., Christopher, T., and Hards, V., 2009a, Microlite transfer by disaggregation of mafic inclusions following magma mixing at Soufriere Hills volcano, Montserrat: Contributions to Mineralogy and Petrology, v. 157, p. 609-624.
Humphreys, M.C.S., Edmonds, M., Christopher, T., and Hards, V., 2009b, Chlorine variations in the magma of Soufriere Hills Volcano, Montserrat: Insights from Cl in hornblende and melt inclusions: Geochemica et Cosmochimica Acta, v. 73, p. 5693-5708.
Huppert, H.E., and Woods, A.W., 2002, The role of volatiles in magma chamber dynamics: Nature, v. 420, p. 493-495.
Jaupart, C., and Allegre, C.J., 1991, Gas content, eruption rate, and instabilities of eruption regime in silicic volcanoes: Earth and Planetary Science Letters, v. 102, p. 413-429.
Johnson, E.R., Wallace, P.J., Cashman, K.V., and Granados, H.D., 2010, Degassing of volatiles (H2O, CO2, S, Cl) during ascent, crystallization, and eruption at mafic monogenetic volcanoes in central Mexico: Journal of Volcanology and Geothermal Research, v. 197, p. 225-238.
Johnson, E.R., Wallace, P.J., Cashman, K.V., Granados, H.D., and Kent, A.J.R., 2008, Magmatic volatile contents and degassing-induced crystallization at Volcán Jorullo, Mexico: Implications for melt evolution and the plumbing systems of monogenetic volcanoes: Earth and Planetary Science Letters, v. 269, p. 478-487.
Kent, A.J.R., 2008, Melt inclusions in basaltic and related volcanic rocks, *in* Putirka, K.D., and Tepley, F.J.I., eds., Minerals, inclusions, and volcanic processes, Volume 69, Mineralogical Society of America, p. 273-331.

Kent, A.J.R., Darr, C.M., Koleszar, A.M., Salisbury, M.J., and Cooper, K.M., 2010, Preferential eruption of andesitic magmas through recharge filtering: Nature Geoscience, v. 3, p. 631-636.
Kohut, W., and Nielsen, R.L., 2004, Melt inclusion formation mechanisms and compositional effects in high-An feldspar and high-Fo olivine in anhydrous mafic silicate liquids: Contributions to Mineralogy and Petrology, v. 147, p. 684-704.
Kress, V.C., and Ghiorso, M.S., 2004, Thermodynamic modeling of post-entrapment crystallization of igneous phases: Journal of Volcanology and Geothermal Research, v. 137, p. 247-260.
Lange, R.A., Frey, H.M., and Hector, J., 2009, A thermodynamic model for the plagioclase-liquid hygrometer/thermometer: American Mineralogist, v. 94, p. 494-506.
Lowenstern, J.B., 2000, A review of the contrasting behavior of two magmatic volatiles: chlorine and carbon dioxide: Journal of Geochemical Exploration, v. 69-70, p. 287-290.
Luhr, J.F., 2001, Glass inclusions and melt volatile contents at Paricutin Volcano, Mexico: Contributions to Mineralogy and Petrology, v. 142, p. 261-283.
Mandeville, C.W., Webster, J.D., Tappen, C., Taylor, B.E., and Timbal, A., 2009, Stable isotope and petrologic evidence for open-system degassing during the climactic and pre-climactic eruptions of Mt. Mazama, Crater Lake, Oregon: Geochemica et Cosmochimica Acta, v. 73, p. 2978-3012.
Mangan, M., and Sisson, T., 2000, Delayed, disequilibrium degassing in rhyolite magma: decompression experiments and implications for explosive volcanism: Earth and Planetary Science Letters, v. 183, p. 441-455.
Marsh, B.D., 1981, On the crystallinity, probability of occurrence, and rheology of lava and magma: Contributions to Mineralogy and Petrology, v. 78, p. 85-98.
Martel, C., Bourdier, J.-L., Pichavant, M., and Traineau, H., 2000, Textures, water content and degassing of silicic andesites from recent plinian and dome-forming eruptions at Mount Pelée volcano (Martinique, Lesser Antilles arc): Journal of Volcanology and Geothermal Research, v. 96, p. 191-206.
Martel, C., Pichavant, M., Bourdier, J.-L., Traineau, H., Holtz, F., and Scaillet, B., 1998, Magma storage conditions and control of eruption regime in silicic volcanoes: experimental evidence from Mt. Pelée: Earth and Planetary Science Letters, v. 156 p. 89-99.
Martel, C., and Poussineau, S., 2007, Diversity of eruptive styles inferred from the microlites of Mt Pelée andesite (Martinique, Lesser Antilles): Journal of Volcanology and Geothermal Research, v. 166, p. 233-254.
Martel, C., Radadi Ali, A., Poussineau, S., Gourgaud, A., and Pichavant, M., 2006, Basalt-inherited microlites in silicic magmas: Evidence from Mount Pelee (Martinique, French West Indies): Geology, v. 3, p. 905-908.
Mastin, L., and Ghiorso, M.S., 2002, Insights into volcanic conduit flow from an open-source numerical model: Geochemistry Geophysics Geosystems, v. 3, p. DOI: 10.1029/2001GC000192.
McBirney, A.R., 1978, Volcanic evolution of the Cascades Range: Annual Review in Earth and Planetary Sciences, v. 6, p. 437-456.

Melnik, O., and Sparks, R.S.J., 1999, Nonlineral dynamics of lava dome extrusion: Nature, v. 402, p. 37-41.
Métrich, N., and Rutherford, M.J., 1992, Experimental study of chlorine behavior in hydrous silicic melts: Geochimica et Cosmochimica Acta, v. 56, p. 607-616.
Miller, T.P., Chertkoff, D.G., Eichelberger, J.C., and Coombs, M.L., 1999, Mount Dutton volcano, Alaska: Aleutian arc analog to Unzen volcano, Japan: Journal of Volcanology and Geothermal Research, v. 89, p. 275-301.
Miller, T.P., and Chouet, B.A., 1994, The 1989-1990 eruptions of Redoubt Volcano: An introduction: Journal of Volcanology and Geothermal Research, v. 62, p. 1-10.
Morrissey, M.M., 1997, Long-period seismicity at Redoubt Volcano, Alaska, 1989-1990 related to magma degassing: Journal of Volcanology and Geothermal Research, v. 75, p. 321-335.
Murphy, M.D., Sparks, R.S.J., Barclay, J., Carroll, M.R., Lejeune, A.-M., Brewer, T.S., Macdonald, R., Black, S., and Young, S., 1998, The role of magma mixing in triggering the current eruption at the Soufriere Hills volcano, Montserrat, West Indies: Geophysical Research Letters, v. 25, p. 3433-3436.
Newman, S., and Lowenstern, J.B., 2002, VolatileCalc: a silicate melt-H2O-CO2 solution model written in Visual Basic for Excel: Computers and Geosciences, v. 28, p. 597-604.
Okumura, S., Nakamura, M., Takeuchi, S., Tsuchiyama, A., Nakano, T., and Uesugi, K., 2009, Magma deformation may induce non-explosive volcanism via degassing through bubble networks: Earth and Planetary Science Letters, v. 281, p. 267-274.
Okumura, S., Nakamura, M., and Tsuchiyama, A., 2006, Shear-induced bubble coalescence in rhyolite melts with low vesicularity: Geophysical Research Letters, v. 33.
Pallister, J.S., Hoblitt, R.P., Meeker, G.P., Knight, R.J., and Siems, D.F., 1996, Magma mixing at Mount Pinatubo: Petrographic and chemical evidence from 1991 deposits, *in* Newhall, C., and Punongbayan, R., eds., Fire and Mud: Eruptions and Lahars of Mount Pinatubo, Quezon City, Philippine Institute of Volcanology and Seismology, and Seattle, University of Washington Press, p. 687-732.
Papale, P., 1999, Strain-induced magma fragmentation in explosive eruptions: Nature, v. 397, p. 425-428.
Papale, P., Moretti, R., and Barbato, D., 2006, The compositional dependence of the saturation surface of H2O + CO2 fluids in silicate melts: Chemical Geology, v. 229, p. 78-95.
Pichavant, M., Martel, C., Bourdier, J.-L., and Scaillet, B., 2002, Physical conditions, structure, and dynamics of a zoned magma chamber: Mount Pelée (Martinique, Lesser Antilles Arc): Journal of Geophysical Research, v. 107.
Pinel, V., and Jaupart, C., 2005, Some consequences of volcanic edifice destruction for eruption conditions: Journal of Volcanology and Geothermal Research, v. 145, p. 68-80.
Prouteau, G., Scaillet, B., Pichavant, M., and Maury, R.C., 1999, Fluid-present melting of ocean crust in subduction zones: Geology, v. 27, p. 1111-1114.
Putirka, K.D., 2005, Mantle potential temperatures at Hawaii, Iceland, and the mid-ocean ridge system, as inferred from olivine phenocrysts: Evidence for thermally driven

mantle plumes: Geochemistry Geophysics Geosystems, v. 6, p. doi: 10.1029/2005GC000915.

—, 2008, Thermometers and barometers for volcanic systems, *in* Putirka, K.D., and Tepley, F.J.I., eds., Minerals, inclusions, and volcanic processes, Volume 69, Mineralogical Society of America, p. 61-120.

Reubi, O., and Blundy, J., 2009, A dearth of intermediate melts at subduction zone volcanoes and the petrogenesis of arc andesites: Nature, v. 461, p. 1269-1273.

Ridolfi, F., Renzulli, A., and Puerini, M., 2010, Stability and chemical equilibration of amphibole in calc-alkaline magmas: an overview, new thermobarometric formulations and applicaton to subduction-related volcanoes: Contributions to Mineralogy and Petrology, v. 160, p. 45-66.

Roggensack, K., Hervig, R.L., McKnight, S.B., and Williams, S.N., 1997, Explosive basaltic volcanism from Cerro Negro Volcano: Influence of volatiles on eruptive style: Science, v. 277, p. 1639-1642.

Roman, D.C., Cashman, K.V., Gardner, C.A., Wallace, P.J., and Donovan, J.J., 2006, Storage and interaction of compositionally heterogeneous magmas from the 1986 eruption of Augustine Volcano, Alaska: Bulletin of Volcanology, v. 68, p. 240-254.

Ross, P.-S., Ukstins Peate, I., McClintock, M.K., Xu, Y.G., Skilling, I.P., White, J.D.L., and Houghton, B.F., 2005, Mafic volcaniclastic deposits in flood basalt provinces: A review: Journal of Volcanology and Geothermal Research, v. 145, p. 281-314.

Ruprecht, P., and Bachmann, O., 2010, Pre-eruptive reheating during magma mixing at Quizapu volcano and the implications for the explosiveness of silicic arc volcanoes: Geology, v. 38, p. 919-922.

Ruscitto, D.M., Wallace, P.J., Johnson, E.R., Kent, A.J.R., and Bindeman, I.N., 2010, Volatile contents of mafic magmas from cinder cones in the Central Oregon High Cascades: Implications for magma formation and mantle conditions in a hot arc: Earth and Planetary Science Letters, v. 298, p. 153-161.

Salisbury, M.J., Bohrson, W.A., Clynne, M.A., Ramos, F.C., and Hoskin, P., 2008, Multiple plagioclase crystal populations identified by crystal size distribution and in situ chemical data: Implications for timescales of magma chamber processes associated with the 1915 eruption of Lassen Peak, CA: Journal of Petrology, v. 49, p. 1755-1780.

Sato, H., Nakada, S., Fujii, T., Nakamura, M., and Suzuki-Kamata, K., 1999, Groundmass pargasite in the 1991-1995 dacite of Unzen volcano: phase stability experiments and volcanological implications: Journal of Volcanology and Geothermal Research, v. 89, p. 197-212.

Scandone, R., Cashman, K.V., and Malone, S.D., 2007, Magma supply, magma ascent and the style of volcanic eruptions: Earth and Planetary Science Letters, v. 253, p. 513-529.

Scott, W.E., Gardner, C.A., Tilling, R.I., and Lanphere, M.A., 1997a, Geologic History of Mount Hood Volcano, Oregon: A Field-Trip Guidebook: U.S. Geological Survey Open-File Report, v. 97, p. 38p.

Scott, W.E., Pierson, T.C., Schilling, S.P., Costa, J.E., Gardner, C.A., Vallance, J.W., and Major, J.J., 1997b, Volcano hazards in the Mount Hood Region, Oregon, *in*

Interior, U.S.D.o.t., ed., Volume Open-File Report 97-89, U.S. Geological Survey, p. 14.

Sparks, R.S.J., 1978, The dynamics of bubble formation and growth in magmas: A review and analysis: Journal of Volcanology and Geothermal Research, v. 3, p. 1-37.

Sparks, R.S.J., and Sigurdsson, H., 1977, Magma mixing: a mechanism for triggering acid explosive eruptions: Nature, v. 267, p. 315-318.

Steiner, A.R., 2009, A petrologic investigation of mafic inputs into the Augustine Volcano (Alaska) magma system over the pas 2,200 years: Fullerton, California State University.

Symonds, R.B., Poreda, R.J., Evans, W.C., Janik, C.J., and Ritchie, B.E., 2003, Mantle and crustal sources of carbon, nitrogen, and noble gases in Cascade-Range and Aleutian-Arc volcanic gases: USGS Open-File Report, v. 03-436.

Villemant, B., and Boudon, G., 1998, Transition from dome-forming to plinian eruptive styles controlled by H2O and Cl degassing: Nature, v. 392, p. 65-69.

Wallace, P.J., 2005, Volatiles in subduction zone magmas: concentrations and fluxes based on melt inclusion and volcanic gas data: Journal of Volcanology and Geothermal Research, v. 140, p. 217-240.

Watts, R.B., Herd, R.A., Sparks, R.S.J., and Young, S.R., 2002, Growth patterns and emplacement of the andesitic lava dome at Soufriére Hills Volcano, Montserrat: Geological Society, London, Memoirs, v. 21, p. 115-152.

Webster, J.D., 1997, Chloride solubility in felsic melts and the role of chloride in magmatic degassing: Journal of Petrology, v. 38, p. 1793-1807.

Webster, J.D., Kinzler, R.J., and Mathez, E.A., 1999, Chloride and water solubility in basalt and andesite melts and implications for magmatic degassing: Geochimica et Cosmochimica Acta, v. 63, p. 729-738.

Wilson, L., 1980, Relationships between pressure, volatile content, and ejecta velocity in three types of volcanic explosive: Journal of Volcanology and Geothermal Research, v. 8, p. 297-313.

Wilson, L., Sparks, R.S.J., and Walker, G.P.L., 1980, Explosive volcanic eruptions-- IV. The control of magma properties and conduit geometry on eruption column behaviour: Geophysical Journal of the Royal Astronomical Society, v. 63, p. 117-148.

Wolf, K.J., and Eichelberger, J.C., 1997, Syneruptive mixing, degassing, and crystallization at Redoubt Volcano, eruption of December, 1989 to May 1990: Journal of Volcanology and Geothermal Research, v. 75, p. 1997.

Woods, A.W., 1995, The dynamics of explosive volcanic eruptions: Reviews of Geophysics, v. 33, p. 495-530.

Woods, M.M., 2004, Compositional and mineralogical relationships between mafic inclusions and host lavas as key to andesite petrogenesis at Mount Hood Volcano, Oregon: Portland, Portland State University.

FIGURES

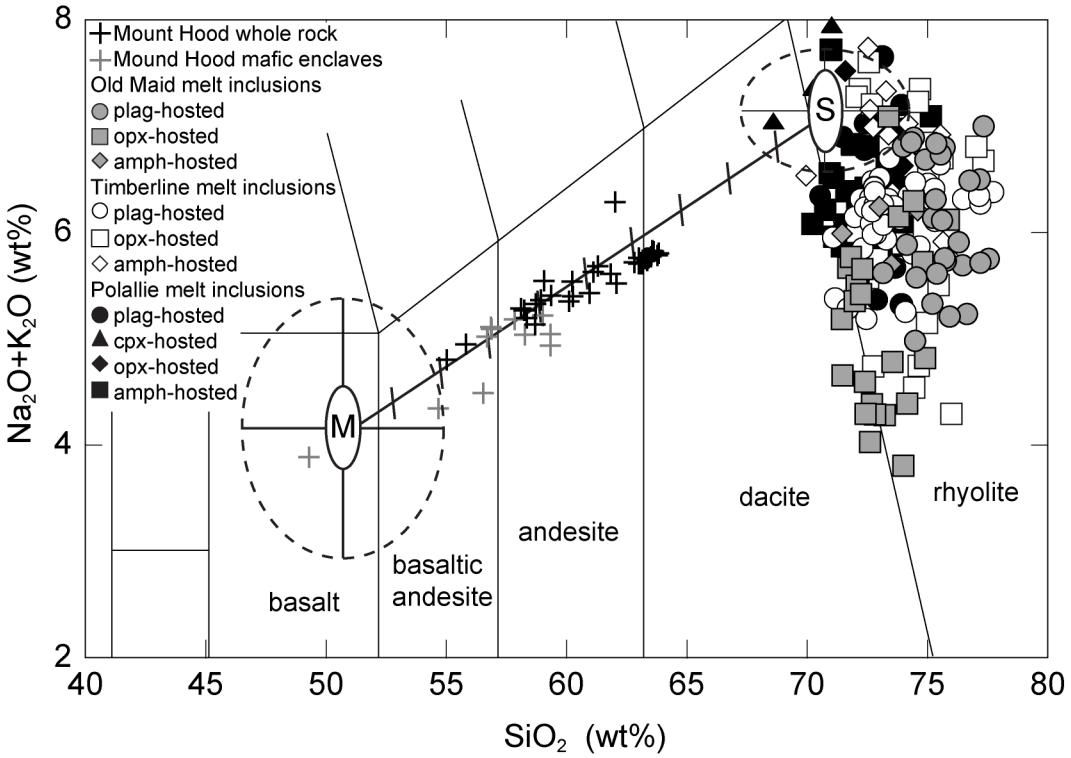

Figure 2.1: Total alkali versus silica for whole rock and melt inclusions from Mount Hood. Whole rock data from Kent et al. (2010) and unpublished data. Dashed circles (M= Mafic, S= Silicic) indicate approximate compositions for the mixing endmembers (Kent et al. 2010).

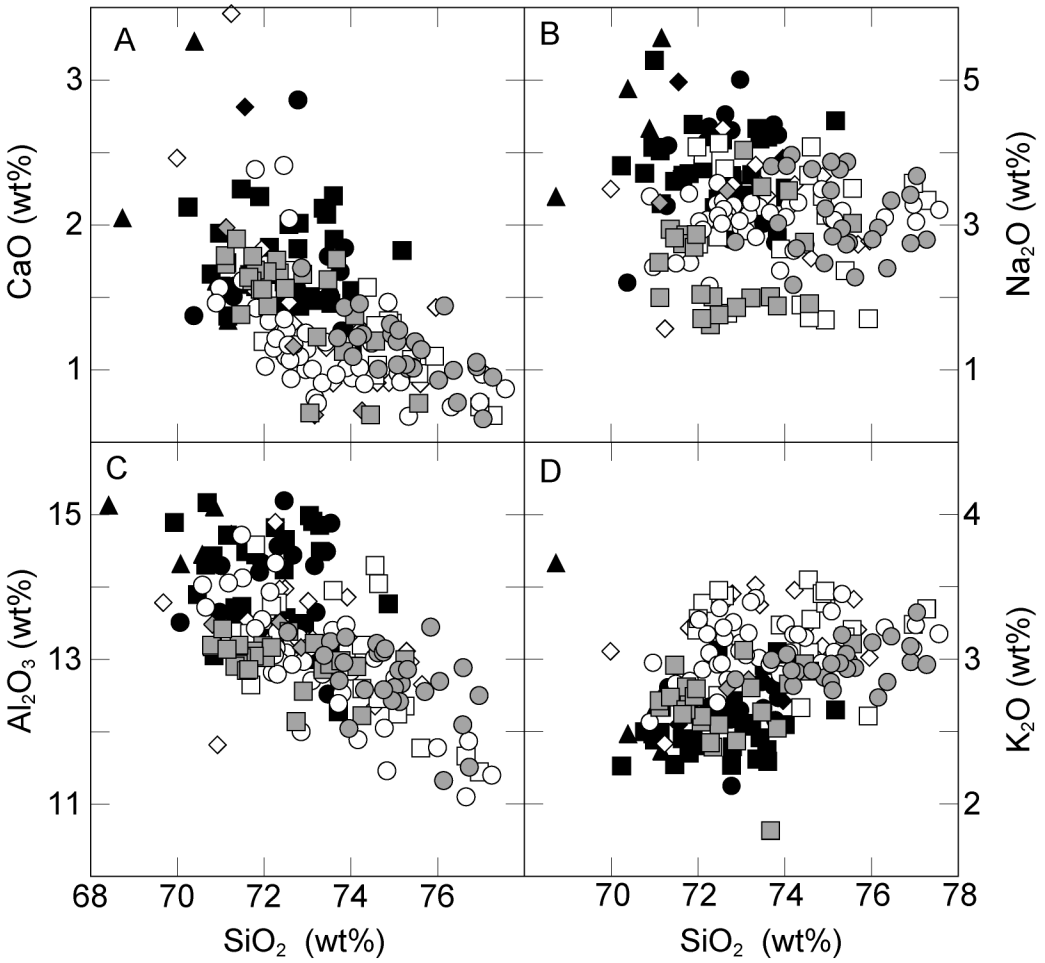

Figure 2.2: SiO_2 versus CaO, Na_2O, Al_2O_3, and K_2O for melt inclusions from Mount Hood. A: SiO_2 versus CaO, B: SiO_2 versus Na_2O, D: SiO_2 versus Al_2O_3, and D: SiO_2 versus K_2O. Symbols as in Fig. 1.

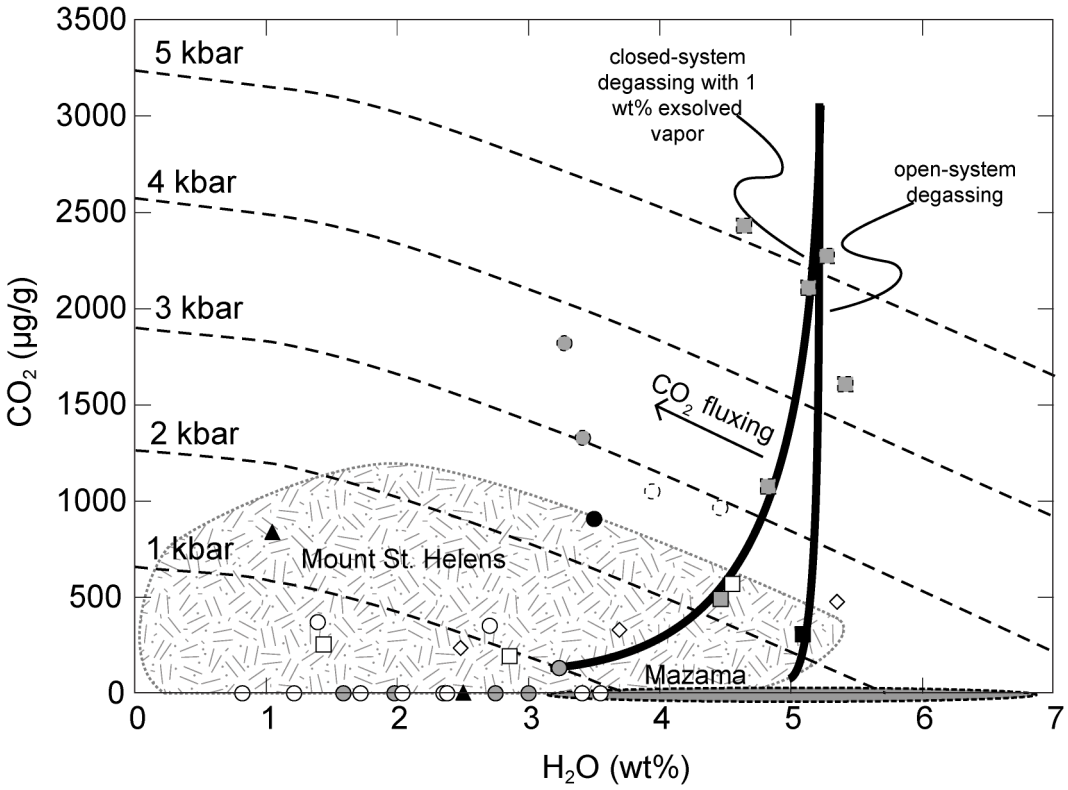

Figure 2.3: H_2O versus CO_2 for melt inclusions from Mount Hood, Mount St. Helens, and the preclimactic and climactic eruptions of Mount Mazama. Mount St. Helens data from Blundy et al. (2010); Mount Mazama data from Mandeville et al. (2009). Isobars and degassing paths calculated using Newman and Lowenstern (2002). Symbols as in Fig. 1. Symbols with dashed outlines have CO_2 beyond analytical calibration (~1000 µg/g) and are included only for informational purposes.

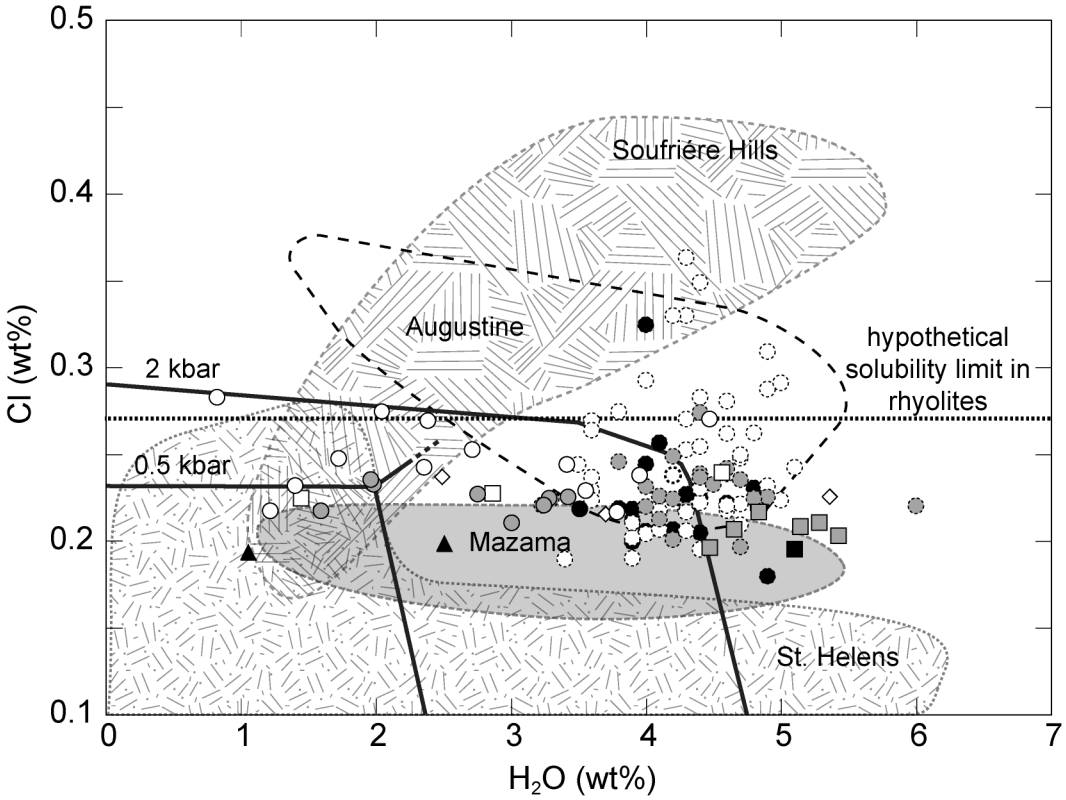

Figure 2.4: H_2O versus Cl for melt inclusions from Mount Hood, Mount St. Helens, Soufriére Hills Volcano, Augustine Volcano, and Mount Mazama. Mount St. Helens data from Blundy et al. (2010), Soufriére Hills Volcano data from Humphreys et al. (2009), Augustine Volcano data from Roman et al. (2006), and Mount Mazama data from Bacon et al. (1992). Symbols as in Fig. 1. Symbols with dashed outlines represent Mount Hood melt inclusions with H_2O contents estimated using the hygrometer of Lange et al. (2009). Hypothetical Cl solubility limit from Métrich and Rutherford (1992); bold solubility paths from Webster (1999).

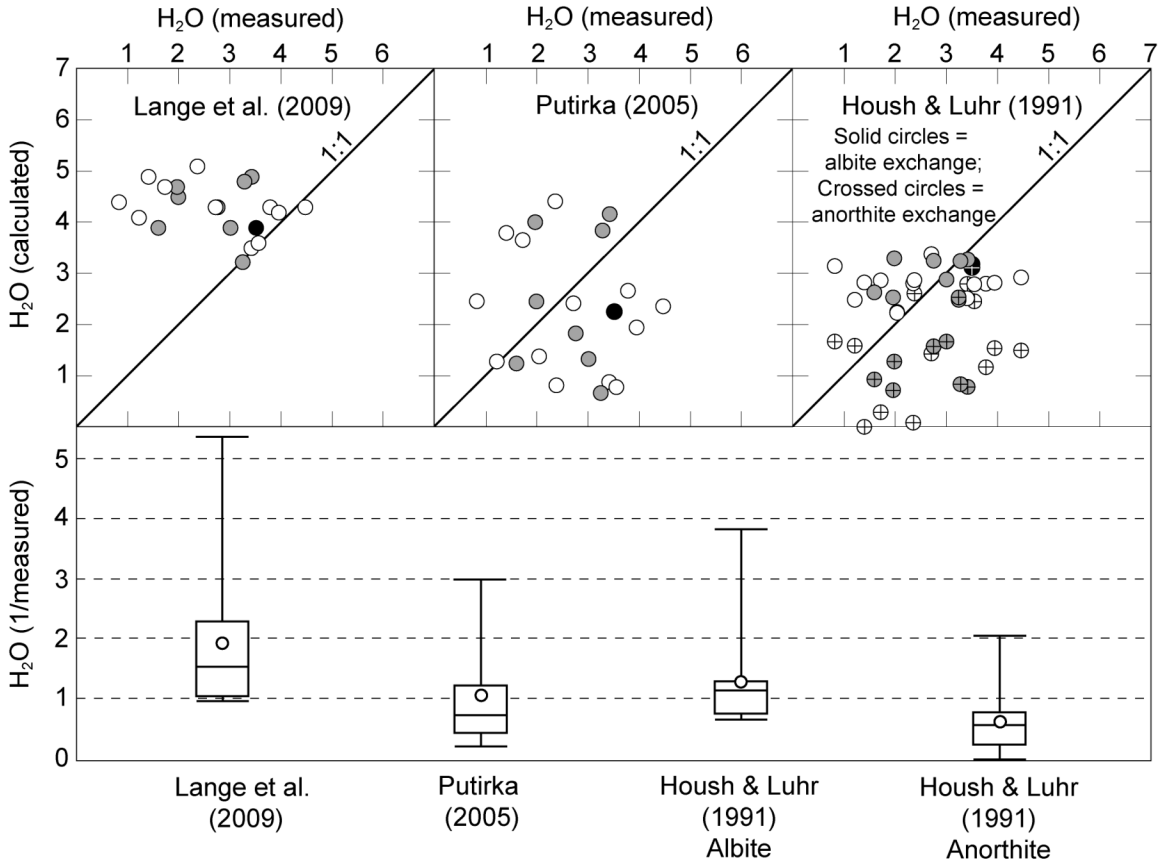

Figure 2.5: Comparison between various hygrometers and measured values of H_2O in melt inclusions from Mount Hood. Symbols as in Fig. 2.1. On Box and Whisker plots, boxes indicate the middle 50% of values, circles are mean values, and black lines are median values. Whiskers represent the full range of the data.

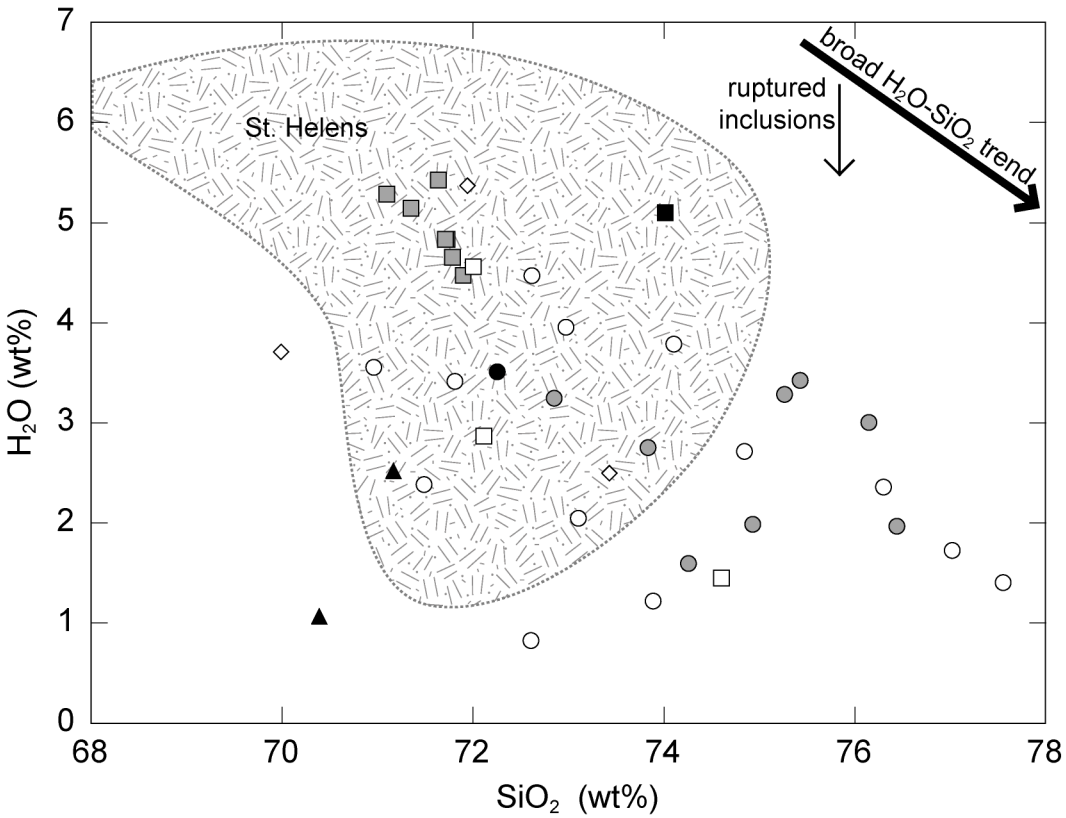

Figure 2.6: SiO_2 versus H_2O for melt inclusions from Mount Hood and the 1980 Plinian eruption of Mount St. Helens. Mount St. Helens data from Blundy et al. (2010). "Ruptured" melt inclusions have lost H_2O after entrapment. Symbols as in Fig. 1.

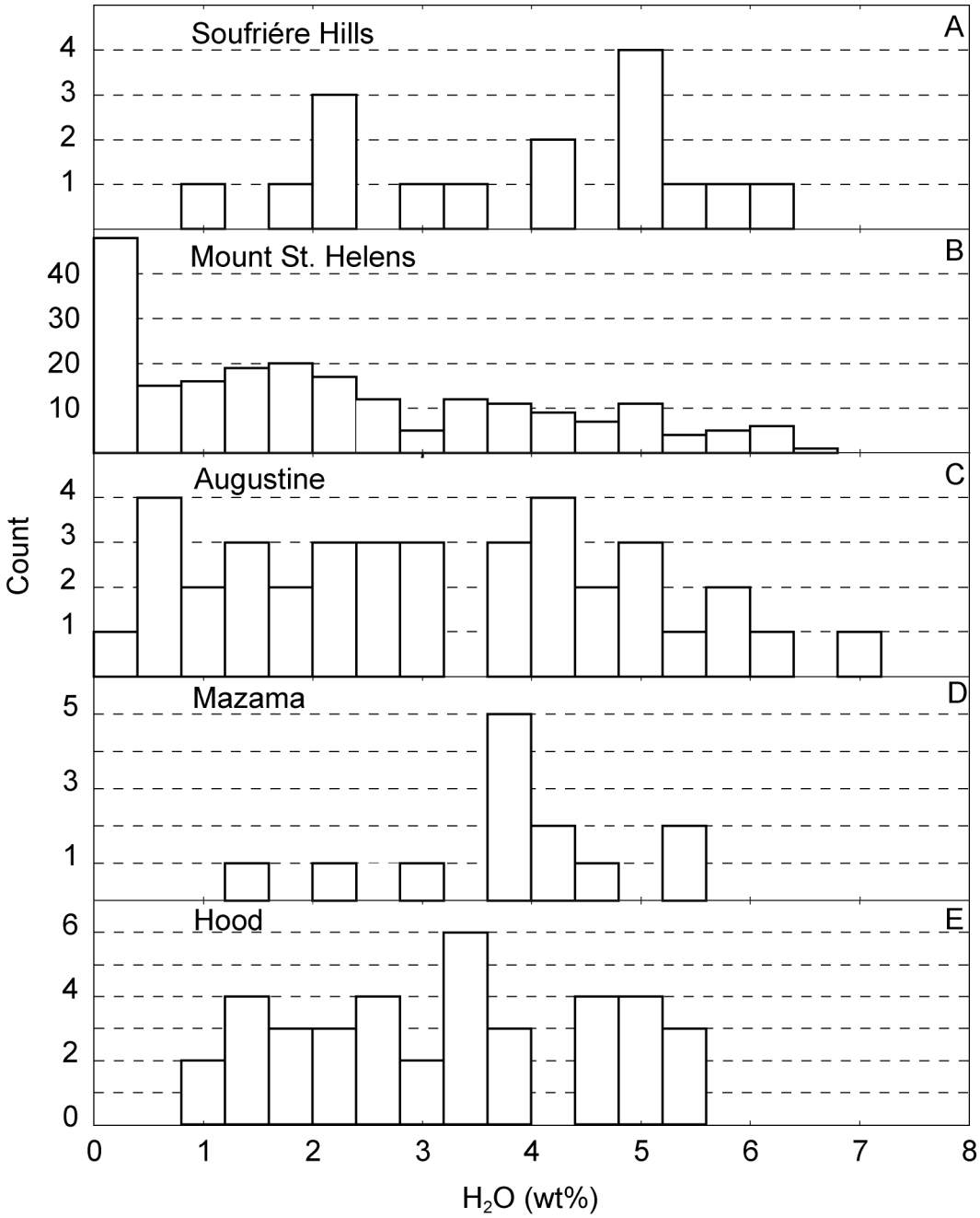

Figure 2.7: H_2O contents for Soufriére Hills Volcano, Mount St. Helens, Augustine Volcano, Mount Mazama, and Mount Hood. A: Soufriére Hills Volcano (Humphreys et al., 2009), B: Mount St. Helens (Blundy et al., 2008), C: Augustine Volcano (Roman et al., 2006), D: Mount Mazama (Bacon et al., 1992), and E: Mount Hood (this study).

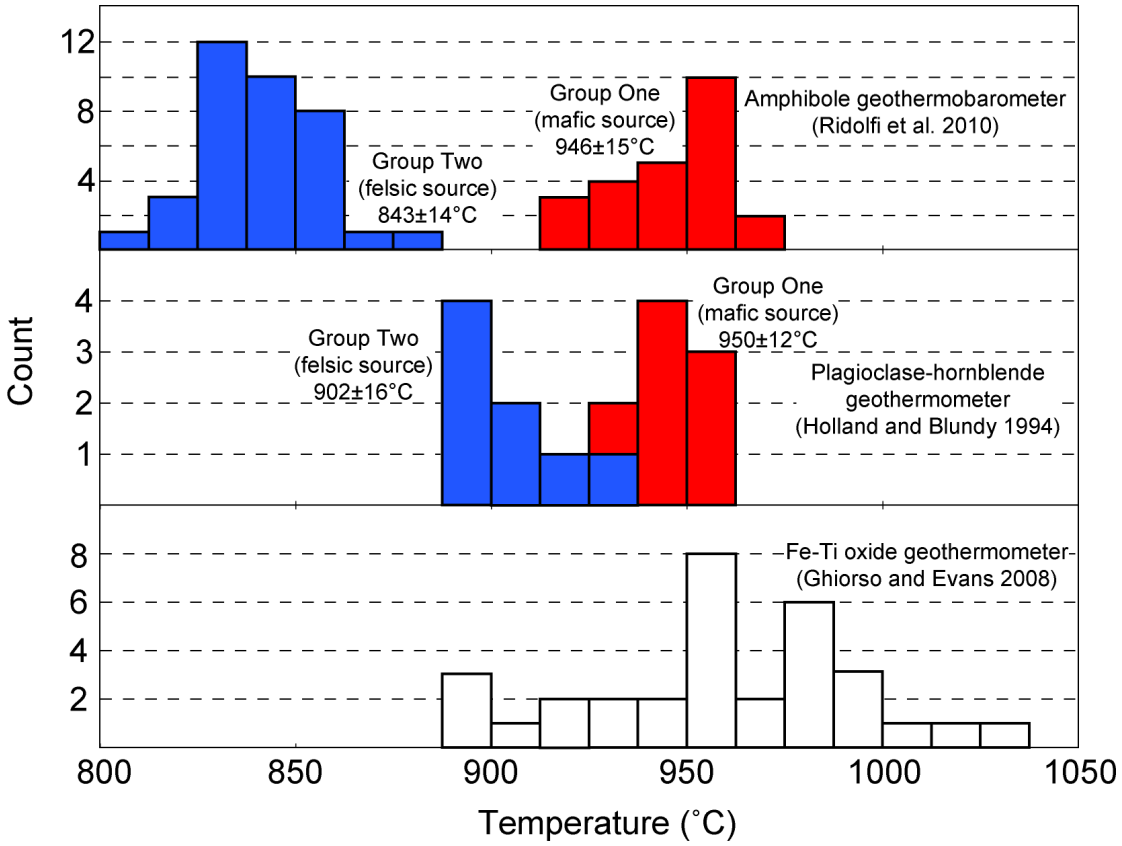

Figure 2.8: Comparison between pre-eruptive temperatures for Mount Hood magmas calculated using different methods: Amphibole composition (Ridolfi et al., 2010), plagioclase-hornblende pairs (Holland and Blundy, 1994), and Fe-Ti oxides (Ghiorso and Evans, 2008). Group One amphiboles contain <45 wt% SiO_2; Group Two amphiboles contain >45 wt% SiO_2.

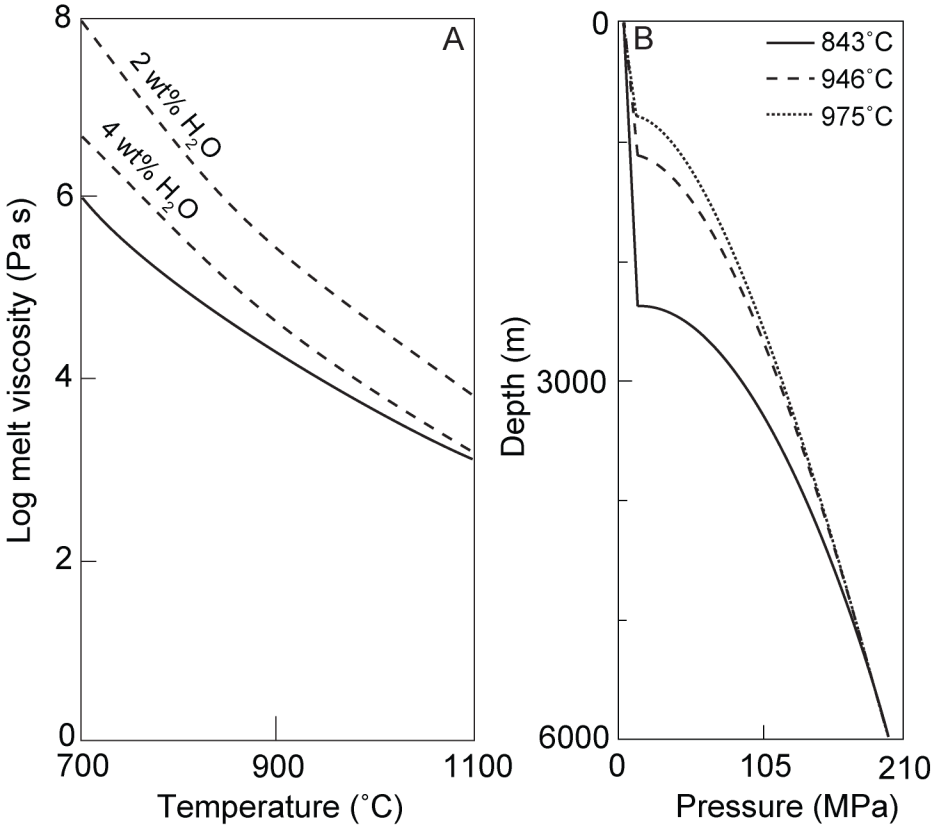

Figure 2.9: Magma viscosities and CONFLOW simulations. A: Magma viscosity in Mount Hood andesite that contains 4 wt% H_2O and 30% crystallinity calculated using CONFLOW (Mastin and Ghiorso, 2000) (solid line) and from Giordano et al. (2008) (dashed lines, 2 wt% and 4 wt% H_2O), using the Roscoe-Einstein equation and the recommended constant of ϕ_m=0.6 from Marsh (1981). B: CONFLOW simulation illustrating delayed fragmentation when magma temperature is increased.

TABLES

Table 2.1: CONFLOW simulation parameters

Magma composition	
CONFLOW simulation parameters	
Magma composition	
SiO_2	67.51
TiO_2	1.08
Al_2O_3	11.78
FeO*	6.90
MnO	0.12
MgO	3.43
CaO	2.92
Na_2O	3.91
K_2O	2.10
P_2O_5	0.24
Anhydrous total	100.00
H_2O	4 wt%
crystallinity	30%
starting pressure	200 MPa
starting depth	6000 m
conduit width	20 m
initial velocity	1 m/s

Table 2.2: Major element and volatile compositions of melt inclusions from Mount Hood.

		Major Elements by EMPA										Volatiles by FTIR[1] and SIMS[2]	
Melt Inclusion	host	SiO_2	TiO_2	Al_2O_3	FeO*	MgO	CaO	Na_2O	K_2O	Cl	Total	H_2O	CO_2
MH08-20-0101	plag	74.26	0.19	11.94	2.04	0.25	1.25	2.68	2.92	0.218	95.74	1.59[1]	b.d
MH08-20-0102a	plag	74.94	0.16	12.99	1.30	0.20	1.25	3.23	2.92	0.233	97.22	1.98[1]	b.d
MH08-20-0102b	plag	73.84	0.30	13.14	2.09	0.22	1.43	3.03	2.88	0.227	97.15	2.75[1]	b.d
MH08-20-0103	plag	76.15	0.19	13.34	1.25	0.22	1.44	2.97	2.74	0.211	98.51	3.00[1]	b.d
MH08-20-0106	plag	72.85	0.26	13.27	1.97	0.40	1.71	2.77	2.86	0.221	96.32	3.24[1]	b.d.
MH08-20-0202a	opx	71.79	0.27	12.92	2.37	0.41	1.69	2.80	2.74	0.207	95.18	4.65[2]	2433[2]
MH08-20-0202b	opx	71.10	0.28	13.09	2.38	0.51	1.79	2.49	2.72	0.211	94.57	5.28[2]	2275[2]
MH08-20-0204	opx	71.73	0.43	13.09	2.02	0.49	1.79	2.76	2.81	0.223	95.35	4.83[2]	
MH08-20-0205	opx	73.05	0.22	12.04	2.92	1.80	0.70	4.04	3.06	0.203	98.03		
MH08-20-0206a	opx	73.47	0.24	13.11	2.40	0.41	1.62	3.53	2.64	0.230	97.65		
MH08-20-0209	opx	71.35	0.43	13.32	2.00	0.51	1.91	2.94	2.74	0.209	95.41	5.14[2]	2108[2]
MH08-20-0210a	opx	71.72	0.35	12.83	2.06	0.51	1.62	2.86	2.65	0.217	94.82	4.83[2]	1077[2]
MH08-20-0210b	opx	71.64	0.21	12.80	2.25	0.46	1.64	2.75	2.62	0.203	94.58	5.42[2]	1608[2]
MH08-20-0211	opx	71.90	0.22	12.74	2.19	0.49	1.56	2.70	2.74	0.196	94.74	4.47[2]	492[2]
MH08-20-0215b	amph	72.68	0.40	13.40	1.93	0.33	1.16	3.47	2.80	0.229	96.41		
MH08-20-0226a	opx	74.08	0.38	12.88	2.28	0.45	1.38	3.48	2.83	0.224	97.99		
MH08-20-0226b	opx	71.46	0.30	13.04	2.08	0.47	1.38	2.83	2.96	0.206	94.73		
MH08-20-0226c	opx	71.96	0.50	12.76	2.09	0.48	1.56	2.87	2.80	0.199	95.22		
MH08-20-0230	plag	73.69	0.38	12.95	1.17	0.20	1.22	3.82	3.00	0.222	96.66		
MH08-20-0234a	plag	75.43	0.25	12.31	1.33	0.25	1.01	3.88	2.94	0.226	97.62	3.42[2]	1330[2]
MH08-20-0234b	plag	75.27	0.24	12.33	1.30	0.25	1.04	3.77	2.98	0.225	97.40	3.28[2]	1821[2]
MH08-20-0235	plag	77.04	0.25	11.41	1.30	0.25	0.66	3.68	3.33	0.221	98.14		
MH08-20-0236	plag	76.89	0.23	11.99	1.40	0.17	1.05	3.42	3.09	0.201	98.45		
MH08-20-0237a	plag	74.15	0.20	12.85	1.18	0.24	1.23	3.97	2.93	0.225	96.97		
MH08-20-0237b	plag	74.04	0.21	12.60	1.24	0.24	1.09	3.83	3.04	0.219	96.50		
MH08-20-0238	plag	75.07	0.19	12.48	1.24	0.23	1.04	3.88	2.97	0.222	97.31		
MH08-20-0239	plag	76.44	0.30	11.22	2.01	0.35	0.78	3.34	3.16	0.236	97.84	1.96[2]	
MH08-20-0242	amph	71.13	0.38	13.37	1.84	0.33	1.98	3.30	2.71	0.168	95.22		
MH08-20-2002	plag	75.47	0.26	12.56	1.32	0.27	1.20	2.76	2.99	0.226	97.05		
MH08-20-2029	plag	75.41	0.43	12.75	2.21	0.32	1.02	2.73	3.04	0.249	98.16		
MH08-20-2031a	plag	74.91	0.25	13.12	2.02	0.28	1.32	2.48	2.88	0.213	97.46		
MH08-20-2031b	plag	75.32	0.26	12.50	1.90	0.26	1.01	2.96	3.17	0.242	97.62		
MH08-20-2044b	plag	76.36	0.19	12.59	1.74	0.34	1.00	2.40	2.85	0.220	97.70		
MH08-20-2059	plag	75.05	0.12	13.00	1.10	0.17	1.20	3.48	2.85	0.197	97.16		
MH08-20-2084	plag	77.26	0.20	12.40	1.23	0.22	0.95	2.80	2.97	0.229	98.25		
MH08-20-2092	plag	75.10	0.23	13.04	2.01	0.25	1.28	2.85	2.79	0.239	97.78		
MH08-20-2098	plag	74.19	0.21	13.20	1.83	0.27	1.46	2.18	2.82	0.225	96.39		
MH08-20-2145	plag	75.62	0.22	12.76	1.45	0.22	1.14	2.28	2.95	0.246	96.88		
MH08-20-2157	plag	76.02	0.34	12.45	1.57	0.29	0.93	2.81	3.12	0.274	97.80		
MH08-20-2195	plag	76.90	0.13	12.78	1.29	0.23	1.02	2.75	2.98	0.232	98.32		
MH08-20-232	plag	74.63	0.31	12.48	1.39	0.29	1.01	3.77	2.92	0.237	97.04		
MH08-20-3020	opx	74.56	0.55	12.12	2.12	0.36	1.20	1.92	2.92	0.211	95.96		
MH08-20-3021	opx	73.66	0.18	12.76	2.24	0.48	1.77	2.01	1.82	0.163	95.08		
MH08-20-3036	opx	71.12	0.41	13.07	2.33	0.51	1.73	2.00	2.67	0.234	94.07		
MH08-20-3043b	opx	72.34	0.26	12.92	2.55	0.43	1.67	2.01	2.40	0.222	94.80		
MH08-20-3060	amph	74.27	0.30	13.19	2.15	0.27	0.72	3.28	2.95	0.236	97.36		
MH08-20-3071a	opx	72.28	0.37	13.09	2.55	0.46	1.76	1.63	2.43	0.218	94.78		
MH08-20-3071b	opx	73.21	0.21	12.46	2.36	0.40	1.23	2.00	2.81	0.228	94.90		
MH08-20-3071c	opx	72.88	0.40	13.28	2.11	0.53	1.66	1.87	2.44	0.225	95.41		
MH08-20-3093a	opx	74.45	0.38	12.80	2.17	0.20	0.69	2.77	2.97	0.216	96.65		
MH08-20-3093b	opx	75.56	0.38	12.89	2.30	0.21	0.77	3.03	3.11	0.213	98.46		
MH08-20-3104a	amph	73.18	0.41	13.05	2.22	0.27	0.69	2.87	2.86	0.249	95.79		
MH08-20-3114a	opx	72.07	0.45	13.01	2.12	0.48	1.68	2.05	2.57	0.225	94.66		
MH08-20-3114b	opx	73.82	0.21	12.83	2.38	0.42	1.13	1.89	2.53	0.145	95.35		
MH08-20-3114c	opx	72.49	0.44	13.06	1.81	0.49	1.56	1.76	2.55	0.234	94.40		
MH08-20-3121a	opx	72.08	0.21	12.94	2.37	0.51	1.44	1.71	2.61	0.226	94.11		

Table 2.2 cont.		Major Elements by EMPA										Volatiles by FTIR[1] and SIMS[2]	
Melt Inclusion	host	SiO_2	TiO_2	Al_2O_3	FeO*	MgO	CaO	Na_2O	K_2O	Cl	Total	H_2O	CO_2
MH08-22-0103	plag	71.81	0.31	14.02	1.98	0.58	1.43	2.49	2.85	0.244	95.72	3.41[1]	b.d.
MH08-22-0119	plag	73.89	0.15	13.30	1.22	0.20	1.02	2.38	2.90	0.218	95.27	1.21[1]	b.d.
MH08-22-0120a	plag	70.96	0.26	13.62	1.85	0.33	1.57	2.43	2.98	0.229	94.23	3.55[1]	b.d.
MH08-22-0120b	plag	71.49	0.29	13.95	1.52	0.22	1.62	2.48	2.83	0.270	94.69	2.38[1]	b.d.
MH08-22-0121	plag	72.61	0.33	13.27	2.00	0.25	1.18	3.14	3.15	0.283	96.21	0.82[1]	b.d.
MH08-22-0122	plag	73.11	0.17	13.20	1.24	0.18	1.01	2.93	3.03	0.275	95.13	2.04[1]	b.d.
MH08-22-0123a	plag	72.45	0.35	13.83	1.81	0.34	2.41	3.59	2.70	0.202	97.69		
MH08-22-0123b	plag	77.02	0.44	11.77	2.17	0.57	0.97	3.06	3.24	0.248	99.49	1.72[1]	b.d.
MH08-22-2019a	plag	74.20	0.21	13.37	1.22	0.18	1.02	2.66	3.17	0.210	96.23		
MH08-22-2049	plag	73.16	0.33	11.90	1.96	0.32	0.81	3.16	3.18	0.288	95.11		
MH08-22-2051	plag	74.48	0.40	11.79	2.13	0.68	1.19	2.74	3.15	0.263	96.83		
MH08-22-2054a	plag	72.82	0.19	12.99	1.44	0.24	1.09	3.28	3.26	0.330	95.64		
MH08-22-2054b	plag	72.02	0.23	12.88	1.48	0.25	1.03	3.06	3.28	0.364	94.59		
MH08-22-2054c	plag	73.33	0.21	13.06	1.52	0.25	0.91	2.85	3.43	0.349	95.90		
MH08-22-2073	plag	75.08	0.30	11.95	1.82	0.43	0.98	3.10	3.33	0.239	97.23		
MH08-22-2076a	plag	72.27	0.23	13.45	1.64	0.23	1.22	2.17	3.05	0.237	94.50		
MH08-22-2090	plag	70.89	0.25	13.92	1.80	0.47	1.46	3.41	2.57	0.207	94.98		
MH08-22-2105a	plag	73.22	0.28	12.86	1.56	0.21	0.77	3.32	3.40	0.310	95.94		
MH08-22-2105b	plag	75.33	0.21	12.63	1.41	0.20	0.68	3.21	3.45	0.292	97.41		
MH08-22-2122a	plag	76.97	0.41	11.00	1.62	0.23	0.78	3.29	3.07	0.224	97.59		
MH08-22-2122b	plag	75.14	0.26	11.36	2.25	0.63	0.92	3.08	3.05	0.222	96.92		
MH08-22-2143a	plag	72.68	0.20	12.86	1.65	0.23	1.18	3.15	2.86	0.206	95.03		
MH08-22-2143b	plag	73.65	0.13	12.69	1.50	0.28	0.97	3.18	2.97	0.221	95.61		
MH08-22-2157a	plag	72.62	0.21	12.69	1.35	0.24	0.94	3.11	3.02	0.231	94.39		
MH08-22-2157b	plag	71.79	0.22	14.61	1.31	0.22	2.39	3.45	2.72	0.190	96.90		
MH08-22-2166a	plag	72.11	0.31	13.32	1.80	0.29	1.34	2.95	2.93	0.264	95.31		
MH08-22-2166b	plag	72.59	0.33	13.05	1.69	0.27	1.07	3.23	3.22	0.293	95.74		
MH08-22-2166c	plag	72.45	0.29	12.98	1.74	0.30	1.35	3.15	2.97	0.224	95.45		
MH08-22-2191	plag	74.31	0.18	12.73	1.86	0.47	0.91	3.32	3.17	0.250	97.21		
MH08-22-2202	plag	72.96	0.23	12.83	1.68	0.23	1.26	3.07	3.06	0.196	95.51		
MH08-22-2203	plag	72.55	0.32	12.96	1.54	0.37	1.17	3.03	2.97	0.255	95.17		
MH08-22-2204a	plag	77.56	0.44	11.30	1.71	0.30	0.87	3.22	3.18	0.232	98.81	1.40[2]	372[2]
MH08-22-2204b	plag	74.85	0.40	12.91	2.40	0.66	1.47	3.51	2.98	0.253	99.43	2.71[2]	352[2]
MH08-22-2206	plag	74.11	0.15	12.43	1.49	0.32	1.02	3.29	3.05	0.217	96.07	3.78[2]	
MH08-22-2211	plag	72.96	0.39	13.17	1.91	0.34	1.00	3.22	3.07	0.330	96.39		
MH08-22-2212	plag	74.02	0.33	12.29	1.45	0.25	0.95	3.12	3.25	0.218	95.88		
MH08-22-2213	plag	76.30	0.31	11.68	1.36	0.25	0.74	3.12	3.22	0.243	97.23	2.35[2]	
MH08-22-2214	plag	72.62	0.32	12.68	1.67	0.25	1.15	3.25	3.15	0.271	95.37	4.47[2]	966[2]
MH08-22-2215	plag	73.40	0.25	12.60	1.61	0.36	1.19	3.26	3.01	0.191	95.89		
MH08-22-2216a	plag	72.43	0.44	12.98	1.58	0.22	1.31	3.30	3.04	0.234	95.54		
MH08-22-2216b	plag	72.58	0.20	14.23	1.38	0.21	2.05	3.34	3.10	0.205	97.29		
MH08-22-2216c	plag	72.50	0.26	13.15	1.34	0.21	1.27	3.14	3.08	0.223	95.19		
MH08-22-2216d	plag	72.50	0.31	12.72	1.54	0.22	1.09	3.15	3.36	0.281	95.18		
MH08-22-2216e	plag	72.21	0.31	12.94	1.49	0.23	1.15	3.09	3.18	0.262	94.86		
MH08-22-2217	plag	72.98	0.24	12.87	1.70	0.18	1.15	2.98	3.12	0.238	95.45	3.95[2]	1051[2]
MH08-22-3004b	amph	71.25	0.44	11.71	3.41	2.01	3.46	1.57	2.42	0.163	96.43		
MH08-22-3011a	opx	74.95	0.32	13.94	2.24	0.26	1.32	3.15	3.39	0.247	99.83		
MH08-22-3011b	opx	74.86	0.37	14.19	2.28	0.26	1.34	3.41	3.46	0.251	100.43		
MH08-22-3024a	amph	75.70	0.28	12.85	2.21	0.28	1.14	2.73	3.20	0.208	98.61		
MH08-22-3028	opx	75.39	0.17	12.14	2.09	0.27	1.07	2.38	3.16	0.241	96.91		
MH08-22-3070	opx	74.93	0.24	12.35	2.35	0.37	1.27	1.70	3.48	0.215	96.91		
MH08-22-3073a	opx	74.38	0.55	12.80	2.24	0.32	1.57	1.91	2.67	0.198	96.63		
MH08-22-3073b	opx	74.56	0.14	12.49	2.36	0.22	1.31	1.73	3.05	0.208	96.07		
MH08-22-3075a	opx	72.68	0.28	13.34	2.33	0.48	1.69	1.79	2.98	0.228	95.80		
MH08-22-3105	opx	75.92	0.11	11.67	2.21	0.30	1.10	1.72	2.61	0.196	95.83		
MH08-22-3121	opx	73.90	0.38	13.85	1.99	0.29	1.17	2.68	3.24	0.267	97.77		
MH08-22-3143a	amph	74.24	0.28	13.75	1.99	0.28	1.28	3.56	3.48	0.218	99.08		

Table 2.2 cont.		Major Elements by EMPA										Volatiles by FTIR[1] and SIMS[2]	
Melt Inclusion	host	SiO_2	TiO_2	Al_2O_3	FeO*	MgO	CaO	Na_2O	K_2O	Cl	Total	H_2O	CO_2
MH08-22-3143b	amph	73.34	0.30	13.69	1.98	0.29	1.19	3.83	3.51	0.234	98.37		
MH08-22-3151a	amph	74.61	0.30	12.98	1.99	0.28	0.91	2.55	3.25	0.213	97.09		
MH08-22-3151b	amph	75.96	0.33	12.54	1.85	0.24	1.43	2.78	3.01	0.185	98.33		
MH08-22-3164a	amph	75.61	0.32	13.00	1.79	0.25	0.90	3.52	3.42	0.192	99.01		
MH08-22-3201a	amph	73.44	0.35	13.17	1.78	0.26	1.15	3.57	3.37	0.237	97.33	2.49[2]	234[2]
MH08-22-3201c	amph	72.81	0.41	13.87	2.16	0.29	1.09	3.56	3.45	0.228	97.86		
MH08-22-3204	amph	71.80	0.27	12.79	1.73	0.08	1.54	2.47	3.21	0.242	94.13		
MH08-22-3206	amph	71.95	0.42	13.42	1.84	0.35	1.83	2.74	2.65	0.226	95.43	5.36[2]	475[2]
MH08-22-3211	amph	70.00	0.38	13.67	2.51	0.87	2.46	3.50	3.05	0.216	96.66	3.70[2]	330[2]
MH08-22-3212	opx	72.12	0.30	14.48	1.97	0.30	1.54	3.99	3.39	0.228	98.31	2.86[2]	196[2]
MH08-22-3214	amph	72.58	0.41	14.78	1.86	0.30	1.46	4.34	3.42	0.242	99.39		
MH08-22-3215	amph	72.68	0.28	13.86	2.01	0.30	1.32	3.77	3.41	0.238	97.87		
MH08-22-3217	opx	72.46	0.28	13.08	2.11	0.36	1.61	2.85	2.75	0.223	95.72		
MH08-22-3218a	opx	74.61	0.46	12.96	2.40	0.73	1.03	4.09	3.28	0.225	99.79	1.44[2]	256[2]
MH08-22-3218b	opx	71.98	0.44	13.26	2.44	0.53	1.20	4.09	3.20	0.280	97.42		
MH08-22-3218c	opx	75.55	0.48	12.25	2.12	0.19	0.98	3.52	3.21	0.231	98.53		
MH08-22-3221	opx	72.01	0.14	12.54	2.05	0.31	1.44	2.75	3.28	0.240	94.75	4.56[2]	570[2]
MH08-22-3222	opx	74.55	0.41	13.09	2.16	0.23	0.97	3.70	3.55	0.217	98.86		
MH08-22-3223	opx	72.62	0.32	13.68	2.11	0.27	1.11	3.79	3.44	0.237	97.57		
MH08-22-3225	amph	74.88	0.40	12.24	2.38	0.36	0.91	3.68	3.09	0.258	98.20		
MH08-22-3232	amph	73.60	0.31	12.64	1.85	0.31	0.91	3.41	2.99	0.216	96.21		
MH08-22-3233	opx	77.27	0.35	11.34	1.78	0.17	0.69	3.35	3.35	0.189	98.50		
MH08-22-3235a	opx	76.96	0.44	11.56	1.91	0.18	0.75	3.59	3.24	0.174	98.79		
MH08-22-3235b	opx	72.48	0.40	13.63	2.24	0.27	1.14	4.14	3.48	0.265	98.05		
MH08-23-0201	plag	71.32	0.17	14.19	1.54	0.26	1.58	4.10	2.81	0.245	96.23		
MH08-23-0202a	plag	72.26	0.22	14.23	1.53	0.26	1.56	4.36	2.68	0.219	97.31	3.51[2]	908[2]
MH08-23-0202b	plag	72.63	0.36	14.46	1.48	0.25	1.58	4.53	2.59	0.206	98.09		
MH08-23-0202c	plag	72.97	0.22	14.34	1.51	0.27	1.49	5.01	2.65	0.207	98.67		
MH08-23-0210	plag	72.21	0.46	14.10	0.50	0.03	1.54	4.16	2.64	0.205	95.83		
MH08-23-0219	amph	73.97	0.30	13.15	1.41	0.02	1.26	3.92	2.72	0.192	96.95		
MH08-23-0226a	opx	71.00	0.45	15.06	1.69	0.21	1.58	5.28	2.45	0.223	97.94		
MH08-23-0228	cpx	71.17	0.45	14.99	2.23	0.23	1.34	5.58	2.37	0.199	98.57	2.51[2]	
MH08-23-0229	cpx	70.40	0.43	14.21	2.38	1.14	3.27	4.88	2.49	0.193	99.37	1.06[2]	836[2]
MH08-23-0231	cpx	70.90	0.38	14.34	1.01	0.01	1.61	4.33	2.60	0.188	95.36		
MH08-23-0232c	opx	71.13	0.39	14.33	1.48	0.03	1.74	4.03	2.50	0.199	95.83		
MH08-23-0232d	opx	70.96	0.39	14.20	1.35	0.03	1.95	4.08	2.49	0.188	95.62		
MH08-23-0233a	opx	74.02	0.22	12.17	1.76	0.09	1.12	3.39	3.04	0.196	96.00	5.10[2]	310[2]
MH08-23-0234b	opx	71.89	0.42	14.39	2.79	0.45	2.20	4.39	2.45	0.209	99.19		
MH08-23-0235	opx	71.65	0.28	13.52	1.60	0.06	1.66	3.69	2.71	0.218	95.39		
MH08-23-0240b	cpx	68.74	0.44	15.02	0.51	0.03	2.05	3.38	3.67	0.178	94.01		
MH08-23-2015	plag	73.47	0.50	14.19	0.79	0.10	1.79	3.38	2.85	0.257	97.34		
MH08-23-2022a	plag	73.75	0.30	14.39	1.64	0.25	1.68	4.39	2.82	0.227	99.45		
MH08-23-2022b	plag	71.28	0.40	13.55	1.00	0.17	1.51	3.27	2.76	0.325	94.26		
MH08-23-2035a	plag	72.74	0.26	13.44	0.59	0.05	1.57	2.80	2.59	0.219	94.26		
MH08-23-2035b	plag	73.51	0.25	13.55	1.05	0.15	1.52	3.02	2.67	0.212	95.94		
MH08-23-2037	plag	73.85	0.32	14.77	1.94	0.37	1.84	4.25	2.74	0.226	100.31		
MH08-23-2041	plag	72.77	0.41	15.08	2.11	0.53	2.87	4.31	2.13	0.200	100.41		
MH08-23-2070a	plag	70.37	0.26	13.41	1.96	0.37	1.38	2.21	4.15	0.231	94.34		
MH08-23-2070b	plag	73.78	0.14	12.42	0.87	0.15	1.27	2.76	2.59	0.180	94.15		
MH08-23-3022a	opx	72.38	0.27	13.03	2.25	0.15	1.36	3.24	3.00	0.213	95.90		
MH08-23-3022b	opx	70.77	0.44	13.79	2.48	0.34	1.67	3.72	2.51	0.265	95.98		
MH08-23-3040	opx	71.15	0.29	12.95	1.99	0.07	1.37	3.30	2.67	0.296	94.10		
MH08-23-3042b	opx	73.59	0.44	14.75	2.68	0.45	2.20	4.23	2.38	0.208	100.94		
MH08-23-3043a	opx	73.36	0.43	14.88	2.59	0.39	2.12	4.34	2.31	0.193	100.62		
MH08-23-3043b	opx	73.43	0.45	14.80	2.42	0.21	2.08	4.19	2.46	0.204	100.25		
MH08-23-3058a	opx	72.46	0.37	13.19	2.12	0.17	1.45	3.36	3.07	0.227	96.40		
MH08-23-3058b	opx	71.80	0.30	13.63	1.97	0.07	1.58	3.71	2.36	0.236	95.64		

Table 2.2 cont.		**Major Elements by EMPA**										**Volatiles by FTIR[1] and SIMS[2]**	
Melt Inclusion	host	SiO_2	TiO_2	Al_2O_3	FeO*	MgO	CaO	Na_2O	K_2O	Cl	Total	H_2O	CO_2
MH08-23-3071	amph	71.57	0.37	14.62	1.88	0.26	2.81	4.97	2.55	0.199	99.22		
MH08-23-3075a	opx	73.61	0.43	14.38	2.27	0.24	1.90	4.21	2.30	0.187	99.53		
MH08-23-3075b	opx	70.24	0.42	14.79	1.32	0.01	2.13	3.82	2.27	0.187	95.19		
MH08-23-3076	opx	72.80	0.35	14.56	1.59	0.05	2.01	3.63	2.40	0.205	97.58		
MH08-23-3081	opx	73.53	0.31	12.89	1.74	0.05	1.46	3.09	2.96	0.218	96.25		
MH08-23-3084a	opx	72.77	0.32	14.13	1.47	0.01	1.84	3.69	2.27	0.239	96.74		
MH08-23-3084b	opx	71.64	0.26	13.61	2.18	0.10	1.59	3.63	2.46	0.364	95.83		
MH08-23-3086	opx	73.84	0.24	13.02	2.00	0.06	1.25	2.83	3.06	0.226	96.52		
MH08-23-3095a	opx	72.11	0.39	14.34	1.60	0.10	1.85	3.78	2.41	0.182	96.76		
MH08-23-3095b	opx	71.46	0.36	14.61	1.66	0.05	2.25	3.61	2.28	0.179	96.45		
MH08-23-3095c	opx	72.56	0.44	14.72	2.22	0.17	2.01	4.18	2.64	0.187	99.13		
MH08-23-3097	opx	75.17	0.30	13.66	2.78	0.42	1.83	4.44	2.66	0.260	101.52		
MH08-23-3102a	opx	73.24	0.29	13.39	1.56	0.02	1.48	3.70	2.54	0.190	96.41		
MH08-23-3102b	opx	73.05	0.26	13.26	1.51	0.00	1.51	3.42	2.56	0.186	95.76		
MH08-23-3102c	opx	74.02	0.26	13.28	1.62	0.17	1.55	3.51	2.55	0.194	97.15		
MH08-23-3102d	opx	72.82	0.28	13.47	1.57	0.13	1.44	3.47	2.72	0.199	96.10		

Table 2.3: Hygrometer calculations and host composition for plagioclase-hosted melt inclusions from Mount Hood. P2005: Putirka (2005); L2009: Lange et al. (2009); HL91Ab: Housh and Luhr (1991) Albite hygrometer HL91An: Housh and Luhr (1991) Anorthite hygometer

	Hygrometers				**Host plagioclase composition by EMPA**										
Melt Inclusion	P2005	L2009	HL91Ab	HL90An	SiO_2	TiO_2	Al_2O_3	FeO*	MgO	CaO	Na_2O	K_2O	Total	An#_pl	Ab#_pl
MH08-20-0101	1.2	3.9	2.6	0.9	54.73	0.02	26.85	0.30	0.02	9.29	5.15	0.22	96.56	0.49	0.49
MH08-20-0102a	2.4	4.5	3.3	1.3	54.05	0.02	27.85	0.69	0.02	10.10	4.96	0.18	97.87	0.52	0.47
MH08-20-0102b	1.8	4.3	3.3	1.6	54.05	0.02	27.85	0.69	0.02	10.10	4.96	0.18	97.87	0.52	0.47
MH08-20-0103	1.3	3.9	2.9	1.7	56.75	0.02	27.21	0.34	0.02	9.31	5.48	0.21	99.33	0.48	0.51
MH08-20-0106	0.7	3.2	2.5	2.5	57.39	0.02	26.56	0.30	0.02	8.18	6.17	0.26	98.90	0.42	0.57
MH08-20-0230	2.9	4.4			57.02	0.03	27.79	0.27	0.01	9.37	5.70	0.24	100.42	0.47	0.52
MH08-20-0234a	4.2	4.9	3.3	0.8	56.12	0.01	28.11	0.36	0.01	10.15	5.31	0.19	100.27	0.51	0.48
MH08-20-0234b	3.8	4.8	3.2	0.8	56.12	0.01	28.11	0.36	0.01	10.15	5.31	0.19	100.27	0.51	0.48
MH08-20-0235	8.5	6.0			53.45	0.02	30.21	0.41	0.01	12.28	4.23	0.13	100.74	0.61	0.38
MH08-20-0236	2.4	4.2			57.42	0.01	27.06	0.29	0.01	8.92	5.93	0.21	99.85	0.45	0.54
MH08-20-0237a	2.7	4.2			57.93	0.01	26.63	0.29	0.02	8.63	6.10	0.24	99.85	0.43	0.55
MH08-20-0237b	2.9	4.3			57.93	0.01	26.63	0.29	0.02	8.63	6.10	0.24	99.85	0.43	0.55
MH08-20-0238	3.6	4.6			57.14	0.02	27.96	0.29	0.01	9.48	5.68	0.22	100.81	0.47	0.51
MH08-20-0239	4.0	4.7	2.5	0.7	56.63	0.01	27.28	0.27	0.02	9.46	5.61	0.21	99.49	0.48	0.51
MH08-20-2002	1.5	4.1			55.82	0.02	28.49	0.28	0.01	9.87	5.44	0.19	100.12	0.49	0.49
MH08-20-2029	1.9	4.2			57.15	0.02	28.20	0.34	0.02	9.38	5.71	0.24	101.06	0.47	0.52
MH08-20-2031a	1.2	4.1			56.00	0.02	28.91	0.28	0.01	10.26	5.17	0.19	100.83	0.52	0.47
MH08-20-2031b	2.7	4.6			56.00	0.02	28.91	0.28	0.01	10.26	5.17	0.19	100.83	0.52	0.47
MH08-20-2044b	1.2	4.0			56.57	0.01	28.19	0.32	0.02	9.24	5.70	0.22	100.28	0.47	0.52
MH08-20-2059	3.7	4.7			53.97	0.02	29.54	0.23	0.01	10.56	4.99	0.18	99.52	0.53	0.46
MH08-20-2084	2.6	4.4			55.38	0.00	29.12	0.25	0.01	10.52	4.97	0.16	100.41	0.53	0.46
MH08-20-2092	2.4	4.4			54.91	0.02	29.42	0.31	0.01	10.91	4.91	0.16	100.65	0.55	0.44
MH08-20-2098	0.2	3.3			58.25	0.01	27.44	0.30	0.02	8.45	5.99	0.26	100.74	0.43	0.55
MH08-20-2145	1.0	3.8			55.27	0.02	28.98	0.29	0.01	10.13	5.21	0.21	100.11	0.51	0.48
MH08-20-2157	2.3	4.4			55.47	0.02	28.61	0.30	0.02	9.64	5.61	0.23	99.89	0.48	0.51
MH08-20-2195	1.5	4.0			57.59	0.01	27.98	0.26	0.01	8.66	6.03	0.23	100.76	0.44	0.55
MH08-20-232	3.3	4.4			57.89	0.02	26.83	0.31	0.02	8.78	5.91	0.25	100.00	0.44	0.54
MH08-22-0103	0.9	3.5	2.5	2.8	58.53	0.01	26.52	0.32	0.01	7.91	5.94	0.28	99.52	0.42	0.57
MH08-22-0119	1.3	4.1	2.5	1.6	57.48	0.02	28.26	0.22	0.01	9.05	5.89	0.22	101.15	0.45	0.53
MH08-22-0120a	0.8	3.6	2.8	2.5	52.09	0.02	27.38	0.29	0.01	9.29	5.62	0.21	94.91	0.47	0.52
MH08-22-0120b	0.8	3.6	2.9	2.6	52.09	0.02	27.38	0.29	0.01	9.29	5.62	0.21	94.91	0.47	0.52
MH08-22-0121	2.5	4.4	3.2	1.7	54.89	0.02	27.88	0.27	0.01	9.93	5.46	0.20	98.66	0.50	0.49
MH08-22-0122	1.4	3.8	2.2	2.2	57.76	0.01	25.14	0.18	0.01	6.82	6.65	0.37	96.94	0.35	0.62
MH08-22-0123a	1.5	3.9			54.19	0.02	28.14	0.26	0.01	10.46	4.88	0.17	98.12	0.54	0.45
MH08-22-0123b	3.7	4.7	2.9	0.3	54.19	0.02	28.14	0.26	0.01	10.46	4.88	0.17	98.12	0.54	0.45
MH08-22-2019a	2.3	4.7			54.35	0.02	28.11	0.22	0.00	10.21	5.07	0.20	98.20	0.52	0.47
MH08-22-2049	4.2	4.9			54.68	0.02	27.49	0.33	0.01	9.78	5.26	0.21	97.78	0.50	0.49
MH08-22-2051	2.6	4.8			51.40	0.04	29.55	0.29	0.00	12.54	3.92	0.09	97.84	0.63	0.36
MH08-22-2054a	2.3	4.2			56.46	0.01	26.61	0.25	0.00	8.69	5.93	0.25	98.20	0.44	0.54

Table 2.3 cont.	Hygrometers				Host plagioclase composition by EMPA										
Melt Inclusion	P2005	L2009	HL91Ab	HL90An	SiO_2	TiO_2	Al_2O_3	FeO*	MgO	CaO	Na_2O	K_2O	Total	An#_pl	Ab#_pl
MH08-22-2054b	2.3	4.3			56.46	0.01	26.61	0.25	0.00	8.69	5.93	0.25	98.20	0.44	0.54
MH08-22-2054c	2.4	4.4			56.46	0.01	26.61	0.25	0.00	8.69	5.93	0.25	98.20	0.44	0.54
MH08-22-2073	2.9	4.6			54.53	0.02	27.61	0.21	0.01	9.98	5.15	0.21	97.74	0.51	0.48
MH08-22-2076a	0.6	3.6			56.39	0.01	26.46	0.26	0.01	8.50	5.97	0.27	97.87	0.43	0.55
MH08-22-2090	2.2	4.1			55.92	0.02	27.06	0.25	0.01	9.29	5.62	0.21	98.38	0.47	0.52
MH08-22-2105a	4.9	4.9			56.20	0.02	26.89	0.24	0.00	8.77	5.75	0.25	98.12	0.45	0.53
MH08-22-2105b	4.4	5.0			56.20	0.02	26.89	0.24	0.00	8.77	5.75	0.25	98.12	0.45	0.53
MH08-22-2122a	4.5	5.0			54.06	0.02	27.59	0.25	0.01	10.29	4.95	0.17	97.34	0.53	0.46
MH08-22-2122b	3.3	4.7			54.06	0.02	27.59	0.25	0.01	10.29	4.95	0.17	97.34	0.53	0.46
MH08-22-2143a	2.4	4.3			55.06	0.02	27.57	0.29	0.01	9.47	5.43	0.22	98.05	0.48	0.50
MH08-22-2143b	3.5	4.6			55.06	0.02	27.57	0.29	0.01	9.47	5.43	0.22	98.05	0.48	0.50
MH08-22-2157a	2.7	4.4			53.85	0.01	25.96	0.24	0.01	8.36	5.57	0.23	94.24	0.45	0.54
MH08-22-2157b	1.2	3.4			53.85	0.01	25.96	0.24	0.01	8.36	5.57	0.23	94.24	0.45	0.54
MH08-22-2166a	1.1	3.6			57.79	0.01	25.58	0.28	0.01	7.63	6.43	0.33	98.06	0.39	0.59
MH08-22-2166b	1.9	4.0			57.79	0.01	25.58	0.28	0.01	7.63	6.43	0.33	98.06	0.39	0.59
MH08-22-2166c	1.2	3.6			57.79	0.01	25.58	0.28	0.006	7.63	6.43	0.33	98.06	0.39	0.59
MH08-22-2191	3.7	4.7			55.04	0.02	27.50	0.25	0.005	9.62	5.42	0.20	98.05	0.49	0.50
MH08-22-2202	2.2	4.4			55.61	0.02	28.35	0.26	0.009	10.31	5.17	0.20	99.93	0.52	0.47
MH08-22-2203	2.4	4.4			55.65	0.03	28.19	0.29	0.012	10.21	5.35	0.20	99.92	0.51	0.48
MH08-22-2204a	3.8	4.9	2.8	0.0	55.38	0.02	28.58	0.29	0.013	10.75	5.05	0.17	100.26	0.54	0.45
MH08-22-2204b	2.4	4.3	3.4	1.4	55.38	0.02	28.58	0.29	0.013	10.75	5.05	0.17	100.26	0.54	0.45
MH08-22-2206	2.7	4.3	2.8	1.2	57.32	0.01	27.32	0.26	0.010	9.18	5.83	0.24	100.17	0.46	0.53
MH08-22-2211	2.6	4.3			58.19	0.01	26.76	0.31	0.010	8.52	6.02	0.24	100.05	0.43	0.55
MH08-22-2212	3.0	4.6			56.57	0.02	28.10	0.24	0.010	9.67	5.48	0.20	100.30	0.49	0.50
MH08-22-2213	4.4	5.1	2.8	0.1	55.64	0.03	28.11	0.21	0.002	10.35	5.22	0.18	99.75	0.52	0.47
MH08-22-2214	2.4	4.3	2.9	1.5	57.29	0.02	27.45	0.23	0.009	9.26	5.63	0.23	100.12	0.47	0.52
MH08-22-2215	1.8	3.9			58.36	0.02	26.13	0.31	0.026	8.16	6.00	0.32	99.33	0.42	0.56
MH08-22-2216a	2.4	4.4			55.40	0.02	28.18	0.23	0.003	10.23	5.24	0.21	99.52	0.51	0.48
MH08-22-2216b	1.4	4.0			55.40	0.02	28.18	0.23	0.003	10.23	5.24	0.21	99.52	0.51	0.48
MH08-22-2216c	2.3	4.4			55.40	0.02	28.18	0.23	0.003	10.23	5.24	0.21	99.52	0.51	0.48
MH08-22-2216d	2.8	4.6			55.40	0.02	28.18	0.23	0.003	10.23	5.24	0.21	99.52	0.51	0.48
MH08-22-2216e	2.5	4.6			55.40	0.02	28.18	0.23	0.003	10.23	5.24	0.21	99.52	0.51	0.48
MH08-22-2217	1.9	4.2	2.8	1.5	57.01	0.01	27.38	0.23	0.006	9.15	5.65	0.24	99.67	0.47	0.52
MH08-23-0201	2.1	4.0			58.86	0.01	26.34	0.31	0.016	8.17	6.28	0.27	100.26	0.41	0.57
MH08-23-0202a	2.3	3.9	3.2	3.1	59.10	0.01	26.07	0.32	0.017	7.77	6.42	0.24	99.95	0.39	0.59
MH08-23-0202b	2.4	4.0			59.10	0.01	26.07	0.32	0.017	7.77	6.42	0.24	99.95	0.39	0.59
MH08-23-0202c	2.9	4.2			59.10	0.01	26.07	0.32	0.017	7.77	6.42	0.24	99.95	0.39	0.59
MH08-23-0210	2.8	4.4			56.65	0.02	27.67	0.27	0.015	9.71	5.44	0.19	99.97	0.49	0.50
MH08-23-2015	1.7	4.1			54.85	0.02	27.70	0.32	0.016	9.76	5.20	0.18	98.05	0.50	0.49
MH08-23-2022a	2.7	4.3			56.39	0.02	26.70	0.31	0.016	9.09	5.43	0.18	98.14	0.48	0.51
MH08-23-2022b	1.8	4.0			56.39	0.02	26.70	0.31	0.016	9.09	5.43	0.18	98.14	0.48	0.51

Table 2.3 cont.	**Hygrometers**				**Host plagioclase composition by EMPA**										
Melt Inclusion	P2005	L2009	HL91Ab	HL90An	SiO_2	TiO_2	Al_2O_3	FeO*	MgO	CaO	Na_2O	K_2O	Total	An#_pl	Ab#_pl
MH08-23-2035a	1.1	3.8			56.53	0.02	27.20	0.33	0.020	9.35	5.56	0.20	99.21	0.48	0.51
MH08-23-2035b	1.4	3.9			56.53	0.02	27.20	0.33	0.020	9.35	5.56	0.20	99.21	0.48	0.51
MH08-23-2037	2.6	4.4			54.36	0.03	27.28	0.37	0.027	10.02	5.04	0.19	97.31	0.52	0.47
MH08-23-2041	1.8	3.9			55.10	0.02	27.55	0.37	0.015	9.92	5.03	0.18	98.17	0.52	0.47
MH08-23-2070a	1.5	4.8			51.35	0.02	29.79	0.29	0.013	12.60	3.81	0.10	97.98	0.64	0.35
MH08-23-2070b	2.5	4.9			51.35	0.02	29.79	0.29	0.013	12.60	3.81	0.10	97.98	0.64	0.35

Table 2.4: Fe-Ti oxide data and geothermometry. Analyses by EMPA.

	Magnetite composition (wt%)													
	EMPA											Mg	Mn	log
sample	spot #	SiO_2	TiO_2	Al_2O_3	FeO*	MnO	MgO	CaO	Cr_2O_3	V_2O_3	Total	atomic	atomic	(Mg/Mn)
MH08-08_ox01	1	0.15	11.47	1.88	76.14	0.40	1.41	0.03	0.12	0.57	92.18	1.27	0.21	0.79
MH08-08_ox01	2	0.10	12.20	1.84	76.87	0.42	1.41	0.01	0.07	0.55	93.47	1.25	0.21	0.78
MH08-08_ox01	3	0.09	12.07	1.86	76.80	0.41	1.41	0.02	0.09	0.52	93.25	1.25	0.21	0.79
MH08-08_ox01	4	0.06	11.52	1.93	76.80	0.39	1.41	0.02	0.10	0.53	92.77	1.26	0.20	0.80
MH08-08_ox01	5	0.07	11.66	1.85	76.85	0.39	1.39	0.01	0.08	0.62	92.94	1.25	0.20	0.80
MH08-08_ox01	**Ave**	**0.10**	**11.79**	**1.87**	**76.69**	**0.40**	**1.41**	**0.02**	**0.09**	**0.56**	**92.92**	**1.26**	**0.20**	**0.79**
MH08-08_ox02	1	0.08	12.09	1.69	76.95	0.40	1.49	0.03	0.11	0.49	93.33	1.32	0.20	0.82
MH08-08_ox02	2	0.06	13.21	1.46	76.66	0.40	1.56	0.04	0.08	0.46	93.93	1.38	0.20	0.83
MH08-08_ox02	3	0.04	13.30	1.43	75.56	0.44	1.58	0.09	0.08	0.45	92.97	1.41	0.22	0.81
MH08-08_ox02	4	0.05	12.60	1.51	76.80	0.41	1.55	0.08	0.07	0.48	93.56	1.38	0.21	0.82
MH08-08_ox02	5	0.04	11.46	1.62	77.50	0.40	1.49	0.01	0.09	0.48	93.08	1.33	0.20	0.82
MH08-08_ox02	**Ave**	**0.05**	**12.53**	**1.54**	**76.69**	**0.41**	**1.54**	**0.05**	**0.08**	**0.47**	**93.37**	**1.36**	**0.21**	**0.82**
MH08-08_ox03	4	0.91	10.45	2.33	77.23	0.38	1.12	0.03	0.09	0.59	93.12	0.99	0.19	0.72
MH08-08_ox03	5	0.09	10.13	2.09	78.28	0.37	1.08	0.02	0.10	0.68	92.83	0.97	0.19	0.71
MH08-08_ox03	**Ave**	**0.50**	**10.29**	**2.21**	**77.76**	**0.37**	**1.10**	**0.03**	**0.09**	**0.63**	**92.98**	**0.98**	**0.19**	**0.72**
MH08-08_ox04	1	0.06	11.91	2.50	76.33	0.35	2.09	0.01	0.07	0.70	94.02	1.83	0.17	1.03
MH08-08_ox05	3	0.05	12.58	1.55	76.81	0.38	1.61	0.03	0.10	0.44	93.55	1.43	0.19	0.87
MH08-08_ox05	4	0.28	12.43	2.03	75.58	0.34	1.65	0.03	0.03	0.44	92.81	1.46	0.17	0.93
MH08-08_ox05	**Ave**	**0.16**	**12.51**	**1.79**	**76.19**	**0.36**	**1.63**	**0.03**	**0.06**	**0.44**	**93.18**	**1.45**	**0.18**	**0.90**
MH08-08_ox08	4	0.05	11.00	1.53	77.52	0.45	1.37	0.05	0.09	0.60	92.66	1.23	0.23	0.73
MH08-08_ox08	5	0.04	12.38	1.40	76.69	0.44	1.44	0.00	0.10	0.50	92.98	1.29	0.22	0.76
MH08-08_ox08	6	0.01	13.24	1.34	76.22	0.44	1.49	0.00	0.05	0.43	93.22	1.32	0.22	0.77
MH08-08_ox08	**Ave**	**0.03**	**12.20**	**1.43**	**76.81**	**0.44**	**1.43**	**0.02**	**0.08**	**0.51**	**92.95**	**1.28**	**0.23**	**0.75**
MH08-08_ox09	1	0.06	12.33	1.58	76.39	0.42	1.54	0.06	0.09	0.40	92.85	1.37	0.21	0.81
MH08-08_ox09	2	0.04	13.73	1.31	75.32	0.50	1.52	0.04	0.05	0.38	92.88	1.36	0.25	0.73
MH08-08_ox09	**Ave**	**0.05**	**13.03**	**1.45**	**75.85**	**0.46**	**1.53**	**0.05**	**0.07**	**0.39**	**92.87**	**1.37**	**0.23**	**0.77**
MH08-08_ox10	1	0.07	10.05	1.84	78.45	0.36	1.40	0.01	0.11	0.53	92.82	1.26	0.18	0.83
MH08-08_ox11	1	0.07	9.41	1.79	78.64	0.31	1.45	0.02	0.11	0.56	92.35	1.32	0.16	0.91
MH08-08_ox11	2	0.05	10.24	1.60	78.36	0.31	1.61	0.01	0.10	0.57	92.85	1.45	0.16	0.96
MH08-08_ox11	3	0.04	11.09	1.70	77.54	0.33	1.69	0.07	0.09	0.54	93.09	1.51	0.17	0.95
MH08-08_ox11	**Ave**	**0.05**	**10.25**	**1.70**	**78.18**	**0.32**	**1.58**	**0.03**	**0.10**	**0.56**	**92.77**	**1.42**	**0.16**	**0.94**
MH08-12_ox01	4	0.08	11.33	2.00	75.23	0.39	3.57	0.11	0.02	0.40	93.13	3.13	0.19	1.21
MH08-12_ox03	1	0.13	16.75	2.34	71.43	0.33	2.62	0.10	0.05	0.49	94.23	2.24	0.16	1.15
MH08-12_ox03	2	0.09	16.58	2.43	71.85	0.37	2.66	0.03	0.04	0.54	94.60	2.27	0.18	1.10
MH08-12_ox03	3	0.10	16.81	2.39	70.75	0.35	2.71	0.27	0.00	0.52	93.89	2.33	0.17	1.14
MH08-12_ox03	**Ave**	**0.11**	**16.71**	**2.39**	**71.34**	**0.35**	**2.67**	**0.13**	**0.03**	**0.52**	**94.24**	**2.28**	**0.17**	**1.13**
MH08-12_ox04	2	0.12	17.70	1.54	72.56	0.44	1.62	0.07	0.02	0.46	94.53	1.40	0.22	0.81
MH08-12_ox04	3	0.10	17.78	1.53	72.46	0.41	1.63	0.05	0.02	0.47	94.44	1.40	0.20	0.84
MH08-12_ox04	**Ave**	**0.11**	**17.74**	**1.54**	**72.51**	**0.43**	**1.62**	**0.06**	**0.02**	**0.47**	**94.49**	**1.40**	**0.21**	**0.83**
MH08-12_ox06	1	0.08	17.68	1.30	72.47	0.47	1.41	0.02	0.02	0.43	93.88	1.23	0.23	0.72
MH08-12_ox06	2	0.09	17.17	1.34	72.91	0.50	1.48	0.02	0.05	0.44	94.00	1.29	0.25	0.72
MH08-12_ox06	3	0.06	16.09	1.43	73.97	0.43	1.47	0.05	0.03	0.41	93.94	1.29	0.22	0.78
MH08-12_ox06	**Ave**	**0.08**	**16.98**	**1.36**	**73.12**	**0.47**	**1.45**	**0.03**	**0.03**	**0.42**	**93.94**	**1.27**	**0.23**	**0.74**

Table 2.4 cont.

Ilmenite composition (wt%)

sample	EMPA spot #	SiO_2	TiO_2	Al_2O_3	FeO*	MnO	MgO	CaO	Cr_2O_3	V_2O_3	Total	Mg atomic	Mn atomic	log (Mg/Mn)
MH08-08_ox01	6	0.02	40.71	0.15	50.44	0.42	2.05	0.01	0.01	0.26	94.08	1.66	0.19	0.93
MH08-08_ox01	7	0.02	40.91	0.14	50.63	0.41	2.10	0.01	0.03	0.33	94.59	1.69	0.19	0.96
MH08-08_ox01	8	0.02	40.36	0.16	51.15	0.40	2.05	0.04	0.03	0.34	94.56	1.65	0.18	0.95
MH08-08_ox01	9	0.04	40.46	0.13	51.33	0.41	2.09	0.02	0.03	0.36	94.88	1.68	0.19	0.95
MH08-08_ox01	10	0.05	40.97	0.17	50.37	0.49	2.24	0.02	0.01	0.25	94.55	1.80	0.22	0.91
MH08-08_ox01	**Ave**	**0.03**	**40.68**	**0.15**	**50.79**	**0.43**	**2.11**	**0.02**	**0.02**	**0.31**	**94.53**	**1.70**	**0.20**	**0.94**
MH08-08_ox02	6	0.00	41.81	0.09	50.61	0.45	2.36	0.01	0.05	0.26	95.64	1.87	0.20	0.97
MH08-08_ox02	7	0.02	41.75	0.10	50.48	0.45	2.34	0.03	0.02	0.27	95.46	1.86	0.20	0.96
MH08-08_ox02	8	0.01	41.85	0.10	49.98	0.44	2.38	0.03	0.00	0.27	95.07	1.90	0.20	0.98
MH08-08_ox02	9	0.01	41.86	0.09	50.46	0.47	2.38	0.03	0.07	0.25	95.60	1.89	0.21	0.95
MH08-08_ox02	10	0.00	41.98	0.11	50.01	0.47	2.37	0.01	-0.01	0.28	95.22	1.89	0.21	0.95
MH08-08_ox02	**Ave**	**0.01**	**41.85**	**0.10**	**50.31**	**0.46**	**2.37**	**0.02**	**0.02**	**0.26**	**95.40**	**1.88**	**0.21**	**0.96**
MH08-08_ox03	1	0.02	41.57	0.12	50.24	0.48	2.14	0.04	0.03	0.26	94.91	1.71	0.22	0.89
MH08-08_ox03	2	0.28	41.34	0.19	49.41	0.49	2.11	0.22	0.02	0.31	94.37	1.70	0.22	0.88
MH08-08_ox03	**Ave**	**0.15**	**41.45**	**0.15**	**49.83**	**0.49**	**2.13**	**0.13**	**0.02**	**0.28**	**94.64**	**1.71**	**0.22**	**0.89**
MH08-08_ox04	4	0.06	36.55	0.29	47.19	0.37	3.05	0.03	0.00	0.28	87.81	2.63	0.18	1.16
MH08-08_ox05	7	0.03	42.22	0.09	50.15	0.42	2.60	0.04	-0.04	0.21	95.76	2.06	0.19	1.04
MH08-08_ox05	8	0.03	40.54	0.15	50.62	0.35	2.34	0.02	0.00	0.26	94.31	1.89	0.16	1.07
MH08-08_ox05	**Ave**	**0.03**	**41.38**	**0.12**	**50.38**	**0.38**	**2.47**	**0.03**	**-0.02**	**0.23**	**95.04**	**1.97**	**0.17**	**1.06**
MH08-08_ox08	1	0.00	41.51	0.08	50.33	0.51	2.22	0.05	0.01	0.26	94.98	1.77	0.23	0.88
MH08-08_ox08	2	0.01	41.45	0.07	50.39	0.49	2.17	0.01	0.01	0.28	94.88	1.74	0.22	0.89
MH08-08_ox08	3	0.01	41.48	0.08	50.19	0.50	2.19	0.01	0.01	0.30	94.76	1.76	0.23	0.89
MH08-08_ox08	**Ave**	**0.00**	**41.48**	**0.08**	**50.30**	**0.50**	**2.19**	**0.02**	**0.01**	**0.28**	**94.87**	**1.76**	**0.23**	**0.89**
MH08-08_ox09	3	0.01	41.31	0.10	49.96	0.43	2.34	0.03	0.01	0.29	94.49	1.88	0.19	0.98
MH08-08_ox09	4	0.03	41.16	0.09	49.61	0.46	2.29	0.02	0.02	0.30	93.97	1.85	0.21	0.94
MH08-08_ox09	**Ave**	**0.02**	**41.24**	**0.10**	**49.79**	**0.44**	**2.31**	**0.03**	**0.01**	**0.29**	**94.23**	**1.86**	**0.20**	**0.96**
MH08-08_ox10	3	0.01	41.49	0.10	49.83	0.48	2.29	0.03	0.03	0.28	94.53	1.84	0.22	0.93
MH08-08_ox11	4	0.01	41.05	0.13	49.85	0.43	2.65	0.01	0.01	0.24	94.37	2.13	0.20	1.03
MH08-08_ox11	5	0.01	41.01	0.09	50.31	0.38	2.52	0.02	0.00	0.35	94.68	2.02	0.17	1.07
MH08-08_ox11	6	0.00	41.13	0.13	50.20	0.40	2.47	0.11	0.00	0.32	94.77	1.98	0.18	1.04
MH08-08_ox11	**Ave**	**0.01**	**41.06**	**0.12**	**50.12**	**0.40**	**2.55**	**0.05**	**0.00**	**0.30**	**94.61**	**2.04**	**0.18**	**1.05**
MH08-12_ox01	1	0.03	40.58	0.20	48.19	0.35	5.01	0.08	-0.01	0.23	94.67	3.95	0.16	1.40
MH08-12_ox03	4	0.03	45.17	0.18	45.56	0.37	3.79	0.09	0.03	0.32	95.54	2.95	0.16	1.25
MH08-12_ox03	5	0.04	43.87	0.22	46.78	0.34	3.54	0.05	0.00	0.34	95.18	2.78	0.15	1.26
MH08-12_ox03	6	0.12	43.37	0.21	44.52	0.34	3.60	1.51	0.02	0.28	93.95	2.85	0.15	1.27
MH08-12_ox03	**Ave**	**0.06**	**44.14**	**0.20**	**45.62**	**0.35**	**3.64**	**0.55**	**0.01**	**0.31**	**94.89**	**2.86**	**0.16**	**1.26**
MH08-12_ox04	5	0.01	45.59	0.05	47.29	0.48	2.44	0.03	0.02	0.29	96.20	1.91	0.21	0.95
MH08-12_ox04	6	0.56	44.90	0.36	45.71	0.49	2.39	0.08	0.01	0.24	94.74	1.88	0.22	0.93
MH08-12_ox04	**Ave**	**0.29**	**45.24**	**0.20**	**46.50**	**0.48**	**2.41**	**0.06**	**0.01**	**0.27**	**95.47**	**1.89**	**0.22**	**0.94**
MH08-12_ox06	4	0.03	45.72	0.03	47.66	0.56	2.23	0.04	0.00	0.31	96.58	1.74	0.25	0.84
MH08-12_ox06	5	0.03	45.42	0.04	47.34	0.48	2.31	0.03	0.00	0.25	95.90	1.81	0.21	0.93
MH08-12_ox06	6	0.04	45.17	0.06	47.14	0.52	2.28	0.17	0.02	0.23	95.63	1.79	0.23	0.89
MH08-12_ox06	**Ave**	**0.03**	**45.44**	**0.04**	**47.38**	**0.52**	**2.27**	**0.08**	**0.01**	**0.26**	**96.03**	**1.78**	**0.23**	**0.89**

Table 2.4 cont.

Geothermometry	Ghiorso & Evans (2008):			Andersen & Lindsley 1985	
sample	T ˚C (Fe-Ti exchange)	log10 fO_2 (relative to NNO)	T ˚C (Fe-Mg exchange)	T	log10 fO_2
MH08-08_ox01	946	0.72	1143	914	-11.04
MH08-08_ox01	961	0.68	1104	924	-10.92
MH08-08_ox01	967	0.73	1104	928	-10.81
MH08-08_ox01	955	0.76	1095	919	-10.91
MH08-08_ox01	950	0.70	1042	915	-11.03
MH08-08_ox01	**956**	**0.72**	**1098**	**920**	**-10.94**
MH08-08_ox02	953	0.65	1074		
MH08-08_ox02	976	0.60	1109		
MH08-08_ox02	977	0.56	1119		
MH08-08_ox02	961	0.62	1106		
MH08-08_ox02	927	0.65	1106		
MH08-08_ox02	**959**	**0.62**	**1103**	**921**	**-11**
MH08-08_ox03	918	0.71	860		
MH08-08_ox03	900	0.69	841		
MH08-08_ox03	**909**	**0.70**	**851**	**891**	**-11.41**
MH08-08_ox04	**1003**	**1.00**	**792**	944	-10.44
MH08-08_ox05	958	0.60	1053		
MH08-08_ox05	979	0.72	1120		
MH08-08_ox05	**969**	**0.66**	**1087**	**928**	**-10.87**
MH08-08_ox08	921	0.69	1085		
MH08-08_ox08	955	0.62	1125		
MH08-08_ox08	975	0.58	1130		
MH08-08_ox08	**950**	**0.63**	**1113**	**916**	**-11.05**
MH08-08_ox09	958	0.64	1108		
MH08-08_ox09	990	0.55	1091		
MH08-08_ox09	**974**	**0.60**	**1100**	**932**	**-10.86**
MH08-08_ox10	**895**	**0.75**	**1085**		
MH08-08_ox11	888	0.83	935		
MH08-08_ox11	907	0.80	1102		
MH08-08_ox11	929	0.75	1153		
MH08-08_ox11	**908**	**0.79**	**1063**	**888**	**-11.34**
MH08-12_ox01	**972**	**0.96**	**997**		
MH08-12_ox03	997	0.09	1064		
MH08-12_ox03	1028	0.32	1177		
MH08-12_ox03	1013	0.17	1172		
MH08-12_ox03	**1013**	**0.19**	**1138**	**985**	**-10.47**
MH08-12_ox04	991	-0.10	1141		
MH08-12_ox04	977	-0.22	1157		
MH08-12_ox04	**984**	**-0.16**	**1149**	**958**	**-11.23**
MH08-12_ox06	990	-0.13	1090		
MH08-12_ox06	978	-0.10	1116		
MH08-12_ox06	955	-0.06	1162		
MH08-12_ox06	**974**	**-0.10**	**1123**	**951**	**-11.23**

CHAPTER THREE

CONDITIONS OF MAGMA MIXING IN ANDESITIC VOLCANOES AS RECORDED IN AMPHIBOLE: EVIDENCE FROM MOUNT HOOD, OREGON

Alison M. Koleszar
Adam J. R. Kent

This manuscript is in preparation for submission to:
Earth and Planetary Science Letters
3251 Riverport Lane
Maryland Heights, MO 63043
USA

ABSTRACT

Lavas erupted from mixing-dominated andesitic volcanoes typically contain multiple populations of amphiboles that record parent magma compositions, temperatures, and pressures prior to mixing. These pre-mixing characteristics can be used to constrain the plumbing structure of the magma supply system below and to describe general models for plumbing systems below different style volcanoes. This is shown for Mount Hood, Oregon, and other recharge-driven intermediate volcanoes such as Soufriére Hills Volcano, Unzen Volcano, and Mont Pelée, where bimodal amphiboles record crystallization in a two-part magmatic system, consisting of two chemically distinct magma bodies at separate pressures and temperatures. These observations suggest similar plumbing systems and mixing mechanisms for many recharge-driven intermediate volcanoes. The bimodal amphibole compositions (Magnesiohornblende and Tschermakitic pargasite) from these volcanoes are notably distinct from the continuum of amphibole compositions from volcanoes such as Mount St. Helens, where mixing is more complicated than simple binary recharge. In non-binary systems, amphiboles display a continuum of compositions inconsistent with simple bimodality and suggest multiple cycles of recharge, mixing and/or hybridization, and storage.

INTRODUCTION

Magma mixing at intermediate composition arc volcanoes is a fundamental process that controls the initiation of eruptions (Eichelberger, 1980; Murphy et al., 1998), the composition of erupted lavas (Anderson, 1976; Kent et al., 2010; Reubi and Blundy, 2009), and the style of eruption (Koleszar et al., in review; Ruprecht and Bachmann,

2010; Sparks and Sigurdsson, 1977). A significant number of intermediate arc volcanoes exhibit recharge-driven behavior (Kent et al., 2010), where nearly every eruption is initiated by mixing between two parental magmas that are compositional endmembers: one that is relatively silicic, and one that is comparatively mafic (e.g., Anderson, 1976; Eichelberger, 1978; Kent et al., 2010). As a result, the compositions of these parent magmas and their physical properties such as temperature and viscosity, as well as the depth and conditions of magma storage prior to mixing, play important roles in determining the behavior of these volcanic systems, and identifying the characteristics of pre-mixing parent magmas is crucial for assessing the dynamics of intermediate arc volcanoes.

Identifying the true parental endmember compositions involved in magma mixing is inherently difficult, however, as the mixing proportions of the two parent magmas dictate the final bulk compositions of hybrid erupted magmas. Mafic enclaves can suggest a starting point for estimates of the endmember mafic composition, but these often consist of material that has been partially hybridized or reflect loss of melt via filter pressing or other mechanisms (e.g., Bacon, 1986; Humphreys et al., 2009a; Tepley et al., 1999). Melt inclusions in intermediate systems often only trap melts derived from the more silicic parent magma, and mafic melt inclusions are nearly absent in lavas with >60 wt% SiO_2, even where significant magmatic contributions have come from a more mafic parent (Koleszar et al., in review; Reubi and Blundy, 2009). In addition, as erupted lavas are mixtures that form shortly before eruption and therefore do not represent equilibrium assemblages, it can be difficult to locate mineral-mineral or mineral-liquid pairs that are truly in equilibrium and experimental studies may be misleading unless the

different chemical, thermal, and physical characteristics of the relevant magmas are considered, both before and after mixing (e.g., Pichavant et al., 2007; Putirka, 2008). All of these characteristics of mixed-magma systems contribute to the difficulty in determining the parent magma compositions and conditions that lead to recharge, mixing, and eventual eruption.

Alternatives to studies of bulk magma compositions or melt inclusions are studies of individual crystals or crystal populations within mixed magmas. As the re-equilibration timescales of most silicate crystalline phases are considerably slower than the timescales of magma mixing and eruption (e.g., Kent et al., 2010; Venezky and Rutherford, 1999), phenocrysts can preserve considerable information about composition and storage conditions of pre-mixing parental magmas (e.g., Gerlach and Grove, 1982; Grove et al., 1988; Humphreys et al., 2009a; Tepley et al., 1999). Previous studies have shown that high-An plagioclase and pargasitic amphibole may be carried in ascending mafic magma (Pichavant et al., 2002), and that mixed intermediate lavas often contain crystal cargo derived from both the mafic and silicic parent magmas prior to eruption (e.g., Humphreys et al., 2009a; Kent et al., 2010; Martel et al., 2006). Crystal size distributions (CSDs) also commonly reveal two populations of phenocrysts (where 'phenocryst' is used as a textural descriptor and has no genetic connotations) representing crystals derived from two distinct magmas that are subsequently hybridized before eruption (e.g., Gourgaud et al., 1989; Hammer et al., 1999; Higgins, 1996; Humphreys et al., 2009a; Humphreys et al., 2009b; Kent et al., 2010; Morrissey, 1997; Pichavant et al., 2002; Sato et al., 1999).

Studies of crystalline phases offer several means for constraining the composition, origin, and pre-mixing storage conditions of the magmas that are involved in magma mixing. Crystal assemblages can also be used to examine phase stability relations, often in concert with major element compositions. Compositional data, together with the application of appropriate geothermometers and geobarometers (e.g., Ghiorso and Evans, 2008; Holland and Blundy, 1994; Ridolfi et al., 2010), can provide information on the storage conditions prior to magma mixing. Modal abundances and CSDs can be used to determine the proportions and sizes of crystalline phases contributed by each parental magma (e.g., Kent et al., 2010; Salisbury et al., 2008). Trace element abundances in phenocrysts can also be used to indicate the sources and evolutionary paths of parental magmas, and trace element profiles can be used to estimate residence times (e.g., Morgan et al., 2004; Singer et al., 1995). Magmatic volatile abundances and fugacities can be estimated from the composition of volatile-bearing phases (e.g., biotite, anhydrite, and amphibole) and measurement of volatiles trapped in melt inclusions within phenocrysts (e.g., Anderson, 1974; Scaillet and Evans, 1999; Wallace, 2005).

In this study we explore the potential for using amphibole compositions in mixed lavas to constrain the pre-mixing storage conditions and compositions of magmas at Mount Hood, Oregon, an andesite-dacite composition arc volcano where erupted magma compositions are controlled by mixing between broadly basaltic and rhyolitic magmas (Kent et al., 2010). We present data for the compositions of amphiboles that demonstrate the presence two distinct populations. Amphibole is a particularly valuable investigative phase in these rocks as it can be used to estimate temperatures and pressures of mineral formation (e.g., Ernst and Liu, 1998; Ridolfi et al., 2010; Rutherford and Devine, 1988),

can constrain activities of some volatile phases (e.g., Ridolfi et al., 2008; Ridolfi et al., 2010; Rutherford and Devine, 1988; Scaillet and Evans, 1999), and has concentrations of rare earth elements (REE) and other trace elements that are high enough to measure using in-situ techniques (e.g., Rowe et al., 2008) and can be used as geochemical indicators of parent magma composition. In addition, under suitable pressure and temperature conditions, amphibole is stable in H_2O-saturated silicic magmas that have a wide range of bulk compositions, from basaltic to rhyolitic (Ridolfi et al., 2010 and references therein).

We use our geochemical data to constrain the structure of the magma supply system below Mount Hood, and we also compare our results with published data from other recharge-driven intermediate volcanic systems at Unzen Volcano, Soufriére Hills Volcano, and Mont Pelée. Geothermobarometry based on amphibole from all of these systems (Ridolfi et al., 2010) clearly indicates two regions of amphibole formation, consistent with magma storage and crystallization in two distinct storage zones. These observations suggest a general model for the plumbing systems of recharge-driven intermediate volcanoes. By comparison, at Mount St. Helens, where mixing is more complicated than simple binary recharge (e.g., Pallister et al., 2008; Streck et al., 2008), phenocrysts display a continuum of compositions inconsistent with simple bimodality and suggest multiple cycles of recharge, mixing and/or hybridization, and storage.

SAMPLES AND ANALYTICAL METHODS

Samples

Amphiboles included in this study were taken from five prismatically-joined blocks (PJBs), one dacitic inclusion, and two mafic enclaves that were collected from

Mount Hood in 2008-2009. These samples are representative of the three most recent eruptive periods at Mount Hood (Old Maid ~200 years ago, Timberline ~1500 years ago, and Polallie 13,000-20,000 years ago). The PJBs have an extremely restricted compositional range and all contain 63.1-63.8 wt% SiO_2, the dacitic inclusion contains 63.4 wt% SiO_2, and the mafic enclaves contain 58.1-59.4 wt% SiO_2 (see Chapter Four). Amphibole compositions were measured in thin sections from each of these samples and screened for valid formulae (i.e., charge-balanced) using the criteria for calcic-amphiboles described in Ridolfi et al. (2010) and Leake et al. (1997).

Major elements

Major and minor elements, together with Cl and F in amphibole were determined by Electron Microprobe Analysis (EMPA) at Oregon State University using a Cameca SX-100 with 15 kV accelerating voltage and 30 nA probe current. Well-characterized mineral and oxide standards were used for calibration. Count times were 20 s on peak (10 s on background) for all elements except Al_2O_3, which had a peak count time of 15 s (7.5 s for background). All data reported here are for analyses in amphibole cores unless stated otherwise (as for transects). Analytical uncertainty (as assessed by replicate analyses of Kakanui hornblende) was typically < 1% for SiO_2, Al_2O_3, FeO^T, MgO, and TiO_2; < 4% for Na_2O, CaO, K_2O, and F; and < 15% for Cl.

Trace elements

Trace elements were analyzed by Laser Ablation Inductively Coupled Plasma Mass Spectrometry (LA-ICP-MS) in the W.M. Keck Collaboratory for Plasma Mass

Spectrometry at Oregon State University using a procedure similar to that described in Kent and Ungerer (2006), and these data were used to calculate Eu-anomalies. A NewWave DUV 193 nm ArF Excimer Laser was used for ablation with a 40 μm spot size, pulse rate of 4 Hz, ablation time of 45 s, and carrier gas (He) flowing at 0.8 L/min. Ablated material was analyzed on a VG PQ ExCell quadrupole ICP-MS using NIST-612 and GSE-1G as calibration standards, with trace element concentrations measured relative to ^{43}Ca as an internal standard. Eu-anomalies (Eu/Eu*) were calculated as $Eu_N/[(Sm_N + Gd_N)/2]$, where the subscript N indicates concentrations that are normalized to pyrolite using the normalization scheme of McDonough and Sun (1995). Analytical uncertainty (as assessed by replicate analyses) for Eu, Sm, and Gd was within 3% (resulting in total uncertainty of ~5 % (1σ) in Eu/Eu*).

RESULTS AND DISCUSSION

Amphibole composition

The amphiboles in this study are classified based on their core composition (Table 3.1) determined by Electron Microprobe (EMP) and fall into two groups: Tschermakitic pargasite (hereafter referred to as Tsch-pargasite) or Magnesiohornblende (Mg-hornblende) when described using the calcic-amphibole classification of Leake et al. (1997) as modified by Ridolfi et al. (2010). These compositions are notably bimodal: Tsch-pargasites from Mount Hood have >11 wt% Al_2O_3 and <45 wt% SiO_2, whereas Mg-hornblendes have <10 wt% Al_2O_3 and >45 wt% SiO_2 (Fig. 3.1b, c). Although the ranges of Cl concentrations and Mg# overlap between the two amphibole groups, the Tsch-pargasites typically have lower Cl and extend to higher Mg# than the Mg-hornblendes

(Fig. 3.1d). Mg-hornblendes have Eu/Eu* <1, whereas this large Eu-anomaly is generally absent from the Tsch-pargasites (Fig. 3.1a). Both species of amphibole range in size from <100 μm to >1000 μm and vary from nearly euhedral to anhedral. Breakdown rims on Mg-hornblende vary in thickness from 0 μm to ~50 μm in thickness; rims on Tsch-pargasite vary from 0 μm to ~20 μm.

Previous studies indicate that the andesites and dacites erupted at Mount Hood are the result of mixing between mafic and silicic magmas shortly before eruption (Darr, 2006; Kent et al., 2010; Woods, 2004); the presence of two populations of amphiboles with distinctly different compositions in these erupted lavas is consistent with crystalline material from each of these pre-eruptive parental magmas supplying amphibole to the erupted hybridized lavas. A similar observation has been made for plagioclase in these lavas (Kent et al., 2010). In the following section we constrain the composition of parental melts that produced each of the amphibole populations we have identified.

Parent magma compositions

For elements with well-constrained mineral-melt partition coefficients, amphibole compositions can be used to characterize the composition of coexisting melts. Lower SiO_2 in the parent melt will drive the reaction pargasite + $4SiO_2$ = albite + hornblende (Holland and Blundy, 1994) to the left, thus high Al_2O_3 Tsch-pargasites are consistent with low SiO_2 activity in the parent melt whereas low Al_2O_3 Mg-hornblendes are indicative of a parent melt with higher SiO_2 activity. As a result, ratios of (molar) Al/Si in amphiboles are strongly linked to the Al/Si ratio of the melt from which they are extracted, and populations of amphiboles that are produced from compositionally distinct

parental melts will have different Al/Si ratios. Sisson and Grove (1993) found $K_D^{Al\text{-}Si}$ to be relatively insensitive to bulk composition for melts ranging from high-alumina basalt to high-silica rhyolite, and it can thus be used to constrain the composition of melts that crystallize amphibole. This is useful particularly useful in plagioclase-phyric magmas such as those at Mount Hood, as the primary driver of melt Al/Si is plagioclase crystallization.

The Al/Si ratios of Tsch-pargasites from Mount Hood range from 0.31 to 0.38 (Table 3.1), consistent with melt Al/Si ratios of 0.29-0.35 based on a $K_D^{Al\text{-}Si}$ of 0.94 (Sisson and Grove, 1993). Kent et al. (2010) used a combination of textural and compositional data to estimate the composition of the pre-mixing mafic endmember at Mount Hood, which has an Al/Si ratio of 0.38-0.56. This suggests that the Al/Si ratio of this magma is therefore too high (essentially "too primitive") to be the source of the Mount Hood Tsch-pargasites, which likely crystallized from a melt with Al/Si 0.29-0.35 (Fig. 3.2). The Al/Si ratio for calculated endmember indicates the bulk (magma) Al/Si ratio, however, not the Al/Si ratio of the melt. Incrementally removing equilibrium plagioclase (composition determined using MELTs, Ghiorso and Sack, 1995) from this bulk composition allows us to estimate a melt composition for this endmember, which matches the Al/Si ratio necessary to crystallize Mount Hood Tsch-pargasite once ~25% plagioclase is removed (Fig. 3.2). This degree of crystallization falls within the range of 23-37% suggested by Kent et al. (2010) for the crystallinity of the parental endmembers at Mount Hood. The calculations suggest that although the pre-mixing mafic endmember at Mount Hood started out as too primitive to be the source of the Tsch-pargasites, magma evolution (i.e., plagioclase crystallization) results in a melt composition in

equilibrium with these amphiboles. A reasonable scenario is that amphibole forms after a period of cooling and crystallization when the mafic melt cools sufficiently to allow amphibole saturation (~970°C; Fig. 3.4). We also note that amphibole formation therefore requires plagioclase fractionation (i.e., crystal-liquid separation), specifically the crystallization of anorthitic plagioclase with Al/Si greater than the Al/Si ratio of the melt.

Mg-hornblendes from Mount Hood have Al/Si ratios that range from 0.17 to 0.25, consistent with a silicic parent magma with Al/Si ratios between 0.18-0.26 (Fig. 3.2) assuming $K_D^{Al\text{-}Si} = 0.94$ (Sisson and Grove, 1993). Melt inclusions from Mount Hood trap high-silica (dacite to rhyolite) melts with Al/Si ratios that range from 0.17 to 0.26 (Koleszar et al., in review), and the silicic endmember calculated by Kent et al. (2010) has an estimated magma Al/Si of 0.21-0.27. We can estimate the Al/Si ratio of the melt by incrementally removing equilibrium plagioclase calculated using the MELTs algorithm, as described above (Ghiorso and Sack, 1995). Removing up to ~20% of this plagioclase from the magma results in Al/Si ratios consistent with a melt in equilibrium with Mg-hornblende from Mount Hood. Both of these melt compositions (high-Si melts trapped in melt inclusions and the estimated silicic melt endmember) therefore represent potential parent melts from which the Mg-hornblende crystallized (Fig. 3.2).

The $K_D^{Fe\text{-}Mg}$ between amphibole and melt varies strongly with the silica content of the melt (Sisson and Grove, 1993). For melts ranging from high-Al basalt to aluminous andesite, $K_D^{Fe\text{-}Mg}$ varies between 0.35-0.38, whereas $K_D^{Fe\text{-}Mg}$ for rhyolite may be closer to 0.01(Sisson and Grove, 1993). The relatively restricted range of $K_D^{Fe\text{-}Mg}$ for more mafic melts allows us to estimate a Fe/Mg ratio for the melt from which the Mount Hood Tsch-

pargasites crystallized (where Fe = Fe^{Total}). These amphiboles have Fe/Mg ratios that range from 0.38 to 0.68. Using the range of K_D^{Fe-Mg} of 0.35-0.38 suggested by Sisson and Grove (1993) for high-Al basalt to aluminous andesite, the mafic parental melt for these amphiboles would have Fe/Mg ratios of 1.0-1.8 (Fig. 3.3). The mafic endmember composition calculated by Kent et al. (Kent et al., 2010) has a Fe/Mg ratio of 0.7-1.1. These calculations suggest that at K_D^{Fe-Mg} of ~0.37, the Fe/Mg ratios for the calculated mafic endmember overlap with the Fe/Mg ratio of the melt from which Tsch-pargasite would have crystallized (Fig. 3.3).

Calculated Eu-anomalies in amphiboles in lavas at Mount Hood also suggest the presence of two parent magmas of different compositions (Table 3.2): Mg-hornblendes have Eu/Eu* << 1 (0.52 ± 0.11; 1σ) consistent with crystallization from a silicic melt that has experienced extensive plagioclase crystallization (Fig. 3.1a). Tsch-pargasites from Mount Hood have less significant Eu anomalies (0.95 ± 0.21; 1σ) (Fig. 3.1a), suggesting that the mafic source for these amphiboles has not lost as much Eu through plagioclase crystallization as the more silicic source for the Mg-hornblendes. If we consider the above estimate that the parental mafic melt may have lost up to 25% plagioclase to reach Al/Si ratios in equilibrium with the observed amphiboles, we can calculate the effect of this on melt Eu/Eu* ratios.

The compatibility of Eu is highly redox sensitive and increases greatly at lower fO_2 (Aigner-Torres et al., 2007). Partition coefficients for anorthitic plagioclase in a basaltic melts at log fO_2 = -12.19 are D_{Eu} = 0.966, D_{Sm} = 0.075, and D_{Gd} = 0.05, but at log fO_2 = -8.65, D_{Eu} decreases dramatically to 0.098 whereas D_{Sm} and D_{Gd} only vary by a factor of 1-2 (Aigner-Torres et al., 2007). The compositions of Tsch-pargasites from

Mount Hood suggest that log fO_2 ranges from -9.2 to -10.5 in the mafic parental magma (Ridolfi et al., 2010) and Fe-Ti oxide compositions suggest that log fO_2 in the erupted mixed lava ranges from -10.4 to -11.4 (Anderson and Lindsley, 1985), so the applicable D_{Eu} for the mafic parental magma is likely in between the values suggested by Aigner-Torres et al. (2007). Using partition coefficients for the more reducing conditions (i.e., fO_2 = -12.19), we find that removing 25% plagioclase decreases Eu/Eu^*_{Melt} from 1.0 to 0.77 (Fig. 3.2). The Eu-anomaly of the amphibole (Eu/Eu^*_{Amph}) in equilibrium with this melt will decrease from 0.85 to 0.65, a smaller decrease than the range of Eu-anomalies present within Tsch-pargasites from Mount Hood ($Eu/Eu^*_{Amph} = 0.95 \pm 0.21$). For less reducing conditions (i.e., fO_2 = -8.65), Eu/Eu^*_{Melt} only decreases from 1.06 to 1.03, and Eu/Eu^*_{Amph} decreases from 0.85 to 0.83. Thus, even at the most reducing conditions, the changes to Eu/Eu* associated with the removal of ~25% plagioclase from the mafic parental melt are within the range of variation in Tsch-pargasite from Mount Hood, and removal of plagioclase is a thus a viable process to generate a magma in equilibrium with these amphiboles.

Geothermobarometry

Previous studies have outlined the difficulty in estimating pre-eruptive magmatic temperatures and pressures in volcanic systems (e.g., Putirka, 2008; Ridolfi et al., 2008). Pressure estimates are particularly challenging, subject to large errors, and prone to giving inconsistent results, as described by Bachmann and Dungan (2002) and Ridolfi et al. (2008). Furthermore, as Ridolfi et al. (2008) note, barometers that rely solely on Al-in-hornblende overestimate pressure by an average of 2.8 kbar, whereas barometers that

consider both Al-in-hornblende and temperature give pressure estimates that are, on average, 3.5 kbar too low. A recent geothermobarometer (Ridolfi et al., 2010) considers Al_T (total aluminum), $^{[6]}Al^*$ (octahedral aluminum index), Mg* (magnesium index), and Si* (silicon index) in calcic amphiboles that crystallized from calc-alkaline magmas, and relies on the observation that amphibole crystallization primarily occurs close to the amphibole stability curve (where small pressure and/or temperature changes will result in amphibole instability). Ridolfi et al. (2010) demonstrate that results from this geothermobarometer (with temperature uncertainties of ± 22˚C and pressure uncertainties of 11-25%) generally agree with temperature and pressure estimates from other methods, including temperatures from Fe-Ti oxide and plagioclase-hornblende geothermometry, and barometry from seismic imaging of magma chambers and volatile saturation in melt inclusions.

Pre-eruptive temperatures for Mount Hood from plagioclase-hornblende geothermometry (Holland and Blundy, 1994) and Fe-Ti oxide geothermometry (Ghiorso and Evans, 2008), and pressure estimates from volatile concentrations in melt inclusions (Newman and Lowenstern, 2002; Papale et al., 2006) suggest that the geothermobarometer of Ridolfi et al. (2010) provides realistic estimates for the P-T conditions for the Mount Hood system (Fig. 3.4; Koleszar et al., in review). Additionally, the use of a single phase (amphibole) avoids problems associated with finding two phases that are in true equilibrium with each other, which can be particularly challenging in mixed magmas that contain multiple populations of phenocrysts (and which may also be extensively zoned), but is necessary for methods such as plagioclase-hornblende geothermometery (Holland and Blundy, 1994) and Fe-Ti oxide geothermometry

(Anderson and Lindsley, 1985; Ghiorso and Evans, 2008). Although equilibrium between Fe-Ti oxides can be verified chemically (Bacon and Hirschmann, 1988) for use in the Fe-Ti oxide geothermometer, oxides re-equilibrate rapidly and are therefore unsuitable for identifying magma temperatures during storage in a magma chamber prior to eruption.

Pressures calculated from H_2O and CO_2 concentrations in melt inclusions (Newman and Lowenstern, 2002; Papale et al., 2006) can also be problematic for obtaining a comprehensive view of volcanic plumbing systems. Results from this method can only be used to estimate minimum entrapment pressures, and require that volatiles are not lost subsequent to melt inclusion entrapment or that trapped melts are not supersaturated prior to entrapment. Additionally, intermediate mixed magmas frequently lack any melt inclusions derived from the hotter, more mafic recharge magma (Reubi and Blundy, 2009), thus pressure estimates from inclusions may only represent the cooler, more silicic parental magma. This is the case with melt inclusions from Mount Hood (Fig. 3.4), which only record pressures associated with the shallow silicic magma body (Koleszar et al., in review). Therefore we use the calculations of Ridolfi et al. (2010) to estimate pre-eruptive temperatures and pressures for lavas erupted from Mount Hood, which allows us to identify two parent magmas with different compositions and storage conditions. These calculations also allow us compare our results to pressures and temperatures for other volcanoes.

Geothermobarometry for Mount Hood

The bimodality of amphiboles evident in compositional data (Fig. 3.1) from Mount Hood is also particularly striking on a P-T diagram (Fig. 3.4), and suggests that Mg-hornblendes from Mount Hood crystallized from a relatively low pressure (< 200 MPa) and low temperature (< 880˚C) magma, whereas the Tsch-pargasites indicate the presence of a higher pressure (> 250 MPa), higher temperature (> 910˚C) magma (Fig. 3.4). The temperature estimate from Tsch-pargasites is likely a minimum temperature for the mafic-derived amphiboles, as the mafic parental magma would have cooled and evolved before amphibole would be stable and able to crystallize (see section 3.2). Although the maximum temperature for Tsch-pargasite stability is ~1000°C (Ridolfi et al., 2010), the estimated liquidus temperature for the mafic Mount Hood endmember is ~1140˚C calculated from MELTs (Ghiorso and Sack, 1995). These P-T results, when combined with the compositional data discussed in section 3.2 and other studies (Gourgaud et al., 1989; Humphreys et al., 2009a; Murphy et al., 1998; Sato et al., 1999) allow us to constrain the nature of the plumbing system and processes that lead to formation of hybridized erupted magmas, which we discuss in Section 4.

Our interpretation of bimodal amphibole populations, informed by our P and T estimates and other data, also differs in some respects from earlier studies. Sato et al. have suggested that Tsch-pargasites in intermediate lavas from Unzen Volcano represent groundmass amphiboles that crystallized after mixing and hybridization (Sato et al., 1999), rather than crystallizing early from a deeper, hotter source as we propose. In contrast, Humphreys et al. (2009a) recognized the mafic source for Tsch-pargasite and suggested that their presence in the groundmass of intermediate lava from Soufriére Hills

Volcano is the result of the disaggragation of mafic enclaves. Pressures calculated using by geothermobarometer (Ridolfi et al., 2010) indicate that Tsch-pargasites from Mount Hood formed at higher pressures than Mg-hornblendes, consistent with the interpretation that the Tsch-pargasites formed in a parent mafic magma prior to recharge and predate the crystallization of the groundmass (Figs. 3.4-3.5). If these pressure estimates are accurate then they largely preclude formation of Tsch-pargasites as groundmass phases following mixing.

Zoning patterns within amphibole are also consistent with early crystallization of Tsch-pargasite, prior to magma mixing. Although many amphiboles in this study are unzoned, some (~5%) amphiboles are composed of a Tsch-pargasite or Mg-hornblende core that is surrounded by a rim of intermediate-Al_2O_3 (9.5-11 wt%) (Fig. 3.6c). This is consistent with early formation of the amphibole cores in either a deep mafic or shallow silicic magma chamber, followed by rim growth that occurs after mixing to produce intermediate magma. Proteau and Scaillet (2003) also observed high-Al_2O_3 cores in amphiboles from Mount Pinatubo, which they interpreted as evidence of high-pressure crystallization prior to magma injection into a shallow reservoir.

We also observe evidence for two separate magma bodies in the consistent differences in Cl content between the two populations of amphibole at Mount Hood (Fig 1d). Sato et al. observed similar characteristics at Unzen Volcano and suggested that the lower Cl concentrations in Tsch-pargasites are the result of crystallization from a partially degassed magma at shallow depths (Sato et al., 2005), however we note that the high-Al contents of these amphiboles (both at Mount Hood and Unzen Volcano) are consistent

with crystallization at greater depth than the Mg-hornblendes (Figs. 3.1a, 3.7). Therefore, an alternative explanation for the low Cl concentrations in Tsch-pargasite is required.

The partition coefficient for Cl/OH ($K_D^{Cl\text{-}OH}$) in amphibole is compositionally dependent, and depends on both the Fe/Mg ratio of the amphibole and the Cl/OH ratio of the parental melt from which it crystallized (Humphreys et al., 2009b; Sato et al., 2005). Relative to OH, Cl will preferentially enter amphibole with high Fe/Mg (Humphreys et al., 2009b; Sato et al., 2005), so $K_D^{Cl\text{-}OH}$ is higher in amphiboles with high Fe/Mg. We observe overlapping ranges of Fe/Mg for Tsch-pargasite and Mg-hornblende from Mount Hood (Fig. 3.3), however, so the effects of the Fe/Mg ratio in amphibole cannot be the sole reason for the high Cl contents of the Mg-hornblendes relative to Tsch-pargasite. The other control on the Cl contents of amphibole is the Cl/OH ratio of the parental melt (Humphreys et al., 2009b; Sato et al., 2005), and melts with higher Cl/OH ratios will produce amphiboles with higher Cl/OH ratios (and therefore higher Cl concentrations, since Cl and OH are stoichiometrically linked in amphibole).

Although we might expect the mafic magma to have higher Cl than the silicic magma because of the higher solubility of Cl in mafic melts relative to silicic melts (e.g., Lowenstern, 2000; Métrich and Rutherford, 1992), we observe higher Cl concentrations in amphibole that crystallized from silicic (rather than mafic) magma (Fig. 3.1d). For Soufríere Hills Volcano, Humphreys et al. (2009b) offered two possible explanations for high $(Cl/OH)_{melt}$ in the silicic magma: 1) exsolution of H_2O from the melt into the vapor phase, which will decrease $(OH)_{melt}$ and therefore increase $(Cl/OH)_{melt}$, or 2) increasing $(CO_2)_{melt}$ due to CO_2 fluxing from magma degassing at depth, which recent studies have

demonstrated is a common occurrence at arc volcanoes (e.g., Blundy et al., 2010). As a deep-seated mafic magma degasses CO_2, the overlying silicic magma body will be fluxed with CO_2-rich vapor, which will decrease H_2O_{melt} in order to stay in equilibrium with this vapor. This will decrease the concentration of Cl in the co-existing vapor, thus driving more Cl into the melt (increasing Cl_{melt}) and consequently, increasing the concentration of Cl in the coexisting amphiboles (Humphreys et al., 2009b).

Architecture of the Mount Hood magma system

Previous studies have identified the role of magma mixing in producing intermediate magmas at Mount Hood (e.g., Cribb and Barton, 1997; Darr, 2006; Kent et al., 2010; Woods, 2004), however the depths at which storage and mixing occurs have been generally unconstrained. The pressure and temperature results discussed in section 3.4 and shown in Fig. 3.4 now allow us to describe the plumbing system below Mount Hood in significantly greater detail (Fig. 3.5).

Pressure and temperature estimates from amphiboles at Mount Hood suggest that amphibole crystallization from hot mafic magma occurs at 9-15 km (Fig. 3.5a), and we suggest that this records the point that ascending mafic magma cools sufficiently to saturate with Tsch-pargasite (Fig. 3.4) while also crystallizing some proportion of plagioclase (Kent et al., 2010). This occurs at temperatures between ~920-970˚C (Fig. 3.6a). Plagioclase U-series results and plagioclase morphology (Eppich et al., in review; Kent et al., 2010) suggests that crystallization occurs relatively rapidly in this magma, consistent with rapid ascent to this depth and subsequent rapid cooling. Concurrently, a long-lived magma chamber containing cooler (~810-880˚C) silicic (rhyolitic) magma

exists at a shallower crustal level (3-7 km or 100-150 MPa; Figs. 3.4 and 3.5b), where unzoned Mg-hornblende has previously crystallized (Fig. 3.6b). U-series measurements suggest plagioclase residence time in excess of at least 4000-5000 years (and possibly greater than 10,000 years) in this silicic magma (Eppich et al., in review), although plagioclase residence ages based on CSD and diffusion modeling are <100 years (Kent et al., 2011). This discrepancy is consistent with the rhyolitic magma being at near- or sub-solidus temperatures for much of its residence time, suggesting little ongoing replenishment or reheating prior to the mafic recharge even that occurs immediately prior to eruption.

Within months to weeks before eruption (Kent et al., 2010) the hotter mafic magma ascends from depth and intrudes into the shallower silicic magma chamber (Figs. 3.4-3.5). This results in rapid hybridization of these magmas (possibly by a mechanism similar to that proposed by Burgisser and Bergantz, 2011) to create the andesites and low-SiO_2 dacites that are erupted from Mount Hood. As the magmas (and their crystal cargos) mix, some amphiboles acquire rims with intermediate compositions (Fig. 3.6c), however rapid mixing and eruption preserves the bimodal distribution of amphibole core compositions.

Applications to other recharge-driven volcanic systems

Summary of other systems

Abundant evidence for mafic recharge and an association between recharge and eruption is apparent in a number of other intermediate arc volcanoes. Examples for which significant amount of petrologic data exist include the 1902 and 1929 eruptions of Mont

Pelée, the 1991-1995 eruptions of Unzen Volcano, and the 2001-2007 eruptions of Soufriére Hills Volcano. Evidence for pre-eruptive recharge includes the presence of mafic enclaves, elevated temperatures in erupted Fe-Ti oxides, multiple populations of plagioclase, and/or reverse compositional zoning in plagioclase (Browne et al., 2006; Gourgaud et al., 1989; Humphreys et al., 2009a; Martel et al., 2006; Murphy et al., 2000; Sato et al., 1999). All of these systems also exhibit bimodal amphibole populations that are remarkably similar to what we describe above for Mount Hood (Fig. 3.7). Tsch-pargasite at Mont Pelée, Unzen Volcano, and Soufriére Hills Volcano is most abundant within mafic enclaves (Browne et al., 2006; Gourgaud et al., 1989; Humphreys et al., 2009a), although both Tsch-pargasite and Mg-hornblende occur within enclaves and the surrounding host lava, consistent with enclave disaggregation and crystal transfer between enclaves and host lava (Humphreys et al., 2009a; Pichavant et al., 2002). We observe a similar distribution of amphiboles at Mount Hood, where Tsch-pargasite is slightly more prevalent in mafic enclaves than in host lavas, but both species are present in both locations. We discuss further pertinent details for Mont Pelée, Soufriére Hills Volcano, and Unzen Volcano below, and results are summarized in Figs. 3.7-3.8.

Amphiboles from the 1902 and 1929 eruptions of Mont Pelée have previously been classified as pargasite and edenitic hornblendes (Gourgaud et al., 1989; Pichavant et al., 2002). When reclassified using the updated scheme in Ridolfi et al. (2010), these amphiboles fall into the same groups (Tsch-pargasite and Mg-hornblende) as amphiboles from Mount Hood and suggest a two-part plumbing system similar to what we propose for Mount Hood (Figs. 3.7-3.8). The shallowest portion of the mafic magma source below Mont Pelée has previously been estimated to be at 400 MPa (Pichavant et al.,

2002), consistent with geobarometry estimates (Ridolfi et al., 2010), which indicate the shallowest Tsch-pargasites record pressures of 420 MPa (Fig. 3.8).

Amphiboles from the 2001-2007 eruptions of Soufriére Hills Volcano have been previously classified as Mg-hastingsite, pargasite, and Mg-hornblende (Humphreys et al., 2009a; Murphy et al., 2000; Murphy et al., 1998), however these compositions also re-classify as Tsch-pargasite and Mg-hornblende using the criteria of Ridolfi et al. (2010). Amphiboles from Soufriére Hills Volcano also illustrate two separate magma reservoirs at 90-140 MPa (~3-5 km) and 360-670 MPa (13-25 km) (Fig. 3.8). Two magma chambers at 5 km and 17 km beneath Soufriére Hills Volcano have previously been proposed on the basis of geodetic data (Foroozan et al., 2010); these depths are in general agreement with the pressures and depths associated with amphibole compositions (Fig. 3.8).

Amphiboles from the 1991-1995 eruption of Unzen Volcano have previously been classified as pargasite and Mg-hornblende (Sato et al., 1999; Venezky and Rutherford, 1999). When these amphibole core compositions are reclassified using the criteria in Ridolfi et al (2010), they also fall into the same two groups (Tsch-pargasite and Mg-hornblende) as amphiboles erupted from Mount Hood, Mont Pelée, and Soufriére Hills Volcano. Al-in-hornblende geobarometry estimates a pressure of 160 MPa for the rhyodacite beneath Unzen Volcano (Venezky and Rutherford, 1999); this is slightly higher than the range of 100-130 MPa suggested by amphibole compositions (Fig. 3.8) but generally within the range of error on both geobarometers.

Bimodal versus multimodal mixed systems

The similarities in amphibole compositions discussed in section 5.1 suggest marked similarities between the plumbing systems of Mount Hood, Mont Pelée, Unzen Volcano, and Soufriére Hills Volcano (Fig. 3.7). Amphibole geothermobarometry also suggests that all four volcanoes are underlain by broadly similar plumbing systems where amphiboles of the same composition form at broadly equivalent conditions of pressure and temperature (Fig. 3.8). Thus erupted lavas contain Tsch-pargasite derived from a deep (> 260 MPa), hot (> 910˚C) mafic source and Mg-hornblende derived from a shallow (< 190 MPa), cool (< 880˚C) silicic source. There are no amphibole cores with intermediate compositions, which suggests that eruption occurs sufficiently soon after mixing to prevent significant amphibole growth. Magmatic temperatures are comparable in all four volcanic systems, although amphibole compositions suggest that the silicic magma body (at the time of amphibole crystallization) may be ~50˚C hotter at Mount Hood than at the other volcanoes (Fig. 3.8). The shallow silicic source likely resides at 100-200 MPa for all four volcanoes, whereas the deep mafic source is located at >250 MPa for Mount Hood and Unzen Volcano and >350 MPa for Soufriére Hills Volcano and Mont Pelée. The differences in these depths may reflect variations in amphibole stability between the different systems. Bulk composition, including H_2O and halogen content, can strongly affect amphibole stability (Rutherford and Devine, 1988), which may be a possible explanation for the slightly deeper occurrence of amphibole at Soufriére Hills Volcano and Mont Pelée than at Mount Hood and Unzen Volcano.

Why should these geographically diverse volcanoes necessarily share such similar plumbing systems? Arc volcanoes commonly erupt lavas with intermediate compositions,

which are generally the product of mixing between mafic and silicic magmas at crustal levels (Anderson, 1976; Eichelberger, 1978; Eichelberger et al., 2006; Reubi and Blundy, 2009). More specifically, most of these magmas represent a mixture of shallow silicic material (potentially crustally-derived) and the magmas ultimately derived from mantle-derived basalts supplied from the subduction zone to the base of the crust (e.g., Hildreth, 2007). Pichavant (2002) proposed that the mafic parental magma at Mont Pelée ascends as relatively evolved hydrous basalt derived from the lower crust or upper mantle, and will begin to crystallize between 400-1000 MPa. Magmas are apt to stall as a result of discontinuities in crustal density, levels of neutral buoyancy, changes in the local stress field, and/or H_2O-saturation (Hildreth, 2007; Scandone et al., 2007), and Pichavant estimates that the ascending mafic parental magma will stall at ~300 MPa as a result of crystallization, which increases the overall magmatic density (and viscosity). This stall depth is also consistent with the crystallization pressures for Tsch-parasites at Soufriére Hills Volcano, Unzen Volcano, and Mount Hood (Fig. 3.8), suggesting a similar origin for the mafic parental magma at each of these volcanoes. Additionally, the derivative nature of this magma is consistent with our observation that Tsch-pargasites at Mount Hood cannot crystallize directly from the primitive mafic parental magma, but instead crystallize once this magma becomes more evolved (Fig. 3.2).

As the mafic parental magma continues to crystallize, the residual liquids (andesites to dacites) are comparatively buoyant and can segregate at shallower depths to create a shallow silicic magma body, and may potentially carry crystal cargo of anorthitic plagioclase and pargasitic hornblende that crystallized at depth (Pichavant et al., 2002). As this shallow silicic magma body cools, it will crystallize low-Al amphibole (Martel et

al., 1999; Pichavant et al., 2002) near the amphibole stability curve, consistent with our observed crystallization depths for Mg-hornblende from Mount Hood, Soufriére Hills Volcano, Unzen Volcano, and Mont Pelée (Fig. 3.8). This silicic magma body may cool to a crystal mush and be uneruptible as a result of its high viscosity (Kent et al., 2010), until it is mobilized by a large flux of mafic material (Pichavant et al., 2002; Zellmer et al., 2003). Consequently, recharge-driven eruptions at each of these volcanoes will produce intermediate lavas containing two populations of amphibole: Tsch-pargasite derived from the mafic parental magma, and Mg-hornblende that formed while the silicic parental magma cooled in the shallow crust. Some of the Tsch-pargasite may have crystallized before emplacement of the silicic magma body and been carried as crystal cargo during the ascent of the silicic derivative magma (Pichavant et al., 2002; Zellmer et al., 2003), however much of the Tsch-pargasite presents in the erupted lavas likely ascends with the mafic recharge magma. Additionally, some Tsch-pargasite may come from the disaggregation of mafic enclaves that are produced during recharge (Humphreys et al., 2009a).

In contrast to these systems, amphibole compositions from the 2004-2006 eruptions of Mount St. Helens illustrate a very different plumbing system than the bimodal recharge-driven volcanoes (Fig. 3.8). Previous studies at Mount St. Helens have suggested that magma is sourced from a variety of depths at different times, and that cyclic magma mixing contributes to the range of compositions observed in erupted lavas (Pallister et al., 2008; Rutherford and Devine, 1988; Streck et al., 2008; Thornber et al., 2008). Amphiboles exhibit cyclic compositional zoning, including cyclic variations in the pressure-sensitive Al-Tschermak substitution, which requires amphibole crystallization at

a variety of depths as magma is cycled through the storage region (Rutherford and Devine, 2008). The amphibole compositions shown in Fig. 3.8 support this observation, and appear to record a near-continuum of compositions, pressures, and temperatures (90-820 MPa, 790-1020˚C; Fig. 3.8). If recharge influenced magma compositions at Mount St. Helens, it likely occurred as repeated minor injections of hotter magma prior to the 2004-2006 eruption (Pallister et al., 2008; Streck et al., 2008). Amphibole and plagioclase compositions record extensive magma convection and overturn over a large range of pressures at Mount St. Helens (Rutherford and Devine, 2008), and seismic and petrologic data an underlying magma body that is continuous between 5-12 km (Pallister et al., 2008). This is in stark contrast to the systems at Mount Hood, Soufriére Hills Volcano, Unzen Volcano, and Mont Pelée, where bimodal amphibole populations are representative of discrete magma bodies at two different depths, and magma mixing immediately preceding eruption.

We find significant differences between amphiboles produced by binary mixing at recharge-driven volcanoes (e.g., Mount Hood, Unzen Volcano, Soufriére Hills Volcano, Mont Pelée) and amphiboles produced by complex extended crystallization over a variety of pre-eruptive conditions (e.g., Mount St. Helens). Although all of these volcanoes are located in arc settings and should therefore share broadly similar parent materials (i.e., mantle-derived basalt ± crustal material), only amphiboles from recharge-driven eruptions show evidence of magma bodies stalled at two different depths, whereas crystallization at Mount St. Helens occurs over a continuous range of pressures (Fig. 3.8). The differences between these two plumbing systems may indicate differences in magma

flux, magma ascent rates, or differences in the composition or stress state within the crust, a potential topic for future research.

CONCLUSIONS

Two populations of calcic amphibole are commonly present in lavas erupted from recharge-driven intermediate volcanoes, where mafic magma mixes with silicic magma shortly before eruption. The composition of these two groups of amphiboles allows identification of the pressures and temperature conditions at which these magmas were stored prior to mixing. Compositional differences between these two amphibole groups, including Al/Si and Fe/Mg ratios and Eu-anomalies, indicate that they crystallized from two different parent magmas prior to mixing. The lack of intermediate amphibole core compositions suggests that mixing occurs shortly before eruption.

The similarities between amphibole compositions and plumbing systems for the recharge-driven eruptions of Mount Hood, Soufriére Hills Volcano, Mont Pelée, and Unzen Volcano suggest a general model for the plumbing system of these types of volcanoes, and the presence of bimodal amphiboles appears to be diagnostic of recharge-driven eruptions. Bimodal amphibole groups and the plumbing structure that they suggest is in striking contrast to the continuum of amphibole compositions and associated pressures and temperatures for volcanoes with more complicated magmatic histories that include multiple sources at various depths, cyclic magma mixing, and extended storage times, such as at Mount St. Helens. We conclude that bimodal amphibole compositions and dual magma bodies are common characteristics of, and possibly unique to, recharge-driven intermediate volcanic eruptions.

ACKNOWLEDGEMENTS

This work was funded by NSF EAR grant EAR-038421 to AJRK and a USGS Kleinman Grant to AMK. Olivier Bachmann, Brandon Browne, and the OSU VIPERs joined us in stimulating discussions that contributed to this manuscript. Frank Tepley, Dale Burns, and Andy Ungerer provided analytical assistance, and Gary Eppich, Kari Cooper, and Edith Koleszar provided valuable assistance in with fieldwork.

REFERENCES

Aigner-Torres, M., Blundy, J., Ulmer, P., and Pettke, T., 2007, Laser ablation ICPMS study of trace element partitioning between plagioclase and basaltic melts: an experimental approach: Contributions to Mineralogy and Petrology, v. 153, p. 647-667.

Anderson, A.T., 1974, Chlorine, sulfur, and water in magmas and oceans: Geological Society of America Bulletin, v. 85, p. 1485-1492.

—, 1976, Magma mixing: Petrological process and volcanological tool: Journal of Volcanology and Geothermal Research, v. 1, p. 3-33.

Anderson, A.T., and Lindsley, D.H., 1985, New (and final) models for the Ti-magnetite/ilmenite geothermometer and oxygen barometer: Eos Trans. AGU, Spring Meeting, v. 66, p. 416.

Bachmann, O., and Dungan, M.A., 2002, Temperature-induced Al-zoning in hornblendes of the Fish Canyon magma, Colorado: American Mineralogist, v. 87, p. 1062-1076.

Bacon, C.R., 1986, Magmatic inclusions in silicic and intermediate volcanic rocks: Journal of Geophysical Research, v. 21, p. 6091-6112.

Bacon, C.R., and Hirschmann, M.M., 1988, Mg/Mn partitioning as a test for equilibrium between coexisting Fe-Ti oxides: American Mineralogist, v. 73, p. 57-61.

Blundy, J., Cashman, K.V., Rust, A., and Witham, F., 2010, A case for CO2-rich arc magmas: Earth and Planetary Science Letters, v. 290, p. 289-301.

Browne, B.L., Eichelberger, J.C., Patino, L.C., Vogel, T.A., Dehn, J., Uto, K., and Hoshizumi, H., 2006, Generation of porphyritic and equigranular mafic enclaves during magma recharge events at Unzen Volcano, Japan: Journal of Petrology, v. 47, p. 301-328.

Burgisser, A., and Bergantz, G.W., 2011, A rapid mechanism to remobilize and homogenize highly crystalline magma bodies: Nature, v. 471, p. 212-215.
Cribb, J.W., and Barton, M., 1997, Significance of crustal and source region processes on the evolution of compositionally similar calc-alkaline lavas, Mt. Hood, Oregon: Journal of Volcanology and Geothermal Research, v. 76, p. 229-249.
Darr, C.M., 2006, Magma chamber processes over the past 475,000 years at Mount Hood, Oregon: Insights from crystal zoning and crystal size distribution studies: Corvallis, Oregon State University.
Eichelberger, J.C., 1978, Andesitic volcanism and crustal evolution: Nature, v. 275, p. 21-27.
—, 1980, Vesiculation of mafic magma during replenishment of silicic magma reservoirs: Nature, v. 288, p. 446-450.
Eichelberger, J.C., Izbekov, P.E., and Browne, B.L., 2006, Bulk chemical trends at arc volcanoes are not liquid lines of descent: Lithos, v. 87, p. 135-154.
Ernst, W.G., and Liu, J., 1998, Experimental phase-equilibrium study of Al- and Ti-contents of calcic amphibole in MORB-- A semiquantitative thermobarometer: American Mineralogist, v. 83, p. 952-969.
Foroozan, R., Elsworth, D., Voight, B., and Mattioli, G.S., 2010, Dual reservoir structure at Soufriére Hills Volcano inferred from continuous GPS observations and heterogeneous elastic modeling: Geophysical Research Letters, v. 37.
Gerlach, D.C., and Grove, T.L., 1982, Petrology of Medicine Lake Highland Volcanics: Characterization of endmembers of magma mixing: Contributions to Mineralogy and Petrology, v. 80, p. 147-159.
Ghiorso, M.S., and Evans, B.W., 2008, Thermodynamics of rhombohedral oxide solid solutions and a revision of the Fe-Ti two-oxide geothermometer and oxygen-barometer: American Journal of Science, v. 308, p. 957-1039.
Ghiorso, M.S., and Sack, R.O., 1995, Chemical mass transfer in magmatic processes. IV. A Revised and internally consistent thermodynamic model for the interpolation and extrapolation of liquid-solid equilibria in magmatic systems at elevated temperatures and pressures.: Contributions to Mineralogy and Petrology, v. 119, p. 197-212.
Gourgaud, A., Fichaut, M., and Joron, J.-L., 1989, Magmatology of Mt. Pelée (Martinique, F.W.I.). I: Magma mixing and triggering of the 1902 and 1929 Pelean nuées ardentes: Journal of Volcanology and Geothermal Research, v. 38, p. 143-169.
Grove, T.L., Kinzler, R.J., Baker, M.B., Donnelly-Nolan, J.M., and Lesher, C.E., 1988, Assimilation of granite by basaltic magma at Burnt Lava flow, Medicine Lake volcano, northern California: Decoupling of heat and mass transfer: Contributions to Mineralogy and Petrology, v. 99, p. 320-343.
Hammer, J.E., Cashman, K.V., Hoblitt, R.P., and Newman, S., 1999, Degassing and microlite crystallization during the pre-climatic events of the 1991 eruption of Mt. Pinatubo, Phillipines: Bulletin of Volcanology, v. 60, p. 355-380.
Higgins, M.D., 1996, Magma dynamics beneath Kameni volcano, Thera, Greece, as revealed by crystal size and shape measurements: Journal of Volcanology and Geothermal Research, v. 70, p. 37-48.

Hildreth, W., 2007, Quaternary Magmatism in the Cascades— Geologic Perspectives: Reston, VA, U.S. Geological Survey.

Holland, T., and Blundy, J., 1994, Non-ideal interactions in calcic amphiboles and their bearing on amphibole-plagioclase thermometry: Contributions to Mineralogy and Petrology, v. 116, p. 433-447.

Humphreys, M.C.S., Christopher, T., and Hards, V., 2009a, Microlite transfer by disaggregation of mafic inclusions following magma mixing at Soufriere Hills volcano, Montserrat: Contributions to Mineralogy and Petrology, v. 157, p. 609-624.

Humphreys, M.C.S., Edmonds, M., Christopher, T., and Hards, V., 2009b, Chlorine variations in the magma of Soufriere Hills Volcano, Montserrat: Insights from Cl in hornblende and melt inclusions: Geochemica et Cosmochimica Acta, v. 73, p. 5693-5708.

Kent, A.J.R., Cooper, K.M., Eppich, G.R., Koleszar, A.M., and Salisbury, M.J., 2011, Crystal residence ages in andesitic volcanoes, International Union of Geodesy and Geophysics General Assembly: Melbourne, Australia.

Kent, A.J.R., Darr, C.M., Koleszar, A.M., Salisbury, M.J., and Cooper, K.M., 2010, Preferential eruption of andesitic magmas through recharge filtering: Nature Geoscience, v. 3, p. 631-636.

Kent, A.J.R., and Ungerer, C.A., 2006, Analysis of light lithophile elements (Li, Be, B) by laser ablation ICP-MS: Comparision between magnetic sector and quadrupole ICP-MS: American Mineralogist, v. 91, p. 1401-1411.

Koleszar, A.M., Kent, A.J.R., Wallace, P.J., and Scott, W.E., in review, Controls on long-term low explosivity at andesitic arc volcanoes: Insights from Mount Hood, Oregon: Journal of Volcanology and Geothermal Research.

Leake, B.E., Woolley, A.R., Arps, C.E.S., Birch, W.D., Gilbert, M.C., Grice, J.D., Hawthorne, F.C., Kato, A., Kisch, H.J., Krivovichev, V.G., Linthout, K., Laird, J., Mandarino, J., Maresch, W.V., Nickel, E.H., Schumaker, J.C., Smith, D.C., Stephenson, N.C.N., Ungaretti, L., Whittaker, E.J.W., and Youzhi, G., 1997, Nomenclature of amphiboles: report of the subcommittee on amphiboles of the International Mineralogical Associate Comission on New Minerals and Mineral Names: Mineralological Magazine, v. 61.

Lowenstern, J.B., 2000, A review of the contrasting behavior of two magmatic volatiles: chlorine and carbon dioxide: Journal of Geochemical Exploration, v. 69-70, p. 287-290.

Martel, C., Pichavant, M., Bourdier, J.-L., Traineau, H., Holtz, F., and Scaillet, B., 1999, Magma storage conditions and control of eruption regime in silicic volcanoes: experimental evidence from Mt. Pelée: Earth and Planetary Science Letters, v. 156, p. 89-99.

Martel, C., Radadi Ali, A., Poussineau, S., Gourgaud, A., and Pichavant, M., 2006, Basalt-inherited microlites in silicic magmas: Evidence from Mount Pelée (Martinique, French West Indies): Geology, v. 34, p. 905-908.

McDonough, W.F., and Sun, S.-s., 1995, The composition of the Earth: Chemical Geology, v. 120, p. 223-253.

Métrich, N., and Rutherford, M.J., 1992, Experimental study of chlorine behavior in hydrous silicic melts: Geochimica et Cosmochimica Acta, v. 56, p. 607-616.

Morgan, D.J., Blake, S., Rogers, N.W., DeVivo, B., Rolandi, G., Macdonald, R., and Hawkesworth, C.J., 2004, Time scales of crystal residence and magma chamber volume from modelling of diffusion profiles in phenocrysts: Vesuvius 1944: Earth and Planetary Science Letters, v. 222, p. 933-946.

Morrissey, M.M., 1997, Long-period seismicity at Redoubt Volcano, Alaska, 1989-1990 related to magma degassing: Journal of Volcanology and Geothermal Research, v. 75, p. 321-335.

Murphy, M.D., Sparks, R.S.J., Barclay, J., Carroll, M.R., and Brewer, T.S., 2000, Remobilization of andesite magma by intrusion of mafic magma at the Soufriére Hills Volcano, Montserrat, West Indies: Journal of Petrology, v. 41, p. 21-42.

Murphy, M.D., Sparks, R.S.J., Barclay, J., Carroll, M.R., Lejeune, A.-M., Brewer, T.S., Macdonald, R., Black, S., and Young, S., 1998, The role of magma mixing in triggering the current eruption at the Soufriere Hills volcano, Montserrat, West Indies: Geophysical Research Letters, v. 25, p. 3433-3436.

Newman, S., and Lowenstern, J.B., 2002, VolatileCalc: a silicate melt-H2O-CO2 solution model written in Visual Basic for Excel: Computers and Geosciences, v. 28, p. 597-604.

Pallister, J.S., Thornber, C.R., Cashman, K.V., Clynne, M.A., Lowers, H.A., Mandeville, C.W., Brownfield, I.K., and Meeker, G.P., 2008, Petrology of the 2004-2006 Mount St. Helens lava dome-- Implications for magmatic plumbing and eruption triggering, *in* Sherrod, D.R., Scott, W.E., and Stauffer, P.H., eds., A Volcano Rekindled: The Renewed Eruption of Mount St. Helens, 2004-2006, Volume 1750, U.S.G.S. Professional Paper.

Papale, P., Moretti, R., and Barbato, D., 2006, The compositional dependence of the saturation surface of H2O + CO2 fluids in silicate melts: Chemical Geology, v. 229, p. 78-95.

Pichavant, M., Costa, F., Burgisser, A., Scaillet, B., Martel, C., and Poussineau, S., 2007, Equilibrium scales in silicic to intermediate magmas-- Implications for experimental studies: Journal of Petrology, v. 48, p. 1955-1972.

Pichavant, M., Martel, C., Bourdier, J.-L., and Scaillet, B., 2002, Physical conditions, structure, and dynamics of a zoned magma chamber: Mount Pelée (Martinique, Lesser Antilles Arc): Journal of Geophysical Research, v. 107.

Prouteau, G., and Scaillet, B., 2003, Experimental constraints on the origin of the 1991 Pinatubo dacite: Journal of Petrology, v. 44, p. 2203-2241.

Putirka, K.D., 2008, Thermometers and barometers for volcanic systems, *in* Putirka, K.D., and Tepley, F.J.I., eds., Minerals, inclusions, and volcanic processes, Volume 69, Mineralogical Society of America, p. 61-120.

Reubi, O., and Blundy, J., 2009, A dearth of intermediate melts at subduction zone volcanoes and the petrogenesis of arc andesites: Nature, v. 461, p. 1269-1273.

Ridolfi, F., Puerini, M., Renzulli, A., Menna, M., and Toulkeridis, T., 2008, The magmatic feeding system of El Reventado volcano (Sub-Andean zone, Ecuador) constrained by texture, mineralogy, and thermobarometry of the 2002 erupted products: Journal of Volcanology and Geothermal Research, v. 176, p. 94-106.

Ridolfi, F., Renzulli, A., and Puerini, M., 2010, Stability and chemical equilibration of amphibole in calc-alkaline magmas: an overview, new thermobarometric formulations and applicaton to subduction-related volcanoes: Contributions to Mineralogy and Petrology, v. 160, p. 45-66.

Rowe, M.C., Kent, A.J.R., and Thornber, C.R., 2008, Using amphibole phenocrysts to track vapor transfer during magma crystallization and transport: An example from Mount St. Helens, Washington: Journal of Volcanology and Geothermal Research, v. 178, p. 593-607.

Ruprecht, P., and Bachmann, O., 2010, Pre-eruptive reheating during magma mixing at Quizapu volcano and the implications for the explosiveness of silicic arc volcanoes: Geology, v. 38, p. 919-922.

Rutherford, M.J., and Devine, J.D., 1988, The May 18, 1980, eruption of Mount St. Helens 3. Stability and chemistry of amphibole in the magma chamber: Journal of Geophysical Research, v. 93, p. 11949-11959.

—, 2008, Magmatic conditions and processes in the storage zone of the 2004-2006 Mount St. Helens dacite, *in* Sherrod, D.R., Scott, W.E., and Stauffer, P.H., eds., A Volcano Rekindled: The Renewed Eruption from Mount St. Helens, 2004-2006, Volume 1750, U.S.G.S. Professional Paper.

Salisbury, M.J., Bohrson, W.A., Clynne, M.A., Ramos, F.C., and Hoskin, P., 2008, Multiple plagioclase crystal populations identified by crystal size distribution and in situ chemical data: Implications for timescales of magma chamber processes associated with the 1915 eruption of Lassen Peak, CA: Journal of Petrology, v. 49, p. 1755-1780.

Sato, H., Holtz, F., Behrens, H., Botcharnikov, R., and Nakada, S., 2005, Experimental petrology of the 1991-1995 Unzen Dacite, Japan. Part II: Cl/OH partitioning between hornblende and melt and its implications for the origin of oscillatory zoning of hornblende phenocrysts: Journal of Petrology, v. 46, p. 339-354.

Sato, H., Nakada, S., Fujii, T., Nakamura, M., and Suzuki-Kamata, K., 1999, Groundmass pargasite in the 1991-1995 dacite of Unzen volcano: phase stability experiments and volcanological implications: Journal of Volcanology and Geothermal Research, v. 89, p. 197-212.

Scaillet, B., and Evans, B.W., 1999, The 15 June 1991 eruption of Mount Pinatubo. I. Phase equilibriua and pre-eruption P-T-fO2-fH2O conditions of the dacite magma: Journal of Petrology, v. 40, p. 381-411.

Scandone, R., Cashman, K.V., and Malone, S.D., 2007, Magma supply, magma ascent and the style of volcanic eruptions: Earth and Planetary Science Letters, v. 253, p. 513-529.

Singer, B.S., Dungan, M.A., and Layne, G.D., 1995, Textures and Sr, Ba, Mg, Fe, K, and Ti compositional profiles in volcanic plagioclase: Clues to the dynamics of calc-alkaline magma chambers: American Mineralogist, v. 80, p. 776-798.

Sisson, T.W., and Grove, T.L., 1993, Experimental investigations of the role of H2O in calc-alkaline differentiation and subduction zone magmatism: Contributions to Mineralogy and Petrology, v. 113, p. 143-166.

Sparks, R.S.J., and Sigurdsson, H., 1977, Magma mixing: a mechanism for triggering acid explosive eruptions: Nature, v. 267, p. 315-318.

Streck, M.J., Broderick, C.A., Thornber, C.R., Clynne, M.A., and Pallister, J.S., 2008, Plagioclase populations and zoning in dacite of the 2004-2006 Mount St. Helens eruption: Constraints for magma origin and dynamics, *in* Sherrod, D.R., Scott, W.E., and Stauffer, P.H., eds., A Volcano Rekindled: The Renewed Eruption from Mount St. Helens, 2004-2006, Volume 1750, U.S.G.S. Professional Paper.

Tepley, F.J.I., Davidson, J.P., and Clynne, M.A., 1999, Magmatic interactions as recorded in plagioclase phenocrysts of Chaos Crags, Lassen Volcanic Center, California: Journal of Petrology, v. 40, p. 787-806.

Thornber, C.R., Pallister, J.S., Lowers, H.A., Rowe, M.C., Mandeville, C.W., and Meeker, G.P., 2008, Chemistry, mineralogy, and petrology of amphibole in Mount St. Helens 2004-2006 dacite, *in* Sherrod, D.R., Scott, W.E., and Stauffer, P.H., eds., A Volcano Rekindled: The Renewed Eruption of Mount St. Helens, 2004-2006, Volume 1750, U.S.G.S. Professional Paper.

Venezky, D.Y., and Rutherford, M.J., 1999, Petrology and Fe-Ti oxide reequilibration of the 1991 Mount Unzen mixed magma: Journal of Volcanology and Geothermal Research, v. 89, p. 213-230.

Wallace, P.J., 2005, Volatiles in subduction zone magmas: concentrations and fluxes based on melt inclusion and volcanic gas data: Journal of Volcanology and Geothermal Research, v. 140, p. 217-240.

Woods, M.M., 2004, Compositional and mineralogical relationships between mafic inclusions and host lavas as key to andesite petrogenesis at Mount Hood Volcano, Oregon: Portland, Portland State University.

Zellmer, G.F., Hawkesworth, C.J., Sparks, R.S.J., Thomas, L.E., Harford, C.L., Brewer, T.S., and Loughlin, S.C., 2003, Geochemical evolution of the Soufriére Hills Volcano, Montserrat, Lesser Antilles Volcanic Arc: Journal of Petrology, v. 44, p. 1349-1374.

FIGURES

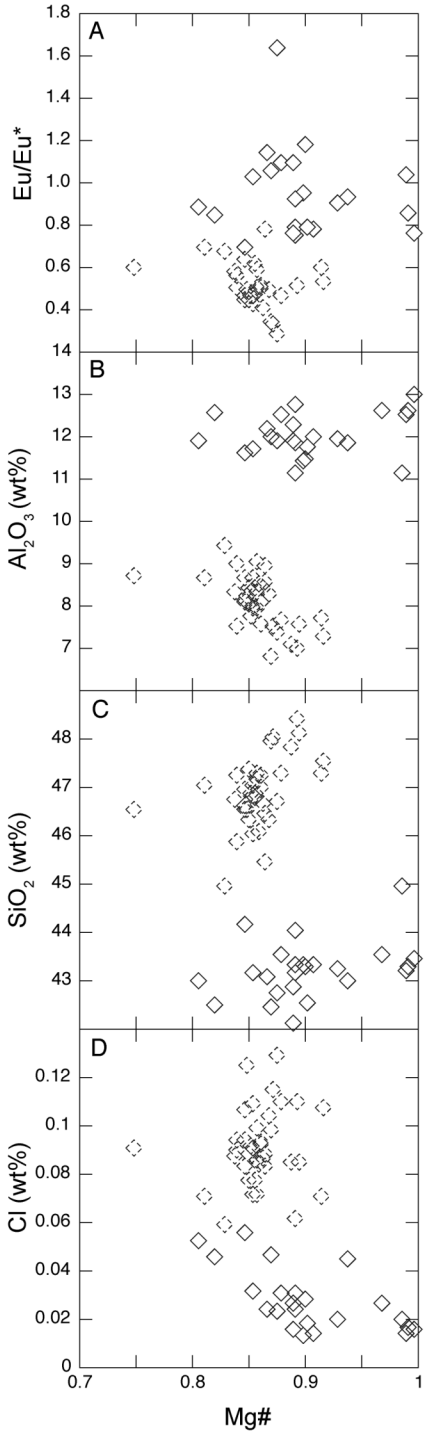

Figure 3.1: Mg# versus Eu/Eu*, Al_2O_3, SiO_2, and Cl for amphiboles from Mount Hood. Symbols with dashed outlines are Mg-hornblende and symbols with solid outlines are Tsch-pargasite. Eu/Eu* calculated as $Eu_N/((Sm_N+Gd_N)/2)$, where the subscript N indicates concentrations are normalized to McDonough and Sun (1995).

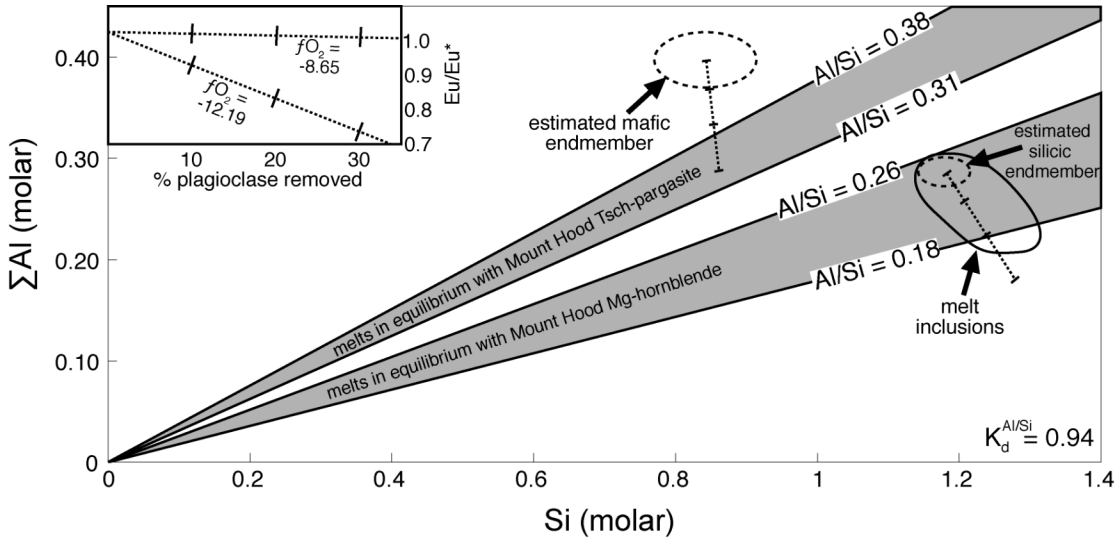

Figure 3.2: Total molar Al versus molar Si for potential parent sources for calcic amphibole at Mount Hood. Al/Si ratios in equilibrium with amphiboles were calculated using Kd = 0.94 (Sisson and Grove 1993). Melt inclusion compositions are from Koleszar et al. (in review). Dashed circles are estimated parent magma compositions for Mount Hood from Kent et al. (2010). Crystallizing and removing equilibrium plagioclase (dotted line) from this bulk composition gives Al/Si ratios consistent with a possible source for the Tsch-pargasites. Ticks are 10% crystallization intervals. Inset shows the change to Eu/Eu* in the melt as plagioclase is removed at fO2 = 12.19 and fO2 = -8.65 (partition coefficients from Aigner-Torres et al. (2007).

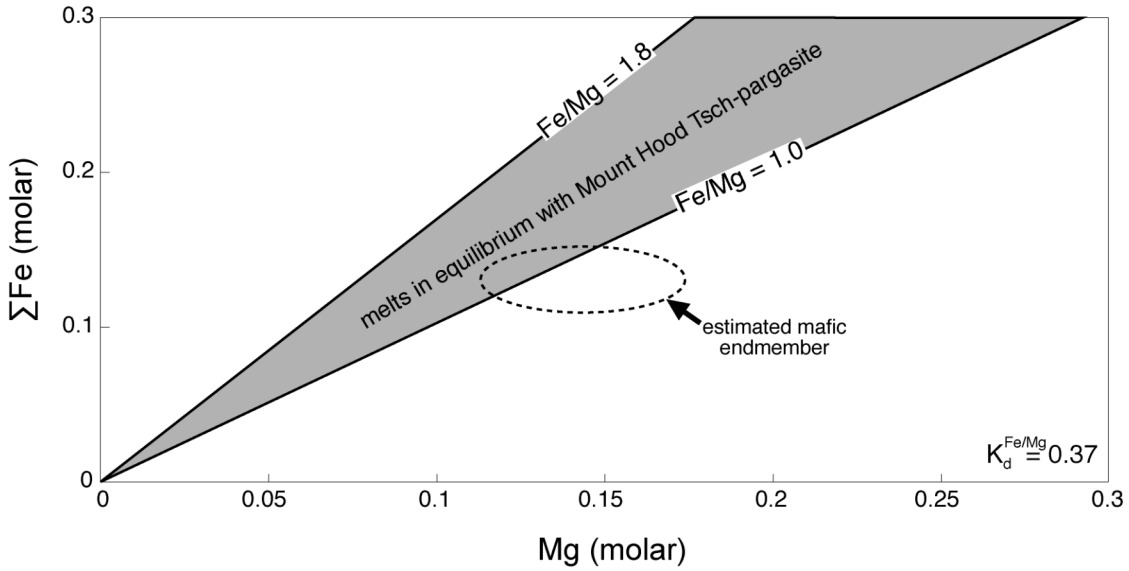

Figure 3.3: Total molar Fe versus molar Mg for potential parent sources for calcic amphibole at Mount Hood. Fe/Mg ratios for melts in equilibrium with Tsch-pargasite were calculated using $K_d = 0.37$ (Sisson and Grove 1993). The dashed circle is the estimated bulk composition for the Mount Hood mafic endmember from Kent et al. (2010).

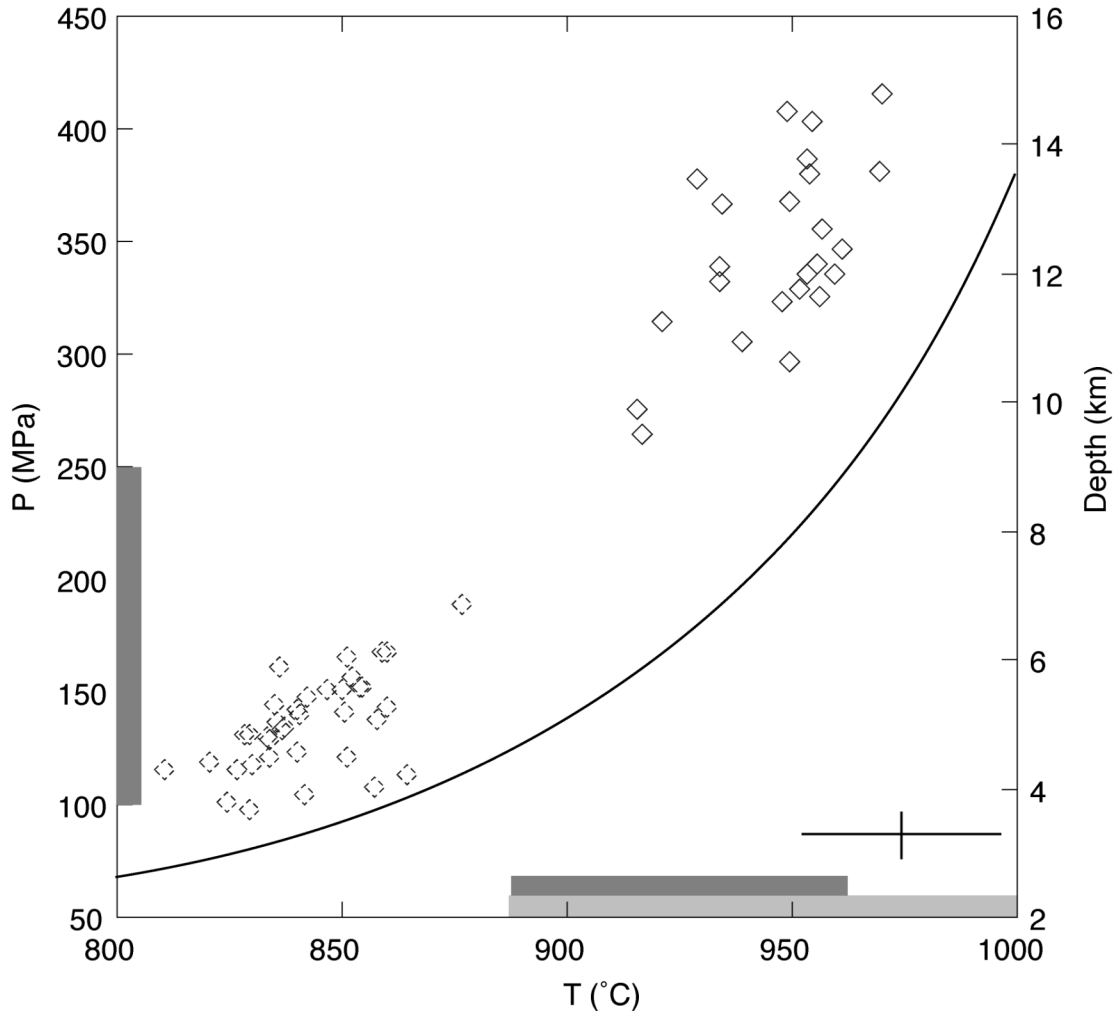

Figure 3.4: Pressures and temperatures for amphiboles from Mount Hood, calculated according to Ridolfi et al. (2010). Dashed symboles are Mg-hornblende, solid symbols are Tsch-pargasite. Error bars are representative errors for P and T calculations. Curved black line indicates maximum thermal stability for amphibole (Ridolfi et al. 2010). Light gray bar indicates eruptive temperatures from Fe-Ti oxides (Ghiorso and Evans, 2008); dark gray bar indicates temperatures from plagioclase-hornblende geothermometry (Holland and Blundy, 1994). Gray vertical bar indicates range of pressures suggested by high-SiO_2 melt inclusions from Mount Hood (see Chapter Two). Further discussion and comparison between geothermobarometers for Mount Hood can be found in Chapter One.

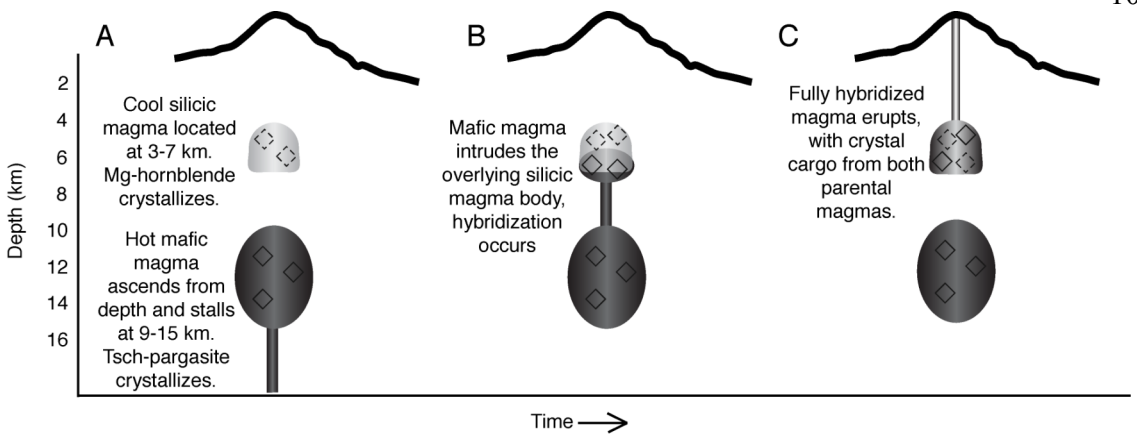

Figure 3.5: Schematic model of the plumbing system below Mount Hood. Edifice not to scale. See text for discussion.

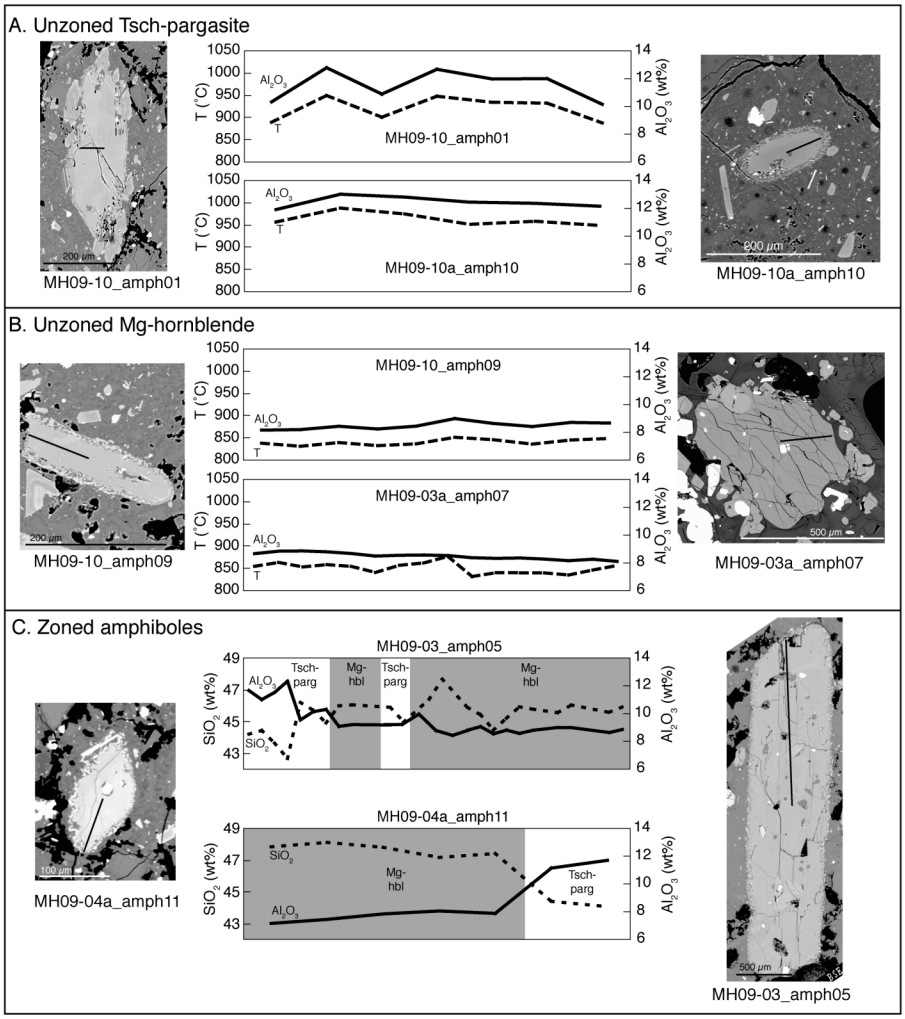

Figure 3.6: Representative amphiboles from Mount Hood. A: Unzoned Tsch-pargasite, B: Unzoned Mg-hornblende, C: Zoned amphiboles. Thermobarometric calculations are unreliable for the quench/late-stage crystallization compositions so SiO_2 is shown instead of temperature.

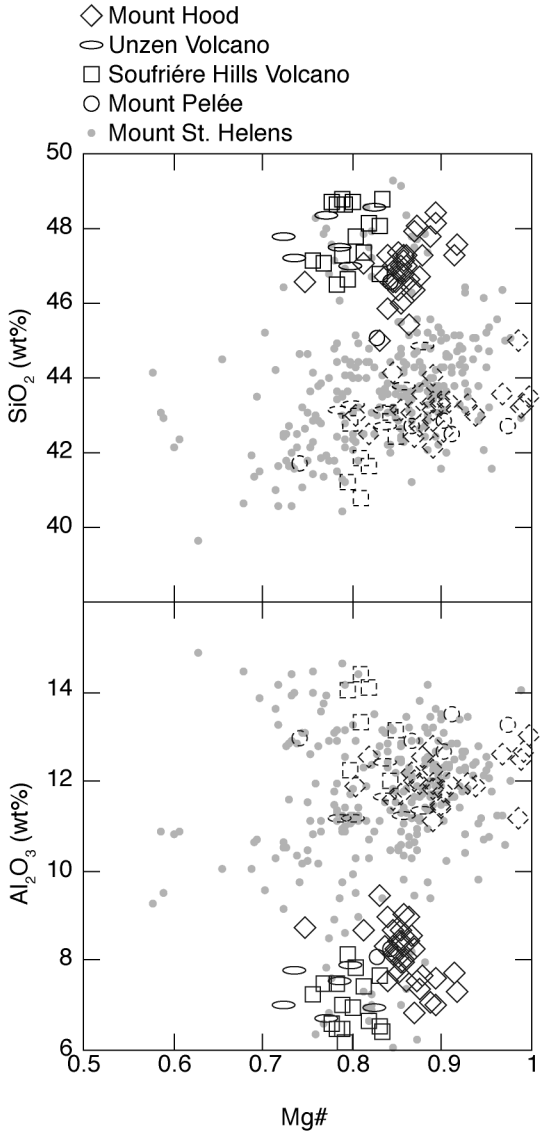

Figure 3.7: Mg# versus SiO_2 and Al_2O_3 for amphiboles from Mount Hood, Unzen Volcano, Soufriére Hills Volcano, Mount Pelée, and Mount St. Helens. Data for Unzen Volcano from Sato et al. 1999, Soufriére Hills Volcano from Humphreys et al. 2009 and Murphey et al. 2000, Mount Pelée from Gourgaud et al. 1989, and Mount St. Helens from Thornber et al. 2008. Symbols with dashed outlines are Mg-hornblende; symbols with solid outlines are Tsch-pargasite. Mount St. Helens amphibole compositions are continuous and are therefore not distinguished by species in these figures.

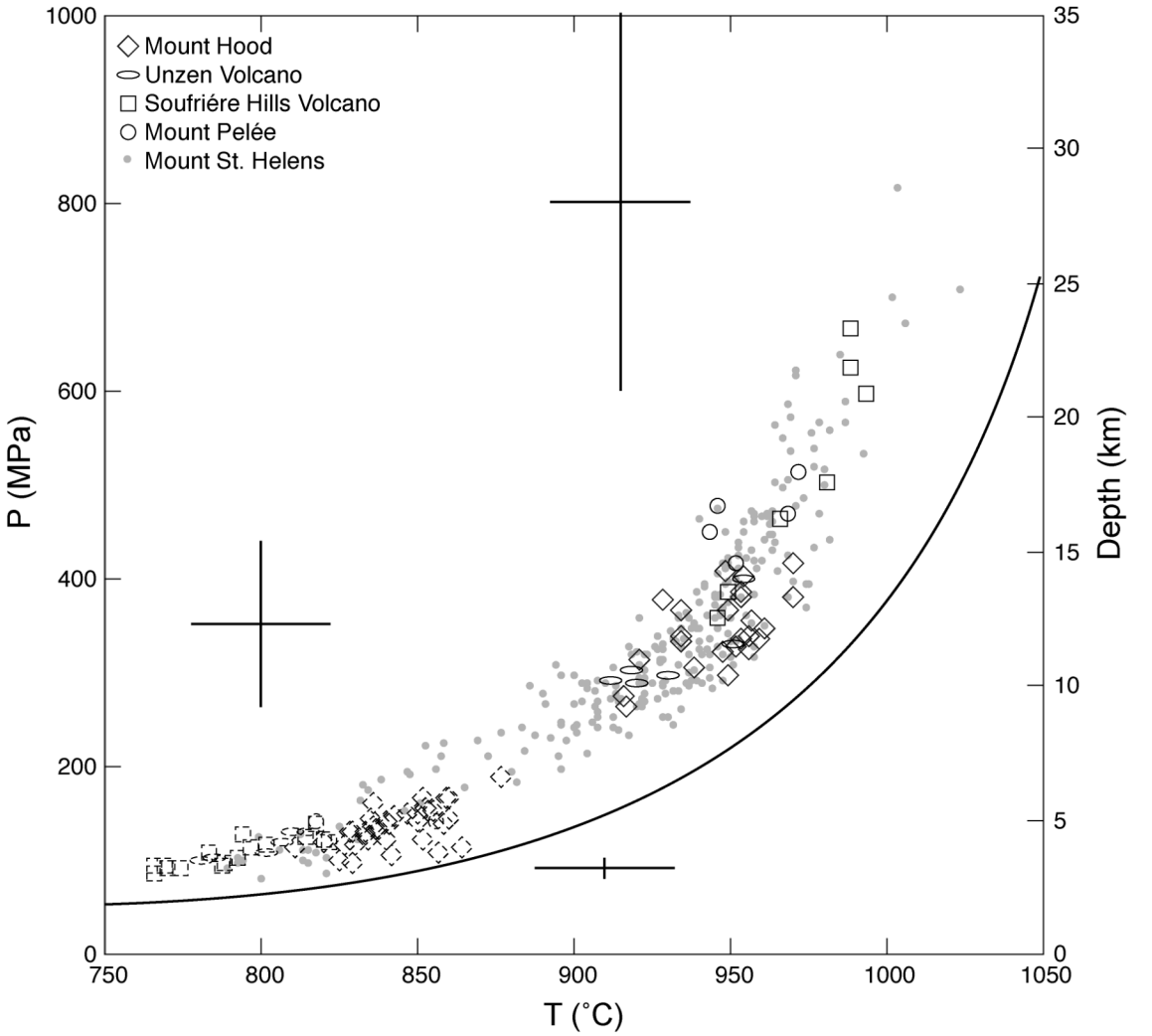

Figure 3.8: Pressures and temperatures for amphiboles from Mount Hood, Unzen Volcano, Soufriére Hills Volcano, Mount Pelée, and Mount St. Helens. Data for Unzen Volcano from Sato et al. 1999, Soufriére Hills Volcano from Humphreys et al. 2009 and Murphey et al. 2000, Mount Pelée from Gourgaud et al. 1989, and Mount St. Helens from Thornber et al. 2008. Symbols with dashed outlines are Mg-hornblende; symbols with solid outlines are Tsch-pargasite. Mount St. Helens amphibole compositions are continuous and are therefore not distinguished by species in this figure. Error bars are represenative for different values of P and T; curved black line indicates maximum thermal stability for amphibole (Ridolfi et al., 2010).

Table 3.1 Major elements (in wt%) of amphiboles from Mount Hood, determined by electron microprobe and temperature, pressure, and $\mathit{f}O2$ calculations from Ridolfi et al. (2010).

sample	SiO_2	TiO_2	Al_2O_3	Fe_2O_3	FeO	MnO	MgO	CaO	Na_2O	K_2O	F	Cl	Total	T (°C)	P (MPa)	$\log \mathit{f}O_2$
MH08-08_amph04	44.04	2.62	11.12	11.77	3.12	0.18	14.29	10.70	2.25	0.26	0.09	0.03	99.24	916	275	-10.5
MH08-08_amph06	45.88	1.88	9.00	10.18	4.92	0.20	14.47	11.10	1.83	0.34	0.15	0.09	98.95	860	168	-11.3
MH08-08_amph07	42.87	2.61	12.27	11.30	3.12	0.19	14.09	10.93	2.33	0.25	-0.01	0.03	98.84	949	368	-10.0
MH08-08_amph08	47.03	1.53	7.97	11.50	4.49	0.23	14.63	10.95	1.65	0.35	0.14	0.09	99.33	834	130	-11.5
MH08-08_amph09	43.54	2.47	12.63	11.77	0.88	0.14	15.21	10.90	2.29	0.19	0.13	0.03	98.94	954	387	-9.6
MH08-08_amph10	46.45	1.73	8.58	10.80	4.14	0.22	14.83	11.14	1.62	0.31	0.11	0.08	98.85	847	151	-11.3
MH08-08_amph12	46.09	1.64	8.55	11.41	4.27	0.25	14.51	10.97	1.75	0.32	0.10	0.08	98.75	850	151	-11.3
MH08-08_amph13	46.84	1.56	7.98	11.17	4.46	0.28	14.55	10.90	1.62	0.31	0.14	0.11	98.73	828	131	-11.7
MH08-08_amph14	44.98	2.01	9.44	10.37	5.18	0.21	14.11	11.16	1.88	0.37	0.12	0.06	98.78	877	189	-11.1
MH08-12_amph05	45.45	1.77	8.95	11.42	4.05	0.22	14.41	10.90	1.77	0.36	0.14	0.09	98.32	859	168	-11.2
MH08-12_amph06	44.98	2.53	11.16	12.94	0.40	0.17	15.76	10.67	2.29	0.21	0.08	0.02	99.87	917	264	-10.1
MH08-12_amph07	46.33	1.72	8.27	11.30	4.00	0.19	14.82	11.02	1.62	0.36	0.15	0.10	98.66	850	141	-11.2
MH08-12_amph08	47.27	1.57	7.68	11.01	3.77	0.24	15.25	11.06	1.54	0.34	0.27	0.11	98.87	834	121	-11.3
MH08-12_amph09	42.99	2.23	11.90	11.31	5.61	0.21	12.97	11.19	2.23	0.36	0.15	0.05	100.01	934	338	-10.5
MH09-03_amph01	43.07	2.14	12.19	11.46	3.70	0.18	13.52	10.87	2.16	0.23	0.18	0.02	98.50	935	367	-10.3
MH09-03_amph02	46.79	1.58	8.42	10.95	4.42	0.20	14.62	10.89	1.72	0.33	0.25	0.08	99.01	835	145	-11.6
MH09-03_amph03A	46.98	1.80	8.12	10.17	4.83	0.20	14.87	11.11	1.70	0.35	0.24	0.09	99.34	837	135	-11.5
MH09-03_amph05	44.18	2.00	11.62	9.79	4.55	0.19	13.99	11.13	2.18	0.29	0.13	0.06	99.06	921	314	-10.5
MH09-03_amph06	46.61	1.67	8.12	10.20	4.73	0.23	14.71	11.04	1.66	0.35	0.15	0.11	98.48	836	137	-11.6
MH09-03_amph07	46.54	1.81	8.72	7.22	8.01	0.17	13.36	11.21	1.58	0.34	0.13	0.09	98.39	836	161	-12.1
MH09-03_amph10	46.32	1.78	8.44	10.61	4.56	0.23	14.55	10.93	1.70	0.39	0.15	0.08	98.59	842	147	-11.5
MH09-03_amph11	46.04	1.73	8.67	9.95	4.53	0.16	14.73	11.05	1.78	0.30	0.02	0.07	98.02	852	157	-11.3
MH09-03_amph12	47.25	1.50	7.57	10.37	4.33	0.22	15.03	11.00	1.58	0.28	0.19	0.09	98.28	820	119	-11.7
MH09-03_amph13	46.73	1.81	8.33	9.86	5.09	0.19	14.67	11.14	1.68	0.32	0.13	0.09	98.99	840	142	-11.6
MH09-03a_amph05	47.05	1.92	8.69	8.51	6.17	0.13	14.88	11.55	1.90	0.31	0.36	0.07	100.50	854	152	-11.4
MH09-03a_amph06	47.17	1.80	8.32	10.10	4.48	0.19	15.15	11.23	1.70	0.28	0.22	0.07	99.58	841	140	-11.4
MH09-03a_amph07	46.56	1.86	8.65	9.79	4.85	0.17	15.01	11.27	1.86	0.34	0.25	0.08	99.58	855	152	-11.2
MH09-03a_amph08	42.50	2.54	12.58	10.10	5.18	0.22	13.19	11.20	2.26	0.30	0.17	0.05	99.19	954	403	-10.2
MH09-04a_amph01	48.41	1.23	7.01	12.37	3.34	0.24	15.50	11.02	1.50	0.26	0.17	0.11	99.83	825	101	-11.2
MH09-04a_amph02	43.55	2.10	12.52	13.25	3.26	0.23	13.29	10.39	2.52	0.24	0.01	0.03	100.05	929	378	-10.5
MH09-04a_amph03	43.35	3.00	11.41	9.96	3.06	0.12	15.20	11.33	2.35	0.27	0.09	0.01	99.11	949	297	-9.9
MH09-04a_amph04	42.75	2.94	11.93	11.32	3.64	0.12	14.25	11.05	2.52	0.29	0.21	0.02	99.81	953	335	-10.0
MH09-04a_amph05	43.17	2.90	11.73	9.65	4.39	0.17	14.31	11.23	2.35	0.40	-0.01	0.03	99.35	948	323	-10.1
MH09-04a_amph06	43.30	2.80	12.64	11.72	0.24	0.09	15.95	11.08	2.48	0.21	0.15	0.02	99.44	970	381	-9.3
MH09-04a_amph07	43.15	2.82	11.85	10.63	3.20	0.13	14.72	11.25	2.34	0.26	0.08	0.02	99.35	951	328	-9.9
MH09-04a_amph08	42.14	3.01	11.93	10.88	3.17	0.15	14.37	11.13	2.33	0.27	0.10	0.02	98.34	961	347	-9.9
MH09-04a_amph09	43.20	2.31	12.50	12.52	0.32	0.17	15.26	10.64	2.51	0.19	0.09	0.01	98.43	954	380	-9.6
MH09-04a_amph10	43.27	2.93	11.49	10.86	2.89	0.16	14.61	10.95	2.25	0.23	0.02	0.03	98.59	939	305	-10.1
MH09-04a_amph11	47.82	1.28	7.10	10.96	3.61	0.23	15.86	10.92	1.99	0.39	0.17	0.09	99.24	842	105	-10.9
MH09-04a_amph12	46.65	1.71	8.44	10.98	4.28	0.28	15.04	11.10	1.98	0.32	0.23	0.09	99.88	860	144	-11.0

Table 3.1 continued

sample	SiO_2	TiO_2	Al_2O_3	Fe_2O_3	FeO	MnO	MgO	CaO	Na_2O	K_2O	F	Cl	Total	T (°C)	P (MPa)	logfO_2
MH09-04a_amph13	43.47	2.14	13.01	11.77	0.11	0.11	15.92	11.27	2.36	0.23	0.07	0.02	99.26	970	416	-9.2
MH09-04a_amph14	47.95	1.29	6.82	12.17	4.04	0.29	15.04	11.04	1.40	0.30	0.13	0.10	99.27	829	98	-11.2
MH09-04a_amph15	43.25	2.20	11.95	13.82	1.93	0.16	14.23	10.76	2.26	0.26	0.09	0.02	99.50	934	332	-10.1
MH09-04a_amph16	46.82	1.73	9.04	10.34	4.38	0.24	14.79	11.08	1.79	0.30	0.13	0.09	99.62	851	166	-11.3
MH09-04a_amph17	46.86	1.53	7.75	12.16	4.47	0.30	14.38	10.91	1.58	0.30	0.22	0.09	99.21	840	124	-11.3
MH09-04a_amph18	42.45	2.99	11.99	9.61	3.80	0.12	14.24	11.05	2.34	0.28	0.15	0.05	98.03	957	355	-10.0
MH09-04a_amph19	43.32	2.95	11.98	9.79	2.76	0.10	15.29	11.44	2.32	0.22	0.06	0.01	99.24	959	336	-9.7
MH09-04a_amph20	42.55	3.02	11.78	11.60	2.82	0.12	14.60	11.07	2.44	0.25	0.36	0.02	99.30	956	326	-9.9
MH09-10_amph01	43.34	1.95	12.76	11.21	3.06	0.25	14.09	11.12	2.17	0.40	0.14	0.06	99.34	949	408	-9.9
MH09-10_amph012	48.12	1.46	7.58	11.76	3.27	0.24	15.55	11.07	1.55	0.25	0.11	0.08	99.80	826	116	-11.4
MH09-10_amph013	47.27	1.53	7.74	12.54	2.59	0.27	15.55	10.95	1.61	0.31	0.15	0.07	99.24	851	121	-10.8
MH09-10_amph03	48.06	1.31	7.53	11.78	3.94	0.28	14.99	10.92	1.49	0.33	0.25	0.12	99.68	811	115	-11.8
MH09-10_amph05	47.28	1.62	7.97	11.44	4.37	0.29	14.75	10.99	1.64	0.31	0.17	0.10	99.70	834	128	-11.5
MH09-10_amph09	46.99	1.60	8.10	10.98	4.29	0.19	14.93	11.09	1.64	0.32	0.17	0.09	99.21	837	134	-11.4
MH09-10A_amph01	46.71	1.39	7.37	11.96	3.84	0.26	15.15	11.09	1.69	0.38	0.09	0.13	98.79	864	113	-10.5
MH09-10A_amph02	46.55	1.48	8.24	11.38	4.69	0.30	14.71	10.62	2.47	0.38	0.66	0.12	100.15	858	138	-11.1
MH09-10A_amph06	47.25	1.33	7.55	11.45	4.97	0.26	14.54	10.97	1.73	0.30	0.14	0.09	99.33	830	118	-11.5
MH09-10A_amph08	47.54	1.44	7.29	14.12	2.48	0.27	15.29	10.81	1.54	0.30	0.17	0.11	99.84	857	108	-10.5
MH09-10A_amph10	43.01	2.66	11.87	9.90	1.85	0.14	15.38	11.01	2.44	0.24	0.20	0.04	97.65	956	340	-9.6
MH09-10A_amph11	47.38	1.61	8.07	11.08	4.63	0.27	14.75	11.11	1.61	0.31	0.19	0.09	99.88	829	131	-11.7

Table 3.2 Trace elements by laser ablation ICP-MS in amphiboles from Mount Hood. Concentrations in μg/g.

sample	Li	Ti	Mn	Cu	Zn	Rb	Sr	Zr	Nb	Ba	Hf	Pb	Th	U
MH08-08_amph04	4	18844	1373		111	0.53	234	69	8.7	69.1	3.4	0.6	0.05	
MH08-08_amph06	20	9613	1991	7.1	171	2.40	77	74	15.0	72.5	2.9	2.7	0.33	0.12
MH08-08_amph07	12	16235	1527	10.9	108	0.38	199	54	6.3	42.0	2.1	0.4		
MH08-08_amph08	6	11027	2172	2.1	212	1.14	79	106	17.1	66.9	3.9	0.6	0.17	0.09
MH08-08_amph10	12	13352	1830	35.3	163	0.59	101	90	13.2	69.7	3.3		0.01	0.06
MH08-08_amph13	21	10590	2443	11.0	211	0.54	65	66	15.6	47.7	3.6	0.6	0.10	
MH08-08_amph14	13	15098	1550	70.8	139	0.42	202	77	11.3	62.0	2.6	0.6	0.02	0.01
MH08-12_amph07	87	11460	1641	5.7	170	0.74	85	91	18.2	57.1	4.0	0.6	0.06	
MH08-12_amph08	259	10889	1882	118.3	208	0.88	74	75	17.9	53.5	3.6	0.6	0.09	
MH08-12_amph09	208	11203	1203	117.2	125	4.67	171	65	6.8	93.9	2.5	2.8	0.40	0.08
MH09-03_amph01	132	13619	1668	21.5	149	0.62	172	63	7.4	51.7	3.4	0.9	0.21	
MH09-03_amph02	93	10838	2061	32.7	214	1.27	87	126	13.1	61.1	6.0	3.2	0.27	0.07
MH09-03_amph03A	23	10866	1665	43.2	155	0.37	91	84	11.5	66.7	3.4	0.7		
MH09-03_amph05	16	14961	1448	7.1	127	0.47	210	56	4.3	38.6	1.5	0.4	0.05	
MH09-03_amph06	23	11088	1697	40.3	168	0.34	91	84	12.5	58.7	3.5	1.1		
MH09-03_amph07	68	12188	1818	90.6	162	0.25	116	117	14.3	75.2	3.7	0.9	0.07	
MH09-03_amph12	71	11200	2030	25.3	192	0.42	85	67	10.4	52.9	2.3	1.3	0.10	
MH09-03_amph13	91	9581	1967	13.9	141	0.71	107	67	10.6	65.3	4.2	0.0	0.15	0.08
MH09-03a_amph05	32	12033	1724	19.2	145	1.25	109	100	14.3	70.8	3.7	0.9	0.06	
MH09-03a_amph06	134	11616	1657	201.2	155	0.37	100	87	12.4	58.5	3.5			
MH09-03a_amph07	82	11991	1630	18.2	153	0.46	102	93	12.5	54.9	3.4	0.5		
MH09-03a_amph08	123	16950	1510	72.7	118	0.55	260	49	6.4	62.2	2.1	0.6		
MH09-04a_amph01	152	9067	2309	41.0	206	0.30	64	80	16.3	42.7	3.9	0.3	0.03	
MH09-04a_amph02	106	17571	1444	49.0	106	0.36	216	48	5.9	59.0	1.1	0.3		
MH09-04a_amph03	85	18097	1588	42.3	104	1.97	238	54	5.1	73.4	1.8	0.5	0.08	0.04
MH09-04a_amph04	50	19390	1484	43.3	102	1.18	277	72	10.5	142.2	1.2	1.9	0.07	
MH09-04a_amph05	96	21195	1119	35.9	89	1.31	270	49	6.1	88.0	1.6	0.5	0.06	
MH09-04a_amph06	81	15092	980	50.6	67	0.67	326	44	3.9	50.6	1.8	0.4		
MH09-04a_amph07	126	18695	1374	41.9	97	0.97	268	44	5.7	59.9	1.3	0.2		
MH09-04a_amph08	75	19598	1081	36.8	86	0.18	268	56	6.0	75.8	2.3			
MH09-04a_amph09	101	19016	1107	62.1	96	0.84	262	52	5.1	85.0	1.1			
MH09-04a_amph10	125	21054	1300	48.3	115	0.30	266	55	7.6	75.2	2.6	1.4		
MH09-04a_amph12	106	10291	1659	26.2	160	0.20	184	73	11.8	60.7	3.4	0.8	0.11	
MH09-04a_amph13	150	15922	1022	34.3	61		255	53	3.8	41.5	2.6	1.4		
MH09-04a_amph14	123	9074	2307	15.2	209	0.69	58	70	15.4	45.2	4.0	0.4		
MH09-04a_amph15	100	16765	1226	36.6	86	0.55	234	65	4.6	80.6	2.3	0.5		0.17
MH09-04a_amph16	137	11983	1761	40.8	163	0.92	113	74	12.1	71.6	3.6	1.2		0.02
MH09-04a_amph17	73	9574	1856	5.5	172	0.36	68	82	16.9	48.9	2.9	0.6		
MH09-04a_amph18	97	20095	1021	36.2	78	0.66	270	59	5.7	71.0	1.9		0.20	0.08
MH09-04a_amph19	99	20878	1109	32.4	86	1.02	271	64	5.0	92.3	3.2	1.0	0.11	
MH09-04a_amph20	42	13745	1130	27.2	84	0.25	244	71	4.3	58.5	2.3	0.9		
MH09-10_amph01	325	13352	1936	66.0	171	1.34	222	60	6.1	49.3	2.2	0.6		0.05
MH09-10_amph013	241	11801	2035	115.9	179	1.00	101	237	12.1	59.0	4.0	0.8		
MH09-10_amph03	85	8554	2242	122.2	197	1.57	54	60	14.4	39.2	3.1	0.6	0.15	
MH09-10_amph09	125	10512	2301	86.6	213	1.11	79	77	15.3	71.4	2.7	0.9	0.09	
MH09-10A_amph01	42	7532	2440	22.5	220	0.52	45	79	13.9	37.1	3.7	0.6		
MH09-10A_amph02	19	9218	2455	125.1	242	1.24	63	99	17.3	73.4	5.4	1.3	0.00	0.07
MH09-10A_amph06	34	9178	2379	12.5	232	0.55	65	102	16.3	52.1	3.9	0.3		
MH09-10A_amph08	34	8641	2431	30.2	244	0.63	56	65	13.2	40.9	2.9	1.1	0.29	0.13
MH09-10A_amph10	83	18327	1246	76.2	104	0.35	282	66	6.3	83.6	2.2	1.3	0.50	0.34
MH09-10A_amph11	88	10394	2032	23.9	190	0.49	80	133	15.1	48.2	6.2	0.6		

Table 3.2 continued

sample	La	Ce	Pr	Nd	Sm	Eu	Gd	Dy	Er	Yb	Eu/Eu*
MH08-08_amph04	5.3	22.5	4.4	25.8	11.1	2.7	10.8	9.7	3.7	3.0	0.75
MH08-08_amph06	14.6	61.7	11.3	66.8	19.3	3.5	22.7	18.9	11.1	8.7	0.51
MH08-08_amph07	3.0	13.3	3.3	17.7	8.3	2.1	8.1	6.8	3.3	2.0	0.76
MH08-08_amph08	15.0	82.6	14.1	78.5	25.5	4.1	28.0	24.3	12.1	9.6	0.46
MH08-08_amph10	13.7	59.0	10.8	57.6	14.8	3.7	13.9	13.5	6.6	4.9	0.78
MH08-08_amph13	16.5	81.8	14.4	85.1	27.3	3.8	25.1	23.1	13.4	8.7	0.43
MH08-08_amph14	9.7	41.3	7.3	44.8	14.4	3.2	14.0	12.0	6.2	5.4	0.68
MH08-12_amph07	16.5	69.8	13.9	84.3	28.6	4.6	26.9	28.1	13.0	9.5	0.49
MH08-12_amph08	18.1	72.0	14.0	84.3	24.9	3.8	24.4	22.9	10.4	8.3	0.47
MH08-12_amph09	4.7	21.4	3.9	22.3	5.7	1.7	6.2	9.0	3.3	4.2	0.88
MH09-03_amph01	7.8	33.7	5.6	30.8	7.6	3.1	8.7	10.7	4.8	3.6	1.14
MH09-03_amph02	13.1	76.5	13.5	69.9	25.7	4.8	21.1	23.8	12.5	11.8	0.62
MH09-03_amph03A	12.4	65.4	12.5	76.4	25.3	3.9	25.7	24.5	13.2	9.8	0.47
MH09-03_amph05	5.0	21.4	3.6	21.4	6.9	1.8	8.9	9.2	4.4	2.7	0.70
MH09-03_amph06	13.2	67.3	14.5	84.0	27.7	4.4	32.3	25.9	13.8	10.0	0.45
MH09-03_amph07	13.3	60.4	12.1	68.5	20.4	4.4	25.2	21.0	10.9	7.1	0.60
MH09-03_amph12	8.8	56.0	9.2	53.6	15.5	3.0	20.9	17.1	7.8	3.0	0.50
MH09-03_amph13	11.9	50.0	9.8	57.6	16.9	3.2	16.0	13.1	7.9	6.8	0.58
MH09-03a_amph05	12.1	57.2	10.4	59.4	20.5	4.7	20.5	17.0	10.8	8.5	0.69
MH09-03a_amph06	10.5	52.6	10.5	61.8	18.9	3.8	21.0	20.3	8.8	6.0	0.59
MH09-03a_amph07	10.9	52.6	9.8	58.7	20.0	4.2	19.7	18.8	9.8	8.6	0.64
MH09-03a_amph08	3.9	18.6	4.0	21.6	7.9	2.1	6.4	7.8	4.3	2.1	0.85
MH09-04a_amph01	17.5	80.4	15.0	89.9	26.4	4.7	29.5	25.2	15.0	10.7	0.51
MH09-04a_amph02	3.0	14.8	2.9	19.0	5.9	2.5	8.3	6.2	2.2	2.0	1.09
MH09-04a_amph03	5.2	15.9	2.5	19.0	7.7	1.9	3.6	6.1	2.2	2.8	0.95
MH09-04a_amph04	3.7	14.5	2.4	20.3	4.8	2.3	3.5	5.5	1.4	1.5	1.64
MH09-04a_amph05	3.6	11.8	2.9	19.9	6.4	2.2	6.4	6.3	3.9	2.4	1.03
MH09-04a_amph06	2.3	10.6	1.9	12.7	3.7	1.2	4.9	2.7	1.4	0.9	0.86
MH09-04a_amph07	2.9	11.0	3.0	16.2	5.1	1.9	7.3	4.6	2.3	1.4	0.93
MH09-04a_amph08	3.5	16.7	3.3	20.8	5.4	2.3	7.8	5.9	2.9	2.3	1.09
MH09-04a_amph09	3.8	12.9	2.2	15.4	3.7	1.7	6.4	5.3	2.1	1.7	1.03
MH09-04a_amph10	4.2	14.0	3.6	15.5	5.0	2.0	5.0	6.0	2.0	1.8	1.18
MH09-04a_amph12	13.5	47.4	10.1	54.5	17.3	2.4	17.2	11.4	8.4	6.2	0.41
MH09-04a_amph13	1.6	8.1	1.7	14.0	5.3	1.3	4.6	3.9	2.2	0.7	0.76
MH09-04a_amph14	22.0	89.3	17.7	98.8	31.1	3.6	32.5	24.8	13.8	10.0	0.34
MH09-04a_amph15	4.3	14.5	3.1	19.5	5.2	2.1	9.7	6.3	2.4	2.7	0.90
MH09-04a_amph16	13.1	49.9	9.8	56.0	18.4	3.0	16.5	16.6	8.7	5.9	0.51
MH09-04a_amph17	18.2	71.8	15.4	94.4	29.4	4.9	34.7	27.6	12.8	9.8	0.46
MH09-04a_amph18	3.7	12.9	3.0	18.7	6.7	2.4	7.4	6.3	2.5	3.1	1.05
MH09-04a_amph19	4.7	14.3	2.9	19.8	7.3	2.1	9.1	6.3	3.6	1.8	0.78
MH09-04a_amph20	3.1	10.7	1.9	11.8	4.7	1.5	6.9	4.5	3.2	1.9	0.79
MH09-10_amph01	6.1	26.8	4.4	23.8	6.0	2.0	9.7	7.8	3.4	3.6	0.79
MH09-10_amph013	12.6	53.3	11.1	67.8	19.6	3.9	19.8	17.2	9.1	6.5	0.60
MH09-10_amph03	19.0	81.4	16.8	103.4	29.5	3.3	30.0	28.0	15.1	10.3	0.34
MH09-10_amph09	15.4	64.6	12.2	72.4	21.4	3.7	22.3	19.2	10.7	6.0	0.51
MH09-10A_amph01	19.5	101.6	20.9	109.9	41.0	3.8	37.5	35.5	17.1	11.6	0.29
MH09-10A_amph02	19.1	83.3	15.5	78.2	25.9	4.1	24.1	23.3	9.7	7.9	0.50
MH09-10A_amph06	17.2	77.1	14.2	83.6	24.7	4.6	23.8	19.5	11.3	8.9	0.57
MH09-10A_amph08	15.0	77.4	14.4	73.4	28.6	4.9	26.5	22.7	9.2	12.6	0.54
MH09-10A_amph10	8.6	21.2	3.7	19.2	5.4	1.9	7.5	4.9	4.1	3.1	0.93
MH09-10A_amph11	18.7	70.7	15.1	87.7	29.0	4.7	36.3	31.3	15.8	10.2	0.45

CHAPTER FOUR

TRACE ELEMENT SYSTEMATICS OF MAGMA MIXING AT MOUNT HOOD, OREGON

Alison M. Koleszar
Adam J. R. Kent

ABSTRACT

Previous studies have identified the andesites and dacites of Mount Hood as the products of magma mixing, and have characterized the endmembers as broadly basaltic and rhyolitic in composition. In this study we combine new whole rock, phenocryst, and melt inclusion compositional data to estimate the trace element compositions and potential sources of the mixing endmembers involved in magmagenesis at Mount Hood. We find that the mafic endmember at Mount Hood is similar to typical Cascades calc-alkaline basalt and is compositionally consistent with isenthalpic flux melting of a peridotite source with contributions of slab fluids ± melts. Fan-shaped arrays of mixing lines, particularly in elements that are compatible in mafic magmas, suggest up to 20% fractional crystallization of the mafic endmember to create an array of derivative endmembers. The silicic endmember has trace element concentrations broadly consistent with rhyolitic plagioclase-hosted melt inclusions from Mount Hood. The composition of this endmember is consistent with partial melting of mafic amphibolite in the middle to lower crust. Although there is potential for arc lavas to be mixed with any number of different compositions of material en route through the crust, the lavas of Mount Hood show remarkable geochemical and petrologic evidence for relatively simple bimodal magma mixing. We observe that the trace element variation in Mount Hood lavas is consistent with this style of mixing.

INTRODUCTION

Mount Hood is a relatively young intermediate arc volcano located in the Cascade Range, and has erupted compositionally restricted andesitic-dacitic lava domes and lava

flows over the last ~0.5 ka (Scott et al., 1997a). A number of studies have identified the importance of magma mixing in generating the intermediate compositions that are erupted at Mount Hood (Cribb and Barton, 1997; Darr, 2006; Kent et al., 2010; Woods, 2004), and recent work has suggested that Mount Hood may be an appropriate general model for the production of andesites at mixing-dominated intermediate arc volcanoes (see Chapter Three and Kent et al., 2010).

Although assigning "endmember" compositions to mixed magmas is fraught with difficulties and likely represents an oversimplification of processes in which magma ascends through 10's of kilometers of materials of potentially varied compositions (Hildreth, 2007), recent work has suggested that magma mixing at Mount Hood may be truly bimodal (see Chapter Three and Kent et al., 2010). Kent et al. (2010) used a combination of compositional and textural data to estimate the compositions of endmember magmas involved as broadly basaltic (50.7±4.3 wt% SiO_2) and rhyolitic (70.9±2.1 wt% SiO_2), however attempts to constrain endmember trace element concentrations have relied on erupted compositions and have been only moderately successful (Woods, 2004). Herein we use new data from intermediate lavas, mafic enclaves, mafic plutonic inclusions, high-SiO_2 melt inclusions, amphibole, and plagioclase phenocrysts to further constrain the magma compositions involved in mixing at Mount Hood, and characterize these lavas in the context of the primitive lavas of the Cascades.

None of the lavas erupted from Mount Hood can be characterized are primitive: all have Mg# < 0.52 and MgO < 4.4 wt% and range from basaltic andesite (one sample) to

dacite, with the majority of erupted lavas andesitic in composition. However, like many of the intermediate lavas of the Cascades, they are likely ultimately derived from one of the common primitive basaltic parents known from the region. The three principle parent magma types in the Cascades have been described in previous studies (e.g., Conrey et al., 1997; Hildreth, 2007; Reiners et al., 2000; Schmidt et al., 2008) include: 1) A moderately trace element depleted basalt that has been called by various names, including mid-ocean ridge basalt (MORB), high-alumina olivine tholeiite (HAOT), and low-potassium tholeiite (LKT), 2) A trace element enriched basalt with high concentrations of high field strength elements (HFSE) relative to large ion lithophile elements (LILE), called OIB, intraplate basalt, within-plate basalt (WIP), or HFSE-rich, and 3) An often-hydrous basalt with high concentrations of LILE relative to HFSE, referred to as calc-alkaline basalt (CAB), high-alumina basalt (HAB), or simply arc basalt. Previous studies have suggested that the lavas at Mount Hood lack significant HFSE depletion (relative to LILE) that is typically associated with arc lavas (Cribb and Barton, 1997), however the data that we present here suggest that the HFSE/LILE ratios of Hood lavas are consistent with HFSE-depletion/LILE-enrichment that is considered a signal of slab input into arc volcanics.

The comprehensive dataset presented in this paper allows for more detailed determination of the trace element budgets of the magma endmembers involved in mixing at Mount Hood. Our data confirm that the lavas produced at Mount Hood are likely to be mixtures of a mafic magma that is compositionally related to the most mafic lavas erupted from Mount Hood, and a high-SiO_2 magma with trace element contents that

are near the concentrations in plagioclase-hosted melt inclusions. Any scenario proposed for the petrogenesis of intermediate lavas at Mount Hood likely represents a non-unique solution, however our results suggest that a relatively simple model of binary mixing between a magma generated by isenthalpic flux melting of a peridotite source and a silicic crystal-rich mush derived from partial melting of mafic amphibolite adequately reproduces most of the trace element variation in lavas erupted from Mount Hood.

SAMPLES

This study incorporates data from melt inclusions, phenocryst phases (plagioclase and amphibole), and whole rock compositions. Whole rock data includes major elements, trace elements, and $^{87}Sr/^{86}Sr$ and $^{143}Nd/^{144}Nd$ ratios. We report trace element data for melt inclusions; major element data are reported elsewhere {Koleszar, in review #305}. Plagioclase and amphibole were analyzed from many of the samples listed in Table 4.1 and described below. Additional information on phenocryst analyses can be found in Chapter Two.

A total of 40 samples were selected for whole rock analyses. Samples were initially divided on the basis of their textural and petrographic characteristics and are described below.

Intermediate lavas

Samples of lava flows, domes, and prismatically-joined blocks (PJBs) in block-and-ash flows are included in this group. Ages range from 475 ka (Main Stage Eruptive Period) to ~220 years (Old Maid Eruptive Period) (Table 4.1). Fourteen of the

intermediate lavas were collected and analyzed by XRF in 2004 by Cris Darr (Darr, 2006); these data are reported in Kent et al. (2010) and these samples were analyzed for trace elements by ICP-MS with the samples described below. We collected the remaining 14 lava samples in the summers of 2008 and 2009.

Lava flow, lava dome, and PJB samples are typically light to medium gray in color, medium-grained, and porphyritic, with phenocrysts of plagioclase, amphibole, orthopyroxene, and minor amounts of FeTi-oxides (Fig. 4.1a). The groundmass is dominated by glass and plagioclase microlites. Additional petrographic descriptions can be found in Darr (2006) and Woods (2004).

Although pumiceous deposits are rare at Mount Hood (Scott et al., 1997b), limited amounts of pumice were ejected in block-and-ash flows following dome collapse events. William E. Scott at the USGS Cascades Volcano Observatory provided samples of pumice from the Polallie and Timberline eruptive periods, and in 2008 we collected pumice from the Old Maid eruptive period (Table 4.1). Pumice samples contain abundant plagioclase, amphibole, and orthopyroxene in a glassy matrix (Fig. 4.1b). Pumice samples were collected primarily for melt inclusions, which are often quenched in rapidly cooled samples. This minimizes the effects of volatile loss and post-entrapment crystallization within melt inclusions (Kress and Ghiorso, 2004; Luhr, 2001).

Porphyritic inclusions

Inclusions of darker porphyritic lava were present in samples we collected from Crater Rock, the remnants of the Old Maid- and Timberline-aged lava dome near the summit of Mount Hood (MH09-07a), and a prismatically-jointed block (PJB) from the

Timberline eruptive period (MH09-10a, Table 4.1). These two inclusions are texturally nearly identical to their host rock and contain a similar mineral assemblage (Fig. 4.1c).

Fine-grained mafic enclaves

Eight of the lava samples (representing a variety of eruptive periods, Table 4.1) contain fine-grained mafic enclaves, which are lighter in color than their host rock (average grainsize ~200 μm, Fig. 4.1d). These enclaves are microvesicular, have broadly similar mineralogy to the lava samples in which they are hosted (primarily plagioclase + orthopyroxene + amphibole ± FeTi-oxides), and are dominated by fine-grained (< 500 μm) equigranular elongate plagioclase (Fig. 4.1c). Occasional large (>1000 μm) plagioclase phenocrysts are also present. These samples are texturally similar to enclaves (or "quenched mafic inclusions") observed at other intermediate arc volcanoes, including Augustine Volcano (Steiner, 2009), Unzen Volcano (Browne et al., 2006) and Mount St. Helens (Heliker, 1995; Lieuallen, 2010). Fine-grained mafic enclaves from Mount Hood are described in detail in Woods (2004).

Plutonic inclusions

Two inclusions are texturally distinct from the mafic enclaves and porphyritic inclusions described above. MH09-01a contains abundant plagioclase, orthopyroxene, clinopyroxene, amphibole, and Fe-Ti oxides interspersed with regions of polygonal plagioclase (Fig. 4.1e), and mineralogically resembles the laminated gabbronorite inclusions at Mount St. Helens (Heliker, 1995). MH08-11b is coarse-grained and sugary

in hand sample, with interlocking grains of plagioclase, orthopyroxene, and clinopyroxene, abundant Fe-Ti oxides, and minor amounts of olivine (Fig. 4.1f), and resembles the gabbroic xenoliths at Augustine Volcano (Larsen et al., 2010; Steiner, 2009) and the subophitic gabbronorite inclusions at Mount St. Helens (Heliker, 1995; Lieuallen, 2010). For simplicity, these two samples will be referred to as plutonic inclusions (Table 4.1).

ANALYTICAL METHODS

Whole rock XRF

Major and selected trace elements were measured in lava, pumice, enclave, and inclusion samples using a ThermoARL Advant'XP+ sequential X-ray fluorescence (XRF) spectrometer at the Washington State University (WSU) GeoAnalytical Laboratory. Samples were powdered by grinding clean rock chips in a carbon-steel ring mill. Once powdered, 3.5 g of sample was combined with 7 g of lithium tetraborate flux, placed in a crucible, and fused at 1000˚C in a muffle furnace for 30 minutes. The fused bead was then reground in the carbon-steel ring mill and fused again. After cooling, the bottom surface of each bead was polished in preparation for XRF analysis. Further details on sample preparation techniques are described elsewhere (Johnson et al., 1999). The data for these 26 analyses are in good agreement with 14 analyses performed by Cris Darr in 2004, using similar procedures (Darr, 2006).

Whole rock ICP-MS

The samples described above were analyzed for trace elements at the WSU GeoAnalytical Laboratory using an Agilent 7700 Inductively Coupled Plasma Mass Spectrometer (ICP-MS). Samples were ground and fused as described above for XRF analyses, but were mixed with Li-tetraborate flux in a ratio of 1:1 and were fused only once. The fused beads were reground to a powder for acid dissolution and analysis (additional analytical information is available at http://www.sees.wsu.edu/Geolab/note/icpms.html).

Whole rock MC-ICP-MS

Approximately 150 mg of powdered rock (prepared as described above for XRF) for 11 lava samples and two plutonic inclusions was shipped to Dr. Petrus le Roux for analysis of $^{87}Sr/^{86}Sr$ and $^{143}Nd/^{144}Nd$ ratios. Powders were dissolved by HF:HNO_3 digestion then Sr and Nd were chromatographically separated (Míková and Denková, 2007). Analy2ses were performed on a NuPlasma HR in the AEON EarthLAB at the University of Cape Town, South Africa. $^{87}Sr/^{86}Sr$ ratios in standard reference material BHVO-2G were within the reported ranges for this material (with 2σ errors; measured $^{87}Sr/^{86}Sr$ = 0.703489±14 and 0.703452±12 with reported value 0.703479±20). Measured ratios of $^{143}Nd/^{144}Nd$ in BHVO were also within the reported range (0.512996±6 and 0.512984±4 with reported value 0.512984±11). Internal errors are typically one in the fifth decimal place (i.e., 0.00001) for $^{87}Sr/^{86}Sr$ and 5-8 in the sixth decimal place (i.e., 0.000005-0.000008) for $^{143}Nd/^{144}Nd$.

EMPA

Major element concentrations in melt inclusions, plagioclase phenocrysts, and amphibole phenocrysts were determined by Electron Microprobe Analysis (EMPA) at Oregon State University using a Cameca SX-100 Electron Microprobe with 15 kV accelerating voltage and 30 nA beam current. Analytical details are described in Koleszar et al. (in review) and Chapter 2.

LA-ICP-MS

Trace elements in plagioclase, amphibole, and melt inclusions were analyzed by Laser Ablation Inductively Coupled Plasma Mass Spectrometry (LA-ICP-MS) in the W.M. Keck Collaboratory for Plasma Mass Spectrometry at Oregon State University using a procedure similar to that described in Kent and Ungerer (2006). A NewWave 193 nm DUV ArF Excimer Laser was used for ablation. Laser spot size was typically 40 μm with a pulse rate of 4 Hz and 45 s ablation time. Helium was used a carrier gas, flowing at ~0.8 L/min. Ablated material was analyzed on a VG PQ ExCell quadrupole ICP-MS using NIST-612 and GSE-1G as calibration standards, with trace element concentrations measured relative to ^{43}Ca as an internal standard for amphibole and plagioclase and ^{29}Si as an internal standard for melt inclusions. Analytical uncertainty and precision (as assessed by replicate analyses of standard reference materials) was typically within 10-15% for most trace elements.

RESULTS

The majority of samples from Mount Hood are typical crystal-rich arc andesites to dacites with 58.9-63.8 wt% SiO_2. Two dark gray porphyritic inclusions that were hosted in dacite are also dacitic in composition, and compositionally equivalent to the host lavas of similar SiO_2 content suggesting that their dark color is the result of lower degrees of vesicularity rather than compositional differences. Pumice samples are compositionally indistinguishable from lavas and prismatically jointed blocks (PJBs).

Major elements

Bulk compositions of intermediate lavas, porphyritic inclusions, mafic enclaves, and plutonic inclusions range from basalt to dacite (Table 4.2, Fig. 4.2) and form linear trends on most Harker diagrams (Fig. 4.3), bracketed by the low-SiO_2 plutonic inclusions and the high-SiO_2 melt inclusions. Intermediate lavas (including pumice, lavas, and PJBs) contain 55.0-63.8 wt% SiO_2, mafic enclaves contain 56.5-59.4 wt% SiO_2, porphyritic inclusions contain 63.4 wt% SiO_2, and pumices contain 58.7-63.2 wt%. With the exception of the plutonic inclusions (which have the most mafic bulk compositions), all whole rock samples are medium-K calc-alkaline basaltic andesites to dacites. The most mafic lava sample is a basaltic andesite from Cloud Cap. Basaltic andesites from the Parkdale lava flow, located 11 km north of Mount Hood, are compositionally similar to Cloud Cap lavas (more information about both of these units can be found in (Darr, 2006)). At a given SiO_2, these basaltic andesites are displaced to higher Na_2O and slightly lower K_2O than the other lavas from Mount Hood. Melt inclusions are rhyolitic, consistent with typical melt inclusions in intermediate rocks (e.g., Reubi and Blundy,

2009) and are discussed in greater detail in Koleszar et al. (in review) and in Chapter Two. The dark gray porphyritic inclusions are dacitic and indistinguishable from dacitic host rock compositions; in future discussion and on most figures they are grouped with "intermediate lavas."

Incompatible trace elements

Incompatible trace element (ITE) concentrations in whole rock samples vary somewhat between the whole rock sample groups (Table 4.3a), and are distinct from the ITE concentrations of plagioclase-hosted melt inclusions (Table 4.3b). The basaltic andesites from Cloud Cap and Parkdale are slightly less enriched than the intermediate lavas (Figs. 4.4a, 4.5a). Most of the mafic enclaves have ITE concentrations intermediate between the Hood intermediate lavas and the Cloud Cap and Parkdale basaltic andesites, although the most depleted mafic enclave is as depleted as the lavas from Cloud Cap and Parkdale (Figs. 4.4a, 4.5a). Consistent with their major elements (Fig. 4.3), the porphyritic (dacitic) inclusions and pumice samples are indistinguishable from intermediate lavas (Figs. 4.4b, 4.5b). Sample EB-04-01, an intermediate lava with 61.9 wt% SiO_2, is anomalously ITE-enriched relative to the other lavas, particularly in LREE, Ba, Th, U, and K (Fig. 4.4b, 4.5b). The plutonic inclusions are more depleted in most ITEs than other samples from Hood (Figs. 4.4c, 4.5c). The depletion is most extreme in MH09-01a, the most mafic plutonic inclusion. Intermediate lavas and mafic enclaves have negative Ti-anomalies, whereas plutonic inclusions have positive Ti anomalies.

Concentrations of ITEs in the lavas from Mount Hood are generally slightly more enriched than CAB or LKT (Fig. 4.4a), the two most ubiquitous basalt compositions present in the Cascades (e.g., Hildreth, 2007; Reiners et al., 2000; Schmidt et al., 2008). Like CAB and to a lesser extent, LKT, lavas and enclaves from Hood are generally enriched in LILE, including Ba, Sr, and Pb. Ratios of U_N/Th_N and K_N/La_N are >1 in lavas and mafic enclaves from Hood, more similar to CAB than to LKT. Moderately high LILE/HFSE ratios (e.g., Ba/Zr, Ba/Nb) and low Nb/Zr characteristic of Nb-depletion (Fig. 4.6) distinguish Hood lavas from the HFSE-rich (OIB-like) lavas of the Cascades (e.g., Conrey et al., 1997; Hildreth, 2007; Leeman et al., 2005; Schmidt et al., 2008). It was previously argued that lavas from Mount Hood lack significant HFSE depletion (Cribb and Barton, 1997), however previously reported Nb concentrations (8-16 μg/g) are considerably higher than the concentrations we measure by both ICP-MS and XRF (7-11 μg/g). On the basis of these new measurements, we conclude that lavas from Hood do exhibit the HFSE/LILE depletion characteristic of Cascades CAB and lavas from many other subduction zones.

$^{87}Sr/^{86}Sr$ and $^{143}Nd/^{144}Nd$

$^{87}Sr/^{86}Sr$ and $^{143}Nd/^{144}Nd$ ratios in samples from Mount Hood are, with only one exception, nearly identical for the 11 lavas and 2 plutonic inclusions that were analyzed (Table 4.4, Fig. 4.7). With the exception of sample CD-04-01, lavas and plutonic inclusions have $^{87}Sr/^{86}Sr$ and $^{143}Nd/^{144}Nd$ ratios consistent with CAB from this portion of the Cascades (Schmidt et al., 2008). There is no consistent relationship between isotopic enrichment and SiO_2 content (Fig. 4.8). The major and trace element concentrations of

CD-04-01 are otherwise indistinguishable from the other Hood samples, so it is unclear why this sample would be isotopically depleted relative to other Mount Hood lavas. MC-ICP-MS signals for Sr, Rb, Nd, Ce, and Sm and stable isotope ratios are consistent with all other samples from this suite (Petrus le Roux, personal communication), suggesting either contamination during sample preparation or perhaps real variation within this one lava from Mount Hood.

DISCUSSION

The new data presented here confirm some of the previous results regarding the generation of andesites to dacites at Mount Hood, and allow us to further explore possible sources for the parental magmas. On the basis of their textural and geochemical characteristics, the samples in this study have been divided into the following categories: 1) "plutonic inclusions," which are crystal cumulates that contain 49.3-54.7 wt% SiO_2, 2) "mafic lavas," which range from 55.0-58.8 wt% SiO_2 and include basaltic andesites from the Cloud Cap lava flow and andesites from the Parkdale lava flows; 3) "mafic enclaves," which contain 56.6-59.4 wt% SiO_2 and are hosted in Mount Hood andesites and dacites; and 4) "intemediate lavas," which range from 58.9-63.8 wt% SiO_2 and include samples of lava flow and dome samples, PJBs present in block-and-ash flows, pumice, and porphyritic inclusions. These four categories and possibilities for their petrogenesis are discussed below.

Controls on magma compositions

Samples of lava, pumice, inclusions, and enclaves exhibit extensive compositional overlap and fall within the range of compositions previously described for Mount Hood (Darr, 2006; Kent et al., 2010; Scott et al., 1997a; Woods, 2004){Cribb, 1997 #110}. The overall shape of ITE-patterns and large positive anomalies in Ba, K, and Sr (Figs. 4.4a-c) in most of the samples from Mount Hood closely resemble arc lavas in general, and more specifically, typical Cascades CAB (e.g., Conrey et al., 1997; Hildreth, 2007; Reiners et al., 2000; Schmidt et al., 2008). Concentrations of HFSE and LREE are slightly higher in the Hood lavas than in typical Cascades CAB (Fig. 4.4-4.5); these enrichments are present in the accreted mantle domains that are proposed to underlie the Columbia segment of the Cascades, which stretches from Mount Jefferson to Mount Rainier and includes Mount Hood (Schmidt et al., 2008).

With the exception of one lava, $^{87}Sr/^{86}Sr$ and $^{143}Nd/^{144}Nd$ ratios (0.7033-0.7035 and 0.51294-0.51296, respectively) are remarkable similar in all samples from Mount Hood and do not correlate with SiO_2 content (Fig. 4.8). These ratios are consistent with the overall lack of isotopic diversity in the Cascades arc (e.g., Hildreth, 2007), but the particularly restricted range at Mount Hood suggests that erupted lavas may be more closely related to each other than at volcanoes with greater diversity in their isotopic signatures, such as Mount Jefferson (Conrey et al., 2001).

Although linear arrays on many major element diagrams (Fig. 4.3) are broadly consistent with fractional crystallization of plagioclase + orthopyroxene ± amphibole to produce the range of compositions observed in more evolved lavas, abundant evidence for magma mixing invalidates a simple fractional crystallization model. For example, the

presence of mafic enclaves indicates mingling between magmas of different compositions and/or physical properties (Sparks and Marshall, 1986), and mineral compositions, textures, and zoning patterns have led previous workers to suggest that andesites at Mount Hood are produced by mixing between separate silicic and mafic magmas (Cribb and Barton, 1997; Darr, 2006; Kent et al., 2010; Woods, 2004).

The trace element data presented here suggest a similar conclusion (that is, that the intermediate lavas at Mount Hood are produced by mixing rather than crystal fractionation). One particular indicator of this is the relationship between Ni and Rb, two trace elements with very different partition coefficients. The bulk partition coefficient for Ni estimated by Schmidt and Grunder (2011) for an arc basaltic andesite parent close in composition to our most mafic lava from Mount Hood is $D_{Ni} = 4.2$, and the extremely incompatibility of Rb in most phases allows us to estimate $D_{Rb} = 0$ e.g., (Blundy et al., 2008). Crystallization of a mafic (low Rb, high Ni) parent produces a hyperbolic relationship between Rb and Ni whereas the lavas from Mount Hood form an approximately linear array (Fig. 4.9). The elevated Ni contents of evolved lavas are therefore indicative of mixing with a mafic magma.

In intermediate lavas erupted from Mount Hood, Kent et al. (2010) and Darr (2006) identified a population of plagioclase (which they call "Population 1 plagioclase") that appears to have crystallized from this mafic magma. The other population of plagioclase ("Population 2") appears derived from a more silicic source (Kent et al., 2010). For samples with measured crystal size distributions (CSDs), Kent et al. (2010) observed a good correlation between the bulk composition of the sample and the proportion of Population 1 plagioclase that they contain, and used this relationship to

extrapolate endmember magma compositions where $X_{Population\ 1} = 0$ for the silicic endmember and $X_{Population\ 2} = 1$ for the mafic endmember. Kent et al. (2010) then used these major element endmembers to calculate a major element "mixing fraction" (MEMF) for all of their samples, which indicates the proportion of the silicic endmember necessary to produce the observed major element composition for each sample. The correlation coefficient between $X_{Population\ 1}$ and MEMF is -0.95, suggesting that MEMF is an acceptable proxy for $X_{Population\ 1}$ for samples in which CSD data are unavailable. We apply this calculation to the range of bulk compositions presented in this study and find that MEMF is ~0.2 in the most mafic lavas (Cloud Cap), 0.3-0.4 in mafic enclaves, ~0.4 in lavas from Parkdale, and 0.4-0.6 in intermediate lavas (Fig. 4.10).

Although Kent et al. (2010) calculated endmember compositions based on a linear regression model between MEMF and major element concentrations, we observe good correlations between MEMF and certain trace element concentrations (Fig. 4.10). ITEs that vary by less than a factor of two over the entire dataset are not well correlated with MEMF. Such small variations across the dataset suggest that the two endmembers have approximately equal concentrations of these elements, and all of the scatter within the data for these elements is primarily a result of analytical scatter and minor modifications such as small degrees of fractional crystallization (e.g., 10% fractional crystallization will result in >10% increase in the concentration of a perfectly incompatible element). The relationship between MEMF and trace element concentrations is best (correlation coefficient > 0.5) for ITEs that vary by a factor of > 5 (e.g., Ba, Th, U, Rb; Fig. 4.10), so that small variations (as a result of fractional crystallization, noise in the data, etc.) are negligible compared to the overall variation in concentration across the dataset.

Using the same linear regression technique that Kent et al. (2010) used to calculate the major element composition of the mixing endmembers, we use the relationship between trace element concentration and MEMF to estimate the ITE concentrations of the endmembers. Unless otherwise noted, the only samples omitted from the linear regressions were the two plutonic inclusions and sample EB-04-01, which is anomalously enriched in many ITEs. The results of these calculations, performed using the LINEST function in Microsoft Excel, are shown in Table 4.6. The calculated endmember compositions adequately explain most of the trace element variation in the intermediate lavas from Mount Hood although the r^2 values for many of the regressions are very low (Table 4.6).

The correlation between MEMF and trace element concentration is best ($r^2 >$ 0.66) for elements that are compatible during crystallization in a mafic magma (Ni, Cr, V, and Sc; Fig. 4.10), although the concentrations of these elements are somewhat variable at lower MEMF and the data consequently form fan-shaped arrays. Additionally, if we calculate the endmember trace element concentrations from the MEMF as a linear regression, we find reasonable concentrations of these four elements in the mafic endmember but invalid (i.e., negative) concentrations of Ni and Cr in the silicic endmember. Although the calculated concentrations of Sc and V in the silicic endmember are > 0, the error bars are large and extend to values < 0 (Sc = 2.4±3.2 μg/g and V = 6.9±21.8 μg/g). One possible explanation for these observations is fractional crystallization of the mafic magma. If we model the mafic endmember as an array of derivative endmembers created by up to 20% fractional crystallization (and assume that the concentrations of Cr and Ni in the silicic endmember are ~0), we can produce the

majority of Ni, Cr, Sc, and V variations in the intermediate lavas without invoking a silicic endmember with negative (i.e., invalid) concentrations (Fig. 4.11). Concentrations of trace elements with partition coefficients near 1 (e.g., V) will remain approximately equal during 20% fractional crystallization, and the concentrations of incompatible elements will increase only slightly. Therefore, elements with $D \leq 1$ do not generally form fan-shaped arrays. Therefore, elements with $D \leq 1$ do not generally form fan-shaped arrays (e.g., Fig. 4.11d).

Although Sc is compatible in a mafic magma and is therefore somewhat affected by fractional crystallization in the mafic endmember, Sc is well correlated with other indices of mixing such the concentration of highly incompatible trace elements and varies by a factor of ~10 between the mafic and silicic endmembers. Consequently, we can use Sc to calculate a trace element mixing fraction (TEMF) similar to the major element mixing fraction (MEMF) calculated by Kent et al. (2010). These two mixing fractions generally correlate well with each other, which is to be expected since Sc correlates with major element compositions and MEMF is calculated from major elements. We consider both MEMF and TEMF in the following discussion, however, because significant differences between MEMF and TEMF can indicate the failure of a simple mixing model. For example, MEMF and TEMF are consistent to within 10% for samples with >60 wt%, but vary by up to 35% for eruptive products (enclaves, etc.) with < 60 wt% SiO_2 (Fig. 4.12). This is consistent with the observation that trace element concentrations are variable at lower SiO_2 and form a fan-shaped array, indicative of multiple mafic endmembers (which we propose are the result of fractional crystallization of the calculated mafic endmember).

Previous studies have suggested that the 55 ka Cloud Cap basaltic andesites at Mount Hood may be a close approximation of the mafic endmember, as they contain only one population of plagioclase and are the most mafic erupted lavas (Cribb and Barton, 1997; Darr, 2006; Kent et al., 2010; Woods, 2004). As Kent et al. (2010) note, however, Cloud Cap lavas are slightly more evolved than the calculated major element endmember and likely experienced some late mixing with a more silicic magma (e.g., Fig. 4.2).

Mafic enclaves at Mount Hood are compositionally intermediate between the lavas from Cloud Cap and Parkdale (Figs. 4.2-3), and are likely composed of material that was partially hybridized during magma mixing, as observed for mafic enclaves from other mixing-dominated intermediate volcanoes (e.g., Browne et al., 2006; Humphreys et al., 2009). Petrologic evidence for mixing includes two populations of amphibole and plagioclase within mafic enclaves from Mount Hood (Kent et al., 2010)(Koleszar et al., in preparation), and geochemical evidence includes concentrations of trace elements that lie along mixing lines (Fig. 4.11). Major element mixing fractions (MEMF) vary from 0.32-0.41 for the mafic enclaves, and trace element mixing fractions (TEMF) vary from 0.20-0.60. As observed with lavas from Cloud Cap, the discrepancy between MEMF and TEMF in mafic (< 60 wt% SiO_2) samples is likely an indicator of variation within the mafic endmember(s).

Origin of the mafic endmember

Having established potential trace element concentrations for the mafic endmember at Mount Hood, we can combine these results with other information on

potential mafic endmembers in the Cascades to explore different possibilities for the petrogenesis of the mafic magma.

The CAB geochemical signature that is apparent in the mafic lavas from Mount Hood, in the calculated mafic endmember, and in many other Cascades basalts is typically attributed either to flux melting of the mantle wedge e.g., (Reiners et al., 2000), or to melting of previously metasomatized (fluxed) mantle (Leeman et al., 2005; Rowe et al., 2009; Smith and Leeman, 2005). Melting of previously metasomatized mantle is likely to generate a continuum of LILE-enrichment and HFSE-depetion in arc lavas, however, rather than two groups of diverging LILE/HFSE ratios observed between CAB and HFSE-rich OIB-like lavas (Reiners et al., 2000). Isenthalpic flux melting, where the degree of melting (F) and the extent of slab contribution (SC) are non-linearly correlated, generates basalts with high LILE/HFSE ratios consistent with CAB (at high degrees of melting) or OIB-like lavas (at low degrees of melting) (Reiners et al., 2000).

This style of melting is consistent with the LILE/HFSE ratios that we observe in the mafic lavas and calculated mafic endmember from Mount Hood. As slab flux increases, the extent of melting will also increase, thus increasing the concentration of LILE (carried in slab fluids) and decreasing the concentration of Nb (as a result of greater extents of melting). As shown in Fig. 4.6, the calculated mafic endmember from Mount Hood has higher Ba/Nb ratios than HFSE-rich OIB-like lavas, suggesting that the Hood CABs are the product of greater slab flux (i.e., higher Ba) and greater extents of melting (i.e., lower Nb) than OIB (Reiners et al., 2000; Rowe et al., 2009). These models suggest that the CAB compositions observed in mafic lavas at Mount Hood can be created by approximately 15-20% melting at ~1275-1350˚C in a peridotite source (Fig. 4.6; Reiners

et al., 2000; Rowe et al., 2009). This temperature range is broadly consistent with calculated segregation temperatures for CAB below Mount Hood, which indicate that melting occurs near the MOHO at ~1300-1350˚C (Leeman et al., 2005).

Although the calculated mafic endmember has LILE/HFSE ratios consistent with CAB, it shares one compositional characteristic with LKT and OIB-like lavas elsewhere in the Cascades. Linear regression of MEMF and trace element concentrations to estimate the trace element budget of the mafic endmember returns anomalously low concentrations of Th, U, and K, which create a Th-U trough and $Ta_N/K_N > 1$ (where the subscript N designates a concentration that has been normalized to pyrolite, McDonough and Sun 1995). These geochemical signatures are absent from all of the lavas from Mount Hood, but are present in the calculated composition for the mafic endmember (Fig. 4.4d). These concentrations of Th and U are lower than the error bars from the linear regression used to calculate them (Table 4.5), such that their error bars extend into concentrations < 0. Low U, Th, and K are common in Cascades LKT (Conrey et al., 1997), however in LKT the normalized concentrations of U, Nb, and Ta are approximately equal so U_N/Ta_N and U_N/Nb_N are ~1 (Fig. 4.4d). In contrast, the calculated concentration of U in the mafic endmember from Mount Hood is extremely low, so U_N/Ta_N and U_N/Nb_N are < 1 (Fig. 4.4d), which rules out an LKT composition for the mafic endmember. Additionally, like all of the lavas from Mount Hood, the calculated mafic endmember has Ba/Nb, Nb/Zr, and Ba/Zr ratios consistent with a CAB source (Fig. 4.6).

Although U, Th, and K concentrations correlate extremely well in lavas from Mount Hood ($R^2 = 0.98$), their concentrations are considerably more variable at low SiO_2

(< 60 wt%) than at high SiO_2 (> 60 wt%). One potential explanation for this is low but variable concentrations of U, Th, and K in the mafic magma. Fractional crystallization, which we propose as a method of instilling variable concentrations of Sc, V, Ni, and Cr in the mafic endmember, is unable to recreate the variation in U, Th, and K because they are incompatible. Consequently, fractional crystallization will not decrease their concentrations, nor will fractional crystallization decouple them from other similarly incompatible elements such as Ta. Thus the variation in U, Th, and K concentrations in the most mafic lavas from Mount Hood may reflect some unknown source variation that transfers to the mafic endmember. To minimize the uncertainty in the mafic endmember concentrations of U, Th, and K, we have recalculated these concentrations using the same linear regression techniques described above but have omitted the mafic enclaves, Cloud Cap, and Parkdale lavas from the regression due to their relatively low SiO_2 contents and thus, their variable U, Th, and K concentrations.

The new calculated concentrations for U, Th, and K (with the mafic lavas and enclaves omitted from the regression) result in a ITE pattern that is remarkably similar to the trace element pattern for CAB, with characteristic enrichments in LILE (Ba, K, Sr) and depletions in HFSE, including at Nb-Ta trough (4.4d). Based on these observations, we propose that the mafic endmember involved in mixing at Mount Hood is typical CAB as has been observed elsewhere in the Cascades. Moderate degrees of fractional crystallization may be necessary to explain the observed variations in some compatible elements (Sc, Ni, Cr), and source variations may be necessary to explain low but variable Th, U, and K.

Origin of the silicic endmember

The lack of erupted high-SiO_2 material at Mount Hood makes it challenging to assess the true incompatible trace element (ITE) budget of the silicic parent magma, however we can calculate endmember compositions using a linear regression as described above for the mafic endmember, and melt inclusion and phenocryst compositions can add additional constraints to our estimates.

There is evidence for the generation of multiple different silicic magmas in the Cascades through a variety of petrogenetic processes, including fractional crystallization (FC), recharge/assimilation/fractional crystallization (R±A±FC), and partial melting of the crust. Simple FC of basalts can produce liquids of andesitic composition by removing crystallized phases, which will drive the composition of the liquids to more silicic compositions (Eichelberger et al., 2006). Removal of crystallized phases becomes more difficult as the melt viscosity increases with increasing differentiation, however with physical separation processes such as filter pressing it is possible to extract dacitic liquids from an andesitic magma (Eichelberger et al., 2006; Hildreth, 2007). Extensive FC will increase the concentration of incompatible trace elements in the derivative liquids, however, so a simple initial test for this process is to evaluate the relationship between SiO_2 and ITEs, both of which should increase monotonically. This is generally the case between the calculated mafic and silicic endmembers from Mount Hood, however the concentrations of some of the MREE-HREE are lower in the silicic endmember. These elements can behave somewhat compatibly in the presence of amphibole, however, so we should not rule out FC on the basis of this evidence alone.

As discussed above, however, the elevated concentrations of Ni in lavas from Mount Hood indicate that the range of compositions is not simply the product of FC but instead requires mixing with a more mafic source (Fig. 4.9). This does not necessarily argue against FC, however, as the silicic endmember could fractionation from the mafic endmember, then remix with some unfractionated mafic endmember (recharge+FC or RFC) to increase the concentration of Cr in the intermediate lavas. RFC does not work to increase the concentration of elements that are depleted in the mafic (recharging) magma, however. For example, the extent of crystallization required to increase the Rb concentration from 2.4 μg/g in the mafic endmember to 33 μg/g in the silicic endmember is > 90% (Fig. 4.9), which is broadly comparable to the extent of fractionation necessary to evolve the major element contents of a typical silicic volcanic rock from a primitive basalt (Borg and Clynne, 1998). Recharge would decrease the concentration of Rb in the evolving magma, however, thus requiring even greater extents of FC to reach 33 μg/g in the silicic endmember. Other incompatible trace elements have only small differences in their concentrations between the mafic and silicic endmembers, however. Only ~20% FC is needed to increase the U concentration from 0.92 μg/g in the mafic endmember to 1.1 μg/g in the silicic endmember, and Nb only varies between 7.9 μg/g and 8.9 μg/g (also equivalent to approximately 20% FC). It is possible that a third composition (an assimilant) is involved in RAFC, however the range of lava compositions erupted from Mount Hood generally fits well to a binary mixing system, so it may be unreasonable to incorporate an assimilant into the model if other plausible explanations for the origin of the silicic endmember are available.

An additional potential source for silicic magma in the Cascades is through partial melting of crustal material (Hildreth, 2007). This process has been invoked as a source for silicic material at a number of volcanic centers in the Cascades, including Mount Jefferson (Conrey et al., 2001), Mount St. Helens (Smith and Leeman, 1987), and Lassen (Borg and Clynne, 1998). The composition of melt produced is dependent on the starting composition of the crust and fH_2O, which controls the presence of fraction of amphibole is the residue (Borg and Clynne, 1998). Mafic amphibolite in the middle to lower crust at high fH_2O has a liquidus temperature of 884˚C-916˚C, and 15-20% partial melting will produce silicic (63-75 wt% SiO_2) melts that contain 3.1-5.2 wt% H_2O and are MREE-depleted; Borg and Clynne (1998) call these Group 2 lavas. These lavas have REE contents that are similar to the calculated silicic endmember for Mount Hood (Fig. 4.5c). The extent of MREE depletion will depend on fH_2O: a high fH_2O amphibole is present in the residue, so melts will be comparatively depleted in MREE. At low fH_2O the dominant phase is plagioclase, so melts will have negative Eu-anomalies. The calculated silicic endmember is slightly depleted in MREE and has a very slightly negative Eu-anomaly, suggesting that it may be the product of partial melting at moderate fO_2. The range of SiO_2 contents in these partial melts is consistent with the SiO_2 content that Kent et al. (2010) calculated for the silicic endmember (70.9 ± 2.1 wt%), and the H_2O content of the partial melts is consistent with measured concentrations of H_2O in melt inclusions from Mount Hood (2.6 ± 1.0 wt%; see Chapter Two).

A potential source for heat to initiate partial melting is heat released during cooling and crystallization of hot mantle-derived magma fluxing through the lower and middle crust beneath Mount Hood. This magma may be related to the mafic endmember,

which has remained relatively constant (plus or minus up to 20% fractional crystallization) for approximately 0.5 Ma (Kent et al., 2010). Alternatively, there may be other intruding (but unerupting) mafic magmas that could provide heat to initiate partial melting.

Amphibole and plagioclase constraints

To test the validity of the composition that we calculated for the silicic endmember at Mount Hood, we can compare its trace element abundances to the trace element concentrations in phases that we expect crystallized from this magma. There are two populations of amphibole present in lavas erupted from Mount Hood, and one of those amphibole populations (magnesiohornblende, or Mg-hornblende) appears to have crystallized from a cool (800-875˚C), shallow (100-200 MPa) silicic magma (see Chapter Three). The Al/Si ratios of these Mg-hornblendes indicate that they were derived from a melt with an Al/Si ratio of 0.18-0.26, which coincides with the range of Al/Si ratios in the silicic endmember predicted by Kent et al. (Kent et al., 2010). Additionally, Kent et al. identified a population of moderately low-An, low-Fe, low-Ti plagioclase that also likely crystallized from the silicic parent melt. Thus we have two species of phenocryst (plagioclase and Mg-hornblende) with known trace element concentrations (and reasonably well defined partition coefficients for certain trace elements), which we can compare to our calculated silicic endmember.

Melt inclusion constraints

In addition to phenocrysts derived from a potential silicic parent, we have analyzed 86 high-SiO_2 (68.7-77.6 wt%) plagioclase-hosted melt inclusions from Mount Hood. Their volatile contents (H_2O and CO_2) record entrapment pressures of 100-250 MPa, suggesting that they are trapped in the shallow portion of the magmatic system and not in the deeper mafic magma. High-SiO_2 contents in melt inclusions do not necessarily indicate a high-SiO_2 magma, however, as melt inclusions are almost exclusively dacite to rhyolite in systems where the whole rock composition exceeds 60 wt% SiO_2 (Reubi and Blundy, 2009). Therefore it is necessary to confirm that the high-SiO_2 melt inclusions at Mount Hood were produced prior to magma mixing, and not after mixing. If they were trapped after mixing, the ITE contents of these melt inclusions are unlikely to reflect the ITE contents of the silicic parent magma at Mount Hood.

Textural and geochemical evidence suggests that these melt inclusions formed prior to magma mixing. Most of these inclusions are contained within large euhedral plagioclase crystals, which are unlikely to have grown in the short time available following recharge (Kent et al., 2010). Additionally, the plagioclase host crystals are uniformly low-Fe (with the exception of rim compositions), suggesting that magma mixing did not occur until very late in the phenocryst growth history, after melt inclusion entrapment. Furthermore, analyses by Cribb and Barton (1997) indicate that groundmass glasses in lavas from Mount Hood typically have higher Al/Si and lower Fe/Mg than the silicic melt inclusions, suggesting that the melt inclusions are trapped prior to magma mixing (and the groundmass glass, obviously, formed after mixing). And finally, the Al/Si ratios of these melt inclusions are consistent with the melt Al/Si ratios that would

be in equilibrium with the Mg-hornblende that likely crystallized from the silicic parent magma at Mount Hood (see Chapter Three). We can test these melt inclusions for equilibrium with their respective plagioclase host using $K_d^{Ca\text{-}Na}$, which varies from 5.5 in a melt with 2 wt% H_2O to 3.4 in a melt with 4 wt% H_2O (Sisson and Grove, 1993). $K_d^{Ca\text{-}Na}$ for the plagioclase-hosted melt inclusions used for trace element modeling is 5.3 ± 1.9, a K_d that is broadly consistent with the expected K_d for plagioclase-hosted melt inclusions with measured H_2O contents of 2.6 ± 1 wt% (see Chapter Two). Based on all of these lines of evidence, we would expect the trace element concentrations of the melt inclusions to be broadly comparable to concentrations in the calculated silicic endmember.

In general, the trace element concentrations in melt inclusions from Mount Hood are comparable (within error) to the calculated silicic endmember (Fig. 4.4e). The only major exception is Sr, which is comparatively depleted in the melt inclusions relative to the calculated silicic endmember. Although Sr is compatible in plagioclase, the Sr depletion in the melt inclusions cannot be explained by post-entrapment crystallization (PEC) of plagioclase on the inclusion walls after entrapment. No evidence of significant (>10%) PEC is apparent in the melt inclusions in this dataset (Koleszar et al., in review) and correcting for 10% PEC (assuming $D_{Sr}^{plag\text{-}dacite} = 2.4$; Severs et al., 2009) only increases the concentration of Sr in the melt inclusion by ~14%, whereas the measured concentrations of Sr in the melt inclusions are less than half of the concentration in the calculated silicic endmember.

Crystallization of plagioclase prior to melt inclusion entrapment is another possible explanation for the difference between the Sr concentrations of the melt

inclusions and of the calculated silicic endmember. Quantitatively, adding 20% Mount Hood plagioclase back into the melt inclusion composition successfully modifies the Sr content of the melt inclusions such that they are equivalent to the concentration in the calculated silicic endmember, but decreases the concentration of other trace elements such that they are no longer comparable to the concentrations in the calculated silicic endmember (Table 4.5, Fig. 4.4e). Assuming $D_{Sr}^{plag\text{-}dacite} = 2.4$ (Severs et al., 2009), the melt in equilibrium with the Mount Hood plagioclase would contain 491 μg/g Sr, indicating that the melt inclusions are too depleted in Sr to be in equilibrium with their host plagioclase. It is unclear why the Sr contents of these melt inclusions are anomalous with respect to their host plagioclase composition and the calculated silicic endmember.

We can use additional plagioclase-melt and amphibole-melt partition coefficients to assess whether the populations of amphibole and plagioclase that we assume crystallized from the silicic endmember are actually in equilibrium with our calculated silicic endmember. Using partition coefficients from Tiepolo (2007) for amphibole in high-SiO_2 melts, we observe good agreement between most trace elements in the calculated silicic endmember and in the melt in equilibrium with Mg-hornblende (Fig. 4.3e). Data coverage is not as good for plagioclase as for amphibole, because few ITEs are present in plagioclase at measurable concentrations above detection limits by LA-ICP-MS. For elements with measurable concentrations in plagioclase and published partition coefficients (Severs et al., 2009), we find that the melt in equilibrium with plagioclase has trace element concentrations that are equivalent (within error) to the calculated silicic endmember except for the elements La and Nd (Fig. 4.3e). Partition coefficients for La and Nd between plagioclase and dacitic melt vary 3-4 fold in the

literature (Severs et al., 2009), however, so La and Nd concentrations can vary by a fact of 3-4 depending on which partition coefficients are selected. This puts them well within error of the concentrations of the calculated silicic endmember. The good agreement between ITE concentrations in melts in equilibrium with Mg-hornblende and the composition of the calculated silicic endmember (Fig. 4.4e) provides additional support for our assertion that the Mg-hornblende crystallized from the silicic endmember, and suggests that our pressure and temperature calculations based on these amphiboles are applicable to the storage conditions of the silicic parent magma (see Chapter Three). These observations also support the conclusions of Kent et al. (2010) and Darr (2006), who interpreted the low-An Mount Hood plagioclase as a crystallization product of the silicic endmember.

The silicic magma is likely at near- or sub-solidus temperatures during much of its residence time, which is at least 4-5 ka (but may exceed 10 ka; Kent et al., 2010; Eppich et al., in review). Thus the silicic magma is likely highly crystalline at the time of mixing (Kent et al. (2000) estimated a crystallinity of 37 ± 10%) and the actual product involved in mixing is likely a crystal-rich mush. This may affect the efficiency at which material (solid phases versus melt) is extracted from the silicic magma (or mush). Therefore, while we have calculated what appears to be a reasonable estimate for the trace element contents of the silicic endmember involved in mixing, these concentrations may differ somewhat from the overall bulk composition of the silicic body.

Ancillary Erupted Material

The models and calculated endmember compositions discussed in the previous sections are adequate to explain most of the variation that we observe in erupted lavas from Mount Hood. The plutonic inclusions and the single most enriched lava are outliers, however, and have trace element (and in the case of the plutonic inclusions, major element) concentrations that cannot be explained by our relatively simple binary mixing model, even if we allow for some variation in the mafic endmember as a result of fractional crystallization.

The most ITE-enriched sample in this study is EB-04-01, an otherwise unremarkable dacite that is enriched in nearly all of the ITEs on Fig. 4.4b, which have nearly the exhibited by the plagioclase-hosted melt inclusions. The high concentration of many ITEs heavily leverages regression statistics, so this sample was omitted from linear regressions to calculate the mafic and silicic endmembers. EB-04-01 is one of the most silicic lavas from Mount Hood (61.86 wt%) but has the lowest fraction plagioclase < 0.5 mm, and its low crystallinity (Total fraction of plagioclase = 0.258; Kent et al., 2010) is more consistent with the more mafic samples than the other dacites. The low overall abundance of phenocrysts is a reasonable explanation for the elevated trace element concentrations of this sample.

The other compositionally distinct samples in this study were the plutonic inclusions, which are highly crystalline and have lower SiO_2 contents than any other samples. The most mafic plutonic inclusion, MH09-01a, is particularly distinct from the rest of the Hood suite. MH09-01a is strongly depleted in incompatible elements (Fig. 4c) and has high concentrations of Al_2O_3 (Fig. 3) and Eu (Figs. 4c, 5c), in addition to large

positive Eu- and Sr-anomalies (Figs. 4c, 5c). These characteristics indicate that MH09-01a is likely composed of plagioclase-dominated crystal residue, and suggest that it is similar to the laminated gabbronorite inclusions at Mount St. Helens (Heliker, 1995), which some authors suggest are xenoliths (e.g., Pallister et al., 2008). Positive Ti-anomalies (Fig. 4d) in both of the plutonic inclusions from Mount Hood are consistent with abundant FeTi-oxides observed in photomicrographs (Fig. 4.1f).

MH09-01a lacks the clear CAB signature that is present in other samples from Hood, but this may be the result of crystal accumulation in the absence of interstitial melt in which highly incompatible elements could reside. The arc-characteristic Nb-Ta trough is virtually absent, but a Zr-Hf trough is present (Fig. 4c). The absence of a Nb-Ta trough, the presence of a Zr-Hf trough, and a large positive Ba-anomaly result in anomalously high Ba/Zr but relatively low Ba/Nb in this sample (Fig. 6). The other plutonic inclusion, MH08-11b, shares the same general characteristics as MH09-01a, although these characteristics are less pronounced (Figs. 4c, 5c, 6) and suggest that MH08-11b may be somewhat contaminated by the lava in which it was hosted.

These plutonic inclusions may represent cumulates of material that crystallized from one of the two Mount Hood endmembers, or, as with Mount St. Helens, they may be composted of material from geochemically and isotopically unique basement rocks (Kent et al., 2008). Geochemical analyses of the phases within these inclusions will be necessary to characterize their petrogenesis.

CONCLUSIONS

Using a comprehensive dataset that combines whole rock, mineralogical, and melt inclusion data, we build on previous studies that have characterized the major element contents of mafic and silicic endmembers involved in magma mixing at Mount Hood (Darr, 2006; Kent et al., 2010; Woods, 2004). Based our observations and modeling, we observe that:

1. Lavas from Mount Hood have trace element signatures that are considered the hallmarks of typical Cascades calc-alkaline basalt (CAB), including Nb-Ta troughs and enrichment in large ion lithophile elements (LILE) relative to high-field strength elements (HFSE), reflecting slab input into the subduction zone;
2. The LILE/HFSE ratios of the mafic lavas from Mount Hood are broadly consistent with moderately high extents of flux melting of a peridotite source (Reiners et al., 2000; Rowe et al., 2009);
3. The silicic endmember is likely formed by partial melting of mafic amphibolite in the lower to middle crust;
4. The trace element concentrations required for the silicic endmember are comparable to the concentrations observed plagioclase-hosted melt inclusions (with the exception of Sr), are broadly consistent with concentrations calculated for a melt in equilibrium with Mount Hood magnesiohornblende and plagioclase, and suggest that Mg-hornblende, low-An plagioclase, melt inclusion entrapment occurred within a shallow silicic magma body;
5. Our estimated trace element budgets for the mixing endmembers at Mount Hood are certainly non-unique solutions and represent the minimum range of

trace element concentrations that is necessary to reproduce the range of concentrations observed in the intermediate lavas. These estimates could be further refined with more rigorous mixing calculations that consider mass balance and thermodynamic constraints.

ACKNOWLEDGEMENTS

We thank Rick Conrey, Andy Ungerer, Frank Tepley, and Dale Burns for analytical assistance for this project and Willie Scott (CVO) for providing pumice samples. This work was supported by National Science Foundation grant EAR-038421 to AJRK and a USGS Kleinman Grant to AMK.

REFERENCES

Blundy, J., Cashman, K.V., and Berlo, K., 2008, Evolving magma storage conditions beneath Mount St. Helens inferred from chemical variations in melt inclusions from the 1980-1986 and current (2004-2006) eruptions, *in* Sherrod, D.R., Scott, W.E., and Stauffer, P.H., eds., A Volcano Rekindled: The Renewed Eruption from Mount St. Helens, 2004-2006, Volume 1750, U.S.G.S. Professional Paper.

Borg, L.E., and Clynne, M.A., 1998, The petrogenesis of felsic calc-alkaline magmas from the southernmost Cascades, California: Origin by partial melting of basaltic lower crust: Journal of Petrology, v. 39, p. 1197-1222.

Browne, B.L., Eichelberger, J.C., Patino, L.C., Vogel, T.A., Dehn, J., Uto, K., and Hoshizumi, H., 2006, Generation of porphyritic and equigranular mafic enclaves during magma recharge events at Unzen Volcano, Japan: Journal of Petrology, v. 47, p. 301-328.

Conrey, R.M., Hooper, P.R., Larson, P.B., Chesley, J., and Ruiz, J., 2001, Trace element and isotopic evidence for two types of crustal melting beneath a High Cascades volcanic center, Mt. Jefferson, Oregon: Contributions to Mineralogy and Petrology, v. 141, p. 710-732.

Conrey, R.M., Sherrod, D.R., Hooper, P.R., and Swanson, D.A., 1997, Diverse primitive magmas in the Cascades Arc, Northern Oregon, and Southern Washington: The Canadian Mineralogist, v. 35, p. 367-396.

Cribb, J.W., and Barton, M., 1997, Significance of crustal and source region processes on the evolution of compositionally similar calc-alkaline lavas, Mt. Hood, Oregon: Journal of Volcanology and Geothermal Research, v. 76, p. 229-249.

Darr, C.M., 2006, Magma chamber processes over the past 475,000 years at Mount Hood, Oregon: Insights from crystal zoning and crystal size distribution studies: Corvallis, Oregon State University.
Eichelberger, J.C., Izbekov, P.E., and Browne, B.L., 2006, Bulk chemical trends at arc volcanoes are not liquid lines of descent: Lithos, v. 87, p. 135-154.
Heliker, C., 1995, Inclusions in Mount St. Helens dacite erupted from 1980 through 1983: Journal of Volcanology and Geothermal Research, v. 66, p. 115-135.
Hildreth, W., 2007, Quaternary Magmatism in the Cascades— Geologic Perspectives: Reston, VA, U.S. Geological Survey.
Humphreys, M.C.S., Christopher, T., and Hards, V., 2009, Microlite transfer by disaggregation of mafic inclusions following magma mixing at Soufriere Hills volcano, Montserrat: Contributions to Mineralogy and Petrology, v. 157, p. 609-624.
Johnson, D.M., Hooper, P.R., and Conrey, R.M., 1999, XRF analysis of rocks and minerals for major and trace elements on a single low dilution Li-tetraborate fused bead: Advances in X-ray Analysis, v. 41, p. 843-867.
Kent, A.J.R., Darr, C.M., Koleszar, A.M., Salisbury, M.J., and Cooper, K.M., 2010, Preferential eruption of andesitic magmas through recharge filtering: Nature Geoscience, v. 3, p. 631-636.
Kent, A.J.R., Rowe, M.C., Thornber, C.R., and Pallister, J.S., 2008, Trace element and Pb isotope composition of plagioclase from dome samples from the 2004-2005 eruption of Mount St. Helens, Washington, *in* Sherrod, D.R., Scott, W.E., and Stauffer, P.H., eds., A Volcano Rekindled: The Renewed Eruption from Mount St. Helens, 2004-2006, Volume 1750, U.S.G.S. Professional Paper.
Kent, A.J.R., and Ungerer, C.A., 2006, Analysis of light lithophile elements (Li, Be, B) by laser ablation ICP-MS: Comparision between magnetic sector and quadrupole ICP-MS: American Mineralogist, v. 91, p. 1401-1411.
Koleszar, A.M., Kent, A.J.R., Wallace, P.J., and Scott, W.E., in review, Controls on long-term low explosivity at andesitic arc volcanoes: Insights from Mount Hood, Oregon: Journal of Volcanology and Geothermal Research.
Kress, V.C., and Ghiorso, M.S., 2004, Thermodynamic modeling of post-entrapment crystallization of igneous phases: Journal of Volcanology and Geothermal Research, v. 137, p. 247-260.
Larsen, J.F., Nye, C.J., Coombs, M.L., Tilman, M., Izbekov, P., and Cameron, C., 2010, Petrology and geochemistry of the 2006 eruption of Augustine Volcano, *in* Power, J.A., Coombs, M.L., and Freymueller, J.T., eds., The 2006 Eruption of Augustine Volcano, Alaska, Volume 1769, U.S.G.S. Professional Paper.
Leeman, W.P., Lewis, J.F., Evarts, R.C., Conrey, R.M., and Streck, M.J., 2005, Petrologic constraints on the thermal structure of the Cascades arc: Journal of Volcanology and Geothermal Research, v. 140, p. 67-105.
Lieuallen, A.E., 2010, Meeting of the Magmas: the Evolutionary History of the Kalama Eruptive Period, Mount St. Helens, Washington: Corvallis, Oregon State University.
Luhr, J.F., 2001, Glass inclusions and melt volatile contents at Paricutin Volcano, Mexico: Contributions to Mineralogy and Petrology, v. 142, p. 261-283.

McDonough, W.F., and Sun, S.-s., 1995, The composition of the Earth: Chemical Geology, v. 120, p. 223-253.
Míková, J., and Denková, P., 2007, Modified chromatographic separation scheme for Sr and Nd isotope analysis in geological silicate samples: Journal of Geosciences, v. 52, p. 221-226.
Pallister, J.S., Thornber, C.R., Cashman, K.V., Clynne, M.A., Lowers, H.A., Mandeville, C.W., Brownfield, I.K., and Meeker, G.P., 2008, Petrology of the 2004-2006 Mount St. Helens lava dome-- Implications for magmatic plumbing and eruption triggering, *in* Sherrod, D.R., Scott, W.E., and Stauffer, P.H., eds., A Volcano Rekindled: The Renewed Eruption of Mount St. Helens, 2004-2006, Volume 1750, U.S.G.S. Professional Paper.
Reiners, P.W., Hammond, P.E., McKenna, J.M., and Duncan, R.A., 2000, Young basalts of the central Washington Cascades, flux melting of the mantle, and trace element signatures of primary arc magmas: Contributions to Mineralogy and Petrology, v. 138, p. 249-264.
Reubi, O., and Blundy, J., 2009, A dearth of intermediate melts at subduction zone volcanoes and the petrogenesis of arc andesites: Nature, v. 461, p. 1269-1273.
Rowe, M.C., Kent, A.J.R., and Nielsen, R.L., 2009, Subduction influence on basaltic oxygen fugacity and trace and volatile elements across the Cascade volcanic arc: Journal of Petrology, v. 50.
Schmidt, M.E., Grunder, A.L., and Rowe, M.C., 2008, Segmentation of the Cascade Arc as indicated by Sr and Nd isotopic variation among diverse primitive basalts: Earth and Planetary Science Letters, v. 226, p. 166-181.
Scott, W.E., Gardner, C.A., Tilling, R.I., and Lanphere, M.A., 1997a, Geologic History of Mount Hood Volcano, Oregon: A Field-Trip Guidebook: U.S. Geological Survey Open-File Report, v. 97, p. 38p.
Scott, W.E., Pierson, T.C., Schilling, S.P., Costa, J.E., Gardner, C.A., Vallance, J.W., and Major, J.J., 1997b, Volcano hazards in the Mount Hood Region, Oregon, *in* Interior, U.S.D.o.t., ed., Volume Open-File Report 97-89, U.S. Geological Survey, p. 14.
Severs, M.J., Beard, J.S., Fedele, L., Hancher, J.M., Mutchler, S.R., and Bodnar, R.J., 2009, Partitioning behavior of trace elements between dacitic melt and plagioclase, orthopyroxene, and clinopyroxene based on laser ablation ICPMS analysis of silicate melt inclusions: Geochemica et Cosmochimica Acta, v. 73, p. 2123-2141.
Sisson, T.W., and Grove, T.L., 1993, Experimental investigations of the role of H2O in calc-alkaline differentiation and subduction zone magmatism: Contributions to Mineralogy and Petrology, v. 113, p. 143-166.
Smith, D.R., and Leeman, W.P., 1987, Petrogenesis of Mount St. Helens dacitic magmas: Journal of Geophysical Research, v. 92, p. 10313-10334.
—, 2005, Chromian spinel-olivine phase chemistry and the origin of primitive basalts of the southern Washington Cascades: Journal of Volcanology and Geothermal Research, v. 140, p. 49-66.

Sparks, R.S.J., and Marshall, L.A., 1986, Thermal and mechanical constraints on mixing between mafic and silicic magmas: Journal of Volcanology and Geothermal Research, v. 29, p. 99-124.

Steiner, A.R., 2009, A petrologic investigation of mafic inputs into the Augustine Volcano (Alaska) magma system over the pas 2,200 years: Fullerton, California State University.

Tiepolo, M., Oberti, R., Zanetti, A., Vannucci, R., and Foley, S., 2007, Trace-element partitioning between amphibole and silicate melt, *in* Hawthorne, F.C., Oberti, R., Della Ventura, G., and Mottana, A., eds., Amphiboles: Crystal Chemistry, Occurrence, and Health Issues, Volume 67, Mineralogical Society of America.

Woods, M.M., 2004, Compositional and mineralogical relationships between mafic inclusions and host lavas as key to andesite petrogenesis at Mount Hood Volcano, Oregon: Portland, Portland State University.

FIGURES

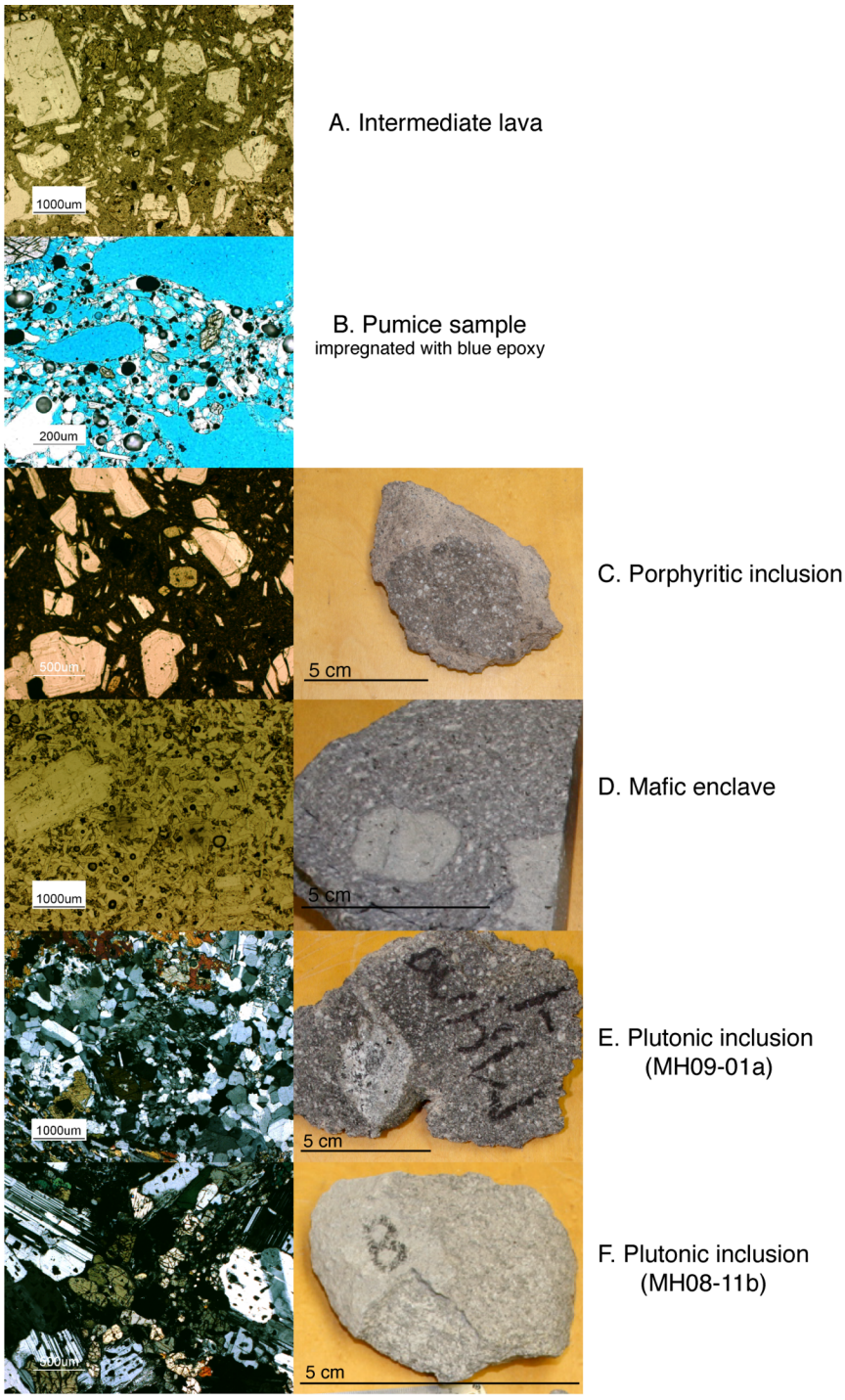

Fig. 4.1: Lava, pumice, inclusion, and enclave textures for samples included in this study.

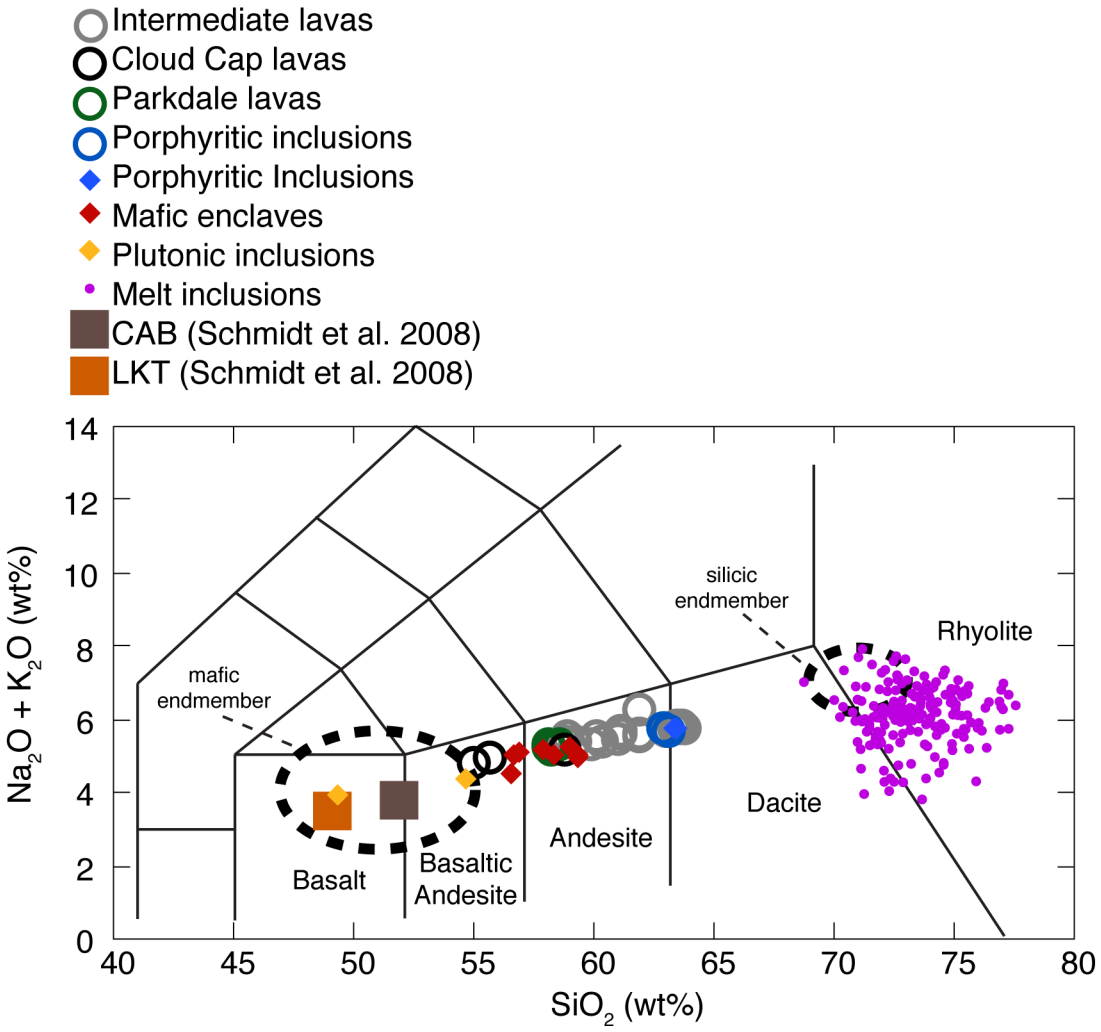

Fig. 4.2: Total alkalis versus silica for melt inclusions and whole rock samples from Mount Hood. Calk-alkaline basalt (CAB) and low-K tholeiite (LKT) are shown for reference (Schmidt and Grunder, 2011). Dashed circles indicate estimated endmember compositions from Kent et al. (2010). Melt inclusion compositions from Koleszar et al. (in review).

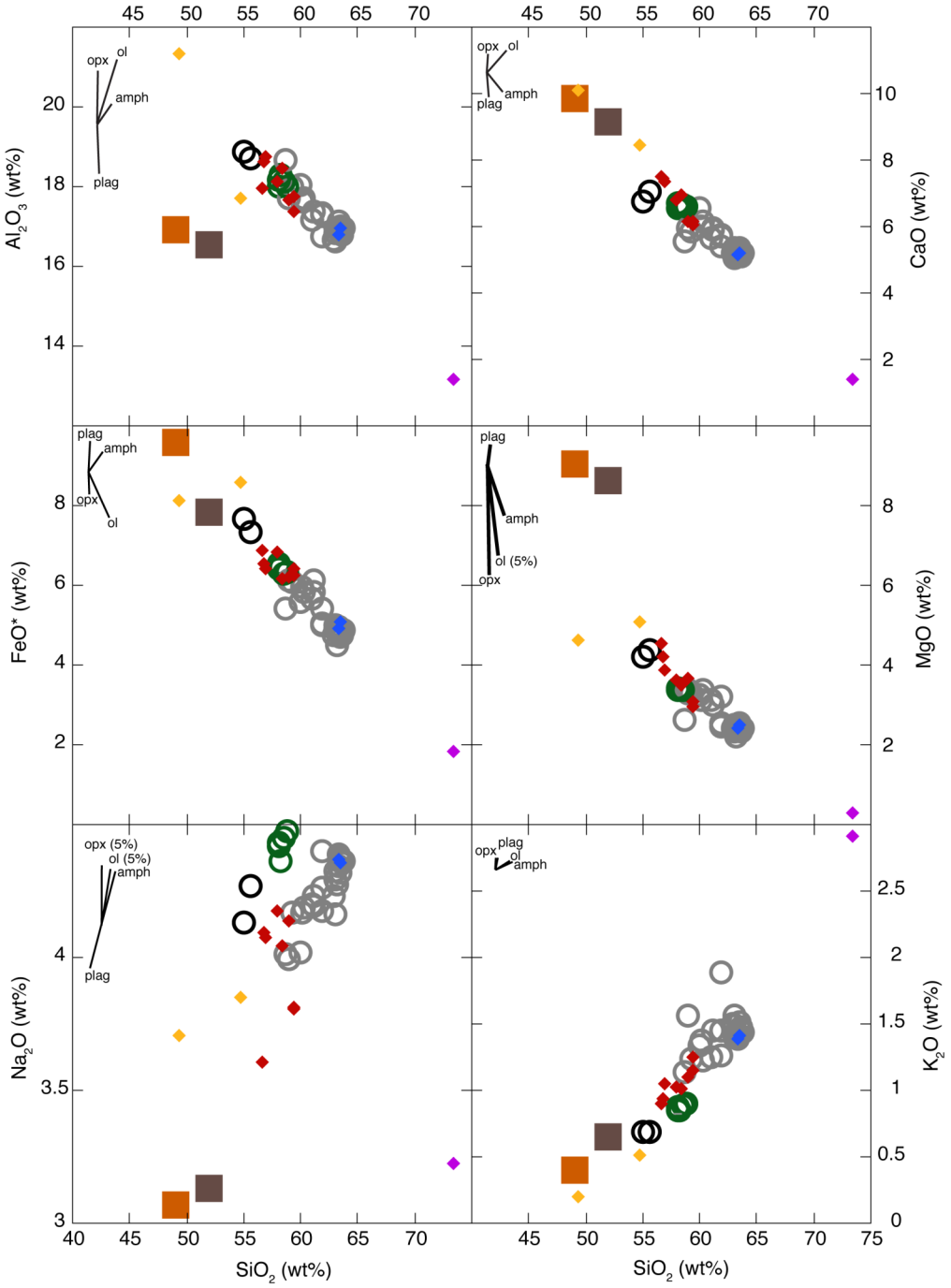

Fig. 4.3: Major element Harker diagrams for lavas, enclaves, and inclusions from Mount Hood. All symbols as in Fig. 2 (pink diamond is average melt inclusion composition). Fractional crystallization vectors indicate 10% crystallization unless otherwise noted. Symbols as in Fig. 4.2.

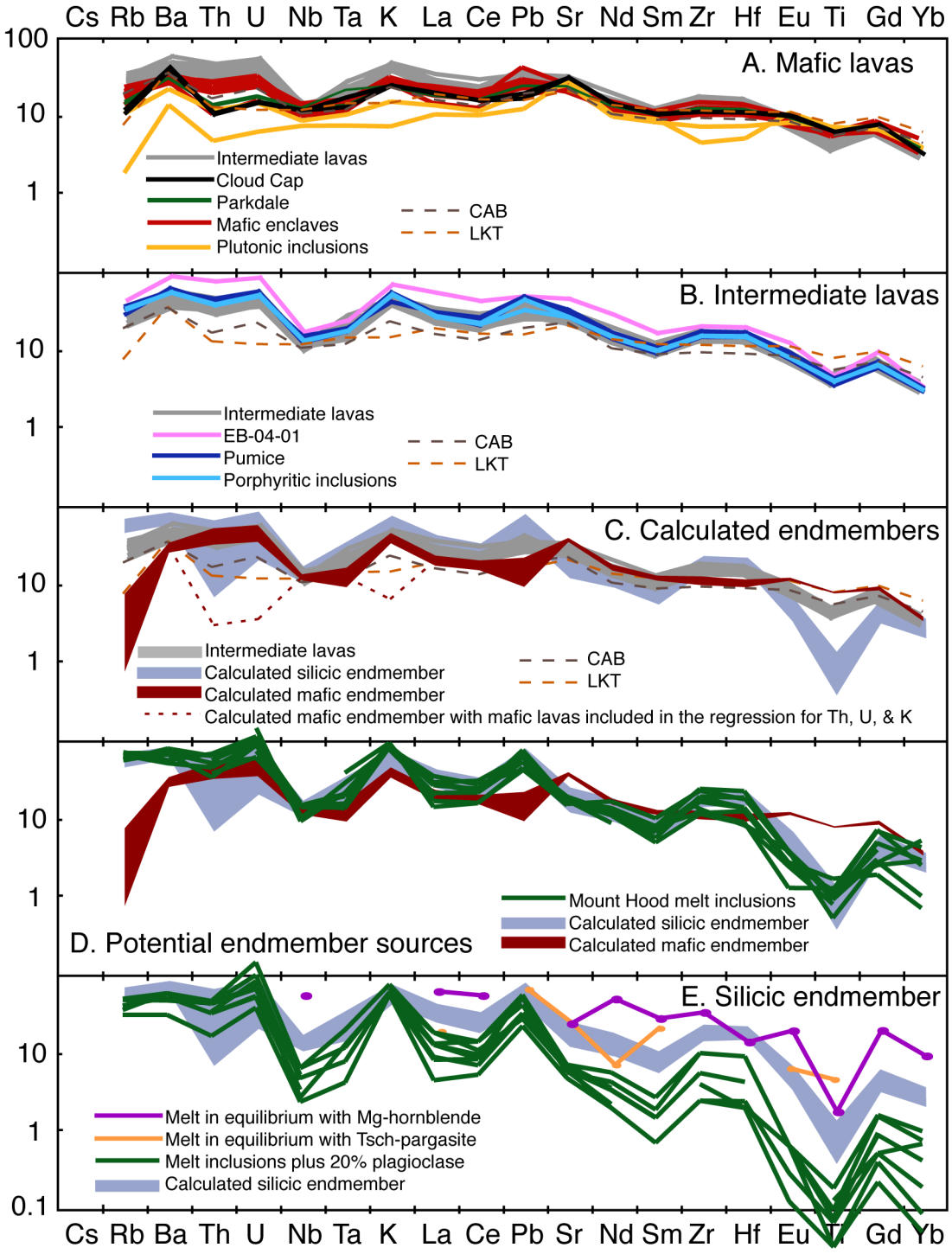

Fig. 4.4: Incompatible trace element concentrations in samples from Mount Hood and calculated melt compositions. Concentrations normalized to pyrolite (McDonough and Sun, 1995). CAB and LKT from Schmidt et al.(Schmidt et al., 2008).

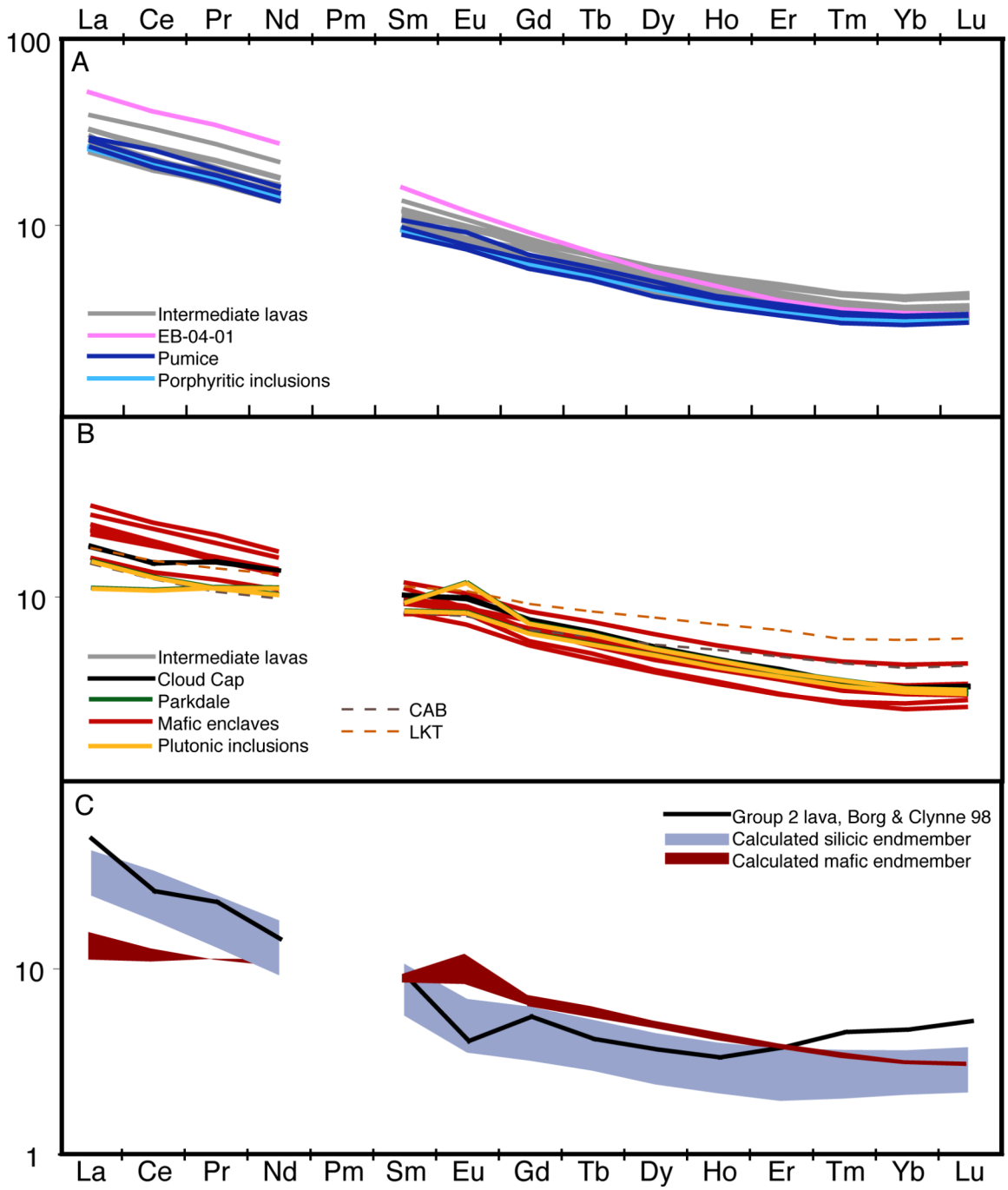

Fig. 4.5: Rare earth element concentrations in samples from Mount Hood, normalized to pyrolite (McDonough and Sun, 1995). CAB and LKT from Schmidt and Grunder (Schmidt et al., 2008).

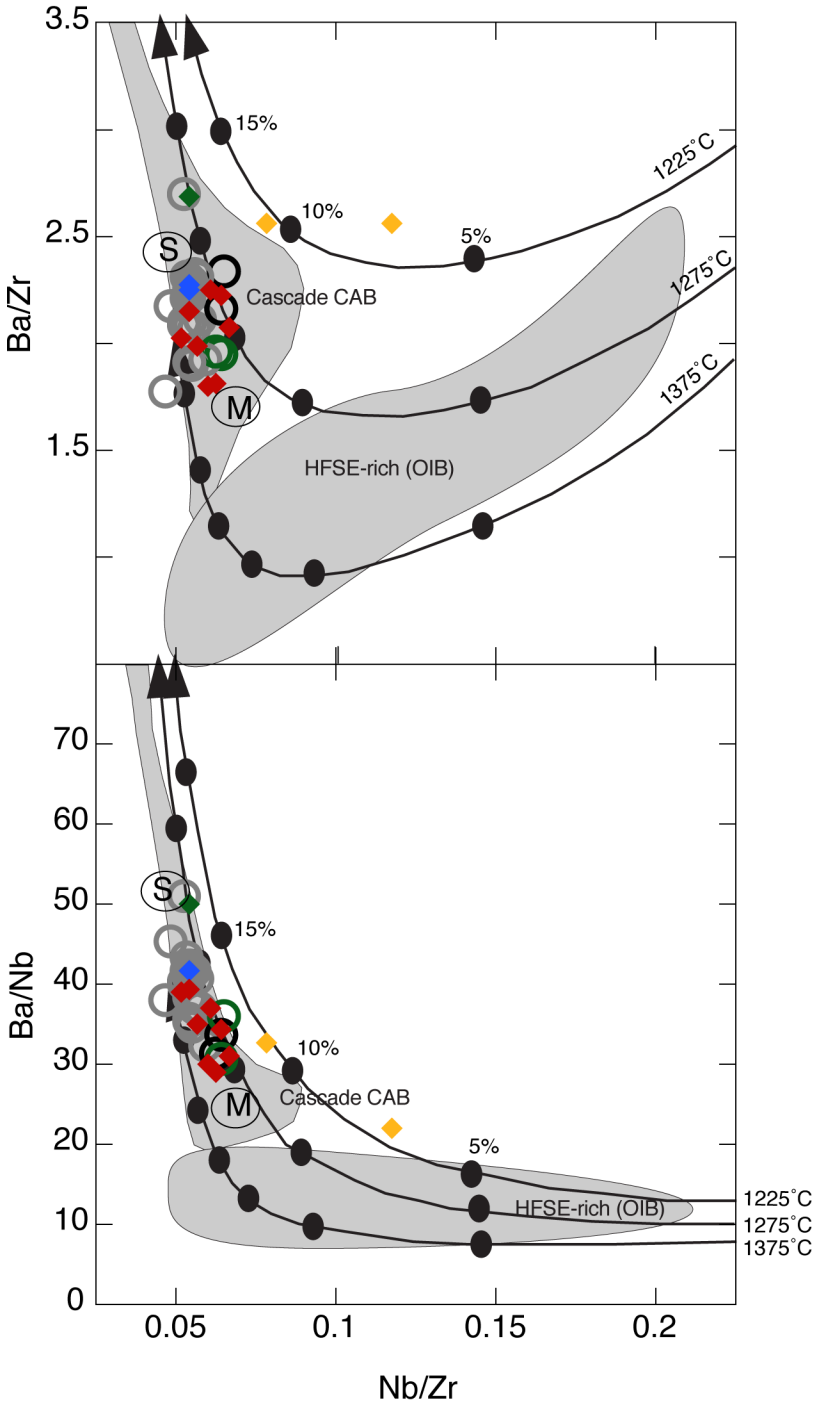

Fig. 4.6: LILE and HFSE ratios for lavas from Mount Hood. Fields for CAB and OIB and isenthalpic melting curves from Reiners et al. (2000). Black circles and percentages indicatedextent of melting of a peridotite source. Symbols as in Fig. 4.2. S and M are calculated silicic and mafic endmembers, respectively.

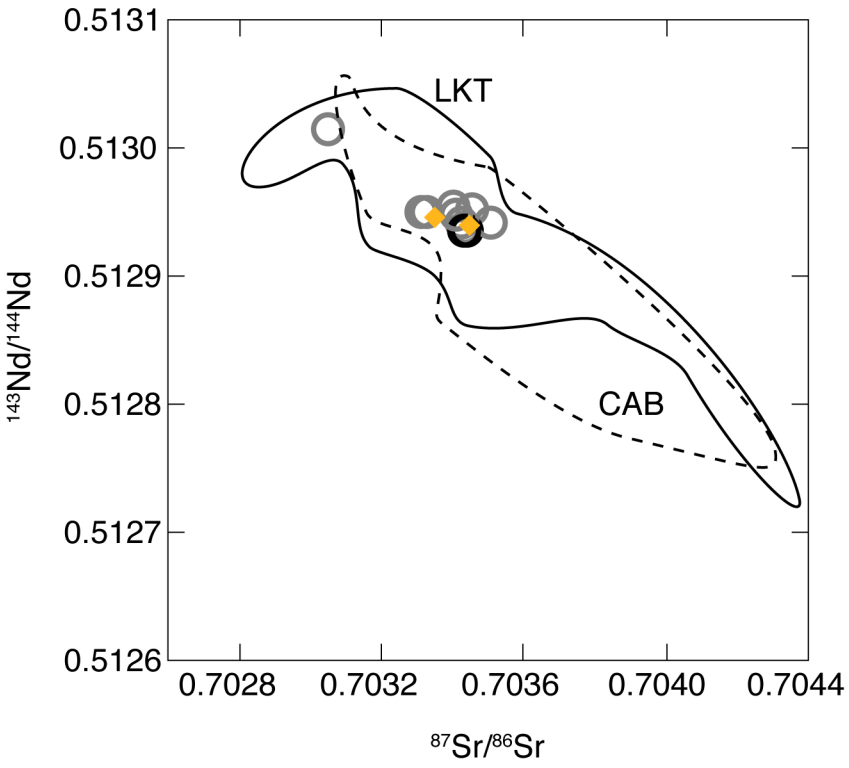

Fig. 4.7: $^{87}Sr/^{86}Sr$ versus $^{143}Nd/^{144}Nd$ for lavas and plutonic inclusions from Mount Hood. Error bars are smaller than symbols. LKT and CAB fields from Schmidt et al. (2008). All samples cluster tightly with the exception of CD-04-01. Symbols as in Fig. 4.2.

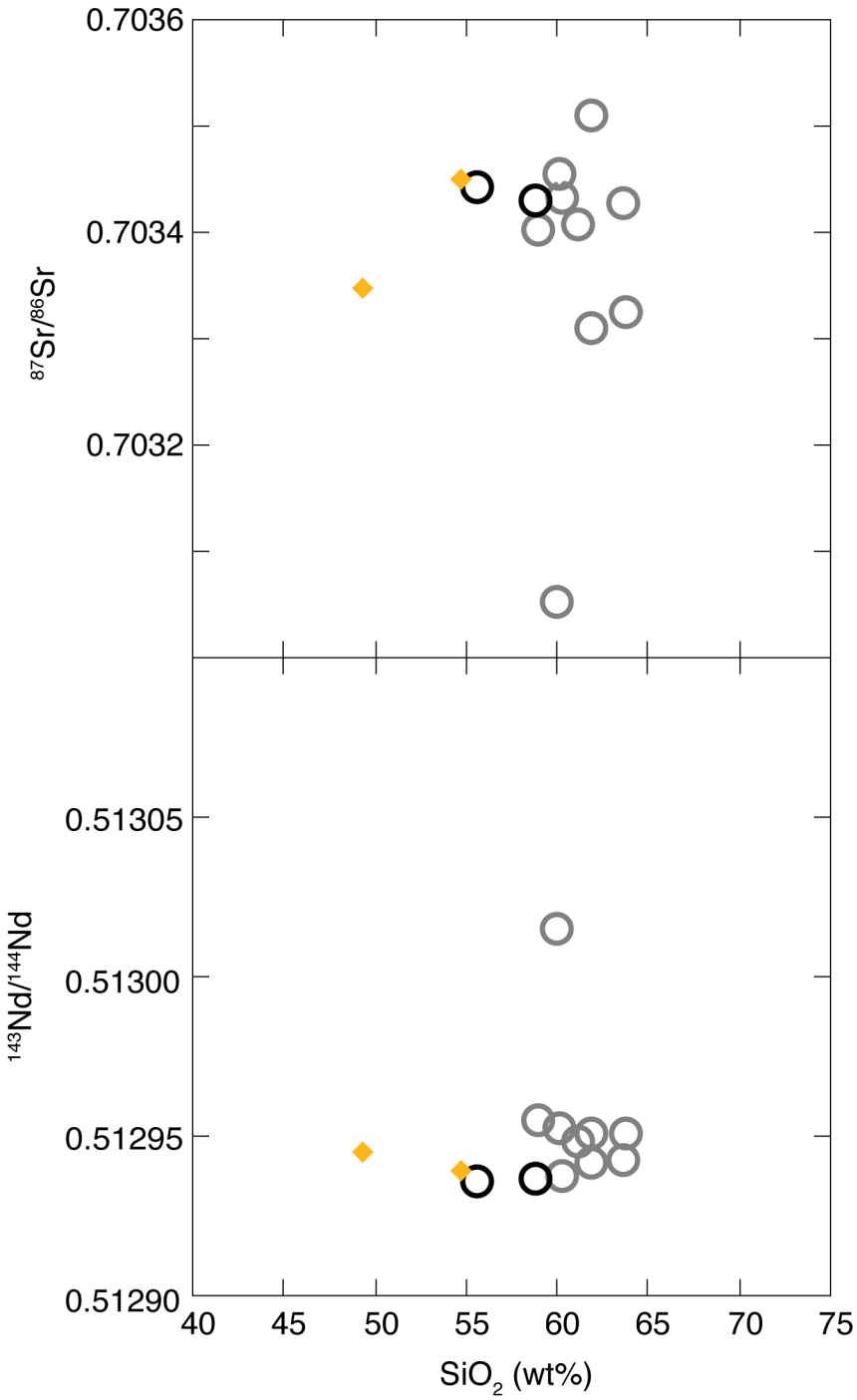

Fig. 4.8: $^{87}Sr/^{86}Sr$ and $^{143}Nd/^{144}Nd$ versus SiO_2 for lavas and plutonic inclusions from Mount Hood. Symbols as in Fig. 4.2.

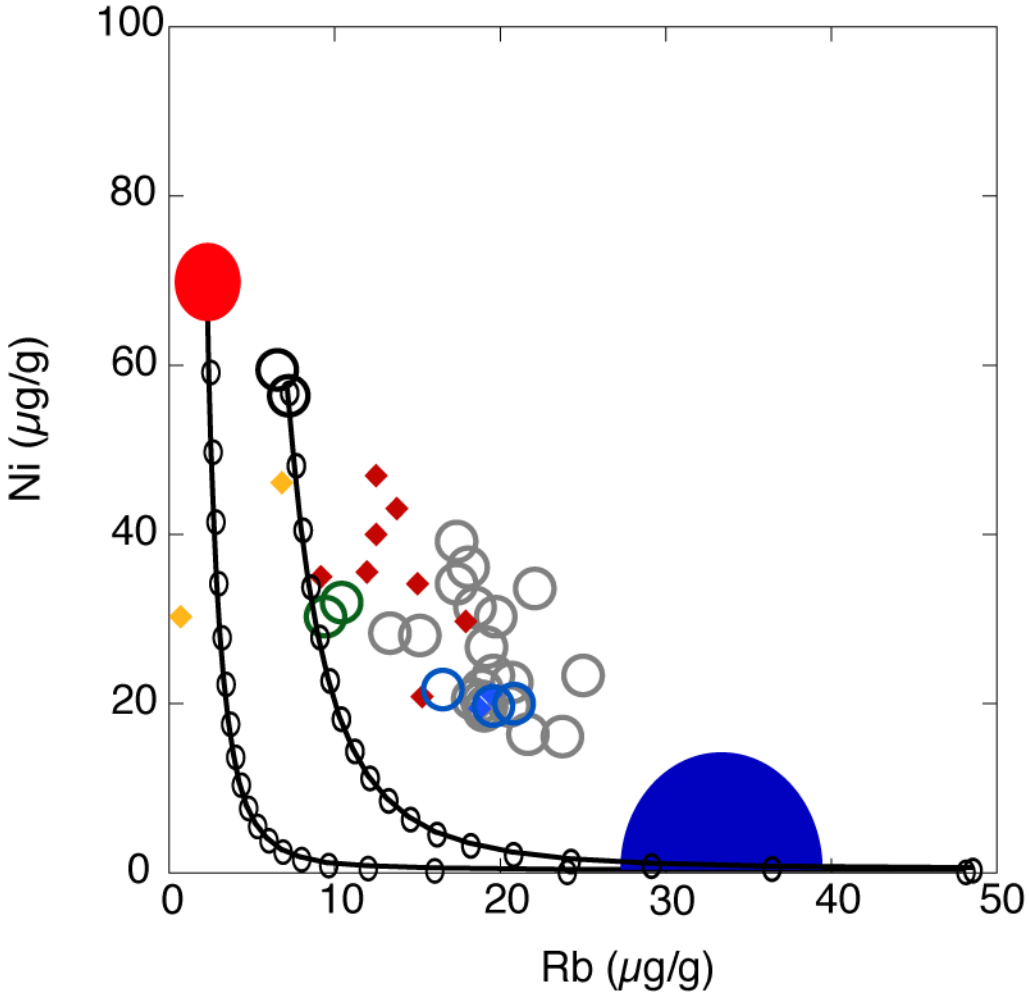

Fig. 4.9: Ni versus Rb for samples from Mount Hood. Symbols as in Fig. 4.2. The curved line shows the change in Ni and Rb content with fractional crystallization, starting at either the Cloud Cap lavas or the calculated mafic endmember. Each tick is 5% fractional crystallization.

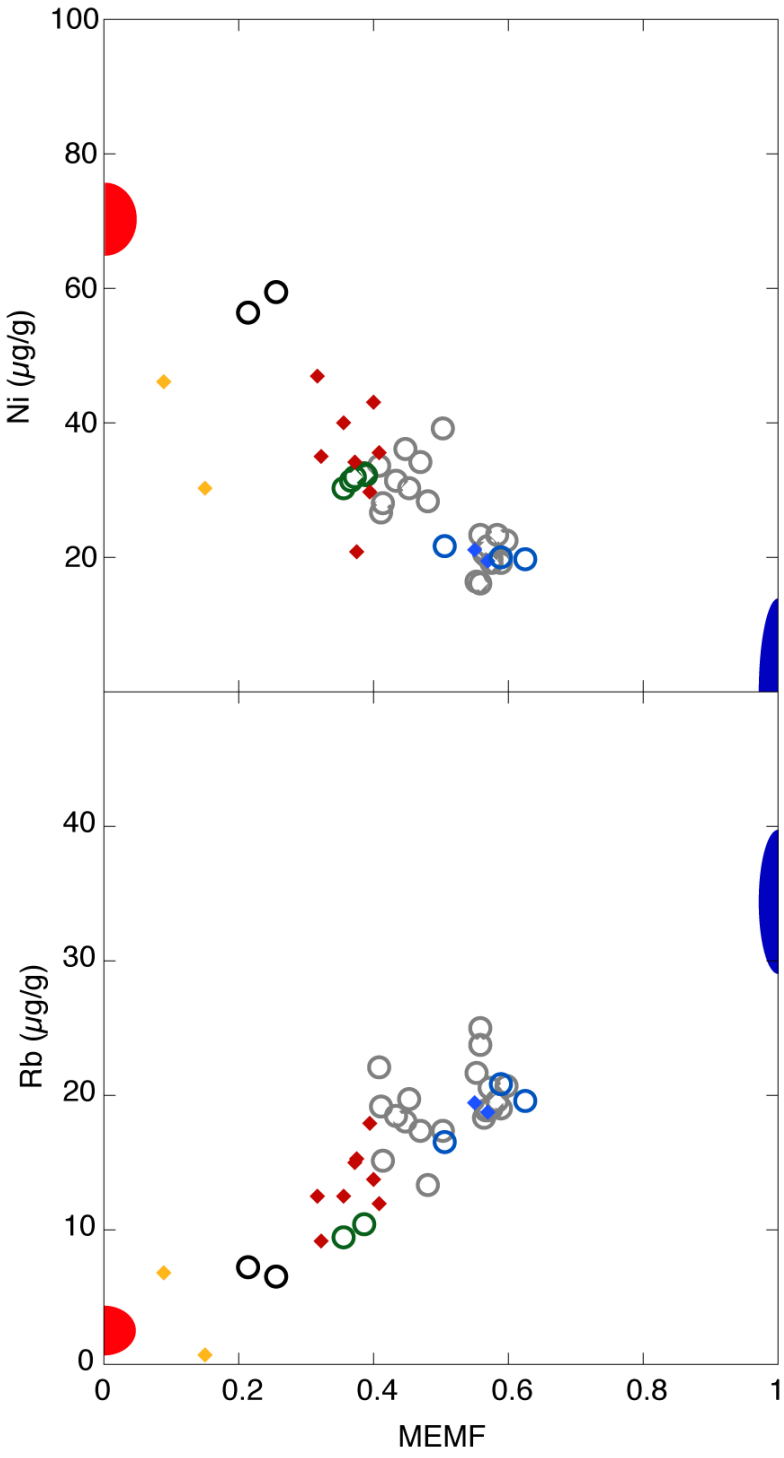

Fig. 4.10: Major element mixing factor (MEMF) versus Ni and Rb. See text for additional details. Symbols as in Fig. 4.2.

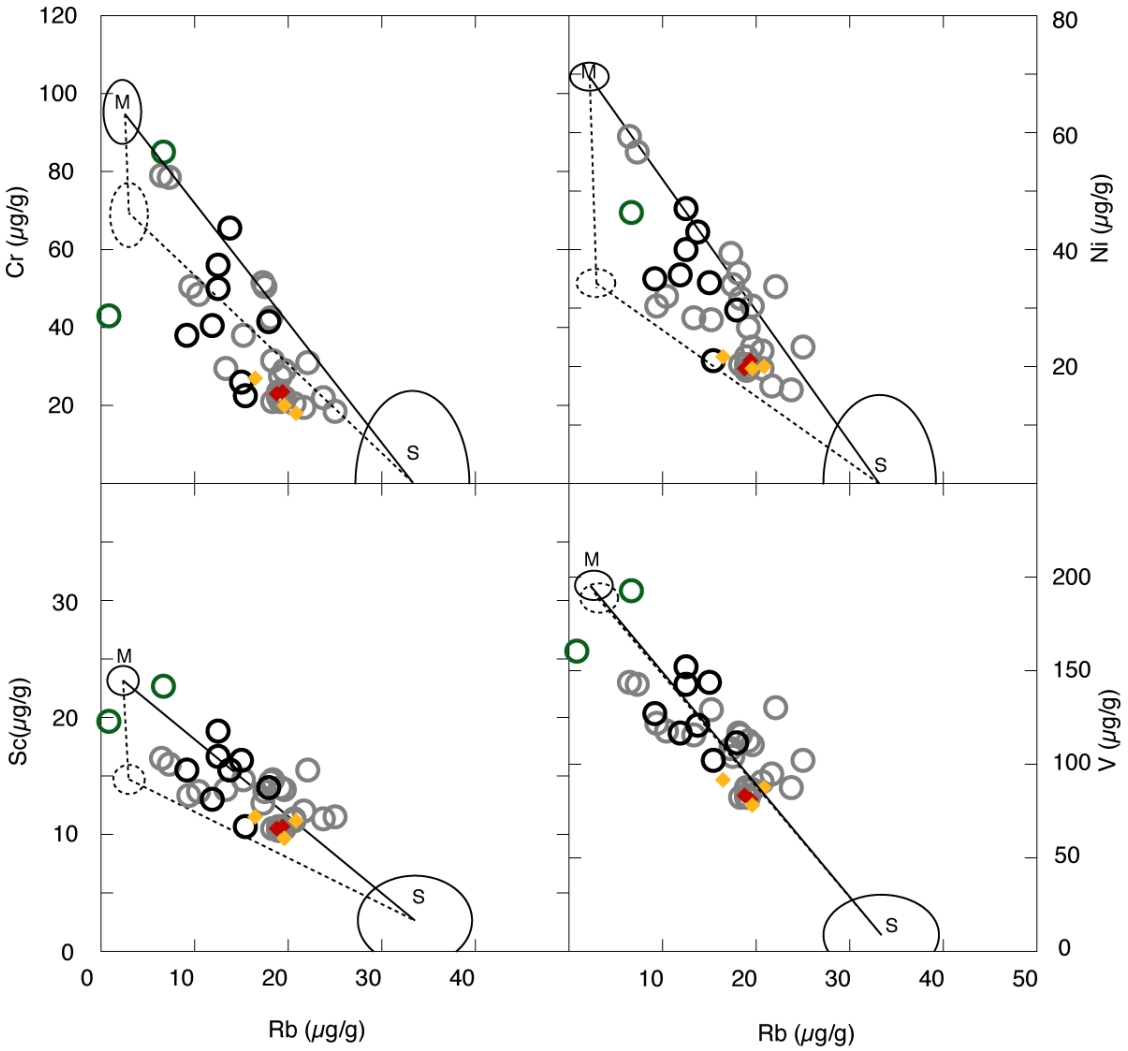

Fig. 4.11: Rb versus Cr, Ni, Sc, and V. Solid lines are mixing lines between the calculated endmembers; dashed lines indicate mixing with the mafic endmember after up to 20% fractional crystallization, resulting in a fanned array of compatible trace elements. Symbols as in Fig. 4.2.

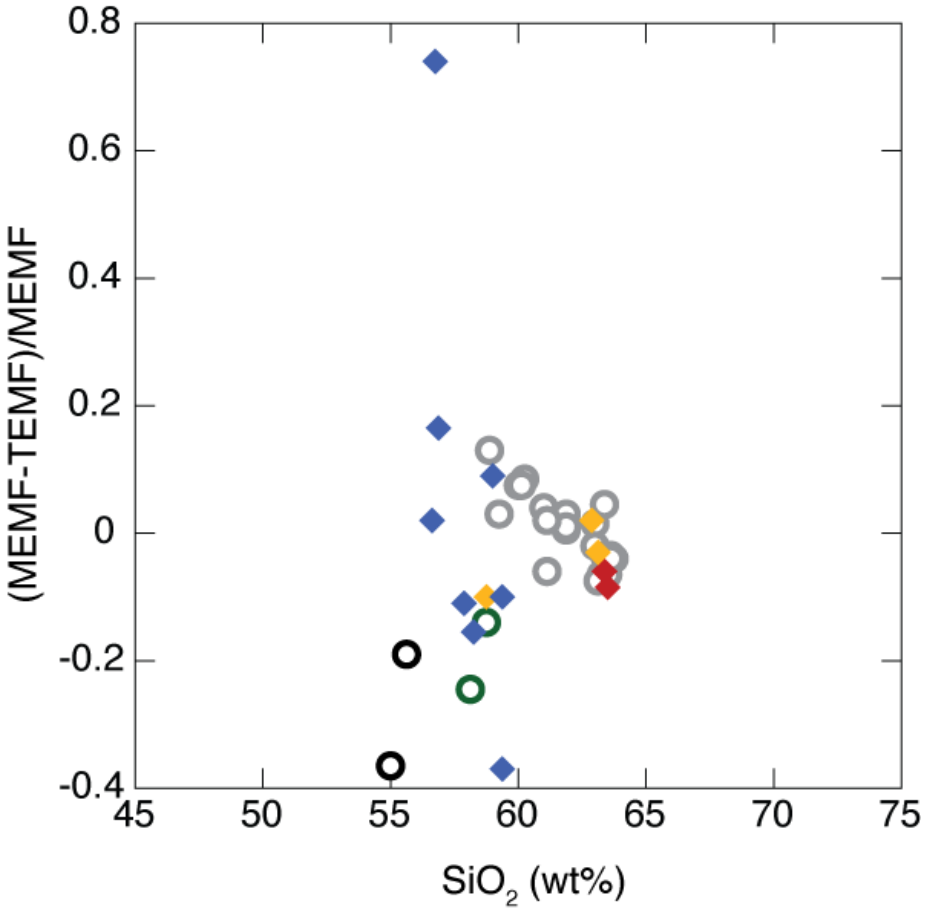

Fig. 4.12: The difference between MEMF and TEMF versus SiO_2. At SiO_2 > 60 wt%, MEMF and TEMF agree very well, but their values deviate more at lower concentrations of SiO_2. This may be indicative of greater variation in the mafic endmember than in the silicic endmember. Symbols as in Fig. 4.2.

Sample	Description	Eruptive Period	SiO_2 (wt%)	Plagioclase	Amphibole	Melt inclusions	Bulk rock
CC04-01	lava	Cloud Cap	55.66				XRF[1], ICP-MS, MC-ICP-MS
CD04-01	lava	Main Stage	59.95				XRF[1], ICP-MS, MC-ICP-MS
CS04-01	lava	Main Stage	58.92				XRF[1], ICP-MS, MC-ICP-MS
CS04-02	lava	Main Stage	59.21				XRF[1], ICP-MS, MC-ICP-MS
EB04-01	lava	Main Stage	61.86				XRF[1], ICP-MS, MC-ICP-MS
HW04-01	lava	Main Stage	60.08				XRF[1], ICP-MS, MC-ICP-MS
HW04-02	lava	Main Stage	61.93				XRF[1], ICP-MS
MH05-01	lava	Main Stage	61.16				XRF[1], ICP-MS
MH05-01a	mafic enclave	Main Stage	57.88				XRF, ICP-MS
MH05-05	lava	Main Stage	61.14				XRF[1], ICP-MS, MC-ICP-MS
MH08-08	PJB	Timberline	63.65	EMPA, LA-ICP-MS	EMPA, LA-ICP-MS		XRF, ICP-MS, MC-ICP-MS
MH08-11a	mafic enclave	Main Stage	56.90				XRF, ICP-MS
MH08-11b	plutonic inclusion	Main Stage	54.70				XRF, ICP-MS
MH08-11c	mafic enclave	Main Stage	56.71				XRF, ICP-MS
MH08-11d	lava	Main Stage	60.30				XRF, ICP-MS, MC-ICP-MS
MH08-12	PJB	Old Maid	63.81	EMPA	EMPA, LA-ICP-MS		XRF, ICP-MS, MC-ICP-MS
MH08-14	lava	Parkdale	58.13				XRF, ICP-MS
MH08-16	lava	Cloud Cap	55.03				XRF, ICP-MS
MH08-18	lava	Main Stage	61.00				XRF, ICP-MS
MH08-18a	mafic enclave	Main Stage	59.03				XRF, ICP-MS
MH08-20	pumice	Old Maid	63.16	EMPA	EMPA, LA-ICP-MS	EMPA, LA-ICP-MS, SIMS	XRF, ICP-MS
MH08-22	pumice	Timberline	62.86	EMPA	EMPA, LA-ICP-MS	EMPA, LA-ICP-MS, SIMS	XRF, ICP-MS
MH08-23	pumice	Polallie	58.73	EMPA	EMPA, LA-ICP-MS	EMPA, LA-ICP-MS, SIMS	XRF, ICP-MS
MH09-01	PJB	Timberline (?)	61.89				XRF, ICP-MS, MC-ICP-MS
MH09-01a	plutonic inclusion	Timberline (?)	49.32				XRF, ICP-MS
MH09-02	PJB	Timberline (?)	63.04				XRF, ICP-MS
MH09-02a	mafic enclave	Timberline (?)	59.37				XRF, ICP-MS
MH09-03	PJB	Polallie	63.06	EMPA	EMPA, LA-ICP-MS		XRF, ICP-MS
MH09-03a	mafic enclave	Polallie	59.37	EMPA	EMPA, LA-ICP-MS		XRF, ICP-MS
MH09-03b	mafic enclave	Polallie	56.56				XRF, ICP-MS
MH09-04	PJB	Old Maid	63.08	EMPA	EMPA, LA-ICP-MS		XRF, ICP-MS
MH09-04A	mafic enclave	Old Maid	58.31	EMPA	EMPA, LA-ICP-MS		XRF, ICP-MS
MH09-07	PJB	Old Maid	63.31				XRF, ICP-MS
MH09-07a	porphyritic inclusion	Old Maid	63.45				XRF, ICP-MS
MH09-08	PJB	Timberline (?)	63.54				XRF, ICP-MS
MH09-10	PJB	Timberline	63.37	EMPA	EMPA, LA-ICP-MS		XRF, ICP-MS
MH09-10a	porphyritic inclusion	Timberline	63.39	EMPA	EMPA, LA-ICP-MS		XRF, ICP-MS
PD04-01B	lava	Parkdale	58.78				XRF[1], ICP-MS, MC-ICP-MS
TL04-01B	lava	Main Stage	63.43				XRF[1], ICP-MS
WR 05-01	PJB	Old Maid	63.67				XRF[1], ICP-MS
PD-05-02	lava	Parkdale	58.57				XRF[1]
PD-05-03	lava	Parkdale	58.19				XRF[1]
PD-05-04	lava	Parkdale	58.09				XRF[1]

Table 4.1: Sample details and analyses included in this study. XRF[1] are analyses from Darr (2006).

Sample ID	SiO_2	TiO_2	AlO_2O_3	FeO*	MnO	MgO	CaO	Na_2O	K_2O	P_2O_5	Total
CC04-01	55.66	1.23	18.73	7.34	0.12	4.37	7.04	4.27	0.69	0.24	99.69
CD04-01	59.95	0.87	18.04	5.59	0.10	3.25	6.55	4.02	1.34	0.19	99.90
CS04-01	58.92	1.00	17.73	6.15	0.11	3.31	5.97	3.99	1.56	0.27	99.02
CS04-02	59.21	1.00	18.00	6.11	0.11	3.31	5.85	4.17	1.24	0.23	99.21
EB04-01	61.86	0.90	16.74	5.00	0.09	2.56	5.71	4.40	1.89	0.31	99.46
HW04-01	60.08	0.99	17.64	5.96	0.11	3.14	6.03	4.17	1.38	0.24	99.73
HW04-02	61.93	0.85	17.31	5.43	0.10	3.20	5.73	4.26	1.27	0.18	100.25
MH05-01	61.16	0.96	17.37	6.13	0.10	3.01	5.90	4.20	1.45	0.23	100.49
MH05-01a	57.88	1.05	18.11	6.82	0.12	3.63	6.79	4.18	1.02	0.26	99.85
MH05-05	61.14	0.94	17.37	5.82	0.10	3.00	5.94	4.23	1.46	0.23	100.24
MH08-08	63.65	0.73	16.85	4.76	0.08	2.33	5.08	4.36	1.48	0.17	99.49
MH08-11a	56.90	0.96	18.76	6.43	0.10	3.86	7.33	4.07	1.06	0.17	99.65
MH08-11b	54.70	1.38	17.70	8.61	0.13	5.07	8.45	3.85	0.51	0.17	100.57
MH08-11c	56.71	0.99	18.64	6.56	0.10	4.19	7.45	4.09	0.94	0.17	99.85
MH08-11d	60.30	0.88	17.71	5.86	0.10	3.36	6.16	4.19	1.23	0.18	99.95
MH08-12	63.81	0.75	16.95	4.87	0.09	2.40	5.18	4.36	1.43	0.17	100.02
MH08-14	58.13	1.13	17.99	6.56	0.10	3.39	6.56	4.43	0.87	0.28	99.44
MH08-16	55.03	1.24	18.88	7.65	0.12	4.23	6.73	4.13	0.69	0.24	98.95
MH08-18	61.00	0.85	17.15	5.69	0.10	3.12	5.64	4.20	1.25	0.19	99.17
MH08-18a	59.03	0.92	17.67	6.22	0.11	3.67	6.15	4.14	1.10	0.19	99.19
MH08-20	63.16	0.69	16.97	4.49	0.08	2.21	5.13	4.28	1.44	0.16	98.61
MH08-22	62.86	0.72	16.68	4.76	0.09	2.44	5.19	4.23	1.50	0.16	98.64
MH08-23	58.73	0.84	18.68	5.42	0.10	2.62	5.56	4.01	1.14	0.21	97.30
MH09-01	61.89	0.78	17.34	5.05	0.09	2.46	5.40	4.18	1.45	0.18	98.81
MH09-01a	49.32	1.32	21.34	8.14	0.13	4.65	10.09	3.71	0.20	0.25	99.13
MH09-02	63.04	0.73	16.97	4.89	0.09	2.48	5.37	4.29	1.48	0.16	99.51
MH09-02a	59.37	0.98	17.74	6.41	0.12	2.94	6.14	3.80	1.15	0.27	98.92
MH09-03	63.06	0.76	16.64	5.01	0.09	2.34	5.06	4.16	1.56	0.19	98.85
MH09-03a	59.37	0.96	17.38	6.26	0.10	3.11	6.05	3.81	1.25	0.26	98.55
MH09-03b	56.56	1.03	17.95	6.86	0.13	4.56	7.48	3.61	0.90	0.23	99.30
MH09-04	63.08	0.76	16.85	4.92	0.09	2.44	5.20	4.33	1.40	0.17	99.23
MH09-04A	58.31	1.00	18.47	6.16	0.10	3.49	6.95	4.04	1.01	0.20	99.73
MH09-07	63.31	0.76	17.12	4.95	0.09	2.43	5.30	4.39	1.38	0.17	99.89
MH09-07a	63.45	0.77	16.94	5.07	0.09	2.49	5.21	4.36	1.42	0.17	99.97
MH09-08	63.54	0.75	17.00	4.93	0.09	2.43	5.22	4.37	1.41	0.17	99.91
MH09-10	63.37	0.75	16.94	4.87	0.09	2.41	5.20	4.35	1.43	0.17	99.56
MH09-10a	63.39	0.75	16.81	4.92	0.09	2.43	5.14	4.37	1.38	0.17	99.45
PD04-01B	58.78	1.12	18.00	6.32	0.10	3.41	6.62	4.47	0.90	0.26	100.00
PD-05-02	58.57	1.13	18.11	6.30	0.10	3.36	6.65	4.45	0.89	0.26	99.83
PD-05-03	58.19	1.15	18.27	6.47	0.11	3.39	6.67	4.36	0.85	0.27	99.73
PD-05-04	58.09	1.15	18.17	6.42	0.11	3.41	6.70	4.42	0.86	0.27	99.59
TL04-01B	63.43	0.74	16.83	4.71	0.09	2.56	5.34	4.32	1.52	0.17	99.70
WR 05-01	63.67	0.77	16.80	4.82	0.09	2.47	5.13	4.36	1.45	0.17	99.72

Table 4.2: Whole rock major and trace elements analyzed by XRF.

Sample ID	Ni	Cr	Sc	V	Ba	Rb	Sr	Zr	Y	Nb	Ga	Cu	Zn	Pb	La	Ce	Th	Nd	U
CC04-01	59	79	18	143	252	7	629	119	18	7.0	21	46	83	3	11	29	1	18	
CD04-01	28	29	15	116	256	14	736	147	15	7.0	22	43	60	5	16	37	4	16	
CS04-01	34	31	16	130	445	22	733	199	19	9.0	22	27	81	7	21	59	5	27	
CS04-02	28	38	16	129	297	16	644	152	18	9.0	20	38	75	5	20	34	3	19	
EB04-01	23	19	11	103	550	25	902	201	18	10.0	20	33	77	9	30	75	7	36	
HW04-01	32	31	15	115	359	20	566	186	20	11.0	21	32	76	5	18	47	3	23	
HW04-02	39	51	14	108	317	18	526	147	16	9.0	20	29	70	6	15	34	2	19	
MH05-01	27	28	14	112	354	20	560	188	20	11.1	20	28	75	7	19	40	3	20	3
MH05-01a	35	38	18	127	316	9	567	179	21	11.1	20	28	82	6	17	43	3	21	0
MH05-05	19	22	10	82	345	21	518	153	15	8.4	19	21	64	7	20	37	2	18	0
MH08-08	34	26	17	144	279	16	637	130	15	7.4	20	108	82	9	16	29	1	16	1
MH08-11a	34	27	17	143	280	16	639	129	15	8.4	22	109	83	10	11	31	2	16	1
MH08-11b	46	85	22	192	191	7	689	77	16	6.7	20	62	91	4	8	20	1	14	1
MH08-11c	40	56	18	152	268	13	630	133	16	7.0	20	71	72	3	11	31	1	18	0
MH08-11d	36	42	14	117	306	19	556	149	16	9.2	20	43	73	5	16	35	2	18	1
MH08-12	20	21	11	83	347	20	525	156	15	8.9	19	13	68	6	18	34	3	14	0
MH08-14	30	50	13	121	274	10	635	145	16	9.5	22	32	90	4	12	32	1	19	0
MH08-16	57	78	17	143	275	7	612	120	18	8.7	21	48	85	3	13	23	1	18	0
MH08-18	34	50	13	104	307	18	503	151	18	9.2	20	32	72	4	16	28	2	19	1
MH08-18a	43	66	15	120	277	15	528	141	16	8.8	21	46	81	5	12	33	2	16	0
MH08-20	20	20	10	78	348	20	524	152	14	8.2	18	26	64	6	19	38	3	19	1
MH08-22	20	18	11	88	353	21	552	158	15	9.6	21	29	66	6	13	36	2	17	1
MH08-23	22	27	12	91	381	17	628	175	14	9.9	22	21	79	7	18	42	3	20	2
MH09-01	17	19	11	95	342	22	542	163	15	9.8	19	27	69	6	18	40	3	19	1
MH09-01a	30	43	19	161	106	1	812	42	17	6.3	22	52	80	1	7	19	0	14	0
MH09-02	20	20	11	91	346	21	555	157	16	9.0	19	33	65	6	15	42	3	21	0
MH09-02a	21	23	11	102	261	16	636	145	12	9.9	20	19	85	7	19	31	1	14	1
MH09-03	16	22	11	87	369	24	498	178	17	10.4	19	28	68	7	20	40	3	20	3
MH09-03a	30	42	14	111	289	18	550	130	16	8.9	20	52	78	5	17	40	2	21	0
MH09-03b	47	50	17	142	226	14	682	112	16	8.1	18	69	80	4	14	34	1	18	2
MH09-04	22	24	11	88	338	20	523	153	15	8.8	20	12	67	6	13	41	3	19	2
MH09-04A	36	40	14	116	245	13	641	111	13	6.8	21	27	75	5	10	22	1	15	1
MH09-07	20	21	11	82	333	19	538	150	15	8.6	20	24	68	5	15	37	2	17	1
MH09-07a	21	24	11	81	340	20	528	151	15	8.9	20	29	69	6	19	34	2	15	0
MH09-08	20	23	10	86	343	20	529	151	15	8.7	21	24	66	6	18	33	3	18	2
MH09-10	19	23	11	84	340	20	524	152	15	9.5	19	35	67	7	21	40	4	18	2
MH09-10a	20	23	11	83	340	20	520	153	16	8.8	19	28	68	8	16	35	3	18	2
PD04-01B	32	49	15	118	283	10	645	143	17	10.0	20	38	86	5	16	32	1	17	
PD-05-02	32	51	14	119	286	11	647	142	16	9.0	20	39	86	5	14	28	1	19	
PD-05-03	32	47	16	116	291	10	649	145	18	9.0	21	40	87	5	13	33	1	17	
PD-05-04	32	48	14	122	285	9	646	143	17	8.0	22	37	89	5	16	34	2	19	
TL04-01B	23	20	11	91	353	22	575	157	15	8.0	20	25	65	7	15	29	4	17	
WR 05-01	23	22	12	86	344	20	537	152	15	8.0	20	17	67	7	18	39	2	18	

Table 4.2, continued

Sample	La	Ce	Pr	Nd	Sm	Eu	Gd	Tb	Dy	Ho	Er	Tm	Yb	Lu	Ba	Th	Nb	Y	Hf	Ta	U	Pb	Rb	Cs	Sr	Sc	Zr
CC04-01	12.46	25.67	4.00	17.57	4.21	1.51	4.14	0.63	3.62	0.68	1.78	0.23	1.42	0.22	251	0.81	7.50	17.52	3.07		0.29	2.46	6.5	0.10	607	16.5	116
CD04-01	16.62	34.73	4.65	18.86	3.95	1.27	3.46	0.52	2.96	0.58	1.51	0.21	1.32	0.21	258	2.83	6.81	14.66	3.87		0.83	4.08	13.4	0.15	695	13.8	145
CS04-01	24.86	54.36	6.82	27.08	5.41	1.63	4.57	0.67	3.77	0.72	1.89	0.26	1.59	0.25	437	4.15	9.63	18.82	5.06		1.24	5.73	22.1	0.28	710	15.5	201
CS04-02	17.20	35.43	4.92	20.50	4.45	1.50	4.12	0.63	3.61	0.69	1.79	0.25	1.52	0.24	290	2.67	8.97	17.79	3.90		0.84	4.24	15.2	0.32	618	14.7	151
EB04-01	33.00	67.33	8.63	33.88	6.35	1.80	4.91	0.70	3.73	0.69	1.70	0.24	1.46	0.22	545	5.69	10.65	17.65	5.26		1.61	6.93	25.0	0.47	853	11.5	202
HW04-01	20.93	43.08	5.61	22.45	4.88	1.51	4.46	0.69	4.01	0.78	2.09	0.29	1.82	0.29	352	3.17	10.18	20.23	4.72		1.00	4.89	18.4	0.18	544	14.7	186
HW04-02	15.67	32.44	4.28	17.61	3.93	1.26	3.66	0.57	3.24	0.63	1.60	0.22	1.38	0.22	308	2.51	8.34	16.09	3.91		0.86	4.86	17.4	0.25	494	12.7	146
MH05-01	20.72	43.89	5.60	22.24	4.83	1.45	4.33	0.67	3.95	0.75	2.01	0.28	1.74	0.27	352	3.35	9.94	19.44	4.65	0.67	1.06	6.48	19.1	0.20	524	14.0	184
MH05-01a	20.02	41.69	5.42	21.72	4.81	1.58	4.46	0.71	4.16	0.80	2.10	0.30	1.87	0.29	315	2.69	10.45	20.38	4.41	0.68	0.78	5.57	9.2	0.13	551	15.5	175
MH05-05	20.92	43.09	5.53	22.12	4.72	1.47	4.34	0.68	3.94	0.76	2.02	0.29	1.74	0.28	353	3.30	9.91	19.52	4.67	0.81	1.04	4.09	19.7	0.28	549	13.9	184
MH08-08	16.74	34.53	4.30	16.99	3.70	1.16	3.30	0.50	2.90	0.56	1.48	0.21	1.30	0.20	342	2.97	8.07	14.38	4.02	0.61	0.98	6.45	19.0	0.47	521	10.4	150
MH08-11a	15.06	31.70	3.95	16.24	3.67	1.29	3.51	0.53	3.02	0.59	1.54	0.21	1.29	0.19	276	2.24	7.00	14.89	3.32	0.47	0.72	9.46	15.0	0.26	666	16.4	128
MH08-11b	9.93	20.97	2.78	12.56	3.33	1.24	3.38	0.54	3.20	0.61	1.59	0.22	1.32	0.20	186	1.01	5.70	14.87	2.00	0.40	0.34	3.59	6.8	0.12	651	22.6	73
MH08-11c	14.79	31.29	4.00	16.70	3.78	1.26	3.62	0.56	3.23	0.62	1.63	0.22	1.36	0.21	263	2.10	6.75	15.63	3.34	0.47	0.71	3.12	12.5	0.21	586	18.8	130
MH08-11d	15.91	34.28	4.28	17.19	3.80	1.24	3.52	0.56	3.24	0.61	1.62	0.23	1.42	0.22	308	2.68	7.68	15.57	3.81	0.55	0.88	4.47	18.1	0.24	521	14.5	147
MH08-12	16.64	34.49	4.29	17.28	3.77	1.15	3.39	0.52	2.97	0.57	1.49	0.22	1.33	0.21	343	2.90	8.12	14.68	3.99	0.61	0.97	6.20	19.2	0.46	527	10.7	149
MH08-14	13.87	30.77	4.29	18.44	4.23	1.48	3.98	0.61	3.33	0.63	1.58	0.22	1.34	0.21	273	1.15	8.93	15.83	3.71	0.57	0.41	4.64	9.5	0.21	614	13.3	140
MH08-16	12.24	26.04	3.96	17.59	4.17	1.54	4.13	0.64	3.63	0.69	1.75	0.23	1.42	0.22	272	0.84	7.55	17.25	3.10	0.47	0.30	2.86	7.3	0.18	599	16.0	116
MH08-18	19.29	33.72	4.97	20.20	4.36	1.30	4.00	0.60	3.42	0.66	1.70	0.23	1.44	0.22	307	2.51	8.33	17.45	3.90	0.60	0.86	4.54	17.4	0.25	475	13.7	148
MH08-18a	14.63	31.18	4.01	16.86	3.86	1.27	3.61	0.57	3.24	0.63	1.60	0.23	1.37	0.22	279	2.06	7.95	15.97	3.64	0.55	0.66	4.90	13.8	0.21	498	15.5	140
MH08-20	16.70	33.54	4.23	16.58	3.53	1.12	3.12	0.49	2.75	0.53	1.41	0.20	1.26	0.20	341	3.02	7.90	13.89	3.94	0.61	0.99	6.31	19.5	0.47	503	9.7	148
MH08-22	18.07	36.59	4.63	18.28	3.87	1.18	3.47	0.54	3.09	0.59	1.54	0.22	1.39	0.22	355	3.41	8.47	15.27	4.20	0.64	1.08	6.74	20.8	0.47	540	11.1	157
MH08-23	18.72	41.64	5.02	19.86	4.22	1.38	3.70	0.57	3.30	0.61	1.62	0.23	1.41	0.22	386	3.12	9.51	15.70	4.55	0.68	0.96	6.90	16.5	0.40	621	11.4	175
MH09-01	18.44	37.71	4.63	18.17	3.87	1.23	3.46	0.53	3.15	0.60	1.58	0.23	1.42	0.22	339	3.57	8.50	15.57	4.17	0.64	1.17	6.79	21.6	0.55	512	12.0	162
MH09-01a	7.08	17.89	2.80	13.68	3.71	1.80	3.83	0.61	3.46	0.66	1.69	0.23	1.38	0.21	103	0.33	4.71	16.35	1.26	0.27	0.12	2.02	0.7	0.02	781	19.6	40
MH09-02	18.22	37.72	4.62	18.32	3.90	1.22	3.46	0.54	3.09	0.59	1.55	0.22	1.38	0.21	347	3.36	8.30	15.32	4.13	0.62	1.08	6.19	20.6	0.48	522	11.4	157
MH09-02a	15.79	33.06	4.09	16.32	3.30	1.07	2.93	0.45	2.60	0.50	1.28	0.18	1.15	0.18	261	2.04	8.99	12.66	3.68	0.63	0.68	6.00	15.3	0.37	613	10.7	144
MH09-03	20.73	42.53	5.15	20.09	4.21	1.26	3.67	0.57	3.28	0.62	1.63	0.24	1.51	0.23	367	3.89	9.57	16.29	4.51	0.73	1.25	6.70	23.7	0.57	469	11.3	176
MH09-03a	17.83	38.61	4.91	20.06	4.46	1.32	3.98	0.60	3.45	0.65	1.64	0.23	1.37	0.22	289	2.92	8.41	16.25	3.43	0.63	0.93	5.89	18.0	0.42	522	14.0	130
MH09-03b	13.96	31.08	4.12	17.40	3.92	1.36	3.57	0.57	3.33	0.64	1.68	0.23	1.44	0.22	226	1.88	7.28	16.10	2.95	0.49	0.60	4.23	12.5	0.27	652	16.6	109
MH09-04	16.50	33.54	4.31	17.09	3.71	1.19	3.31	0.52	2.93	0.57	1.50	0.21	1.33	0.21	339	2.85	8.19	14.82	4.05	0.60	0.93	5.99	18.9	0.47	511	10.3	151
MH09-04A	10.40	22.48	3.11	13.51	3.22	1.23	3.09	0.48	2.67	0.51	1.29	0.18	1.07	0.17	245	0.84	6.59	12.70	2.91	0.44	0.36	5.52	12.0	0.23	619	13.0	109
MH09-07	15.82	33.20	4.18	16.62	3.64	1.16	3.24	0.51	2.93	0.56	1.45	0.21	1.28	0.20	332	2.77	8.03	14.47	3.82	0.59	0.93	4.45	18.3	0.38	505	10.6	147
MH09-07a	16.17	33.87	4.23	16.96	3.69	1.15	3.25	0.51	2.96	0.56	1.46	0.21	1.29	0.20	335	2.80	8.01	14.53	3.92	0.61	0.93	4.61	19.4	0.52	492	10.6	149
MH09-08	16.01	33.64	4.20	16.71	3.58	1.17	3.30	0.51	2.92	0.56	1.49	0.21	1.32	0.20	339	2.83	8.14	14.59	3.93	0.61	0.95	5.51	19.0	0.41	494	10.5	146
MH09-10	16.80	34.82	4.36	17.21	3.72	1.14	3.34	0.51	2.90	0.56	1.48	0.21	1.31	0.21	340	2.88	8.13	14.60	3.93	0.61	0.95	6.20	19.1	0.46	492	10.7	149
MH09-10a	16.71	34.98	4.37	17.43	3.79	1.15	3.36	0.51	3.03	0.58	1.51	0.21	1.30	0.20	343	2.90	8.21	14.93	4.02	0.62	0.97	6.26	18.8	0.47	495	10.5	151
PD04-01B	14.33	31.34	4.30	18.42	4.26	1.47	3.97	0.60	3.43	0.64	1.64	0.22	1.35	0.21	280	1.25	8.94	16.22	3.64		0.44	4.75	10.5	0.23	615	13.7	143
TL04-01B	18.40	37.32	4.73	18.54	3.95	1.20	3.47	0.53	3.01	0.58	1.58	0.22	1.39	0.22	355	3.41	8.59	15.17	4.20		1.07	5.99	20.7	0.47	543	11.2	157
WR 05-01	16.55	33.38	4.29	17.04	3.67	1.17	3.32	0.52	2.90	0.56	1.44	0.20	1.31	0.21	343	2.92	8.41	14.41	3.99		0.97	5.99	19.5	0.47	523	10.5	148

Table 4.3a: Bulk rock trace elements analyzed by ICP-MS.

Sample	MH08-20-0234b	MH08-20-0237a	MH08-20-2031b	MH08-20-2059	MH08-20-2098	MH08-20-2145	MH08-22-2051	MH08-22-2073	MH08-22-2105a	MH08-22-2105b	MH08-22-2166a	MH08-22-2166c	MH08-22-2191
Li	46.0	55.2	62.2	61.4	64.6	52.4	26.4	3.7	4.2	46.7	52.5	5.4	22.7
V	6.8	5.5	3.5	3.5	2.6	5.5	27.4	15.9	1.7	7.2	12.4	17.4	1.6
Mn	264	235	322	242	282	35	58	44	257	233	26	250	289
Cu	57	33	25	5	34	2	15	2	16	25	19	18	15
Zn	40	40	57	36	50	45	56	43	50	46	56	54	60
Sr	127	124	111	139	178	134	124	17	87	82	156	20	18
Ba	556	489	570	615	537	64	542	488	423	422	549	523	543
La	26.2	18.0	23.5	22.9	16.9	22.9	21.5		11.2	13.3	29.4	28.2	
Ce	47.8	39.2	63.7	45.0	44.4	48.4	49.9	47.0	32.3	32.6	53.3	56.6	
Pr	5.0	4.4	5.8	4.7	4.3	4.6	5.6	4.9	3.4	3.2	6.4	5.2	4.3
Nd	19.4	12.5	21.1	13.5	18.6	17.9	16.9	19.5		14.8	18.1	25.6	16.9
Sm	2.7	2.0	3.9	2.8	4.2	3.3	3.5	3.8			3.4	5.0	2.4
Eu	0.6	0.3	0.6	0.6	0.6	0.7	0.4	0.1	0.4	0.3			0.4
Gd	2.6	2.2	4.6	1.9	3.4	3.2	1.3	1.7	4.8	2.0	2.2	1.8	
Dy	1.7	1.6	4.4	1.4	1.6	3.1	3.5	0.6	0.2		3.9	2.3	2.5
Er	1.8	1.8	2.1	1.6	1.6	1.4	0.5		1.5	1.5	1.5	1.6	
Yb	1.1	0.9	2.3	0.5	1.6	1.6	0.4	1.6	1.3		2.2	2.8	
Th	7.28	5.35	5.55	6.43	6.52	6.44	5.12	3.77	4.50	6.83	5.37	3.40	
Nb	11.87	9.65	12.99	8.18	11.74	12.11	12.12	11.45		9.00	14.75	12.34	7.56
Y	13.97	9.67	21.17	9.22	15.57	14.27	13.49	1.98	11.32	8.79	22.43	23.88	12.22
Hf	6.57	3.28	8.00	2.93	2.86	4.82	4.86	3.14	4.36	4.34	6.49	6.25	2.98
Ta	0.89	0.60		1.32	0.55	0.95	0.71	0.64	1.79		1.25	0.62	0.98
U	1.89	1.88	2.58	2.34	2.93	2.23	1.53	1.58	2.34	2.94	1.93	2.24	3.76
Pb	9.73	9.36	11.59	14.13	9.78	13.46	12.57	11.27	8.18	7.51	8.70	7.69	9.69
Rb	43	41	49	47	53	43	43	39	50	54	47	47	45
Sc	4.77	2.94	8.92	1.55	6.38	7.46	1.60	1.62		7.14	7.71		
Zr	249	123	317		172	214	241	156		152	266	298	150
Ti	1474	1156	1789	792	1247	1596	236	1746	1599	1183	1746		178
W	0.72	0.42	0.23	0.22	0.83	0.63					1.34		

Table 4.3b: Melt inclusion trace elements analyzed by LA-ICP-MS. All concentrations in µg/g.

Sample	$^{87}Sr/^{87}Sr$	±2s	$^{143}Nd/^{144}Nd$	±2s
CC04-01	0.703442	11	0.512936	5
CD04-01	0.703053	11	0.513015	5
CS04-01	0.703403	11	0.512955	6
EB04-01	0.703511	11	0.512942	5
HW04-01	0.703456	11	0.512952	6
MH05-05	0.703407	10	0.512948	5
MH08-08	0.703427	8	0.512942	5
MH08-11b	0.703451	12	0.512939	5
MH08-11d	0.703432	11	0.512938	5
MH08-12	0.703326	12	0.512951	7
MH09-01	0.703310	12	0.512951	8
MH09-01a	0.703347	12	0.512945	6
PD04-01B	0.703429	10	0.512936	6

Table 4.4: Sr and Nd isotopes analyzed by MC-ICP-MS.

	Calculated mafic endmember		Calculated silicic endmember		Intermediate Lavas		Melt Inclusions		Melt in equilbrium with Mg-hornblende	Melt in equilbrium with plagioclase
	Low	High	Low	High	Low	High	Low	High		
Rb	0.4	4.4	27.3	39.3	6.5	25.0	39.0	53.7		
Ba	166	220	377	543	251	545	216	647		296
Th	2.51	4.10	0.54	5.18	0.81	5.69	3.40	7.28		
U	0.70	1.14	0.42	1.71	0.29	1.61	1.53	3.76		
Nb	7.20	8.62	6.79	10.93	6.81	10.65	7.56	14.75	36	
Ta	0.34	0.59	0.52	1.30	0.47	1.15	0.55	1.79		
K	7956	10707	9883	17919	10186	15690	178	1789	2277	6472
La	10.92	14.77	15.68	27.45	12.24	33.00	11.16	29.38	31	12.39
Ce	24.93	33.24	29.72	55.13	25.67	67.33	11.13	63.68	71	
Pb	1.36	3.22	6.00	11.70	4.08	6.93	3.83	14.13		9.85
Pr	3.96	4.92	3.24	6.18	3.96	8.63	0.75	6.37		
Sr	684	767	236	490	469	853	70	1223	472	491
Nd	18.33	21.89	11.23	22.14	16.62	33.88	12.47	25.64	32	8.89
Sm	4.44	5.09	2.21	4.21	3.58	6.35	1.99	4.98	6.2	8.48
Zr	100.15	128.93	145.90	234.00	116.29	201.65	122.78	316.69	350	
Hf	2.54	3.19	4.13	6.12	3.07	5.26	2.86	8.00	3.9	
Eu	1.67	1.83	0.53	1.04	1.14	1.80	0.14	0.75	2.4	0.98
Ti	8941	9323	457	1624	4353	5982	14	1789	2277	6472
Gd	4.44	4.97	1.69	3.31	3.24	4.91	1.25	4.79	10.6	0.00
Yb	1.44	1.66	0.90	1.56	1.28	1.82	0.38	2.81	3.1	
Cr	87.46	103.08	0*	0*	116.29	201.65	122.78	316.69		
Ni	65.10	74.15	0*	0*	3.07	5.26	2.86	8.00		
Sc	21.98	24.00	0*	5.53	1.14	1.80	0.14	0.75		
V	189	203	0*	29	4353	5982	14	1789		

Table 4.5: Trace element concentrations in intermediate mixed lavas and calculated potential endmembers for Mount Hood. Plagioclase composition (for calculations) from Darr (2006). Amphibole compositions (for calculations) from Chapter Two. Partition coefficients for equilibrium melts are from Tiepolo et al. (2007). Melt inclusion compositions are from Koleszar et al. (in review). 0* indicates that calculated concentration was < 0

Table 4.6: Endmember compositions from linear regression (using Excel's LINEST function).
See first example for explanation of LINEST output.

		LINEST output			Mafic endmember	±	Silicic endmember	±
La	**slope**	8.72	12.85	**intercept**	12.85	1.92	21.57	5.89
	±	3.96	1.92	**±**				
	r^2	0.13	2.45	**s(y)**				
	F	4.84	33.00	**degrees of freedom**				
	regression sum of squares	29.18	198.84	**residual sum of squares**				
Ce		13.34	29.08		29.08	4.15	42.43	12.70
		8.55	4.15					
		0.07	5.30					
		2.43	33.00					
		68.32	926.43					
Rb		30.88	2.40		2.40	1.96	33.29	6.00
		4.04	1.96					
		0.64	2.50					
		58.49	33.00					
		365.98	206.50					
Ba		267.14	192.96		192.96	27.11	460.10	82.97
		55.86	27.11					
		0.41	34.60					
		22.87	33.00					
		27388.18	39514.70					
Th		5.19	0.23		0.23	0.45	5.42	1.36
		0.92	0.45					
		0.49	0.57					
		31.95	33.00					
		10.35	10.69					
U		1.69	0.07		0.07	0.12	1.76	0.38
		0.26	0.12					
		0.57	0.16					
		43.37	33.00					
		1.09	0.83					
Nb		0.92	7.94		7.94	0.68	8.86	2.07
		1.39	0.68					
		0.01	0.86					
		0.44	33.00					
		0.32	24.62					

Table 4.6 cont.

	LINEST output		Mafic endmember	±	Silicic endmember	±
Ta	0.45	0.46	0.46	0.13	0.91	0.39
	0.26	0.13				
	0.08	0.16				
	2.94	33.00				
	0.08	0.87				
K	15891.55	3049.79	3049.79	865.11	18941.34	2647.52
	1782.41	865.11				
	0.71	1104.20				
	79.49	33.00				
	96921010	40235799				
Pb	6.56	2.29	2.29	0.93	8.85	2.85
	1.92	0.93				
	0.26	1.19				
	11.68	33.00				
	16.49	46.61				
Sr	-362.35	725.23	725.23	41.38	362.88	126.63
	85.25	41.38				
	0.35	52.81				
	18.07	33.00				
	50389.31	92047.79				
Nd	-3.43	20.11	20.11	1.78	16.68	5.45
	3.67	1.78				
	0.03	2.27				
	0.87	33.00				
	4.50	170.61				
Sm	-1.56	4.77	4.77	0.33	3.21	1.00
	0.67	0.33				
	0.14	0.42				
	5.38	33.00				
	0.93	5.70				
Zr	75.41	114.54	114.54	14.39	189.95	44.05
	29.66	14.39				
	0.16	18.37				
	6.47	33.00				
	2182.35	11138.76				
Hf	2.26	2.86	2.86	0.32	5.12	0.99
	0.67	0.32				
	0.26	0.41				
	11.40	33.00				
	1.96	5.67				

Table 4.6 cont.

	LINEST output		Mafic endmember	±	Silicic endmember	±
Eu	-0.97	1.75	1.75	0.08	0.78	0.25
	0.17	0.08				
	0.49	0.11				
	31.69	33.00				
	0.36	0.37				
Ti	-8091.79	9132.09	9132.09	190.69	1040.29	583.56
	392.87	190.69				
	0.93	243.39				
	424.21	33.00				
	25129007	1954823				
Gd	-2.21	4.70	4.70	0.26	2.50	0.81
	0.55	0.26				
	0.33	0.34				
	16.33	33.00				
	1.87	3.77				
Yb	-0.32	1.55	1.55	0.11	1.23	0.33
	0.22	0.11				
	0.06	0.14				
	2.02	33.00				
	0.04	0.62				
Cr	-128.85	95.27	95.27	7.81	-33.58	23.90
	16.09	7.81				
	0.66	9.97				
	64.12	33.00				
	6371.51	3279.38				
Ni	-86.51	69.62	69.62	4.53	-16.89	13.85
	9.32	4.53				
	0.72	5.78				
	86.07	33.00				
	2872.10	1101.17				
Sc	-20.65	23.01	23.01	1.04	2.37	3.17
	2.13	1.04				
	0.74	1.32				
	93.61	33.00				
	163.58	57.67				
V	-188.75	195.60	195.60	7.11	6.85	21.77
	14.66	7.11				
	0.83	9.08				
	165.80	33.00				
	13672.87	2721.43				

Table 4.6 cont.

	LINEST output		Mafic endmember	±	Silicic endmember	±
Dy	-1.84	4.11	4.11	0.23	2.26	0.70
	0.47	0.23				
	0.32	0.29				
	15.19	33.00				
	1.31	2.84				
Yb	-0.32	1.55	1.55	0.11	1.23	0.33
	0.22	0.11				
	0.06	0.14				
	2.02	33.00				
	0.04	0.62				
Pr	0.27	4.44	4.44	0.48	4.71	1.47
	0.99	0.48				
	0.00	0.61				
	0.07	33.00				
	0.03	12.43				
Tb	-0.33	0.72	0.72	0.04	0.39	0.12
	0.08	0.04				
	0.33	0.05				
	16.01	33.00				
	0.04	0.08				
Ho	-0.33	0.78	0.78	0.04	0.44	0.14
	0.09	0.04				
	0.29	0.06				
	13.31	33.00				
	0.04	0.10				
Er	-0.77	1.98	1.98	0.13	1.21	0.38
	0.26	0.13				
	0.21	0.16				
	8.73	33.00				
	0.22	0.85				
Tm	-0.07	0.26	0.26	0.02	0.19	0.06
	0.04	0.02				
	0.10	0.02				
	3.86	33.00				
	0.00	0.02				
Lu	-0.05	0.24	0.24	0.02	0.19	0.05
	0.04	0.02				
	0.05	0.02				
	1.65	33.00				
	0.00	0.02				

Table 4.6 cont.

	LINEST output		Mafic endmember	±	Silicic endmember	±
Pr	0.27	4.44	4.44	0.48	4.71	1.47
	0.99	0.48				
	0.00	0.61				
	0.07	33.00				
	0.03	12.43				
Calculated using only intermediate lavas (no mafic enclaves)						
Th	-0.44	3.31	3.31	0.79	2.86	2.32
	1.52	0.79				
	0.00	0.45				
	0.08	18.00				
	0.02	3.72				
U	0.15	0.92	0.92	0.22	1.06	0.65
	0.42	0.22				
	0.01	0.13				
	0.12	18.00				
	0.00	0.29				
K	4569.33	9331.45	9331.45	1375.51	13900.78	4018.26
	2642.75	1375.51				
	0.14	788.21				
	2.99	18.00				
	1857276	11182965				

CHAPTER FIVE

SUMMARY OF CONCLUSIONS AND SYNTHESIS

This dissertation comprises a comprehensive dataset for samples of lava, pumice, melt inclusions, mafic enclaves, plutonic inclusions, and phenocrysts from Mount Hood and seeks to examine the magmatic sources, plumbing, and eruptive style of this intermediate arc volcano. We confirm previous assertions that the majority of lavas at Mount Hood are produced from relatively simple binary mixing (Darr, 2006; Kent et al., 2010; Woods, 2004), and we find that a linear regression technique for extrapolating the major element contents of the mixing endmembers (Kent et al., 2010) works acceptably well to characterize the trace element budgets of these endmembers (Chapter Four). Additionally, we observe that the "recharge filter" that is responsible for the remarkably homogeneous intermediate lavas at Mount Hood (Kent et al., 2010) is also the likely cause of long-term low explosivity of Mount Hood (Chapter Two), and is indicative of a two-part magma plumbing system that may be a general model for a number of other recharge-driven arc volcanoes (Chapter Three). Finally, we find that the results presented in this dissertation, in concert with previous results by other authors (Cribb and Barton, 1997; Darr, 2006; Kent et al., 2010; Woods, 2004), converge on a generally consistent model for the production, hybridization, and eruption of intermediate lavas at Mount Hood.

Mantle to lower crust

A comprehensive model for what we now know about Mount Hood, from the mantle to the surface, begins with Chapter Four, which uses bulk rock, phenocryst, and trace element data to identify the trace element budget of the endmembers involved in creating Mount Hood intermediate lavas (Fig. 5.1). The trace element concentrations that we measure in lavas ranging from basaltic andesite to dacite are consistent with previous studies suggesting that the lavas at Mount Hood are produced by mixing between two endmembers (Cribb and Barton, 1997; Darr, 2006; Kent et al., 2010; Woods, 2004), thus we use linear regression to establish a trace element budget for each of these magmas. These results enable us to further define the composition of these endmembers and to discuss their petrogenetic origins. Additionally, we observe that the endmembers, like the homogeneous andesites-dacites that Mount Hood has erupted for ~0.5 Ma, show little to no variation with time.

The most mafic lavas from Mount Hood, and the calculated mafic endmember, exhibit trace element depletions and enrichments that are broadly consistent with typical Cascades calc-alkaline basalt (CAB). This is a hydrous basalt with high concentrations of large ion lithophile elements (LILE) relative to high field strength elements (HFSE) (Leeman et al., 2005; Reiners et al., 2000; Rowe et al., 2009; Schmidt et al., 2008). CAB has also been named high-alumina basalt (HAB) or simply arc basalt. More specifically, the calculated mafic endmember is enriched in LILE like Ba, K, and Sr, and depleted in HFSE like Zr and Hf (see Chapter Four). Consequently, ratios of these elements (LILE/HFSE) can be used to distinguish CAB from the other two principle parent magma

types in the Cascades, which include: 1) A moderately trace element depleted basalt that has been called by various names including mid-ocean ridge basalt (MORB), high-alumina olivine tholeiite (HAOT), and low-potassium tholeiite (LKT), and 2) A trace element enriched basalt with high concentrations of HFSE relative to LILE called OIB, intraplate basalt, within-plate basalt (WIP), or HFSE-rich (Conrey et al., 1997; Hildreth, 2007; Reiners et al., 2000; Schmidt et al., 2008).

The CAB geochemical signature that is apparent in the calculated Mount Hood mafic endmember is typically attributed to flux melting of the mantle wedge {e.g., \Reiners, 2000 #129} and/or melting of previously metasomatized (fluxed) mantle (Leeman et al., 2005; Rowe et al., 2009; Smith and Leeman, 2005). One potential source for the CAB signature in the calculated mafic endmember is 15-20% isenthalpic melting of a peridotite source that has been influenced by 3-6% "slab component," which may consist of either slab-derived melts or slab-derived fluids (Reiners et al., 2000; Rowe et al., 2009). This mechanism generates the LILE/HFSE ratios observed in the calculated mafic endmember (see Chapter Four). Melt production at depths > 75 km can produce the slight HREE depletion (and high Dy_N/Yb_N ratios) that we observe in lavas from Mount Hood. These criteria provide our first quantitative constraint on the ultimate (i.e., mantle-derived) source for at least one of the magma sources at Mount Hood. These lavas likely segregate at 35-50 km depth (Leeman et al., 2005) and begin their ascent, undergoing polybaric crystallization over a large range of pressures (400-1000 MPa or approximately 14-70 km; Pichavant et al., 2002) to produce the moderately evolved basalt that contributes to the magma budget at Mount Hood.

As the mafic magmas ascend through the lower crust they liberate heat through cooling and crystallization, which can initiate partial melting of the mafic lower crust. At high fH_2O the mafic lower crust will retain amphibole in the residue during partial melting, so approximately 15-20% partial melting will produce melts that have elevated SiO_2 but are relatively depleted in MREE (Borg and Clynne, 1998). This process produces the Group 2 lavas described by Borg and Clynne (Borg and Clynne, 1998), which are felsic compositions with ~63-75 wt% SiO_2, 3.1-5.2 wt% H_2O, and liquidus temperatures of 884-916˚C (Borg and Clynne, 1998). The trace element concentrations of these Group 2 lavas are comparable to the silicic endmember that we calculate for Mount Hood, thus we suggest that the silicic endmember is also generated by partial melting of the mafic lower crust at high fO_2. Heat to initiate melting may be supplied by the ascending mafic parental magma discussed previously.

Lower to upper crust

The ascending mafic magma will eventually stall (Fig. 5.1), and magmas are most apt to stall as a result of gas saturation, changes to crustal properties (e.g., brittle-ductile transition) and/or density discontinuities. An ascending mafic magma will crystallize as it cools and as H_2O increases, facilitating stalling at approximately 300 MPa as a result of the magma density (and probably viscosity) increase that accompanies crystallization (Pichavant et al., 2002). At these conditions the ascending mafic magma cools, crystallizes further, and eventually saturates in amphibole, establishing the system that is explored in Chapter Three of this dissertation.

Crystallization of phenocrysts within the parent magma prior to magma mixing is suggested by previous studies that identified two populations of plagioclase in lavas from Mount Hood (Darr, 2006; Kent et al., 2010). One of these plagioclase populations (Population 1 in Kent et al. (2010) and Darr (2006)) contains elevated TiO_2, FeO, Sr/Ba, and anorthite content, and is consistent with crystallization from a mafic magma. As described in greater detail in Chapter Three, we observe two populations of amphibole in lavas from Mount Hood, and we suggest that one of the populations crystallized from approximately the same magma as the Population 1 plagioclase (Darr, 2006; Kent et al., 2010). These amphiboles are Tschermakitic pargasite (Tsch-pargasite) and have Al/Si ratios consistent with a mafic parent. Thermobarometric calculations (Holland and Blundy, 1994; Ridolfi et al., 2010) suggest that they crystallized in a hot (920-970˚C) mafic magma that has stalled at depths between 9-15 km (Fig. 5.1).

The silicic melts that were produced by partial melting of the mafic lower crust will also continue to cool and crystallize, and amphibole will become stable at temperatures ~100˚C below the liquidus for those melts (Borg and Clynne, 1998). In addition to the Tsch-pargasites described above (which we interpret as products of the mafic magma), we observe a second population of amphiboles that are magnesiohornblende (Mg-hornblende) with Al/Si ratios indicative of a silicic source. We estimate that these amphiboles crystallized at depths of 3 to 7 km and at temperatures between 810-880˚C using the thermobarometric model Ridolfi et al. (2010). A low velocity zone exists below Mount Hood at a depth of approximately 4 km, although this velocity decrease is small and it is unclear if it could be related to the silicic magma body that we propose is present near this depth (Jones and Malone, 2005). Residence times for

plagioclase that crystallizes from this shallow silicic body (what Kent et al. call "Population 2 plagioclase") are at least on the order of 4000-5000 years, but are potentially greater than 10,000 years (Eppich et al., in review). The long residence times indicate that the silicic magma stalls for an extended period of time and may be a crystal mush by the time of mixing. Kent et al. (2010) suggest that this magma is 'stuck' due to its high viscosity, but propose that it can be remobilized with mafic recharge.

Upper crust to surface

Shortly before eruption (within days to weeks), mafic recharge occurs when mafic magma ascends from 9-15 km and intrudes the silicic magma body situated at 3-7 km depth (Fig. 5.1), initiating the process that we describe in Chapter Two. Magma mixing occurs rapidly, potentially in a manner similar to that recently proposed by (Burgisser and Bergantz, 2011). Amphibole thermobarometry (Holland and Blundy, 1994; Ridolfi et al., 2010) reveals that the homogenized magma at the time of recharge is at least 100°C hotter than the silicic magma prior to mixing, and viscosity models suggest that this can decrease magmatic viscosity by at least a factor of four (Giordano et al., 2008; Mastin and Ghiorso, 2002). Explosive volcanic eruptions require fragmentation of the ascending magma, however the ease with which magma can fragment is highly dependent on the magmatic viscosity (Papale, 1999). The viscosity decrease associated with mafic recharge thus may be able to delay fragmentation or prevent it entirely, as Ruprecht and Bachmann (Ruprecht and Bachmann, 2010) propose for Volcán Quizapu and as we discuss for Mount Hood in Chapter Two.

Our observations of magmatic volatile contents, extent of degassing, and magnitude of temperature increase (and concomitant viscosity decrease) following recharge suggest that reduction in magma viscosity following recharge is likely to have played a decisive role in preventing explosive eruptions at Mount Hood over the lifetime of the current edifice.

This hypothesis also fits well with the observed processes of magma genesis at this volcano, and suggests that the dependence on mafic recharge to initiate eruptions at Mount Hood not only favors the eruption of mixed intermediate lavas with bimodal phenocryst populations, but also appears to favor non-explosive effusive eruptions. Although similar processes have been observed at other recharge-driven intermediate volcanoes such as Soufriére Hills Volcano, Augustine Volcano, Unzen Volcao, and Mont Pelée, we view Mount Hood as a near-endmember in the spectrum of intermediate arc volcanic systems where recharge and mixing have a particularly dominant effect on phenocryst assemblages, erupted compositions, eruption initiation, and eruption style.

REFERENCES

Borg, L.E., and Clynne, M.A., 1998, The petrogenesis of felsic calc-alkaline magmas from the southernmost Cascades, California: Origin by partial melting of basaltic lower crust: Journal of Petrology, v. 39, p. 1197-1222.

Burgisser, A., and Bergantz, G.W., 2011, A rapid mechanism to remobilize and homogenize highly crystalline magma bodies: Nature, v. 471, p. 212-215.

Conrey, R.M., Sherrod, D.R., Hooper, P.R., and Swanson, D.A., 1997, Diverse primitive magmas in the Cascades Arc, Northern Oregon, and Southern Washington: The Canadian Mineralogist, v. 35, p. 367-396.

Cribb, J.W., and Barton, M., 1997, Significance of crustal and source region processes on the evolution of compositionally similar calc-alkaline lavas, Mt. Hood, Oregon: Journal of Volcanology and Geothermal Research, v. 76, p. 229-249.

Darr, C.M., 2006, Magma chamber processes over the past 475,000 years at Mount Hood, Oregon: Insights from crystal zoning and crystal size distribution studies: Corvallis, Oregon State University.
Giordano, D., Russell, J.K., and Dingwell, D.B., 2008, Viscosity of magmatic liquids: A model: Earth and Planetary Science Letters, v. 271, p. 123-134.
Hildreth, W., 2007, Quaternary Magmatism in the Cascades— Geologic Perspectives: Reston, VA, U.S. Geological Survey.
Holland, T., and Blundy, J., 1994, Non-ideal interactions in calcic amphiboles and their bearing on amphibole-plagioclase thermometry: Contributions to Mineralogy and Petrology, v. 116, p. 433-447.
Jones, J., and Malone, S.D., 2005, Mount Hood earthquake activity: Volcanic or tectonic origins?: Bulletin of the Seismological Society of America, v. 95, p. 818-832.
Kent, A.J.R., Darr, C.M., Koleszar, A.M., Salisbury, M.J., and Cooper, K.M., 2010, Preferential eruption of andesitic magmas through recharge filtering: Nature Geoscience, v. 3, p. 631-636.
Leeman, W.P., Lewis, J.F., Evarts, R.C., Conrey, R.M., and Streck, M.J., 2005, Petrologic constraints on the thermal structure of the Cascades arc: Journal of Volcanology and Geothermal Research, v. 140, p. 67-105.
Mastin, L., and Ghiorso, M.S., 2002, Insights into volcanic conduit flow from an open-source numerical model: Geochemistry Geophysics Geosystems, v. 3, p. DOI: 10.1029/2001GC000192.
Papale, P., 1999, Strain-induced magma fragmentation in explosive eruptions: Nature, v. 397, p. 425-428.
Pichavant, M., Martel, C., Bourdier, J.-L., and Scaillet, B., 2002, Physical conditions, structure, and dynamics of a zoned magma chamber: Mount Pelée (Martinique, Lesser Antilles Arc): Journal of Geophysical Research, v. 107.
Reiners, P.W., Hammond, P.E., McKenna, J.M., and Duncan, R.A., 2000, Young basalts of the central Washington Cascades, flux melting of the mantle, and trace element signatures of primary arc magmas: Contributions to Mineralogy and Petrology, v. 138, p. 249-264.
Ridolfi, F., Renzulli, A., and Puerini, M., 2010, Stability and chemical equilibration of amphibole in calc-alkaline magmas: an overview, new thermobarometric formulations and applicaton to subduction-related volcanoes: Contributions to Mineralogy and Petrology, v. 160, p. 45-66.
Rowe, M.C., Kent, A.J.R., and Nielsen, R.L., 2009, Subduction influence on basaltic oxygen fugacity and trace and volatile elements across the Cascade volcanic arc: Journal of Petrology, v. 50.
Ruprecht, P., and Bachmann, O., 2010, Pre-eruptive reheating during magma mixing at Quizapu volcano and the implications for the explosiveness of silicic arc volcanoes: Geology, v. 38, p. 919-922.
Schmidt, M.E., Grunder, A.L., and Rowe, M.C., 2008, Segmentation of the Cascade Arc as indicated by Sr and Nd isotopic variation among diverse primitive basalts: Earth and Planetary Science Letters, v. 226, p. 166-181.

Smith, D.R., and Leeman, W.P., 2005, Chromian spinel-olivine phase chemistry and the origin of primitive basalts of the southern Washington Cascades: Journal of Volcanology and Geothermal Research, v. 140, p. 49-66.

Woods, M.M., 2004, Compositional and mineralogical relationships between mafic inclusions and host lavas as key to andesite petrogenesis at Mount Hood Volcano, Oregon: Portland, Portland State University.

FIGURES

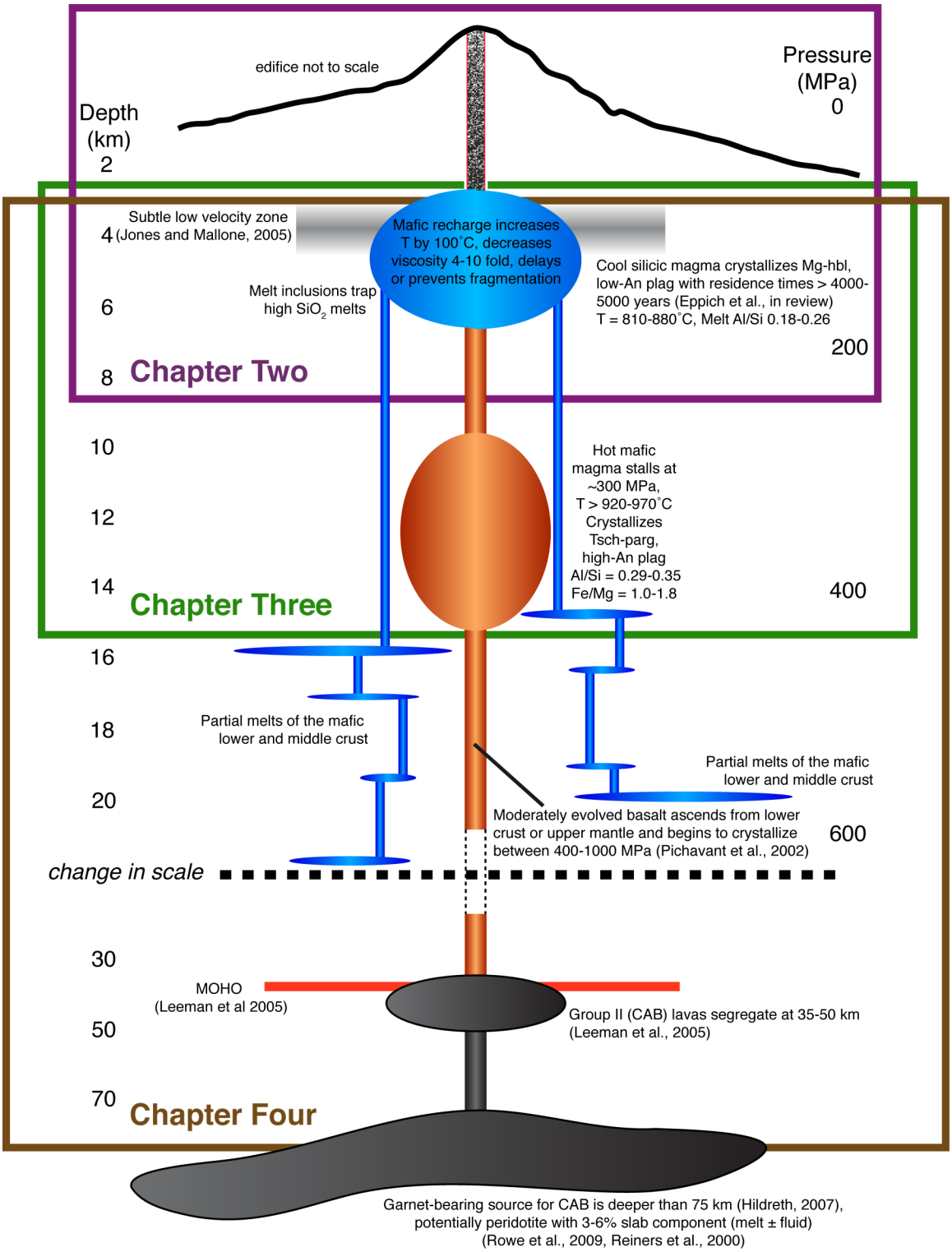

Fig. 5.1: Schematic model of the source regions and plumbing system of Mount Hood, with references to relevant chapters of this dissertation.

BIBLIOGRAPHY

Aigner-Torres, M., Blundy, J., Ulmer, P., and Pettke, T., 2007, Laser ablation ICPMS study of trace element partitioning between plagioclase and basaltic melts: an experimental approach: Contributions to Mineralogy and Petrology, v. 153, p. 647-667.

Anderson, A.T., 1974, Chlorine, sulfur, and water in magmas and oceans: Geological Society of America Bulletin, v. 85, p. 1485-1492.

—, 1976, Magma mixing: Petrological process and volcanological tool: Journal of Volcanology and Geothermal Research, v. 1, p. 3-33.

Bachmann, O., and Dungan, M.A., 2002, Temperature-induced Al-zoning in hornblendes of the Fish Canyon magma, Colorado: American Mineralogist, v. 87, p. 1062-1076.

Bacon, C.R., 1986, Magmatic inclusions in silicic and intermediate volcanic rocks: Journal of Geophysical Research, v. 21, p. 6091-6112.

Bacon, C.R., and Hirschmann, M.M., 1988, Mg/Mn partitioning as a test for equilibrium between coexisting Fe-Ti oxides: American Mineralogist, v. 73, p. 57-61.

Bacon, C.R., Newman, S., and Stolper, E.M., 1992, Water, CO2, Cl, and F in melt inclusions in phenocrysts from three Holocene explosive eruptions, Crater Lake, Oregon: American Mineralogist, v. 77, p. 1021-1030.

Baxter, P.J., 2000, Impacts of Eruptions on Human Health, *in* Sigurdsson, H., ed., Encyclopedia of Volcanoes: San Diego, Academic Press.

Blong, R.J., 1984, Volcanic Hazards: Sydney, Academic Press.

Blundy, J., and Cashman, K., 2008, Petrologic reconstruction of magmatic system variables and processes, *in* Putirka, K.D., and Tepley, F.J.I., eds., Minerals, Inclusions, and Volcanic Processes, Volume 69: Reviews in Mineralogy and Geochemistry: Chantilly, Mineralogical Society of America, p. 179-239.

Blundy, J., Cashman, K., and Humphreys, M., 2006, Magma heating by decompression-driven crystallization beneath andesite volcanoes: Nature, v. 443, p. 76-80.

Blundy, J., Cashman, K.V., and Berlo, K., 2008, Evolving magma storage conditions beneath Mount St. Helens inferred from chemical variations in melt inclusions from the 1980-1986 and current (2004-2006) eruptions, *in* Sherrod, D.R., Scott, W.E., and Stauffer, P.H., eds., A Volcano Rekindled: The Renewed Eruption from Mount St. Helens, 2004-2006, Volume 1750, U.S.G.S. Professional Paper.

Blundy, J., Cashman, K.V., Rust, A., and Witham, F., 2010, A case for CO2-rich arc magmas: Earth and Planetary Science Letters, v. 290, p. 289-301.

Borg, L.E., and Clynne, M.A., 1998, The petrogenesis of felsic calc-alkaline magmas from the southernmost Cascades, California: Origin by partial melting of basaltic lower crust: Journal of Petrology, v. 39, p. 1197-1222.

Browne, B.L., Eichelberger, J.C., Patino, L.C., Vogel, T.A., Dehn, J., Uto, K., and Hoshizumi, H., 2006, Generation of porphyritic and equigranular mafic enclaves during magma recharge events at Unzen Volcano, Japan: Journal of Petrology, v. 47, p. 301-328.

Browne, B.L., and Gardner, J.E., 2006, The influence of magma ascent path on the texture, mineralogy, and formation of hornblende reaction rims: Earth and Planetary Science Letters, v. 246, p. 161-176.
Burgisser, A., and Bergantz, G.W., 2011, A rapid mechanism to remobilize and homogenize highly crystalline magma bodies: Nature, v. 471, p. 212-215.
Clynne, M.A., 1999, A complex magma mixing origin for rocks erupted in 1915, Lassen Peak, California: Journal of Petrology, v. 40, p. 105-132.
Clynne, M.A., Calvert, A.T., Wolfe, E.W., Evarts, R.C., Fleck, R.J., and Lanphere, M.A., 2008, The Pleistocene Eruptive History of Mount St. Helens, Washington, from 300,000 to 12,800 Years Before Present, *in* Sherrod, D.R., Scott, W.E., and Stauffer, P.H., eds., A Volcano Rekindled: The Renewed Eruption of Mount St. Helens, 2004-2006, Volume Professional Paper 1750: Reston, U.S. Geological Survey.
Collins, S.J., Pyle, D.M., and Maclennan, J., 2009, Melt inclusions track pre-eruption storage and dehydration of magmas at Etna: Geology, v. 37, p. 571-574.
Conrey, R.M., Hooper, P.R., Larson, P.B., Chesley, J., and Ruiz, J., 2001, Trace element and isotopic evidence for two types of crustal melting beneath a High Cascades volcanic center, Mt. Jefferson, Oregon: Contributions to Mineralogy and Petrology, v. 141, p. 710-732.
Conrey, R.M., Sherrod, D.R., Hooper, P.R., and Swanson, D.A., 1997, Diverse primitive magmas in the Cascades Arc, Northern Oregon, and Southern Washington: The Canadian Mineralogist, v. 35, p. 367-396.
Coombs, M.L., Bull, K.F., Vallance, J.W., Schneider, D.J., Thoms, E.E., Wessels, R.L., and McGimsey, R.G., 2010, Timing, distribution, and volume of proximal products of the 2006 eruption of Augustine Volcano, *in* Power, J.A., Coombs, M.L., and Freymueller, J.T., eds., The 2006 Eruption of Augustine Volcano, Alaska: U.S. Geological Survey Professional Paper 1769.
Cribb, J.W., and Barton, M., 1997, Significance of crustal and source region processes on the evolution of compositionally similar calc-alkaline lavas, Mt. Hood, Oregon: Journal of Volcanology and Geothermal Research, v. 76, p. 229-249.
Darr, C.M., 2006, Magma chamber processes over the past 475,000 years at Mount Hood, Oregon: Insights from crystal zoning and crystal size distribution studies: Corvallis, Oregon State University.
Dingwell, D.B., 1996, Volcanic Dilemma: Flow or Blow?: Science, v. 273.
Eichelberger, J.C., 1978, Andesitic volcanism and crustal evolution: Nature, v. 275, p. 21-27.
—, 1980, Vesiculation of mafic magma during replenishment of silicic magma reservoirs: Nature, v. 288, p. 446-450.
Eichelberger, J.C., Carrigan, C.R., Westrich, H.R., and Price, R.H., 1986, Non-explosive silicic volcanism: Nature, v. 323, p. 598-602.
Eichelberger, J.C., Izbekov, P.E., and Browne, B.L., 2006, Bulk chemical trends at arc volcanoes are not liquid lines of descent: Lithos, v. 87, p. 135-154.
Ernst, W.G., and Liu, J., 1998, Experimental phase-equilibrium study of Al- and Ti-contents of calcic amphibole in MORB-- A semiquantitative thermobarometer: American Mineralogist, v. 83, p. 952-969.

Foroozan, R., Elsworth, D., Voight, B., and Mattioli, G.S., 2010, Dual reservoir structure at Soufriére Hills Volcano inferred from continuous GPS observations and heterogeneous elastic modeling: Geophysical Research Letters, v. 37.

Friedman, J.D., and Williams, D.L., 1982, Structural and heat flow implications of infrared anomalies at Mt. Hood, Oregon, 1972-1977: Journal of Geophysical Research, v. 87, p. 2793-2803.

Gerlach, D.C., and Grove, T.L., 1982, Petrology of Medicine Lake Highland Volcanics: Characterization of endmembers of magma mixing: Contributions to Mineralogy and Petrology, v. 80, p. 147-159.

Ghiorso, M.S., and Evans, B.W., 2008, Thermodynamics of rhombohedral oxide solid solutions and a revision of the Fe-Ti two-oxide geothermometer and oxygen-barometer: American Journal of Science, v. 308, p. 957-1039.

Ghiorso, M.S., and Sack, R.O., 1995, Chemical mass transfer in magmatic processes. IV. A Revised and internally consistent thermodynamic model for the interpolation and extrapolation of liquid-solid equilibria in magmatic systems at elevated temperatures and pressures.: Contributions to Mineralogy and Petrology, v. 119, p. 197-212.

Giordano, D., Russell, J.K., and Dingwell, D.B., 2008, Viscosity of magmatic liquids: A model: Earth and Planetary Science Letters, v. 271, p. 123-134.

Gonnermann, H.M., and Manga, M., 2003, Explosive volcanism may not be an inevitable consequence of magma fragmentation: Nature, v. 426, p. 432-435.

Gourgaud, A., Fichaut, M., and Joron, J.-L., 1989, Magmatology of Mt. Pelée (Martinique, F.W.I.). I: Magma mixing and triggering of the 1902 and 1929 Pelean nuées ardentes: Journal of Volcanology and Geothermal Research, v. 38, p. 143-169.

Grove, T.L., Kinzler, R.J., Baker, M.B., Donnelly-Nolan, J.M., and Lesher, C.E., 1988, Assimilation of granite by basaltic magma at Burnt Lava flow, Medicine Lake volcano, northern California: Decoupling of heat and mass transfer: Contributions to Mineralogy and Petrology, v. 99, p. 320-343.

Guffanti, M., and Weaver, C.S., 1988, Distribution of late Cenozoic volcanic vents in the Cascade Range; volcanic arc segmentation and regional tectonic considerations: Journal of Geophysical Research, v. B93, p. 6513-6529.

Hammer, J.E., Cashman, K.V., Hoblitt, R.P., and Newman, S., 1999, Degassing and microlite crystallization during the pre-climatic events of the 1991 eruption of Mt. Pinatubo, Phillipines: Bulletin of Volcanology, v. 60, p. 355-380.

Hauri, E.H., Wang, J., Dixon, J.E., King, P.L., Mandeville, C., and Newman, S., 2002, SIMS analysis of volatiles in silicate glasses 1. Calibration, matrix effects and comparisons with FTIR: Chemical Geology, v. 183, p. 99-114.

Heliker, C., 1995, Inclusions in Mount St. Helens dacite erupted from 1980 through 1983: Journal of Volcanology and Geothermal Research, v. 66, p. 115-135.

Higgins, M.D., 1996, Magma dynamics beneath Kameni volcano, Thera, Greece, as revealed by crystal size and shape measurements: Journal of Volcanology and Geothermal Research, v. 70, p. 37-48.

Hildreth, W., 2007, Quaternary Magmatism in the Cascades— Geologic Perspectives: Reston, VA, U.S. Geological Survey.

Holland, T., and Blundy, J., 1994, Non-ideal interactions in calcic amphiboles and their bearing on amphibole-plagioclase thermometry: Contributions to Mineralogy and Petrology, v. 116, p. 433-447.
Housh, T.B., and Luhr, J.F., 1991, Plagioclase-melt equilibria in hydrous systems: American Mineralogist, v. 76, p. 477-492.
Humphreys, M.C.S., Christopher, T., and Hards, V., 2009a, Microlite transfer by disaggregation of mafic inclusions following magma mixing at Soufriere Hills volcano, Montserrat: Contributions to Mineralogy and Petrology, v. 157, p. 609-624.
Humphreys, M.C.S., Edmonds, M., Christopher, T., and Hards, V., 2009b, Chlorine variations in the magma of Soufriere Hills Volcano, Montserrat: Insights from Cl in hornblende and melt inclusions: Geochemica et Cosmochimica Acta, v. 73, p. 5693-5708.
Huppert, H.E., and Woods, A.W., 2002, The role of volatiles in magma chamber dynamics: Nature, v. 420, p. 493-495.
Jaupart, C., and Allegre, C.J., 1991, Gas content, eruption rate, and instabilities of eruption regime in silicic volcanoes: Earth and Planetary Science Letters, v. 102, p. 413-429.
Johnson, D.M., Hooper, P.R., and Conrey, R.M., 1999, XRF analysis of rocks and minerals for major and trace elements on a single low dilution Li-tetraborate fused bead: Advances in X-ray Analysis, v. 41, p. 843-867.
Johnson, E.R., Wallace, P.J., Cashman, K.V., and Granados, H.D., 2010, Degassing of volatiles (H2O, CO2, S, Cl) during ascent, crystallization, and eruption at mafic monogenetic volcanoes in central Mexico: Journal of Volcanology and Geothermal Research, v. 197, p. 225-238.
Johnson, E.R., Wallace, P.J., Cashman, K.V., Granados, H.D., and Kent, A.J.R., 2008, Magmatic volatile contents and degassing-induced crystallization at Volcán Jorullo, Mexico: Implications for melt evolution and the plumbing systems of monogenetic volcanoes: Earth and Planetary Science Letters, v. 269, p. 478-487.
Jones, J., and Malone, S.D., 2005, Mount Hood earthquake activity: Volcanic or tectonic origins?: Bulletin of the Seismological Society of America, v. 95, p. 818-832.
Kent, A.J.R., 2008, Melt inclusions in basaltic and related volcanic rocks, *in* Putirka, K.D., and Tepley, F.J.I., eds., Minerals, inclusions, and volcanic processes, Volume 69, Mineralogical Society of America, p. 273-331.
Kent, A.J.R., Cooper, K.M., Eppich, G.R., Koleszar, A.M., and Salisbury, M.J., 2011, Crystal residence ages in andesitic volcanoes, International Union of Geodesy and Geophysics General Assembly: Melbourne, Australia.
Kent, A.J.R., Darr, C.M., Koleszar, A.M., Salisbury, M.J., and Cooper, K.M., 2010, Preferential eruption of andesitic magmas through recharge filtering: Nature Geoscience, v. 3, p. 631-636.
Kent, A.J.R., Rowe, M.C., Thornber, C.R., and Pallister, J.S., 2008, Trace element and Pb isotope composition of plagioclase from dome samples from the 2004-2005 eruption of Mount St. Helens, Washington, *in* Sherrod, D.R., Scott, W.E., and Stauffer, P.H., eds., A Volcano Rekindled: The Renewed Eruption from Mount St. Helens, 2004-2006, Volume 1750, U.S.G.S. Professional Paper.

Kent, A.J.R., and Ungerer, C.A., 2006, Analysis of light lithophile elements (Li, Be, B) by laser ablation ICP-MS: Comparision between magnetic sector and quadrupole ICP-MS: American Mineralogist, v. 91, p. 1401-1411.

Kohut, W., and Nielsen, R.L., 2004, Melt inclusion formation mechanisms and compositional effects in high-An feldspar and high-Fo olivine in anhydrous mafic silicate liquids: Contributions to Mineralogy and Petrology, v. 147, p. 684-704.

Koleszar, A.M., Kent, A.J.R., Wallace, P.J., and Scott, W.E., in review, Controls on long-term low explosivity at andesitic arc volcanoes: Insights from Mount Hood, Oregon: Journal of Volcanology and Geothermal Research.

Kress, V.C., and Ghiorso, M.S., 2004, Thermodynamic modeling of post-entrapment crystallization of igneous phases: Journal of Volcanology and Geothermal Research, v. 137, p. 247-260.

Lange, R.A., Frey, H.M., and Hector, J., 2009, A thermodynamic model for the plagioclase-liquid hygrometer/thermometer: American Mineralogist, v. 94, p. 494-506.

Larsen, J.F., Nye, C.J., Coombs, M.L., Tilman, M., Izbekov, P., and Cameron, C., 2010, Petrology and geochemistry of the 2006 eruption of Augustine Volcano, *in* Power, J.A., Coombs, M.L., and Freymueller, J.T., eds., The 2006 Eruption of Augustine Volcano, Alaska, Volume 1769, U.S.G.S. Professional Paper.

Leake, B.E., Woolley, A.R., Arps, C.E.S., Birch, W.D., Gilbert, M.C., Grice, J.D., Hawthorne, F.C., Kato, A., Kisch, H.J., Krivovichev, V.G., Linthout, K., Laird, J., Mandarino, J., Maresch, W.V., Nickel, E.H., Schumaker, J.C., Smith, D.C., Stephenson, N.C.N., Ungaretti, L., Whittaker, E.J.W., and Youzhi, G., 1997, Nomenclature of amphiboles: report of the subcommittee on amphiboles of the International Mineralogical Associate Comission on New Minerals and Mineral Names: Mineralological Magazine, v. 61.

Leeman, W.P., Lewis, J.F., Evarts, R.C., Conrey, R.M., and Streck, M.J., 2005, Petrologic constraints on the thermal structure of the Cascades arc: Journal of Volcanology and Geothermal Research, v. 140, p. 67-105.

Lieuallen, A.E., 2010, Meeting of the Magmas: the Evolutionary History of the Kalama Eruptive Period, Mount St. Helens, Washington: Corvallis, Oregon State University.

Lowenstern, J.B., 2000, A review of the contrasting behavior of two magmatic volatiles: chlorine and carbon dioxide: Journal of Geochemical Exploration, v. 69-70, p. 287-290.

Luhr, J.F., 2001, Glass inclusions and melt volatile contents at Paricutin Volcano, Mexico: Contributions to Mineralogy and Petrology, v. 142, p. 261-283.

Mandeville, C.W., Webster, J.D., Tappen, C., Taylor, B.E., and Timbal, A., 2009, Stable isotope and petrologic evidence for open-system degassing during the climactic and pre-climactic eruptions of Mt. Mazama, Crater Lake, Oregon: Geochemica et Cosmochimica Acta, v. 73, p. 2978-3012.

Mangan, M., and Sisson, T., 2000, Delayed, disequilibrium degassing in rhyolite magma: decompression experiments and implications for explosive volcanism: Earth and Planetary Science Letters, v. 183, p. 441-455.

Marsh, B.D., 1981, On the crystallinity, probability of occurrence, and rheology of lava and magma: Contributions to Mineralogy and Petrology, v. 78, p. 85-98.
Martel, C., Bourdier, J.-L., Pichavant, M., and Traineau, H., 2000, Textures, water content and degassing of silicic andesites from recent plinian and dome-forming eruptions at Mount Pelée volcano (Martinique, Lesser Antilles arc): Journal of Volcanology and Geothermal Research, v. 96, p. 191-206.
Martel, C., Pichavant, M., Bourdier, J.-L., Traineau, H., Holtz, F., and Scaillet, B., 1998, Magma storage conditions and control of eruption regime in silicic volcanoes: experimental evidence from Mt. Pelée: Earth and Planetary Science Letters, v. 156 p. 89-99.
—, 1999, Magma storage conditions and control of eruption regime in silicic volcanoes: experimental evidence from Mt. Pelée: Earth and Planetary Science Letters, v. 156, p. 89-99.
Martel, C., and Poussineau, S., 2007, Diversity of eruptive styles inferred from the microlites of Mt Pelée andesite (Martinique, Lesser Antilles): Journal of Volcanology and Geothermal Research, v. 166, p. 233-254.
Martel, C., Radadi Ali, A., Poussineau, S., Gourgaud, A., and Pichavant, M., 2006a, Basalt-inherited microlites in silicic magmas: Evidence from Mount Pelee (Martinique, French West Indies): Geology, v. 3, p. 905-908.
—, 2006b, Basalt-inherited microlites in silicic magmas: Evidence from Mount Pelée (Martinique, French West Indies): Geology, v. 34, p. 905-908.
Mastin, L., and Ghiorso, M.S., 2002, Insights into volcanic conduit flow from an open-source numerical model: Geochemistry Geophysics Geosystems, v. 3, p. DOI: 10.1029/2001GC000192.
McBirney, A.R., 1978, Volcanic evolution of the Cascades Range: Annual Review in Earth and Planetary Sciences, v. 6, p. 437-456.
McDonough, W.F., and Sun, S.-s., 1995, The composition of the Earth: Chemical Geology, v. 120, p. 223-253.
Melnik, O., and Sparks, R.S.J., 1999, Nonlineral dynamics of lava dome extrusion: Nature, v. 402, p. 37-41.
Métrich, N., and Rutherford, M.J., 1992, Experimental study of chlorine behavior in hydrous silicic melts: Geochimica et Cosmochimica Acta, v. 56, p. 607-616.
Míková, J., and Denková, P., 2007, Modified chromatographic separation scheme for Sr and Nd isotope analysis in geological silicate samples: Journal of Geosciences, v. 52, p. 221-226.
Miller, T.P., Chertkoff, D.G., Eichelberger, J.C., and Coombs, M.L., 1999, Mount Dutton volcano, Alaska: Aleutian arc analog to Unzen volcano, Japan: Journal of Volcanology and Geothermal Research, v. 89, p. 275-301.
Miller, T.P., and Chouet, B.A., 1994, The 1989-1990 eruptions of Redoubt Volcano: An introduction: Journal of Volcanology and Geothermal Research, v. 62, p. 1-10.
Morgan, D.J., Blake, S., Rogers, N.W., DeVivo, B., Rolandi, G., Macdonald, R., and Hawkesworth, C.J., 2004, Time scales of crystal residence and magma chamber volume from modelling of diffusion profiles in phenocrysts: Vesuvius 1944: Earth and Planetary Science Letters, v. 222, p. 933-946.

Morrissey, M.M., 1997, Long-period seismicity at Redoubt Volcano, Alaska, 1989-1990 related to magma degassing: Journal of Volcanology and Geothermal Research, v. 75, p. 321-335.

Murphy, M.D., Sparks, R.S.J., Barclay, J., Carroll, M.R., and Brewer, T.S., 2000, Remobilization of andesite magma by intrusion of mafic magma at the Soufriére Hills Volcano, Montserrat, West Indies: Journal of Petrology, v. 41, p. 21-42.

Murphy, M.D., Sparks, R.S.J., Barclay, J., Carroll, M.R., Lejeune, A.-M., Brewer, T.S., Macdonald, R., Black, S., and Young, S., 1998, The role of magma mixing in triggering the current eruption at the Soufriere Hills volcano, Montserrat, West Indies: Geophysical Research Letters, v. 25, p. 3433-3436.

Newman, S., and Lowenstern, J.B., 2002, VolatileCalc: a silicate melt-H2O-CO2 solution model written in Visual Basic for Excel: Computers and Geosciences, v. 28, p. 597-604.

Okumura, S., Nakamura, M., Takeuchi, S., Tsuchiyama, A., Nakano, T., and Uesugi, K., 2009, Magma deformation may induce non-explosive volcanism via degassing through bubble networks: Earth and Planetary Science Letters, v. 281, p. 267-274.

Okumura, S., Nakamura, M., and Tsuchiyama, A., 2006, Shear-induced bubble coalescence in rhyolite melts with low vesicularity: Geophysical Research Letters, v. 33.

Pallister, J.S., Hoblitt, R.P., Meeker, G.P., Knight, R.J., and Siems, D.F., 1996, Magma mixing at Mount Pinatubo: Petrographic and chemical evidence from 1991 deposits, *in* Newhall, C., and Punongbayan, R., eds., Fire and Mud: Eruptions and Lahars of Mount Pinatubo, Quezon City, Philippine Institute of Volcanology and Seismology, and Seattle, University of Washington Press, p. 687-732.

Pallister, J.S., Thornber, C.R., Cashman, K.V., Clynne, M.A., Lowers, H.A., Mandeville, C.W., Brownfield, I.K., and Meeker, G.P., 2008, Petrology of the 2004-2006 Mount St. Helens lava dome-- Implications for magmatic plumbing and eruption triggering, *in* Sherrod, D.R., Scott, W.E., and Stauffer, P.H., eds., A Volcano Rekindled: The Renewed Eruption of Mount St. Helens, 2004-2006, Volume 1750, U.S.G.S. Professional Paper.

Papale, P., 1999, Strain-induced magma fragmentation in explosive eruptions: Nature, v. 397, p. 425-428.

Papale, P., Moretti, R., and Barbato, D., 2006, The compositional dependence of the saturation surface of H2O + CO2 fluids in silicate melts: Chemical Geology, v. 229, p. 78-95.

Pichavant, M., Costa, F., Burgisser, A., Scaillet, B., Martel, C., and Poussineau, S., 2007, Equilibrium scales in silicic to intermediate magmas-- Implications for experimental studies: Journal of Petrology, v. 48, p. 1955-1972.

Pichavant, M., Martel, C., Bourdier, J.-L., and Scaillet, B., 2002, Physical conditions, structure, and dynamics of a zoned magma chamber: Mount Pelée (Martinique, Lesser Antilles Arc): Journal of Geophysical Research, v. 107.

Pinel, V., and Jaupart, C., 2005, Some consequences of volcanic edifice destruction for eruption conditions: Journal of Volcanology and Geothermal Research, v. 145, p. 68-80.

Prouteau, G., and Scaillet, B., 2003, Experimental constraints on the origin of the 1991 Pinatubo dacite: Journal of Petrology, v. 44, p. 2203-2241.
Prouteau, G., Scaillet, B., Pichavant, M., and Maury, R.C., 1999, Fluid-present melting of ocean crust in subduction zones: Geology, v. 27, p. 1111-1114.
Putirka, K.D., 2005, Mantle potential temperatures at Hawaii, Iceland, and the mid-ocean ridge system, as inferred from olivine phenocrysts: Evidence for thermally driven mantle plumes: Geochemistry Geophysics Geosystems, v. 6, p. doi: 10.1029/2005GC000915.
—, 2008, Thermometers and barometers for volcanic systems, *in* Putirka, K.D., and Tepley, F.J.I., eds., Minerals, inclusions, and volcanic processes, Volume 69, Mineralogical Society of America, p. 61-120.
Reiners, P.W., Hammond, P.E., McKenna, J.M., and Duncan, R.A., 2000, Young basalts of the central Washington Cascades, flux melting of the mantle, and trace element signatures of primary arc magmas: Contributions to Mineralogy and Petrology, v. 138, p. 249-264.
Reubi, O., and Blundy, J., 2009, A dearth of intermediate melts at subduction zone volcanoes and the petrogenesis of arc andesites: Nature, v. 461, p. 1269-1273.
Ridolfi, F., Puerini, M., Renzulli, A., Menna, M., and Toulkeridis, T., 2008, The magmatic feeding system of El Reventado volcano (Sub-Andean zone, Ecuador) constrained by texture, mineralogy, and thermobarometry of the 2002 erupted products: Journal of Volcanology and Geothermal Research, v. 176, p. 94-106.
Ridolfi, F., Renzulli, A., and Puerini, M., 2010, Stability and chemical equilibration of amphibole in calc-alkaline magmas: an overview, new thermobarometric formulations and applicaton to subduction-related volcanoes: Contributions to Mineralogy and Petrology, v. 160, p. 45-66.
Roggensack, K., Hervig, R.L., McKnight, S.B., and Williams, S.N., 1997, Explosive basaltic volcanism from Cerro Negro Volcano: Influence of volatiles on eruptive style: Science, v. 277, p. 1639-1642.
Roman, D.C., Cashman, K.V., Gardner, C.A., Wallace, P.J., and Donovan, J.J., 2006, Storage and interaction of compositionally heterogeneous magmas from the 1986 eruption of Augustine Volcano, Alaska: Bulletin of Volcanology, v. 68, p. 240-254.
Ross, P.-S., Ukstins Peate, I., McClintock, M.K., Xu, Y.G., Skilling, I.P., White, J.D.L., and Houghton, B.F., 2005, Mafic volcaniclastic deposits in flood basalt provinces: A review: Journal of Volcanology and Geothermal Research, v. 145, p. 281-314.
Rowe, M.C., Kent, A.J.R., and Nielsen, R.L., 2009, Subduction influence on basaltic oxygen fugacity and trace and volatile elements across the Cascade volcanic arc: Journal of Petrology, v. 50.
Rowe, M.C., Kent, A.J.R., and Thornber, C.R., 2008, Using amphibole phenocrysts to track vapor transfer during magma crystallization and transport: An example from Mount St. Helens, Washington: Journal of Volcanology and Geothermal Research, v. 178, p. 593-607.
Ruprecht, P., and Bachmann, O., 2010, Pre-eruptive reheating during magma mixing at Quizapu volcano and the implications for the explosiveness of silicic arc volcanoes: Geology, v. 38, p. 919-922.

Ruscitto, D.M., Wallace, P.J., Johnson, E.R., Kent, A.J.R., and Bindeman, I.N., 2010, Volatile contents of mafic magmas from cinder cones in the Central Oregon High Cascades: Implications for magma formation and mantle conditions in a hot arc: Earth and Planetary Science Letters, v. 298, p. 153-161.

Rutherford, M.J., and Devine, J.D., 1988, The May 18, 1980, eruption of Mount St. Helens 3. Stability and chemistry of amphibole in the magma chamber: Journal of Geophysical Research, v. 93, p. 11949-11959.

—, 2008, Magmatic conditions and processes in the storage zone of the 2004-2006 Mount St. Helens dacite, *in* Sherrod, D.R., Scott, W.E., and Stauffer, P.H., eds., A Volcano Rekindled: The Renewed Eruption from Mount St. Helens, 2004-2006, Volume 1750, U.S.G.S. Professional Paper.

Salisbury, M.J., Bohrson, W.A., Clynne, M.A., Ramos, F.C., and Hoskin, P., 2008, Multiple plagioclase crystal populations identified by crystal size distribution and in situ chemical data: Implications for timescales of magma chamber processes associated with the 1915 eruption of Lassen Peak, CA: Journal of Petrology, v. 49, p. 1755-1780.

Sato, H., Holtz, F., Behrens, H., Botcharnikov, R., and Nakada, S., 2005, Experimental petrology of the 1991-1995 Unzen Dacite, Japan. Part II: Cl/OH partitioning between hornblende and melt and its implications for the origin of oscillatory zoning of hornblende phenocrysts: Journal of Petrology, v. 46, p. 339-354.

Sato, H., Nakada, S., Fujii, T., Nakamura, M., and Suzuki-Kamata, K., 1999, Groundmass pargasite in the 1991-1995 dacite of Unzen volcano: phase stability experiments and volcanological implications: Journal of Volcanology and Geothermal Research, v. 89, p. 197-212.

Scaillet, B., and Evans, B.W., 1999, The 15 June 1991 eruption of Mount Pinatubo. I. Phase equilibriua and pre-eruption P-T-fO2-fH2O conditions of the dacite magma: Journal of Petrology, v. 40, p. 381-411.

Scandone, R., Cashman, K.V., and Malone, S.D., 2007, Magma supply, magma ascent and the style of volcanic eruptions: Earth and Planetary Science Letters, v. 253, p. 513-529.

Schmidt, M.E., Grunder, A.L., and Rowe, M.C., 2008, Segmentation of the Cascade Arc as indicated by Sr and Nd isotopic variation among diverse primitive basalts: Earth and Planetary Science Letters, v. 226, p. 166-181.

Scott, W.E., Gardner, C.A., Tilling, R.I., and Lanphere, M.A., 1997a, Geologic History of Mount Hood Volcano, Oregon: A Field-Trip Guidebook: U.S. Geological Survey Open-File Report, v. 97, p. 38p.

Scott, W.E., Pierson, T.C., Schilling, S.P., Costa, J.E., Gardner, C.A., Vallance, J.W., and Major, J.J., 1997b, Volcano hazards in the Mount Hood Region, Oregon, *in* Interior, U.S.D.o.t., ed., Volume Open-File Report 97-89, U.S. Geological Survey, p. 14.

Severs, M.J., Beard, J.S., Fedele, L., Hancher, J.M., Mutchler, S.R., and Bodnar, R.J., 2009, Partitioning behavior of trace elements between dacitic melt and plagioclase, orthopyroxene, and clinopyroxene based on laser ablation ICPMS analysis of silicate melt inclusions: Geochemica et Cosmochimica Acta, v. 73, p. 2123-2141.

Singer, B.S., Dungan, M.A., and Layne, G.D., 1995, Textures and Sr, Ba, Mg, Fe, K, and Ti compositional profiles in volcanic plagioclase: Clues to the dynamics of calc-alkaline magma chambers: American Mineralogist, v. 80, p. 776-798.

Sisson, T.W., and Grove, T.L., 1993, Experimental investigations of the role of H2O in calc-alkaline differentiation and subduction zone magmatism: Contributions to Mineralogy and Petrology, v. 113, p. 143-166.

Smith, D.R., and Leeman, W.P., 1987, Petrogenesis of Mount St. Helens dacitic magmas: Journal of Geophysical Research, v. 92, p. 10313-10334.

—, 2005, Chromian spinel-olivine phase chemistry and the origin of primitive basalts of the southern Washington Cascades: Journal of Volcanology and Geothermal Research, v. 140, p. 49-66.

Sparks, R.S.J., 1978, The dynamics of bubble formation and growth in magmas: A review and analysis: Journal of Volcanology and Geothermal Research, v. 3, p. 1-37.

Sparks, R.S.J., and Marshall, L.A., 1986, Thermal and mechanical constraints on mixing between mafic and silicic magmas: Journal of Volcanology and Geothermal Research, v. 29, p. 99-124.

Sparks, R.S.J., and Sigurdsson, H., 1977, Magma mixing: a mechanism for triggering acid explosive eruptions: Nature, v. 267, p. 315-318.

Steiner, A.R., 2009, A petrologic investigation of mafic inputs into the Augustine Volcano (Alaska) magma system over the pas 2,200 years: Fullerton, California State University.

Streck, M.J., Broderick, C.A., Thornber, C.R., Clynne, M.A., and Pallister, J.S., 2008, Plagioclase populations and zoning in dacite of the 2004-2006 Mount St. Helens eruption: Constraints for magma origin and dynamics, *in* Sherrod, D.R., Scott, W.E., and Stauffer, P.H., eds., A Volcano Rekindled: The Renewed Eruption from Mount St. Helens, 2004-2006, Volume 1750, U.S.G.S. Professional Paper.

Symonds, R.B., Poreda, R.J., Evans, W.C., Janik, C.J., and Ritchie, B.E., 2003, Mantle and crustal sources of carbon, nitrogen, and noble gases in Cascade-Range and Aleutian-Arc volcanic gases: USGS Open-File Report, v. 03-436.

Tepley, F.J.I., Davidson, J.P., and Clynne, M.A., 1999, Magmatic interactions as recorded in plagioclase phenocrysts of Chaos Crags, Lassen Volcanic Center, California: Journal of Petrology, v. 40, p. 787-806.

Thornber, C.R., Pallister, J.S., Lowers, H.A., Rowe, M.C., Mandeville, C.W., and Meeker, G.P., 2008, Chemistry, mineralogy, and petrology of amphibole in Mount St. Helens 2004-2006 dacite, *in* Sherrod, D.R., Scott, W.E., and Stauffer, P.H., eds., A Volcano Rekindled: The Renewed Eruption of Mount St. Helens, 2004-2006, Volume 1750, U.S.G.S. Professional Paper.

Tiepolo, M., Oberti, R., Zanetti, A., Vannucci, R., and Foley, S., 2007, Trace-element partitioning between amphibole and silicate melt, *in* Hawthorne, F.C., Oberti, R., Della Ventura, G., and Mottana, A., eds., Amphiboles: Crystal Chemistry, Occurrence, and Health Issues, Volume 67, Mineralogical Society of America.

Venezky, D.Y., and Rutherford, M.J., 1999, Petrology and Fe-Ti oxide reequilibration of the 1991 Mount Unzen mixed magma: Journal of Volcanology and Geothermal Research, v. 89, p. 213-230.

Villemant, B., and Boudon, G., 1998, Transition from dome-forming to plinian eruptive styles controlled by H2O and Cl degassing: Nature, v. 392, p. 65-69.
Wallace, P.J., 2005, Volatiles in subduction zone magmas: concentrations and fluxes based on melt inclusion and volcanic gas data: Journal of Volcanology and Geothermal Research, v. 140, p. 217-240.
Wallace, P.J., and Gerlach, T.M., 1994, Magmatic vapor source for sulfur dioxide released during volcanic eruptions: Evidence from Mount Pinatubo: Science, v. 265, p. 496-499.
Watts, R.B., Herd, R.A., Sparks, R.S.J., and Young, S.R., 2002, Growth patterns and emplacement of the andesitic lava dome at Soufriére Hills Volcano, Montserrat: Geological Society, London, Memoirs, v. 21, p. 115-152.
Webster, J.D., 1997, Chloride solubility in felsic melts and the role of chloride in magmatic degassing: Journal of Petrology, v. 38, p. 1793-1807.
Webster, J.D., Kinzler, R.J., and Mathez, E.A., 1999, Chloride and water solubility in basalt and andesite melts and implications for magmatic degassing: Geochimica et Cosmochimica Acta, v. 63, p. 729-738.
Wilson, L., 1980, Relationships between pressure, volatile content, and ejecta velocity in three types of volcanic explosive: Journal of Volcanology and Geothermal Research, v. 8, p. 297-313.
Wilson, L., Sparks, R.S.J., and Walker, G.P.L., 1980, Explosive volcanic eruptions-- IV. The control of magma properties and conduit geometry on eruption column behaviour: Geophysical Journal of the Royal Astronomical Society, v. 63, p. 117-148.
Wolf, K.J., and Eichelberger, J.C., 1997, Syneruptive mixing, degassing, and crystallization at Redoubt Volcano, eruption of December, 1989 to May 1990: Journal of Volcanology and Geothermal Research, v. 75, p. 1997.
Woods, A.W., 1995, The dynamics of explosive volcanic eruptions: Reviews of Geophysics, v. 33, p. 495-530.
Woods, M.M., 2004, Compositional and mineralogical relationships between mafic inclusions and host lavas as key to andesite petrogenesis at Mount Hood Volcano, Oregon: Portland, Portland State University.
Zellmer, G.F., Hawkesworth, C.J., Sparks, R.S.J., Thomas, L.E., Harford, C.L., Brewer, T.S., and Loughlin, S.C., 2003, Geochemical evolution of the Soufriére Hills Volcano, Montserrat, Lesser Antilles Volcanic Arc: Journal of Petrology, v. 44, p. 1349-1374.